



HAL
open science

Analysis of structural robustness: characterization of accidental/exceptional events and of their impacts on infrastructures

Mohammad El Hajj Diab

► **To cite this version:**

Mohammad El Hajj Diab. Analysis of structural robustness: characterization of accidental/exceptional events and of their impacts on infrastructures. Civil Engineering. Université Paris-Est, 2019. English. NNT: 2019PESC2079 . tel-02900079

HAL Id: tel-02900079

<https://theses.hal.science/tel-02900079>

Submitted on 15 Jul 2020

HAL is a multi-disciplinary open access archive for the deposit and dissemination of scientific research documents, whether they are published or not. The documents may come from teaching and research institutions in France or abroad, or from public or private research centers.

L'archive ouverte pluridisciplinaire **HAL**, est destinée au dépôt et à la diffusion de documents scientifiques de niveau recherche, publiés ou non, émanant des établissements d'enseignement et de recherche français ou étrangers, des laboratoires publics ou privés.



Thèse présentée pour obtenir le grade de
Docteur de l'Université Paris-Est

Ecole doctorale : “Science, Ingénierie et Environnement”

Spécialité : “Génie Civil”

Par

Mohammad EL HAJJ DIAB

Titre

ANALYSE DE LA ROBUSTESSE STRUCTURALE
Caractérisation des actions accidentelles et/ou
exceptionnelles et de leurs effets sur les structures

Analysis of structural robustness

*Characterization of accidental/exceptional actions and their impacts on
structures*

Soutenue le 24 octobre 2019, devant le jury composé de :

M. Stéphane GRANGE	<i>Président du jury</i>
M. Mohammed HJIAJ	<i>Rapporteur</i>
M. Alan O'CONNOR	<i>Rapporteur</i>
M. Jérémy BLEYER	<i>Examineur</i>
M. Robby CASPEELE	<i>Examineur</i>
M. Jean-François DEMONCEAU	<i>Examineur</i>
M. Cédric DESPREZ	<i>Conseiller d'étude</i>
M. André ORCESI	<i>Directeur de thèse</i>

ACKNOWLEDGMENTS

I would like to express my deepest gratitude to my supervisor Dr. André ORCESI, deputy head of the Urban and Civil Engineering Testing and Modeling Laboratory – EMGCU at IFSTTAR, for his constant guidance and support throughout this PhD. Furthermore, I am especially thankful for his significant contribution to my academic, professional and personal development. My sincere thanks to Dr. Cédric DESPREZ, researcher at EMGCU Laboratory, IFSTTAR, for all his advice, his thoughtful insights and encouragement during this work.

I am deeply grateful to Dr. Jérémy BLEYER, researcher at Navier laboratory, for the many discussions concerning this work and his particular interest in imparting invaluable knowledge. I am also grateful to Prof. Patrick De BUHAN, Navier laboratory, Dr. Pierre MARCHAND, researcher at EMGCU laboratory, and Dr. Anne-Sophie COLAS, researcher at EMGCU laboratory, for their valuable support and thoughtful advice.

I would like to thank Prof. Mohammed HJIAJ, INSA Rennes, and Prof. Alan O’CONNOR, Trinity College Dublin, for accepting to review this dissertation.

I extend profound appreciation to Prof. Stéphane GRANGE, INSA Lyon, for giving me the honour to be president of the jury for the PhD defense. I would also like to thank Prof. Jean-François DEMONCEAU, University of Liege, and Prof. Robby CASPEELE, Ghent University, for agreeing to examine my work.

I am thankful to Dr. Jean-Michel TORRENTI, head of MAST department, Dr. François TOUTLEMONDE, deputy head of MAST department, and Dr. Jean-Noël ROUX, deputy head of Navier laboratory, for their assistance in the follow-up committee of my PhD.

I am grateful to all members of EMGCU laboratory (researchers, technicians and PhD students). I have appreciated during these three years the friendly atmosphere. Special thanks to Dr. Jean-Luc CLEMENT, delegate scientific director at IFSTTAR, Dr. Pierre ARGOUL, head of EMGCU laboratory, Dr. Renaud-Pierre MARTIN, deputy head of EMGCU laboratory, and Mrs. Minh ORCESI, secretary of EMGCU laboratory.

And last, but certainly not least, I would like to express my sincere gratitude to my parents, Ahmad and Mona, to whom I largely owe all I have achieved in my life thus far. I count myself lucky to have this family, my brothers, Rami and Wassim, my sister and her husband, Darine and Youssef, and my lovely nephew Hady.

RESUMÉ

Plusieurs exemples de structures ont subi des endommagements conséquents, avec dans certains cas un effondrement, à la suite d'une propagation de la défaillance résultant d'une action accidentelle ou exceptionnelle. Ces évènements catastrophiques soulignent l'importance d'un dimensionnement n'étant pas limité à la seule vérification de la sécurité dans des conditions accidentelles, mais qui préserve une capacité résiduelle suffisante pour ne pas engendrer d'effondrement progressif sous l'action d'évènements exceptionnels n'ayant pas été identifiés à l'étape de dimensionnement.

Les codes de conception actuels recommandent d'avoir un niveau de robustesse approprié pour éviter un effondrement disproportionné en cas d'évènement exceptionnel. Une difficulté majeure est de quantifier la robustesse d'une structure sous de telles situations exceptionnelles. Dans le domaine de l'ingénierie structurale, le cadre réglementaire des Eurocodes définit la robustesse structurale comme « l'aptitude d'une structure à résister à des événements tels que les incendies, les explosions, les chocs ou les conséquences d'une erreur humaine, sans présenter de dégâts disproportionnés par rapport à la cause d'origine ». Pour prendre en compte cette exigence, la détermination d'indicateurs est essentielle pour évaluer la capacité d'une structure à faire face à ces évènements, à estimer la capacité à éviter un effondrement disproportionné et également à être un outil d'aide à la décision. Plusieurs métriques ont été récemment proposées dans la littérature. Cependant, les méthodes en question ne sont pas encore pleinement intégrées dans les pratiques d'ingénierie.

L'objectif principal de cette thèse est de proposer une approche pour quantifier la robustesse structurale. L'effondrement progressif est pris en compte via un couplage itératif entre un calcul à la rupture et un calcul non linéaire aux éléments finis. Des indices sont introduits pour mesurer un niveau de robustesse et être utilisés comme outil d'aide à la décision. Des cas d'étude sont considérés pour illustrer les concepts proposés (étude de plusieurs scénarios de défaillance, identification des scénarios les plus critiques et évaluation de la capacité structurale à éviter une propagation de la défaillance).

ABSTRACT

Several examples of structures have been severely damaged, or even reached the total collapse, after the propagation of some local failure, resulting from an accidental or exceptional event. These catastrophic events highlight the importance of the structural design not to be limited to safety under normal conditions, but also to preserve structural integrity under an exceptional event not identified at the design stage.

Modern design codes recommend ensuring an appropriate level of robustness to prevent from disproportionate collapse under an exceptional event. One of the major difficulties is to quantify the concept of structural robustness when checking the structural safety under exceptional situations. In this respect, the Eurocodes define the structural robustness as “the ability of a structure to withstand events like fire, explosions, impact or the consequences of human error, without being damaged to an extent disproportionate to the original cause”. To meet such requirements, robustness indicators are essential to assess the capacity of the structure to withstand events, estimate the safety against disproportionate collapse, and finally be used as a decision support for design choices. Several robustness metrics have been recently proposed in the literature. However, despite developments in this field, these methods are still not fully used in engineering practice to effectively assess structural robustness.

The main objective of this PhD is to propose an approach to quantify the structural robustness. Progressive collapse is modelled based on an iterative coupling between the yield design approach and a non-linear analysis. Some indices are introduced to measure the structural robustness and be used as a decision support tool. Case studies are considered to illustrate the proposed concepts (study of a large number of scenarios, identification of the most critical ones, and evaluation of the structural capacity to prevent failure propagation).

TABLE OF CONTENTS

Chapter I General introduction	1
I.1 Background	1
I.2 Issues with structural robustness	6
I.3 Organization of the dissertation	9
Chapter II Concept of structural robustness.....	11
II.1 Introduction	11
II.1.1 The difficulty of dealing with unidentified actions	11
II.1.2 A multi-aspect problem	12
II.1.2.1 Non-linear material behaviour	12
II.1.2.2 Geometrical non-linearities	12
II.1.2.3 Alternative equilibrium state	12
II.1.2.4 Dynamic effects	14
II.1.2.5 Debris loading.....	14
II.1.3 Disparity of definitions between research and normative communities.....	15
II.2 Engineering approach	19
II.2.1 Tying method.....	22
II.2.2 Alternative load path method	23
II.2.3 Local resistance design method	23
II.2.4 Risk-based assessment method.....	24
II.3 Scientific community approaches.....	25
II.3.1 Robustness indices in the literature	26
II.3.1.1 Indices based on structural response	26
II.3.1.1.1 Deterministic indices	26
II.3.1.1.2 Probabilistic indices.....	30
II.3.1.2 Indices based on structural characteristics.....	34
II.3.2 Analytical characterization of alternative load paths	34
II.3.3 Numerical modelling for propagation of failure.....	37
II.3.3.1 Finite Element Method (FEM)	37

II.3.3.1.1 Local approach	37
II.3.3.1.2 Global approach.....	39
II.3.3.1.3 Semi-global approach	40
II.3.3.2 Discrete Element Method (DEM).....	42
II.3.3.3 Applied Element Method (AEM)	43
II.3.3.4 Cohesive Element Method (CEM)	44
II.3.4 Experimental testing for building recommendations.....	45
II.4 Feedback on current approaches and identification of improvement needs.....	46
II.4.1 Feedback on robustness measures	47
II.4.2 Feedback on progressive collapse analysis	48
II.5 Conclusions	48
Chapter III Modelling of progressive collapse	51
III.1 Introduction	51
III.2 Yield design approach.....	52
III.2.1 General principles	52
III.2.2 Static approach of the potential safe loads	56
III.2.3 Kinematic approach of the potential safe loads	56
III.3 Numerical modelling of yield design approach	59
III.3.1 Components of the yield design implementation.....	59
III.3.2 Yield criterion characterization for a beam element cross-section	60
III.3.3 Static approach for the global structure.....	68
III.3.4 Kinematic approach for the global structure	70
III.3.5 Illustration on a simple beam case study and comparison with a non-linear static analysis	72
III.3.5.1 Configuration B1 with pinned supports at both ends.....	74
III.3.5.2 Configuration B2 with one pinned support and one roller support.....	77
III.3.5.3 Configuration B3 with fixed supports at both ends.....	78
III.3.5.4 Comparison of computation cost.....	79
III.3.6 How to use the benefits of the yield design approach for progressive collapse analysis?	80
III.4 Coupling between the yield design approach and a non-linear analysis.....	81
III.4.1 General principles	81
III.4.2 Application on a beam element	84
III.4.3 Application on a steel-framed building	86
III.4.3.1 Presentation of the case study	86

III.4.3.2 Illustration of local failure scenario C1	89
III.4.3.2.a Coupling strategy.....	89
III.4.3.2.b Non-linear static analysis on the whole structure.....	90
III.4.3.3 Illustration of local failure scenario C2.....	92
III.4.3.3.a Coupling strategy.....	92
III.4.3.3.b Non-linear static analysis on the whole structure.....	98
III.4.3.4 Illustration of local failure scenario C3.....	100
III.4.3.4.a Coupling strategy.....	100
III.4.3.4.b Non-linear static analysis on the whole structure.....	102
III.4.3.5 Illustration of local failure scenario C4.....	103
III.4.3.5.a Coupling strategy.....	103
III.4.3.5.b Non-linear static analysis on the whole structure.....	107
III.4.4 General discussion.....	109
III.5 Conclusions	110
Chapter IV Quantification of structural robustness.....	111
IV.1 Introduction	111
IV.2 Characterization of local failure scenarios.....	113
IV.3 Proposed structural robustness indices	122
IV.3.1 Robustness Propagation Failure Index (<i>RPM</i>)	122
IV.3.2 Robustness Energy Index (<i>REI</i>).....	123
IV.3.3 Discussion on the most critical scenarios	124
IV.4 Structural robustness assessment of a steel-framed building structure.....	126
IV.4.1 Identification and characterization of the applied local failure scenarios.....	126
IV.4.2 Structural response under the local failure scenarios.....	130
IV.4.3 Calculation of robustness indices.....	134
IV.5 Comparison with different structural configurations of steel-framed structure.....	143
IV.5.1 Presentation of design configurations	143
IV.5.2 Analysis of structural response	146
IV.5.3 Assessment of structural robustness with <i>RPM</i>	151
IV.5.4 Assessment of structural robustness with <i>REI(UC)</i>	155
IV.5.5 Assessment of structural robustness with several criteria.....	159
IV.5.6 General discussion	168
IV.6 Conclusions	169

Chapter V Analysis of factors influencing the structural robustness assessment.....	171
V.1 Introduction	171
V.2 Effect of loads combination and dynamic amplification factor	172
V.2.1 Presentation of case studies	172
V.2.2 Structural response under the local failure scenarios	174
V.2.3 Assessment of structural robustness with <i>RPFI</i>	178
V.2.4 Assessment of structural robustness with <i>REI(UC)</i>	180
V.2.5 Assessment of structural robustness with several criteria	183
V.2.6 General discussion.....	190
V.3 Effect of bay dimension	191
V.3.1 Presentation of case study	191
V.3.2 Assessment of structural robustness with <i>RPFI</i>	192
V.3.3 Assessment of structural robustness with <i>REI(UC)</i>	195
V.3.4 Assessment of structural robustness with several criteria	196
V.3.5 General discussion.....	197
V.4 Effect of steel ductility	198
V.5 Discussion on the other factors influencing the structural robustness assessment.....	205
V.5.1 Threshold UC associated with an unacceptable collapse	205
V.5.2 Boundary conditions of the substructure.....	206
V.5.3 Local failure scenarios.....	206
V.5.4 Debris loading	207
V.5.5 Three-dimensional analysis	207
V.6 Conclusions	208
Chapter VI General conclusions.....	211
I.1 How to propose a simplified modelling of progressive collapse?	212
I.2 How to identify the degree of failure propagation?	213
I.3 How to assess the maximum structural capacity with respect to some performance criteria?	214
I.4 General Perspectives	215
References	217
Annex A Detailed results for the structural robustness assessment in Chapter IV	233
Annex B Detailed results for the structural robustness assessment in Chapter V.....	239

CHAPTER I

GENERAL INTRODUCTION

I.1 BACKGROUND

In the history of structural engineering, the developments in the understanding of materials, structural behaviour and mathematics, have progressively enabled to model and solve structural problems, by using equilibrium of forces and compatibility of geometry, and formulating fundamental theoretical principles. Throughout the late 19th and 20th centuries, materials science and structural analysis underwent important developments from geometrical nonlinearity's (large deformations) to material nonlinearity's (elasto-plastic materials) in structural design, considering non-linear relation between applied force and displacements. More recently, the development of powerful computers has allowed finite element analysis to become a significant tool for structural non-linear analysis and design. These technological developments meet a growing demand for larger, taller, and more complex structures, in line with the needs of people, such as high towers and buildings, airports and large scale bridges for transportation, nuclear reactors, dams or wind turbines for energy supply, etc. Such structures are critical in the sense that their failure, or even worse their total failure by collapse, may have tremendous impacts on society and environment.

The world has witnessed many incidents of progressive collapses on various types of structure (bridges, airports, towers, etc.), under several types of triggering events (blast, impact, construction errors, etc.). The associated consequences, whether human, economic or environmental, have often put robustness issues on the table and pushed the civil engineering community to further analyze structural behaviour under abnormal actions. After the Second World War, Baker et al. (1948) studied the behaviour of structures against bomb explosions and debris impacts in London during the war, where progressive collapse was identified in several cases of structural failures. Later, one of the most famous historical failures was the progressive and partial collapse of the Ronan Point tower in London (UK) on the 16th May

1968. This 22-storey block was built using large concrete prefabricated sections casted off-site and bolted together to construct the building. A piped gas explosion in the corner of the 18th floor flat led to dislodge one of the load bearing walls in the corner of building (Pearson and Delatte, 2005). The loss of this wall caused the collapse of the above corner floor areas as shown in Figure I.1a, then the subsequent collision with the lower floors led to the collapse of the entire corner area of the building (Figure I.1b). The investigation at the time of Griffiths et al. (1968) indicated that the wall had limited resistance to lateral loading. The explosion even though not significant in magnitude, caused the failure of this weak structural element, which initiated failure propagation. Moreover, the errors in construction, due to workmanship flaws at critical structural connections, caused a lack of continuity and structural redundancy in the structure, which led to the poor resistance against progressive collapse. This event, where the consequences were deemed disproportionate compared to the local failure, represented a decisive moment when structural robustness began to gain importance. Hence, a first wave of research interest released in the progressive collapse of structures, and provisions against progressive collapse (tying method, alternative load path method, notion of key element) were introduced in the British Code "The Building Regulations 1970" (Pearson and Delatte, 2005).



(a) Location of initial damage



(b) Collapsed area

Figure I.1: Collapse of the Ronan Point Tower (photo credit: Derek Voller/CC BY-SA 2.0).

More recently, the dramatic collapse of the twin towers of the World Trade Center by the terrorist attacks of 11 September 2001 in New York City in the United States led to a significant and worldwide impact on the general interest in structural safety. The collapse caused the death of 2,752 people, in addition to the enormous economic and political consequences. The structure of these 110-storey towers consisted of a network of closely-spaced perimeter columns and deep beam spandrels forming together a steel frame-tube system, with a core creating a secondary system by more widely-spaced columns as shown in Figure I.2. There was also a steel truss system (hat truss) to connect the perimeter and core columns, which was located at the top four floors. The floors consisted of lightweight

concrete on a fluted steel deck, and they were supported a grid of lightweight steel bar trusses (Sunder et al., 2005).

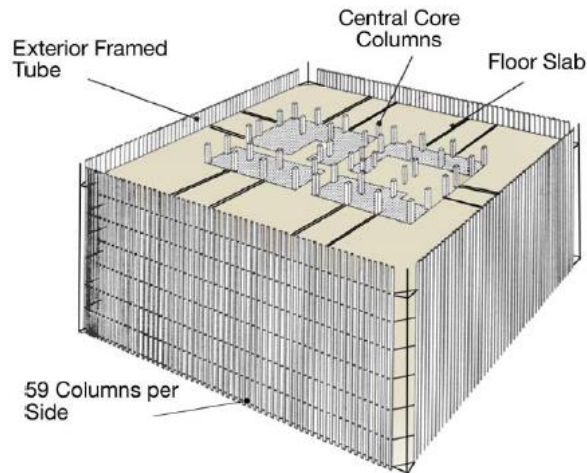


Figure I.2: Structure of the World Trade Center twin towers (source: <https://www.nist.gov/>).

The impact of the aircraft damaged key structural components such as perimeter and core columns, as well as floor slabs. Most of the thermal insulation of the remaining members within the affected area was also destroyed. Although the structure was designed to sustain aircraft impact, the ensuing intense fire that spread over several floors degraded critical load-bearing components in the affected area. Subsequently, the failure propagated under the effect of collision with the lower parts until the total collapse as shown in Figure I.3.



(a) Initial damaged structures
(Photo credit: Dackel
Princess/CC BY-SA 2.0)

(b) Progressive collapse (Photo credit:
Thomas Nilsson)

(c) Total collapse (Photo credit:
Eric J. Tilford)

Figure I.3: Collapse of the World Trade Center twin towers.

Following this event the public opinion grew alarmed, which led to the intensification of research studies to introduce novel instructions and provisions in the codes of construction and structural design. This is shown by the number of published records (Web of Science

extraction in the category “civil engineering”) explicitly including the topics “robustness” (Figure I.4-a) or “progressive collapse (Figure I.4-b) in the document title, abstract or list of keywords. One shows the growing interest of the scientific community to study the problematic issues related to the structural robustness. Many of studies have been funded and released on structural robustness, exceptional actions and progressive collapse issues.

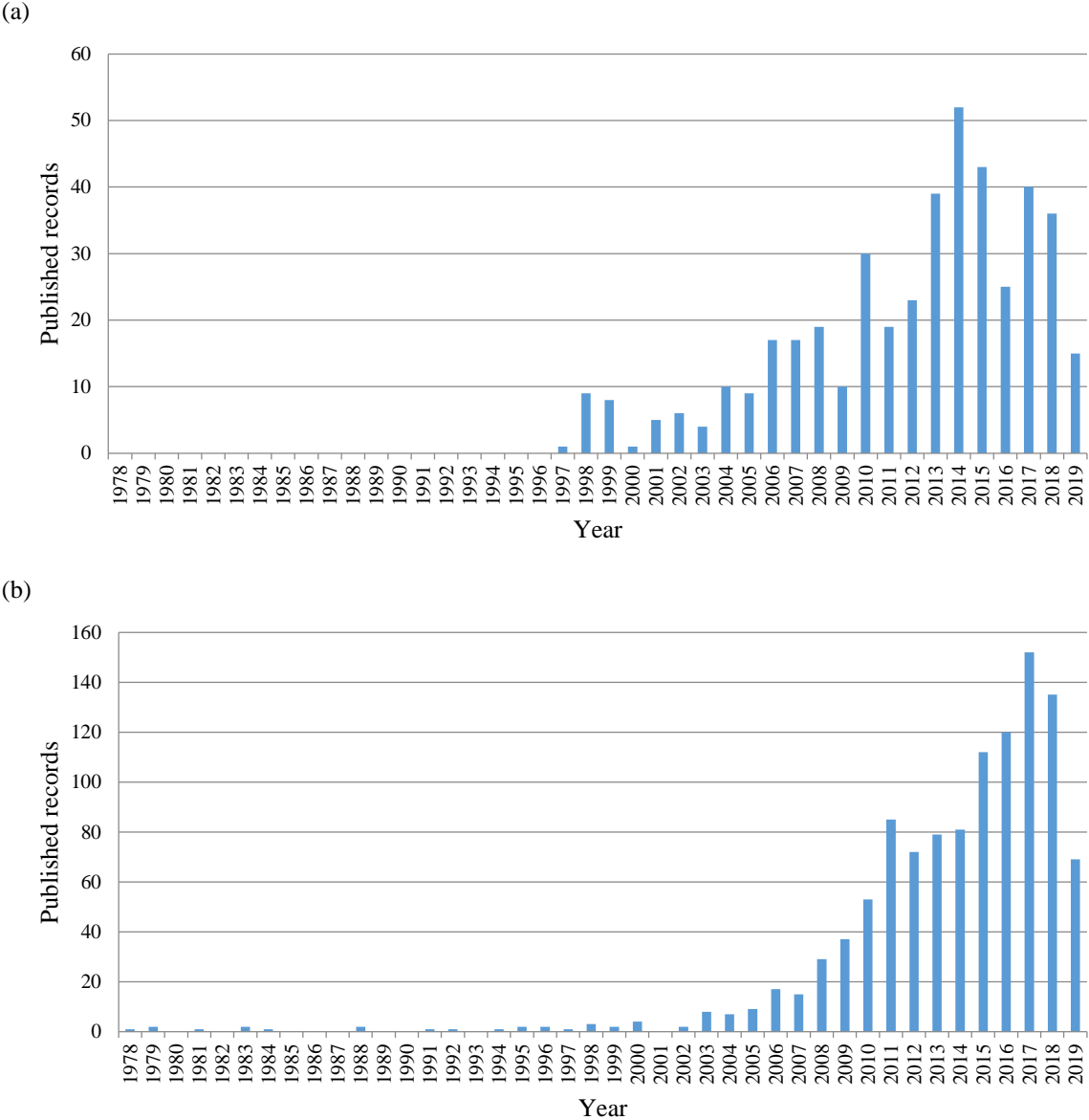


Figure I.4: Yearly published records in Web of Science (collection data extracted in June 2019 in civil engineering category) for topics (a) “robustness” and (b) “progressive collapse”.

Other major catastrophic structural collapses can be mentioned such as the one of the I-35W bridge in Minneapolis, United States of America, on the 1st of August 2007. The probable cause of this collapse, according to the report of (NTSB, 2008), was the design error of the gusset plates at some nodes.

In August 2018, a 200-meter section of the cable-stayed Genoa Bridge collapsed in Italy (Figure I.5), which caused the death of 43 people who were crossing the bridge at that time. This cable stayed bridge was characterized by a prestressed concrete structure for the piers, pylons and deck and a hybrid system for the stays constructed from steel cables with prestressed concrete shells poured on. There were two stays per span for this bridge whereas modern cable-stayed bridges usually adopt multi-cable arrays, which offer alternative load paths in case one cable capacity is lost. Why exactly the bridge collapsed is yet to be understood and this dramatic event led to a broad controversy in public opinion about the safety of the civil engineering structures. It made clear the priority of robustness in any structure to face time-related deterioration and increased loading conditions.



Figure I.5: Collapse of Genoa Bridge (Photo credit: Scatto di Salvatore Fabrizio/CC BY-SA 4.0).

Recently, the incident of the fire that broke out beneath the roof of Notre-Dame Cathedral in Paris (Figure I.6) on April 15, 2019 is an example of the risks that threaten historical structures. Even if the action did not affect critical structural elements and the consequences remained confined on the roof, this event reminded the vulnerability of historical structures under the occurrence of exceptional actions.



Figure I.6: Notre-Dame de Paris cathedral fire (Photo credit: Godefroy Troude /CC BY-SA 4.0).

I.2 ISSUES WITH STRUCTURAL ROBUSTNESS

Design of structures against unidentified actions is a controversial topic, especially for the engineering community considering the unknown aspects of the initial cause of damage, and as the worth of structural robustness issues was recognised mainly after catastrophic events where structural progressive collapse occurred.

In practice, civil engineers have several factors to deal with at the design stage, among which serviceability, structural safety and cost of construction, the goal being to ensure adequate serviceability/safety levels while minimizing construction costs. The standards and codes of civil engineering provide rules and guidelines for structural design to check (i) the serviceability limit states concerning the comfort of people and the functioning of the structure under normal conditions while maintaining the appearance of the structure, and (ii) ultimate limit states, linked with the safety of people, under abnormal conditions. Some accidental actions are then taken into account, such as for example the seismic actions or explosions (NF EN 1990, 2003). These actions have a very low probability of occurrence, and can lead to a high level of consequences, where huge human and financial losses are expected.

During its service life, a structure might not be able to resist some actions, if these actions were not considered at the design stage, or for example in case of advanced degradation of structural components. An event might lead to a local failure with a partial collapse of some structural elements that can propagate and cause the failure of other components in the structure. The extent of failure propagation depends on the magnitude of the local failure, and the capacity of the structure to prevent or to mitigate this propagation.

Demonceau (2008) and Huvelle (2011) distinguish the concepts of accidental and exceptional events. The accidental actions refer to the fully identified actions that are taken into account in the structural design (type of loading is identified, as well as the maximum amplitude of action). Conversely, exceptional actions are supposed not to be taken into account in the structural design. The reason of ignoring can be that the nature of action is unknown during design due to a knowledge gap, which is the case of black swan events (Nafday, 2011). Also, the nature of the exceptional action might be identified, but the intensity could go beyond the expected magnitude. Similar concepts of accidental and exceptional actions are also presented in other terms by referring to identified and unidentified accidental actions (NF EN 1991-1-7, 2007).

One main issue is to assess the structural response against the action, which relates to the final state of failure compared to the local failure. This evaluation allows assessing the propagation of the failure, and investigating whether the collapse is disproportionate or not to the local failure. As illustration, the collapse of Saint-Étienne River Bridge (allowing a

strategic connection in the La Réunion Island) in France in March 2007 is an example of structural collapse of a bridge under some extreme natural event (Sétra, 2013). Following the cyclone Gamède there was a soil scouring under one of the piers, which led to the failure of this pier. Subsequently, the thirteen bays of the bridge collapsed, as shown in Figure I.7. This example clearly represents the successive failures from the local failure of one pier that propagates and causes a disproportionate collapse of the structure.



Figure I.7: Collapse of Saint-Étienne River Bridge (Photo credit: Jacques Mossot).

Conversely, some structures succeed to resist some exceptional scenarios and prevent a propagation of failure until collapse. As an example, 18-wheeler truck crashed into a column of the I-10 Bridge on June 2018, in Houston, United States of America. This collision caused a significant damage for the column, where it almost totally failed as shown in Figure I.8. This structure succeeded to redistribute the forces in the remaining structural components following the collision, which helped the structure to prevent the propagation of the collapse.



Figure I.8: I-10 bridge collision (source: <https://www.aggregatetechnologies.com/>).

Increasing the capacity of the structure to withstand exceptional actions and develop alternative load paths is then a crucial point for robustness purpose. The roof of the Hubert H.

Humphrey Metrodome, which is a sport stadium located in downtown Minneapolis (United States of America), damaged under the weight of snow accumulated during a heavy snow storm on December 12, 2010. The roof consisted of an inflatable dome, where after a large deflection under the excessive snow load the structure succeeded to find an alternative load path by developing a membrane action as shown in Figure I.9. The structure managed to resist through the cables of the roof that had the required ductility to allow the large deformation without rupture, and the anchorage of the roof with the structure that supported the redistribution of the forces. This example shows the importance of developing an alternative load path to limit the consequences of an exceptional action, especially for critical structures.



(a) Before collapse



(b) After collapse

Figure I.9: Hubert H. Humphrey Metrodome roof collapse (Photo credit: Bobak Ha'Eri/CC-BY-SA-3.0).

It is worth mentioning that there is no consensus yet on a methodology to quantify structural robustness. There are different points of view on the structural requirements under local failure, and the types of scenarios that have to be studied when assessing the robustness. Furthermore, the structural response modelling under progressive collapse is considered as a complex phenomenon, where one may encounter numerical convergence issues, as well as the large computational cost especially to investigate a large number of scenarios.

I.3 ORGANIZATION OF THE DISSERTATION

The aim of structural robustness is to improve the performance of structures against progressive collapse, even under conditions that were not considered at the design stage. It should be made clear that the purpose of structural robustness is not to protect the structure of any kind of actions, whatever their magnitude, but rather to prevent a local failure, resulting from an unexpected action, to spread and lead to a disproportionate failure. Developed concepts should help the structural engineer to find the critical zones of the structure, and then to make appropriate decisions to improve its ability to prevent the progressive collapse. In this regard, this research work aims to propose a framework to analyze the structural robustness and the propagation of failure in a structure. The goal is to introduce quantitative measures of structural robustness against accidental or exceptional actions, by modelling with a sufficient accuracy the structural response under progressive collapse.

The following chapters of the manuscript are divided as follows:

Chapter II presents a review of the main aspects concerning structural robustness, where the scientific and technical challenges are discussed with the different definitions of robustness found in the literature. The design approaches proposed by the normative community are presented with a comparison between some international codes. The research activities are detailed along the following main axes: first the deterministic and probabilistic indices proposed for structural robustness quantification, second the analytical and numerical methods used to model the structural response under an exceptional event, and third the experimental characterization of alternative load paths, using properties of materials (ductility) and redundancy. Further, this chapter identifies some remaining issues and introduces the philosophy of the proposed strategy to be described in the later chapters.

Chapter III introduces the yield design theory which is used to identify the ultimate state of a structure under loading. The static and the kinematic approaches are described as well as the numerical modelling of the yield design approach used in the subsequent steps of the analysis. Considering the infinitesimal strain assumption of the yield design theory, an iterative coupling between the yield design approach and a non-linear analysis of the directly affected part is proposed to model progressive collapse within the structure, also taking into account development of materials and geometrical non-linearities. This coupling strategy is applied to some case studies such as steel elements and steel frame structures for illustration.

Chapter IV uses this structural modelling for the purpose of robustness quantification. Some indices are proposed among which the so-called Robustness Propagation Failure Index (*RPMI*), which aims to identify the structural capacity to prevent the propagation of the failure, and the Robustness Energy Index (*REI*), which identifies the critical level of local

failure that can lead to some unacceptable consequences. These indices can be used separately or both together to provide a combined measure of the initial scenario and the extent of failure propagation through the structure (identification of scenarios with minimum initial magnitude and maximum propagation extent). The steel framed building introduced in Chapter III is considered to investigate the ability of the approach to investigate a large number of scenarios, identify the most critical ones and be used when comparing several strengthening options.

Chapter V illustrates the sensitivity of the proposed approach to some factors or parameters among which the load combination and dynamic amplification factor, the structural geometry or the materials ductility. The corresponding effects are illustrated each time with the steel frame structure introduced in Chapter III. This chapter concludes with a discussion on the assumptions considered in this approach and the need for further research work.

In Chapter VI, the general conclusions of the thesis are drawn and recommendations for future investigations are provided.

CHAPTER II

CONCEPT OF STRUCTURAL ROBUSTNESS

II.1 INTRODUCTION

Design against accidental actions aims to ensure an adequate level of structural safety to prevent structural failures and associated consequences. When dealing with exceptional unidentified events, with a high uncertainty about the type, the magnitude and the loading mode of the action, it is quite challenging to refer to an appropriate level of structural safety.

This chapter identifies first some scientific and technical challenges related to the concept of structural robustness. Then, one details major approaches dealing with robustness: those adopted by the engineering community, and those proposed by the scientific community. Finally, one concludes by identifying some improvement needs which motivate the approach proposed in this dissertation.

II.1.1 The difficulty of dealing with unidentified actions

The quantification of structural robustness includes the assessment of structural resistance against different types of abnormal scenarios. These scenarios can be classified into two categories: dependent, and independent scenarios (Arup, 2011). The application of a dependent scenario means that the hazard event or the abnormal condition is fulfilled identified (type, intensity and location). Furthermore, the analysis involves the modelling of the effect of the scenario on the structure, the resulting damage that could result, and the propagation of the failure. Otherwise, the independent scenarios refer only to a local failure scenario without considering the associated hazard. The use of independent scenarios is a commonly adopted approach, where one assesses the capacity of the structure to withstand the propagation of failure without explicitly modelling the cause of the local failure (Kunnath et al., 2018).

II.1.2 A multi-aspect problem

The structural resistance against abnormal actions depends on several factors, which are related to the structural characteristics and the structural behaviour. In the case of progressive collapse, many aspects may influence the structural response such as geometrical and material non-linearities, dynamic effects, and the propagation of failure.

II.1.2.1 Non-linear material behaviour

The material behaviour of a structure under normal conditions is supposed to be linear, where the stresses and strains are in the elastic range. However, under ultimate conditions, the stresses on some elements may exceed their elastic load capacity and undergo plastic yielding (Janssens, 2012). In this case, the inelastic behaviour of material can lead after a certain inelastic strain to a degradation of the material characteristics or even to its rupture. Also, one points out the crucial role of the ductility of materials, meaning the ability of a material to sustain plastic strains without rupture. The ductile material provides the ductility of elements, which allows large deformations without failure (Droogné et al., 2016). Consequently, the ductility contributes to develop multiple load paths and to dissipate the energy resulting from the action or the local failure (AlHafian, 2013). Besides, the strain hardening of materials, e.g. the strengthening of a metal under the effect of its plastic deformation, provides a strength reserve after yielding (Knoll and Vogel, 2009).

II.1.2.2 Geometrical non-linearities

The response of a structure under an exceptional action can lead to geometrical changes, where large rotations and displacements can exist. The geometrical changes lead to a modification in the forces redistribution on the structure (AlHafian, 2013). Furthermore, the geometrical changes can have a negative effect on the resistance capacity of structure, where the capacity to support applied loads decreases with the geometrical change such as P- Δ effect (Scholz, 1990; Babazadeh et al., 2016). The geometrical changes can also have a positive effect, where the capacity to support applied loads increases after a large geometrical deformation, such as the catenary effects in both beams and slabs (Botte et al., 2014).

II.1.2.3 Alternative equilibrium state

The capacity of the structure to find an alternative equilibrium state after the damage occurrence is an important aspect of structural resistance, where it allows to stop the propagation of the failure, thus limiting its consequences. The redundancy of the structure

plays a main role to develop an alternative equilibrium state by redistributing the forces due to applied loads, on all constituent elements (Mohammadkhani-Shali, 2007). Hence, it is associated with the ability of the structural system to provide multiple load paths, which allows to withstand the applied loads in case of failure of some elements by redistributing the efforts to the rest of the structure.

The alternative equilibrium state is also related to the ability of a damaged structure to develop a second line of defence, which is a mechanism with an alternative structural functioning developed after a large displacement (Knoll and Vogel, 2009). This alternative functioning enables to increase the structural capacity to resist the applied loads. The compressive membrane and the tensile membrane actions can be considered as a second line of defence. Figure II.1 presents typical load-deflection curves of an unrestrained and a fully restrained concrete slab, where it shows the development of a compressive membrane action in the restrained slab, due to the compressive forces that increase the bending strength of beams. Furthermore, the large deflection can change the redistribution of efforts in beams, where the moment efforts decrease, while the tensile efforts increase, thus allowing to a supplemental resistance through formation of the catenary configuration in case beams are unable to resist the applied loads through flexural action alone (Botte et al., 2014).

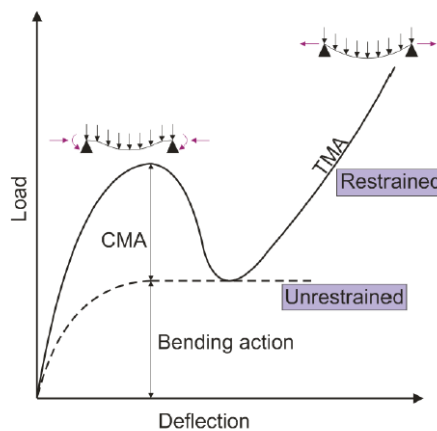


Figure II.1: Compressive membrane (CMA) and tensile membrane (TMA) actions in a fully restrained concrete slab (Botte et al., 2014).

If an alternative equilibrium state cannot be developed or it is insufficient, the segmentation of the structure can be an efficient strategy to stop the propagation of failure. Hence, the structure is segmented by dedicated segment borders that are able to block the propagation of failure. This strategy allows to isolate and to limit the failure in a segment, thus preventing propagation of failure to other segments (fib bulletin 82, 2017).

II.1.2.4 Dynamic effects

The dynamic effects can result from the accidental action applied on the structure, in the case of a threat dependent scenario (Hoffmann et al., 2015; Korndorfer et al., 2015). In the case of a threat-independent scenario, the sudden removal of a structural component releases significant internal energy that disturbs the initial load equilibrium of external loads and internal forces, where the additional load redistributed to adjacent members upon the loss of the structural component is suddenly applied (Janssens, 2012).

The non-linear dynamic analysis is considered as the most theoretically rigorous and accurate method to simulate progressive collapse (Arup, 2011). However, this method is very time-consuming and vulnerable to non-convergence issues (Kunnath et al., 2018).

In order to avoid some dynamic analysis, the Eurocodes (NF EN 1990, 2003) propose that the non-linear dynamic response can be estimated by using the non-linear static analysis and amplifying the gravity loading with a dynamic amplification factor. This strategy is also presented in other international codes such as UFC 4-023-03 (2009), and GSA (2013).

Furthermore, (Izzuddin et al., 2008) proposed an energy-based approximate procedure for the analysis of a sudden column loss in building structures, which enables to define the pseudo-static response. This method proposes a three-step dynamic assessment of the structural response with avoiding a heavy non-linear dynamic analysis: (i) determination of the nonlinear static response under gravity loading using a detailed finite element or a simplified analytical model, (ii) dynamic assessment using a simplified energy-equivalence approach coupled with the nonlinear static response that allows obtaining the maximum dynamic displacement, and (iii) ductility assessment of the connections.

II.1.2.5 Debris loading

It is worth noting that the debris loading is an important aspect of the progressive collapse. There is no current guidance to take into account this type of loading, that may have dynamic effects caused by the collision between falling debris and other structural components (Tagel-Din, 2009; Arup, 2011). Modelling debris is complex, especially in the models based on continuum mechanics such as Finite Element models, where the difficulties lie in the simulation of the elements separation from each other, the formation and movement of debris during progressive collapse, and the debris collision.

II.1.3 Disparity of definitions between research and normative communities

The term "robustness" is used in several sectors, and its definition also differs according to the field of application, which can cause some confusion. Figure II.2 shows the number of published documents in the Web of Science database categories related to the topic robustness. A total of 194,792 records (including articles, proceeding papers, book chapters among others) can be found, which shows the variety of domains in which the term robustness appears.

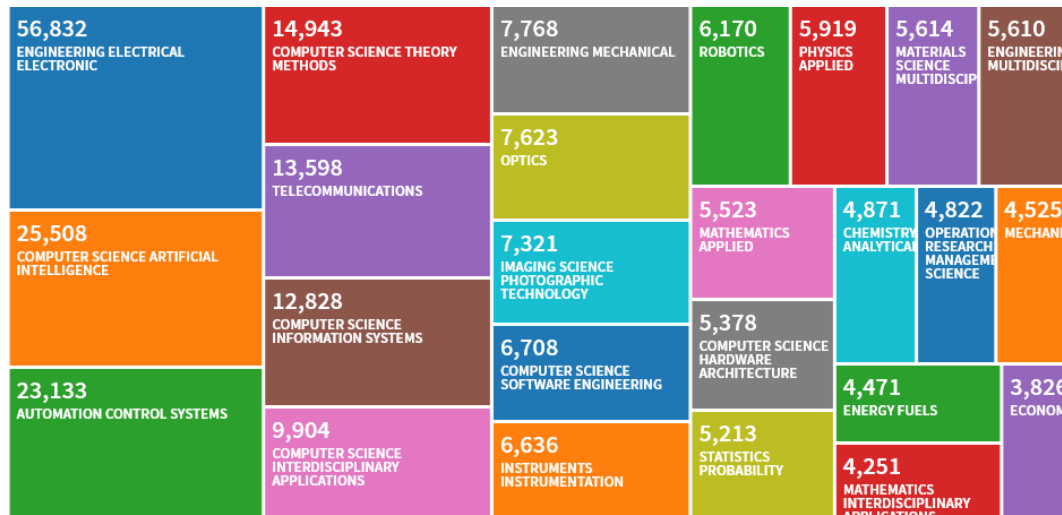


Figure II.2: Records for topic “robustness” in Web of Science (collection data extracted in June 2019).

Table II.1 shows some definitions in several domains, relating either to the performance under an abnormal situation in terms of limiting the consequences, or to the insensitivity of systems to variable factors.

Software Engineering	Robustness is the ability of software systems to react appropriately to abnormal conditions (Meyer, 1997).
Quality Control & Product Development	The state where the technology, product, or process performance is minimally sensitive to factors causing variability (either in manufacturing or user’s environment) and aging at the lowest manufacturing cost (Taguchi and Chowdhury, 1999).
Ecosystems	The capacity of a system to maintain a desired state despite fluctuations in the behaviour of its component parts or its environment (Carlson and Doyle, 2002; Anderies et al., 2004).
Control Systems	The degree to which a system is insensitive to effects which are not considered in the design, such as disturbances, measurement noise, unmodeled dynamics, etc. The system should be able to withstand these neglected effects when

	performing the tasks of interest (Slotine et Li, 1991).
Statistics	A robust statistical technique is insensitive against small deviations in the assumptions (Huber, 1996; Huber and Ronchetti, 2009).
Design Optimization	A robust solution in an optimization problem is one that has the best performance under its worst case (max-min rule) (Kouvelis and Yu, 1997).
Bayesian Decision Making	By introducing a wide class of priors and loss functions, the elements of subjectivity and sensitivity to a narrow class of choices, are both reduced (Insua and Ruggeri, 2000).
Language	The robustness of language is a measure of the ability of human speakers to communicate despite incomplete information, ambiguity, and the constant element of surprise (Briscoe, 1997).

Table II.1: Several associated definitions of "robustness" in different fields (Faber et al., 2006).

In the civil engineering field, there is no consensus on a single definition of "structural robustness". Several definitions of structural robustness can be found in design standards (see Table II.2) and reflect the view of engineering community, where one can identify two main points :

- the situation that the structure is facing is an action that leads to a localised failure in the structure, where the local failure is the part of structure that is assumed to have collapsed, or been severely disabled, by the accidental event (NF EN 1991-1-7, 2007) ;
- the local failure should not propagate disproportionately.

NF EN 1991-1-7 (2007)	The ability of a structure to withstand events like fire, explosions, impact or the consequences of human error, without being damaged to an extent disproportionate to the original cause.
The building regulations 2010 (DCLG, 2013)	The building shall be constructed so that in the event of an accident the building will not suffer collapse to an extent disproportionate to the cause.
GSA guidelines (2003)	The ability of a structure or structural components to resist damage without premature and/or brittle failure due to events like explosions, impacts, fire or consequences of human error, due to its vigorous strength and toughness.
American	Strength and stability shall be checked to ensure that structures are

Society of Civil Engineers (ASCE, 2016)	capable of withstanding the effects of extraordinary (i.e., low-probability) events, such as fires, explosions, and vehicular impact without disproportionate collapse.
---	---

Table II.2: Definitions of structural robustness in some design standards.

One may distinguish the concepts of progressive collapse and disproportionate collapse. Progressive collapse initiates with a localised damage to a single or a few structural components and develops throughout the structural system, affecting other components. Disproportionate collapse relates to a judgement on consequences in the final configuration, which may involve a major part or the whole structural system, characterised by a disproportion in size compared to the original event or its resulting local failure (Adam et al., 2018). Hence, the disproportion aspect is linked with the amount of consequences in the final stage of failure propagation. Thus, the progressive collapse can be disproportionate or not based on the comparison between the initial damage extent and the final state of the structure.

In parallel, the research community has worked on the development of structural robustness concepts, with a view to develop methods and approaches that allow to improve and to assess the resistance of structures against exceptional actions and avoid the catastrophic collapses. There is a need to determine precisely the definition and objectives of structural robustness to avoid the overdesign of structures and optimize the project cost, also ensuring adequate structural safety levels.

The different definitions of structural robustness provided by the scientific community (see Table II.3) present the various existing points of view. Some studies define structural robustness as the insensitivity of a structure to a local damage, by perfectly resisting to some local failure without any propagation. Damage or collapse of components other than those directly affected is then unacceptable (Vrouwenvelder, 2008; Starossek and Haberland, 2010; Arup, 2011). Others mention that the ability of damaged structural components experiencing large displacements to develop a second line of defence without collapse is favorable (Brett and Lu, 2013; Huvelle et al., 2015). Some research works accept partial collapse provided that it is not disproportionate with respect to the local failure (Faber, 2007; Bontempi et al., 2007; Agarwal and England, 2008; Biondini et al., 2008; fib, 2012; Droigné et al., 2018).

Furthermore, COST Action TU0601 (2011) mentions that the structural robustness aims to provide a sufficient resistance of structures to survive to a damage, where some studies recommend that the damage can be the loss of one of the critical structural elements (Sétra, 2013; fib, 2012). Ghosn et al. (2016) mention that the initial damage can include several main structural components, provided that the structure ensures the safe evacuation of its users or occupants after the damage. Moreover, JCSS (2008) acknowledges that the structural robustness depends not only on the structural properties (e.g. strength, ductility,

redundancy, continuity), but also on the risk of failure and the probability of occurrence of the event.

The evaluation of consequences in some studies is related to the direct and indirect economic consequences (COST Action TU0601, 2011; Joint Committee of Structural Safety (JCSS), 2008; Sétra, 2013), whereas it can be simply related to the sum of the affected area in other frameworks (Haberland, 2007a). Besides, the research works have mainly focused on the investigation of accidental or exceptional events, while Cavaco et al. (2018) mention that the structural robustness is also related to the ageing and deteriorating scenarios where damage develops gradually in time.

Faber (2007)	The ability of a considered system to sustain a given damage state subject to the prevailing exposure conditions and thereby limit the consequences of exposure events to the direct consequences.
Bontempi et al. (2007)	The robustness of a structure, intended as its ability not to suffer disproportionate damage as a result of limited initial failure, is an intrinsic requirement, inherent to the structural system organization.
Agarwal and England (2008)	The ability of a structure to avoid disproportionate consequences in relation to the initial damage.
Vrouwenvelder (2008)	The notion of robustness is that a structure should not be too sensitive to local damage, whatever the source of damage.
Biondini et al. (2008)	Structural robustness can be viewed as the ability of the system to suffer an amount of damage not disproportionate with respect to the causes of the damage itself.
Knoll and Vogel (2009)	The property of systems that enables them to survive unforeseen or unusual circumstances.
Starossek and Haberland (2010)	The insensitivity of a structure to initial damage. A structure is robust if an initial damage does not lead to disproportionate collapse.
Brett and Lu (2013)	The ability of a structure in withstanding an abnormal event involving a localized failure with limited levels of consequences, or simply structural damage.
Huvelle et al. (2015)	The ability of a structure to remain globally stable in case of exceptional event leading to local damage.
Ghosn et al. (2016)	The ability of a structure to carry service loads to assure the safe evacuation of its users or occupants after one or several main structural components are damaged.

Droogné et al. (2018)	Ability to avoid disproportional damage and progressive collapse.
Cavaco et al. (2018)	The robustness is an intrinsic structural property for a defined loading scenario and performance indicator, both independent of time and environmental conditions.
JCSS (2008)	The robustness of a system is defined as the ratio between the direct risks and the total risks (total risks is equal to the sum of direct and indirect risks), for a specified time frame and considering all relevant exposure events and all relevant damage states for the constituents of the system.
COST Action TU0601 (2011)	The attitude of a system to survive to a damage.
Arup (2011)	Quality in a structure of insensitivity to local failure, in which modest damage (whether due to accidental or malicious action) causes only a similarly modest change in the structural behaviour.
International Federation for Structural Concrete (fib, 2012)	It should be avoided with adequate reliability that accidental and/or exceptional events, or failure of a structural component, cause disproportional damage of a large part of the structure or even total collapse of the whole structure.
Sétra (2013)	The capacity of a structure to resist actions despite the loss of one of these critical structural elements.

Table II.3: Definitions of structural robustness in literature.

II.2 ENGINEERING APPROACH

Currently, the principle of structural robustness exists in several international codes. The evolution of these codes has been usually triggered after significant catastrophic events, which led to a revision in the principles of structural engineering.

The Ronan Point collapse in Newham (United Kingdom) in 1968 drew attention to the importance of structural robustness and to protect structures from progressive collapse (Pearson and Delatte, 2005). Hence, as a consequence of this collapse, a first effort of research in structural robustness was initiated and provisions for structural robustness of building structures were introduced in the "UK Building (fifth Amendment) Regulations 1970" (Minister of Housing and Local Government, 1970). These provisions and recommendations are slightly developed in the current UK code "the Approved Document A of the Building Regulations" (Department of Communities and Local Government, 2013), which states that "the building shall be constructed so that in the event of an accident the

building will not suffer collapse to an extent disproportionate to the cause". The Eurocodes are generally adopting the UK approach given in the "Approved Document A of the Building Regulations", but in addition a risk-based approach was adopted to evaluate the risk of accidental actions on structures (EN 1990, 2003; NF EN 1991-1-7, 2007).

The Eurocodes document NF EN 1990 presents the main principles for the realization of robust structures, and NF EN 1991-1-7 defines the term of structural robustness and provides the main strategies and recommendations of design to ensure the robustness of structures as shown in Figure II.3. The Eurocodes (NF EN 1991-1-7) divide the accidental actions into two categories: identified, and unidentified actions. On the one hand, the type and notional values of the identified accidental actions are determined, and the structure should be designed to resist these actions. On the other hand, in the case of the unidentified accidental actions, where the potential failure of the structure arising from an unspecified cause, the Eurocodes require that the failure shall be mitigated.

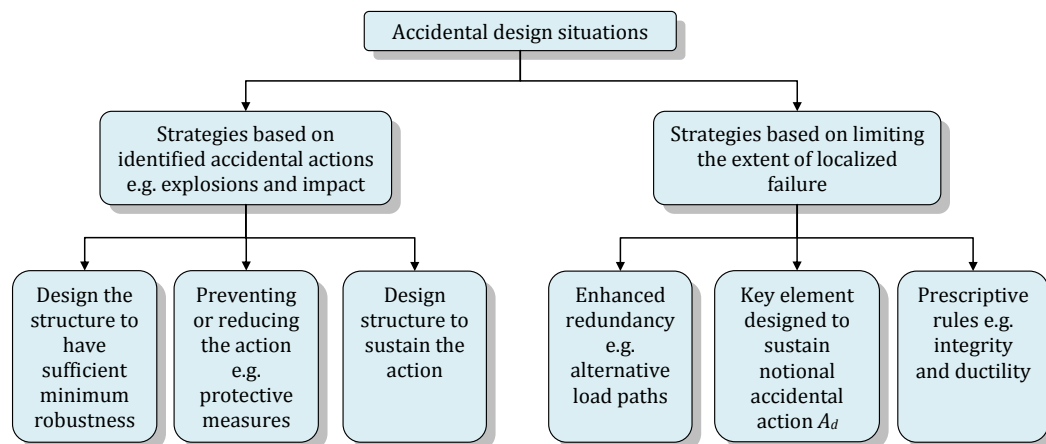


Figure II.3: Strategies for accidental design situations (NF EN 1991-1-7, 2007).

Furthermore, the Eurocodes (NF EN 1991-1-7, 2007) mention that the recommended strategies and methods to improve the structural robustness depend on the degree of safety needed, where the structures are classified in three categories based on the consequences of the failure:

- CC1 (low consequences of failure): there are no specific considerations to take into account;
- CC2 (medium consequences of failure): this category of structures requires a simplified analysis where static equivalent action models or prescriptive rules may be applied (redundancy, ductility, etc...);
- CC3 (high consequences of failure): for this category, it is necessary to carry out an in-depth analysis of the failure scenarios in the context of a risk analysis for example,

and to use refined methods that permit to take into account the dynamic effect, the non-linearities and the interaction between the load and the structure.

Besides, the Eurocodes (NF EN 1991-1-7, 2007) mention that a localised failure may be accepted, if it does not endanger the stability of the structure, and if the overall load-bearing of the structure is maintained and allows the necessary emergency measures to be taken.

Four groups of design approaches can be found in the international codes that aim to improve the structural robustness for buildings :

- tying method,
- alternative load path (ALP) method,
- specific local resistance design method,
- risk-based assessment method.

Table II.4 summarizes these methods in some international codes and standards. One can note that the most widely recognized approaches are the tying rules, the alternative load path (ALP) methods and local resistance methods.

Area	Code	Tying	ALP	Local resistance	Risk-based
Europe	EN 1991-1-7	+	+	+	+
United Kingdom	The building regulations 2010	+	+	+	~
United States of America	ASCE/SEI 7-16	+	+	+	~
	NYC BC 2014	-	+	+	~
	IBC 2009	+	-	-	-
	UFC 4-023-03	+	+	+	~
	GSA 2013	-	+	-	~
China	CECS 392:2014	+	+	+	-
Canada	NBCC 1995	+	+	+	~
Australia	NCC 2016	-	+	+	+

(+) method considered, (-) method not considered, (~) method implicitly considered

Table II.4: Structural robustness design methods considered by the international codes (Adam et al., 2018).

The tying method is considered as an indirect design approach, since it is an implicit provision of resistance to progressive collapse by providing minimum levels of strength, continuity and ductility. The alternative load path (ALP) method and the local resistance method are considered as direct design approaches, since they are implemented through performance-based methods using specific design criteria and explicit structural analysis. The

risk-based methods are explicitly considered by the Eurocodes and the Australian code, but they are implicitly considered by several codes and standards (Table II.4).

II.2.1 Tying method

This method recommends to provide effective tying of the frame building in both horizontal and vertical directions, as shown in Figure II.4, where one identifies minimum requirements of tying strength and ductility. These tying rules contribute to provide a continuity between the structural members, and improve the redundancy of the structure, and the capacity to develop alternative load paths when there is a local damage to the structure. However, these prescriptive rules represent instructions of required tying forces without identifying quantitatively the effectiveness of these provisions to increase the resistance of the structure. Thus it is an indirect design approach.

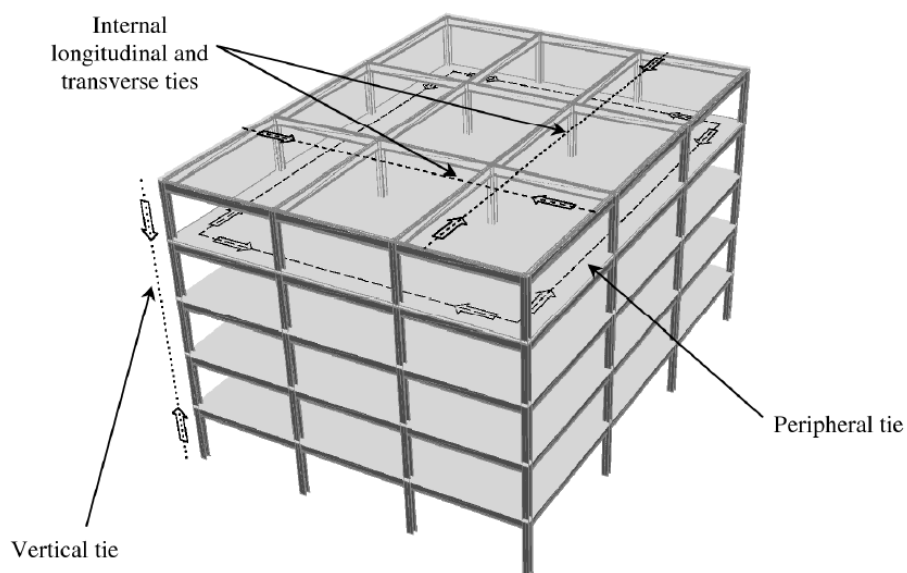


Figure II.4: Structural tying of framed building (Stylianidis, 2011).

The Eurocodes (NF EN 1991-1-7, 2007) recommend that the horizontal ties in a framed structure should be designed to sustain the following tensile forces:

- for internal ties: $T_i = 0.8(g_k + \psi q_k)sL$ or 75 kN , whichever is the greater; (II.1)

- for perimeter ties: $T_p = 0.4(g_k + \psi q_k)sL$ or 75 kN , whichever is the greater. (II.2)

where g_k is the permanent action, q_k is the variable action, s is the spacing of ties, L is the span of the tie, and ψ is the relevant factor in the expression for combination of action effects for the accidental design situation. For the vertical ties, the Eurocodes (NF EN 1991-1-7, 2007) mention that the structure should be tied continuously from the foundations to the roof level without determination of a tensile force threshold.

II.2.2 Alternative load path method

This method aims to ensure that the structure has a sufficient capacity to resist the loss of one of its components, usually a column as shown in Figure II.5. Hence, it enables to check if the redundancy and the continuity of the structure are able to redistribute the forces in an efficient manner, also if the directly affected elements have sufficient ductility that allow large deformations without rupture. This method has the advantage of being threat-independent, where the notional remove of an element represents the consequences of an abnormal event without explicit consideration of this event.

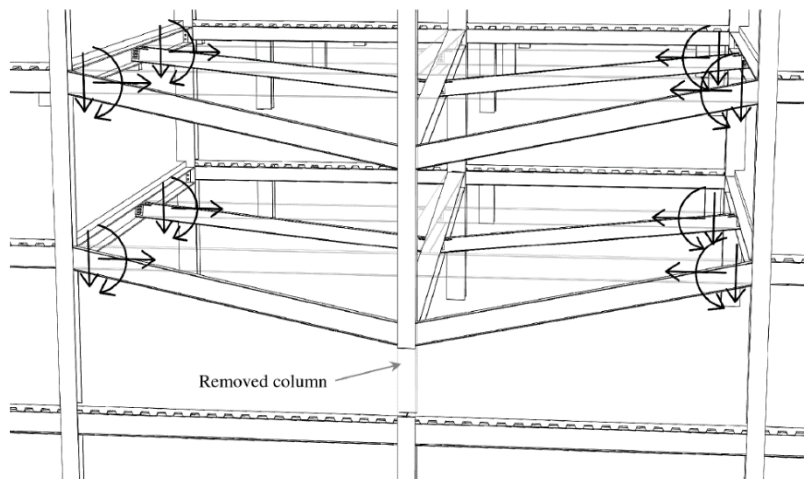


Figure II.5: Alternative load path method (Stylianidis, 2011).

II.2.3 Local resistance design method

In some cases, the loss of a specific element may lead to undesirable consequences or it is likely to be more prone to accidental actions, where the appropriate solution is to protect this element or to be strengthened as there is no capability or it is too costly to provide alternative load paths. The protection of elements can be achieved by use of protective devices like the fender system for bridge pier protection against vessel collision as shown in Figure II.6. Furthermore, the element can be considered as a key element to be designed to sustain an accidental design action.



Figure II.6: Fender system for bridge pier protection (source: <https://www.compositeadvantage.com>).

II.2.4 Risk-based assessment method

The Eurocodes NF EN 1991-1-7 (Annex B) give explicit guidance on the application of risk assessment in terms of the decision making process, where Figure II.7 represents the general overview of a five step risk analysis.

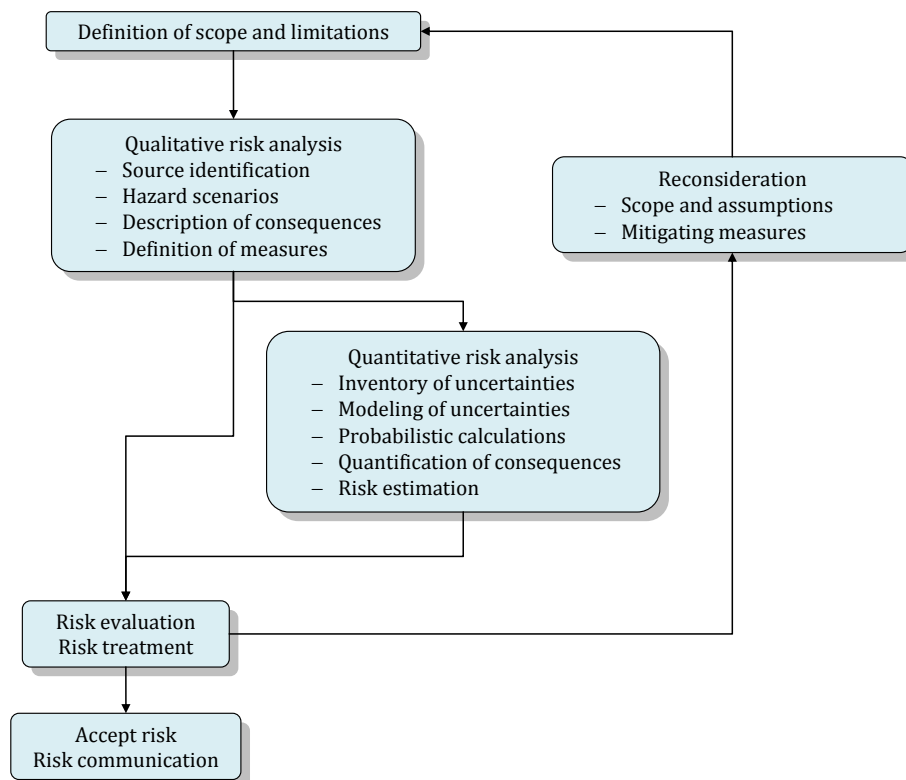


Figure II.7: Overview of risk analysis (NF EN 1991-1-7, 2007).

First, one defines the structural system, and all matters related to the use of the structure. Second, one identifies all hazards and corresponding hazard scenarios, also with related consequences. The probabilities of hazard scenarios and related consequences, identified beforehand, are then estimated, by taking into account associated uncertainties. The evaluation of the risk acceptance is usually based on the principle of ALARP (as low as reasonably practicable), where there are two bounds of risk: the upper tolerability limit and the lower tolerability limit (Arup, 2011). In case the risk is below the lower bound, no measures need to be taken, while if it is above the upper bound the risk is considered as unacceptable. Moreover, in case the risk is between the upper and lower bound an economical optimal solution should be sought. The risk acceptance levels are usually specified based on two criteria: the individual acceptable level of risk and the socially acceptable level of risk. The mitigation measures can be by elimination, reducing or controlling the hazard.

Furthermore, the Eurocodes (NF EN 1991-1-7, 2007) propose an index to evaluate the risk of structures subject to accidental actions, as defined below :

$$RI_I = \sum_{i=1}^{N_H} P(H_i) \sum_{j=1}^{N_D} \sum_{k=1}^{N_S} P(D_j|H_i) P(S_k|D_j) C(S_k) \quad (\text{II.3})$$

where, N_H is the number of the different hazards H_i applied on the structure, N_D represents the different ways of damage D_j that can occur, N_S represents the number of adverse states S_k that can be described as the performance of the damaged structure with corresponding consequences $C(S_k)$, $P(H_i)$ is the probability of occurrence of the i^{th} hazard, $P(D_j|H_i)$ is the conditional probability of the j^{th} damage state of the structure given the i^{th} hazard, and $P(S_k|D_j)$ is the conditional probability of the k^{th} adverse overall structural performance given the j^{th} damage state.

II.3 SCIENTIFIC COMMUNITY APPROACHES

The research works on structural robustness focus on several aspects among which one can cite the three following ones: (i) the quantification of structural robustness, (ii) the modelling of progressive collapse, and (iii) the experimental tests close or above ultimate limits. In order to optimize and develop structural design including structural robustness concepts, a qualitative approach is found to be insufficient, because of its inability to assess the structural performance and the consequences under abnormal events or conditions (Adam et al., 2018). The quantification of structural robustness should assess the capacity of the structure to withstand actions and the safety against progressive collapse. Hence, the quantification of structural robustness can be used as a decision tool, that allows to decide whether a level of robustness is acceptable or not.

Besides, the investigation of the structural capacity against an exceptional action requires the modelling of the progressive collapse. Further, the progressive collapse analysis involves many aspects such as geometrical and material non-linearities, dynamic effects, and the propagation of failure (Tagel-Din, 2009). Several methods have been proposed, some of them providing a detailed representation of the structural response, while others propose a simplified structural modelling.

Furthermore, many experimental studies have been carried out, where the objective is to study the performance of the structure and the materials under progressive collapse. Hence, these studies allow to calibrate models or to check their accuracy.

II.3.1 Robustness indices in the literature

The importance and the need for structural robustness quantification in structural design has encouraged researchers to develop and propose many indices for structural robustness quantification. Various approaches can be found and reflect the diversity of points of view on the notion of the structural robustness. In particular, one can distinguish measures based on the structural characteristics from those based on structural response (also called performance-based measures).

II.3.1.1 Indices based on structural response

The indices based on the performance of the structure under accidental and/or exceptional actions are the most used, since they allow the user to directly assess the structural response under some applied scenarios, and the capacity of structure to withstand these scenarios. These indices are applied either in a deterministic way or in a probabilistic approach, where the inherent uncertainties of the model are taking into account (relating to the material properties, the applied loads or the geometrical data).

II.3.1.1.1 Deterministic indices

Several deterministic robustness indices based on the load capacity of structure are detailed thereafter, which aim to evaluate the robustness by determining the effect of the damage on the structural capacity. In this context, Furuta et al. (1985) presented several robustness indices:

- Reserve redundant factor :

$$RI_2 = \frac{L_{intact}}{L_{design}} \quad (II.4)$$

where L_{intact} is the load carrying capacity (collapse load) of the intact (undamaged) structure, and L_{design} is the design load.

- Residual redundant factor :

$$RI_3 = \frac{L_{damaged}}{L_{intact}} \quad (II.5)$$

where $L_{damaged}$ is the load carrying capacity (collapse load) of the damaged structure.

- Strength redundant factor :

$$RI_4 = \frac{L_{intact}}{L_{intact} - L_{damaged}} \quad (II.6)$$

The reserve redundant factor (RI_2) evaluates the capacity of the structure to resist an overloading of the structural system compared to the design load. Otherwise, the residual (RI_3) and the strength (RI_4) redundant factors assess the redundancy of the structure by checking its ability to redistribute the forces after some damage. Hence, they quantify the loss of the load carrying capacity resulting from the damage, by evaluating the residual capacity and the reserve strength of the structure after the damage.

The concept of measuring the structural robustness by the residual capacity of the structure after a local failure was further developed by Khandelwal and El-Tawil (2008), where they proposed a pushdown analysis to quantify the robustness of a structure with lost critical members. This analysis consists of applying a local failure, which can be the loss of one or more critical member(s), and identifying the failure load, where the gravity loads are incremented until collapse of the structure occurs, defined as an inability to support the applied loading. Moreover, the residual capacity is expressed by the overload factor (RI_5), defined as the ratio of failure load to the nominal gravity loads:

$$RI_5 = \frac{\text{Failure load}}{\text{Nominal gravity loads}} \quad (II.7)$$

Khandelwal and El-Tawil (2011) proposed three different ways to apply the pushdown analysis on a building system:

- Uniform Pushdown : after applying the notional local failure, a non-linear static analysis is applied by increasing the gravity loads on the entire structure. The failure load corresponds to the load for which there is a collapse in the system, where the collapsed part corresponds normally to the weakest part of the damaged

structure. Hence, the failure may occur outside the bays of the local failure. Thus, this method cannot appropriately analyze the propagation of failure from the initial failure of the structure to the adjacent part ;

- Bay Pushdown : in this method, only the damaged bays that suffered damage are subject to an incremental load. The remaining part of the structure is subject to the nominal gravity loads. A non-linear static analysis is used as well, and the failure load corresponds to the failure in the damaged bays. Thus, this method puts attention on the damaged bays ;
- Incremental Dynamic Pushdown : this method aims to take into account the dynamic effect. It consists of successive dynamic analyses with increasing gravity loads in the damaged bays until a collapse of the structure occurs. In each dynamic analysis case, the structure is considered undamaged initially, while the loading is being applied. The local failure is applied instantaneously, by removing some elements and identifying if the structure can, or cannot, resist the damage, including the dynamic effect. As this method requires multiple non-linear dynamic analyses, its disadvantage is the significant computational time needed.

The pushdown analysis was applied also by Fascetti et al. (2015), where they proposed two indices (RI_6 and RI_7). These indices allow to evaluate the structural robustness in a general manner and they are not related to only one scenario. The local robustness evaluation is used in the assessment, where notional removal columns scenarios are applied, and a single point load is applied on the top node of the removed columns. Therefore, the applied load $\alpha_1(DL) + \alpha_2(LL)$ on the structure is kept constant, where DL and LL are the dead and live loads, respectively, α_1 and α_2 are the corresponding load factors. Besides, the concentrated load applied at the node corresponding to the lost column is increased by a multiplier $\lambda(t)P$, where P is the axial load on the column before its removal, as shown in Figure II.8. The proposed robustness indices are described below :

$$RI_6 = \frac{n_r}{n_f} \quad (II.8)$$

where, n_r is the minimum number of columns that need to be removed to initiate progressive collapse of the building, and n_f is the total number columns in the respective floor of the structure.

$$RI_7 = \sum_{i=1}^{n_r} i * L_{n,cr} \quad (II.9)$$

The removing of columns is done sequently, where i represents each phase of the sequence of column removal, and $L_{n,cr}$ is the axial load multiplier for the critical column

removed in each phase. These two indices allow to identify the potential risk associated with each column removal, and the most critical scenario that can lead to a progressive collapse.

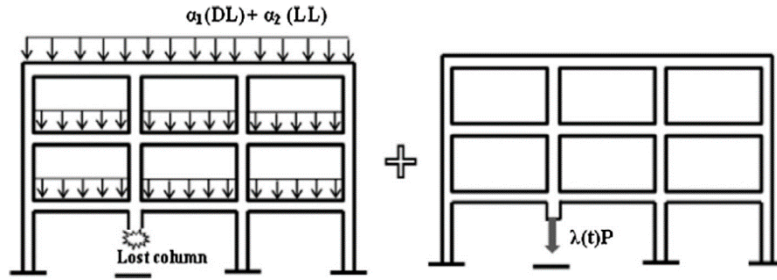


Figure II.8: Local robustness evaluation method (Fascetti et al., 2015).

Fallon et al. (2016) proposed a robustness index that describes the decrease of the damaged structure capacity relative to a given design load, this index is defined as follows :

$$RI_g = \frac{L_{damaged} - L_{design}}{L_{intact} - L_{design}} \quad (\text{II.10})$$

where $L_{damaged}$ is the load carrying capacity of the damaged structure, L_{intact} is the load carrying capacity of the intact (undamaged) structure, and L_{design} is the given design load.

Furthermore, there are robustness indices based on the evaluation of the extent of damage. In this context, Starossek and Haberland (2011) proposed an index that compares the total damage resulting from an initial failure with the limit value of acceptable level of damage specified by design objectives. This index is defined as follows:

$$RI_g = 1 - \frac{P}{P_{lim}} \quad (\text{II.11})$$

where P is the maximum total damage resulting from initial failure, and P_{lim} is the acceptable level of total damage.

The quantification of the damage can be related to the affected volumes, floor areas (e.g. in the case of building structures) or repair costs. This index enables to indicate whether the propagation of the initial failure exceeds the limit level of acceptable damage ($RI_g < 0$) or not ($0 \leq RI_g \leq 1$).

Otherwise, there are also robustness indices based on the energy quantification. The energy based methods are used in some studies to evaluate the propagation of an initial failure. The use of energy based methods for robustness quantification is based on two main objectives (Fang and Li, 2009) :

- improving the energy absorption capacity of structures,
- reducing the energy released during damage propagation.

Starossek and Haberland (2011) proposed an index based on a comparison between the energy released by the initial failure and the energy required for a collapse progression :

$$RI_{10} = 1 - \max_j \left(\frac{E_{r,j}}{E_{f,k}} \right) \quad (\text{II.12})$$

where $E_{r,j}$ is the energy released during the initial failure of a structural element j , and $E_{f,k}$ is the energy required for the failure of the subsequently affected structural element k .

According to this index, which takes values in the interval $] -\infty, 1]$, there is propagation of the failure if $RI_{10} \leq 0$, meaning that $E_{r,j}$ is greater than $E_{f,k}$, which indicates that the released energy is sufficient to cause the failure of another element. If $0 < RI_{10} \leq 1$, it indicates that the initial failure will not propagate, and that the structure has an acceptable level of robustness to withstand the applied initial damage.

II.3.1.1.2 Probabilistic indices

The concept of evaluating structural redundancy has been developed to incorporate probabilistic redundancy measures, in order to take into account the effect of uncertainties that can be related to the material properties, the applied loads or the geometrical data (Frangopol and Nakib, 1991). The robustness indices proposed in the literature are generally based on a reliability index, or a failure probability associated with a particular limit state.

Frangopol and Curley (1987) proposed an index inspired from the strength redundant factor in Equation (II.6), where the load carrying capacity is replaced by the reliability index, as defined below :

$$RI_{11} = \frac{\beta_{intact}}{\beta_{intact} - \beta_{damaged}} \quad (\text{II.13})$$

where β_{intact} is the reliability index of the intact system, and $\beta_{damaged}$ is the reliability index of the damaged system.

The proposed index quantifies the structural robustness by comparing the reliability index of the structure in an intact situation with the one in a damaged situation. Therefore, this index enables to evaluate the residual structural capacity after exposure to a local failure. This index takes values in the interval $[0, +\infty[$, where $RI_{11} \rightarrow \infty$ if the structure is quite insensitive to the local failure ($\beta_{damaged} \approx \beta_{intact}$).

Fu (1987) proposed a redundancy index based on the structural system reliability, with using failure probabilities, as defined below:

$$RI_{12} = \frac{P_{f(dmg)} - P_{f(sys)}}{P_{f(sys)}} \quad (II.14)$$

where $P_{f(dmg)}$ is the probability of damage at the component level, and $P_{f(sys)}$ is the probability of system collapse.

Fu and Frangopol (1990) mentioned that the system residual strength after the initial failure can be described by the difference between the probability of damage occurrence and the probability of system collapse, where it allows to estimate the safety margin between damage initiation and system collapse. Thus, it represents the capacity of the structure to prevent the entire structural system failure upon failure of any component.

Several indices have been proposed later, which can be seen as alternative versions of the previous indices, as those proposed by Mohammadkhani-Shali (2007). These indices, generally obtained through the use of a non-linear analysis, express the performance and the residual strength capacity of the structure. One of these indices is defined as follow:

$$RI_{13} = \frac{\beta_{s,d}}{\beta_{s,i}} \quad (II.15)$$

where $\beta_{s,i}$ and $\beta_{s,d}$ are the reliability indices of the intact system and of structural system when one component failed, respectively. This robustness index RI_{13} takes values in the interval $[-\infty, 1[$, where it tends to 1 when the structure is very robust ($\beta_{s,d} \rightarrow \beta_{s,i}$, which means that the damage did not affect the performance of the structure), and it tends to $-\infty$ when the damaged structure cannot resist and the probability of failure tends to 1.

Furthermore, Kagho Gouadjio (2013) proposed an index that aims to determine the extent from local to global damage, as defined below :

$$RI_{14} = 1 - \frac{P_{global}}{P_{local}} \quad (II.16)$$

where, P_{local} is the probability of local failure, and P_{global} is the probability of global failure.

The global failure may be associated with the formation of a failure mechanism, the loss of global rigidity in the structure, or other critical functions of the structural system (Kagho Gouadjio, 2013). The robustness index RI_{14} varies between the interval $[0, 1[$, the lower and upper bounds indicating non robust and robust structures, respectively. Seck (2018) considered index RI_{14} within a developed approach to determine the probabilities of local and global failure, based on an event tree analysis summarizing all the distinct potential scenarios, from the local damage to the global failure.

The quantification of the structural robustness is often related to extreme events. Nevertheless, the characterisation of structure tolerance to ageing and deterioration can also be useful. In this context, Cavaco et al. (2018) proposed an approach to assess robustness of deteriorated structures for integration in structural management systems. This method was applied to the corrosion risk, and the proposed index was formulated as below :

$$RI_{15} = \int_0^1 \frac{\beta(X_p=x)}{\beta(X_p=0)} dx \tag{II.17}$$

where the damage dx produced by corrosion is measured in terms of reinforcement bars weight loss percentage X_p . This index allows to evaluate the ability of the structure to keep performing according to the design objectives when damage occurs, in terms of the deterioration in the structure. The value of the robustness index RI_{15} varies between the interval $[0, 1[$, where 0 means a non robust structure for which minimal damage level produces total performance loss, and 1 refers to a robust structure where performance is not affected by local damage.

Other robustness indices are based on the risk analysis, which is also recommended by some of international codes such as the Eurocodes (NF EN 1991-1-7, 2007). In this context, Baker et al. (2008) proposed a robustness index based on probabilistic risk assessment with the view to evaluate the progressive collapse risk. This index enables to evaluate the margin between the direct risk associated with local failure, and the indirect risk associated with subsequent structural failure. Consequences are divided into direct consequences (associated with the local failure and assumed to be proportional to the initial cause), and indirect consequences (associated with structural failure subsequent to the local failure and disproportionate to the initial cause).

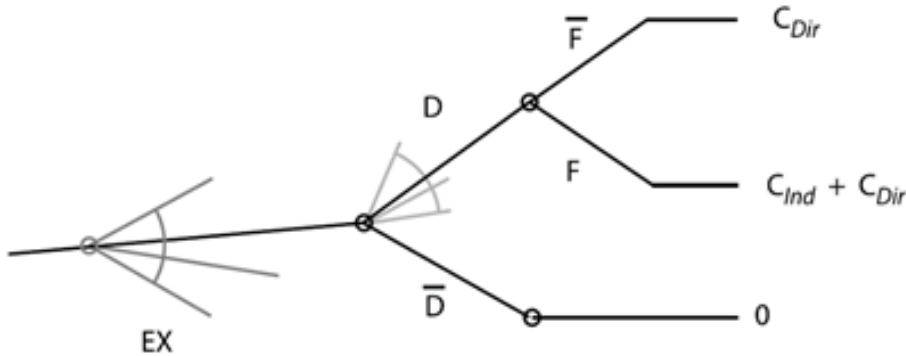


Figure II.9: An event tree for robustness quantification (Baker et al., 2008)

Figure II.9 shows an event tree for robustness quantification, where EX defines some exposure, which has the potential of damaging components in the system. \bar{D} relates to “no

damage occurrence” (then the analysis is finished). D corresponds to the occurrence of some damage, and a variety of damage states D can result. For each state, there is a probability that the failure remains confined to the local failure and does not propagate (\bar{F}), where the total consequences are affined to the direct consequences (C_{Dir}). Otherwise the failure propagates and causes the system failure (F), in this case the total consequences are affined to the sum of direct and indirect consequences ($C_{Dir} + C_{Ind}$). The proposed index by Baker et al. (2008) is defined as below :

$$RI_{16} = \frac{R_{Direct}}{R_{Direct} + R_{Indirect}} \quad (II.18)$$

where, R_{Direct} is the direct risk, and $R_{Indirect}$ is the indirect risk, which are calculated as follow :

$$R_{Direct} = \int_{EX_{BD}} \int_D C_{Dir}(D) P(D|EX) P(EX) dEX dD \quad (II.19)$$

$$R_{Indirect} = \int_{EX_{BD}} \int_D C_{Indir}(F) P(F|D, EX) P(D|EX) P(EX) dEX dD \quad (II.20)$$

There are many difficulties in the application of a risk-based approach (COST Action TU0601, 2011). Shortcomings can be addressed in the international codes and guidelines, that are related to the characterization of the probabilities of exposure occurrence and the failure probabilities for specific scenarios. Further, there are difficulties to estimate the consequences with taking into account the financial losses resulting from the collapse, human losses, and other consequences that can be related.

There are many efforts to develop practical guidelines for the risk, the assessment and the acceptance criteria for structural robustness. The Joint Committee of Structural Safety provided a framework for risk based decision making (JCSS, 2008), where they describe the main axes for a practical application. Further, the task group TU0601 of the European network COST Action published also some document (COST Action TU0601, 2011) that provides information and guidelines for the risk based approach to the practising engineer concerned with the design of buildings. These documents provide information about the hazards, for example on the rate of occurrence and intensity. The various consequences that should be considered in the risk assessment are described, where they can be in the spheres of life safety, economic and business costs, environmental effects, reputational costs, etc.

II.3.1.2 Indices based on structural characteristics

Some robustness indices in the literature are based on the structural characteristics that influence the structural capacity. There are indices based on the stiffness matrix of the structure, where this matrix can be used to assess the stability of a structure after a local failure. Haberland (2007) proposed an index that compares the static system stiffness in an intact state with that after removing a structural element or a connection. This index is defined as below :

$$RI_{17} = \min_j \left(\frac{\det K_j}{\det K_0} \right) \quad (\text{II.21})$$

where K_0 is the stiffness matrix of the intact structure, and K_j is the stiffness matrix of the structure after removing a structural element or a connection j . This index enables to identify critical elements that change and affect more the stiffness matrices.

Biondini et al. (2008) also proposed some indices to compare the stiffness matrices of a structure before and after local failure, also including the ageing effects of the structure over time and checking serviceability conditions under linear behaviour.

The redundancy of the structure is related to the system typology, so it is an important factor on the structural robustness. Brett and Lu (2013) proposed an index based on the system typology, where it is defined as follow:

$$RI_{18} = \frac{Q(S')}{Q(S)} \quad (\text{II.22})$$

where $Q(S')$ is the well-formedness of intact structure, and $Q(S)$ is the well-formedness of damaged structure. The concept of well-formedness $Q(\cdot)$ is being a stiffness-based measure of the quality of the topology and connectivity of the structure (Agarwal et al., 2003).

II.3.2 Analytical characterization of alternative load paths

In the context of applying the Alternative load paths method, which is provided in modern codes and standards, researches were realised at the University of Liege to develop an analytical approach that allows predicting the response of steel building frames submitted to a column loss, and in particular, the associated catenary actions (Jaspart et al., 2011). Demonceau (2008) proposed an analytical model to predict the load-displacement curve of two-dimensional (2D) structures subjected to a column loss scenario (see Figure II.10). This method describes the behaviour of a substructure that contains only the lower beams of the directly affected part as shown in Figure II.11, where they are exposed to the higher tension forces. Moreover, this method focuses on the behaviour in phase 3 (see Figure II.10), when second order effects are predominant. The effect of the indirect affected part is modeled by a

horizontal spring with a stiffness K_H . Huvelle et al. (2015) developed the model of Demonceau to take into account the global interaction between the different parts of the structure, and the local phenomena occurring in the yield zones, submitted to moment and normal forces. The joint is considered as a set of 6 parallel springs submitted to a bending moment M and an axial force N (see Figure II.12), and the section at the extremities of these springs is assumed to remain straight, using the Bernoulli assumption. This approach is described by the Equations provided in Table II.5. Further development of this method was done by Demonceau et al. (2018), to apply it in three-dimensional (3D) and to take into account the dynamic effects.

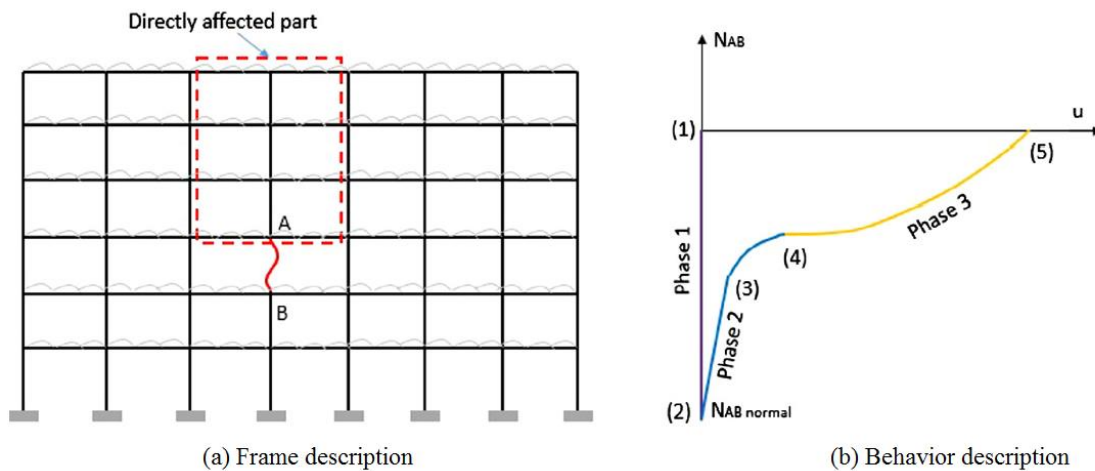


Figure II.10: Behaviour of a 2D frame subjected to a column loss scenario (Huvelle et al., 2015).

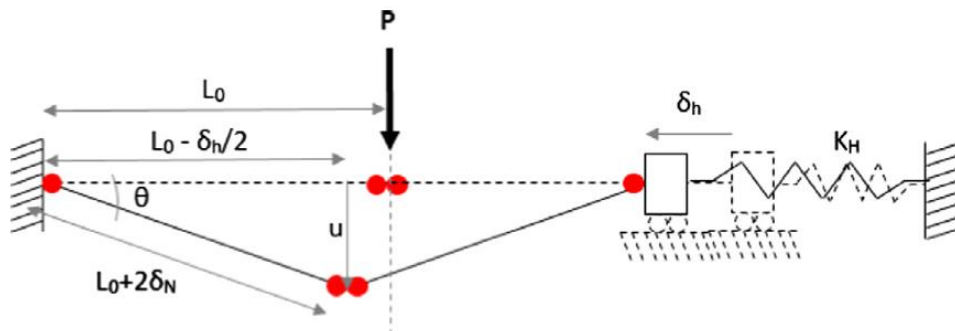


Figure II.11: Substructure considered in the Demonceau model (Demonceau, 2008).

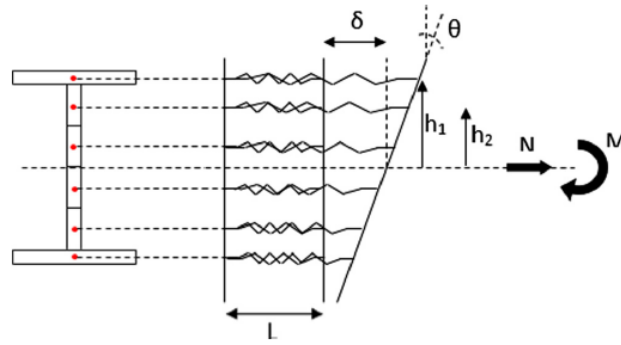


Figure II.12: Spring model for the beam cross-section (Huvelle et al., 2015).

Unknowns	Equations
u	$u = \text{input data}$
θ	$\sin(\theta) = \frac{u}{L_0 - 2L + \Delta_L}$
δ	$\cos(\theta) = \frac{L_0 - 2L - \delta_H - 2\delta}{L_0 - 2L + \Delta_L}$
δ_H	$\delta_H = \frac{F_H}{K_H}$
Δ_L	$\Delta_L = \frac{F_H(L_0 - 2L)}{EA}$
M	$M = \sum F_i h_i$
F_H	$F_H = \sum F_i$
$F_i (i = [1:6])$	$F_i = f(\delta_i)$
$\delta_i (i = [1:6])$	$\delta_i = \delta + h_i \theta$
P	$-P(L_0 - \delta_H) + F_H u + 2M = 0$

P : force simulating the loss of the column

u : vertical displacement at the top of the lost column

K_H : stiffness of the horizontal spring simulating the lateral restraint of the indirectly affected part

F_H : horizontal force acting on the spring K_H

δ_H : horizontal elongation of the spring K_H

M : bending moment at the extremities of the beams of the directly affected part

θ : rotation at the extremities of the beams of the directly affected part

L_0 : initial length of the beams

Δ_L : elastic elongation of the beams of the directly affected part

L : length of the plastic hinge (plasticized zones)

F_i : horizontal force acting on the spring i of the cross section

δ_i : horizontal elongation of the spring i of the cross section

Table II.5: Unknowns and Equations of the Huvelle et al. (2015) model.

II.3.3 Numerical modelling for propagation of failure

With the aim to evaluate the structural robustness, a number of scenarios are applied to investigate the structural response and the capacity of the structure to withstand the applied scenarios. In this respect, the structural modelling has to identify the damage consequences that can exist, which allows to evaluate the disproportionality of the consequences compared to the original cause. Therefore, the structural modelling has to follow the propagation of collapse, also to identify the consequences in the initial stage and the final stage after collapse. Some structural modelling methods are used by the scientific community to model the progressive collapse, where one can set out the following techniques described thereafter: (i) Finite Element Method (FEM), (ii) Discrete Element Method (DEM), (iii) Applied Element Method (AEM), and (iv) Cohesive Element Method (CEM).

II.3.3.1 Finite Element Method (FEM)

The finite element method is the most widely used method in the structural modelling, in particular to simulate the progressive collapse (Adam et al., 2018). The modelling by finite element method can be done with different levels of discretization, where the discretization level basically depends on the dimension of the structure and the level of precision required. Generally, there are three levels of discretization: local, global, and semi-global (Franz-Josef, 1996). Figure II.13 gives an example of a benchmark project (SMART) in which such various approaches were compared (Juster-Lermitte, 2010).

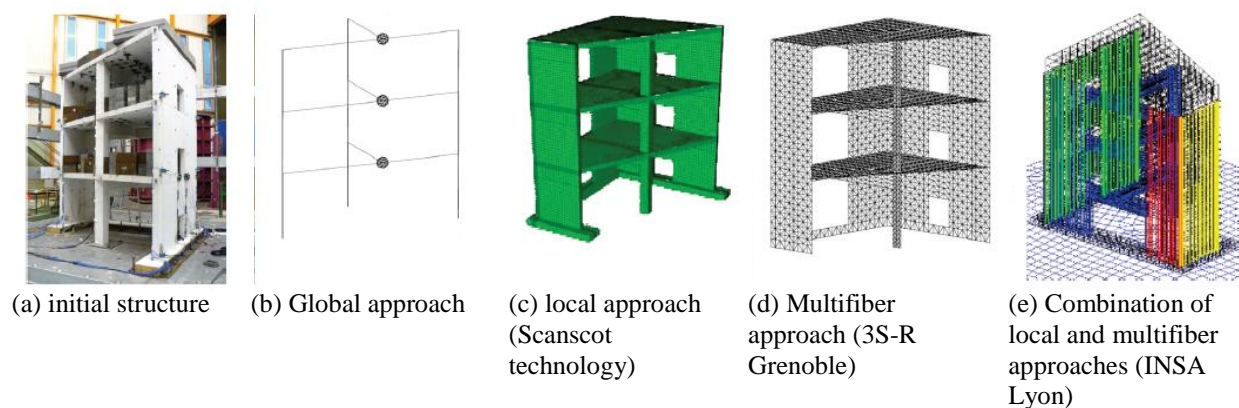


Figure II.13: Finite element models used in the project SMART (CEA) (Juster-Lermitte, 2010).

II.3.3.1.1 Local approach

In a local approach, the structural elements are discretized with small solid elements as shown in Figure II.14, where these elements can be modeled in two-dimensional (2D) or three-dimensional (3D) (Franz-Josef, 1996). This method allows the detailed representation of

the structure as close to reality as possible. Furthermore, each solid element can be described by a specific constitutive law that represents the behaviour of the considered material. The behaviour on each point of the structure is fully described with local variables of stresses ($\underline{\underline{\sigma}}$) and strains ($\underline{\underline{\epsilon}}$).

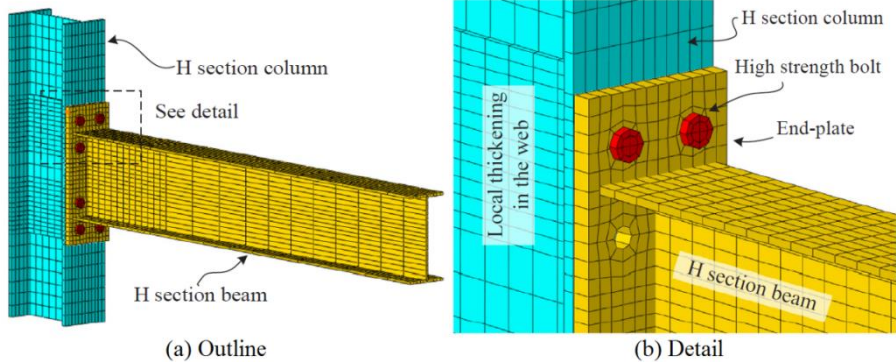


Figure II.14: Modelling with Finite Element Method – Local approach (Yin and Shi, 2018).

This approach allows detailed and accurate representation of the structural response, with local information about the stresses and strains on each point of structure, and the state of materials that identifies if the behaviour of the material is in the elastic or plastic range, besides the state of damage of materials. Figure II.15 shows how such local approach can give information on plastic deformation associated with some limit state (Mohammadkhani-Shali, 2007). However, despite the increasing evolution of computing capabilities, this method requires significant computation time, especially when dealing with geometrical non-linearities. Therefore, this type of modelling is preferred to model small structures (Adam et al., 2018).

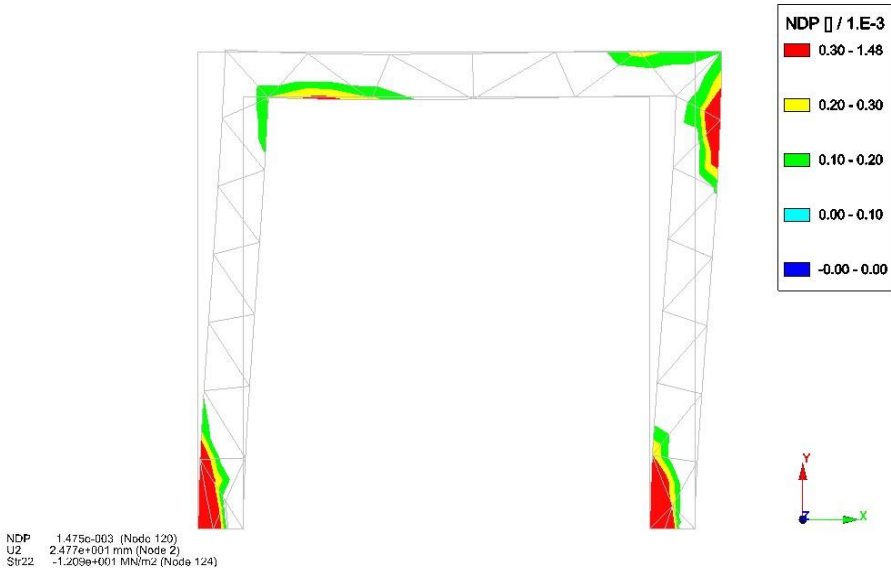


Figure II.15: Plastic deformations obtained within a probabilistic local approach (Mohammadkhani-Shali, 2007).

The local approach has been used in many studies with the aim to assess the structural components behaviour under exceptional situations (Sasani et al., 2011b). Sadek et al. (2011) studied the performance of steel and reinforced concrete beam-column assemblies under a column removal scenario (see Figure II.16), where they investigated the structural design of framing systems as intermediate moment frames (IMFs) and special moment frames (SMFs). Furthermore, the results of the simulation assessment with finite-element based modelling were compared to the experimental results, where they showed a good agreement and that the model is able to accurately represent the behaviour and failure of the assemblies.



Figure II.16: Computational and experimental assessment of RC beam-column assembly under a column removal scenario (Sadek et al., 2011).

II.3.3.1.2 Global approach

In a global approach, the structure is modelled with beam/shell elements (Figure II.17). The behaviour of these elements is described by a global constitutive law, depending on its geometry and materials, where the state of elements is described with global vectors of deformation and forces.

On the one hand, the benefit of this approach is that it enables to simulate the entire structure with saving significantly on computation time. On the other hand, this type of modelling does not allow to determine local information about the behaviour of materials, especially in case of heterogeneous sections such as reinforced concrete elements. Therefore, there might be some difficulties to simulate and to identify the damage in the element sections. Moreover, in this type of analysis the failure mechanisms are located in the presupposed areas of plastic hinges (Franz-Josef, 1996; Desprez, 2010).

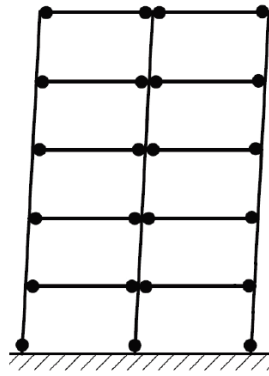


Figure II.17: Modelling with Finite Element Method – Global approach (Takeda et al., 1970).

The simplification of modelling offered by the global approach allows to simulate the progressive collapse of an entire building in three-dimensional (3D) with nonlinear dynamic analysis (Kokot et al., 2012), as shown in Figure II.18.

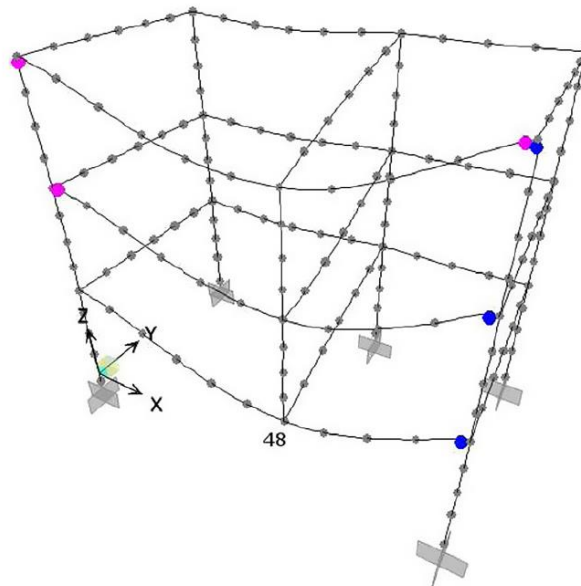


Figure II.18: Nonlinear dynamic response of a reinforced concrete building under a column loss scenario using global approach (FEM) (Kokot et al., 2012).

II.3.3.1.3 Semi-global approach

The semi-global approach is an intermediate scale of discretization between local and global approaches, where the element is divided on multilayer or multifiber elements parallel to the axis of the structural element as shown in Figure II.19. This approach simplifies the modelling of a structure compared to a local approach while providing a higher degree of analysis than a global approach (Mazars and Grange, 2017). Each layer or fiber is described by its own constitutive law.

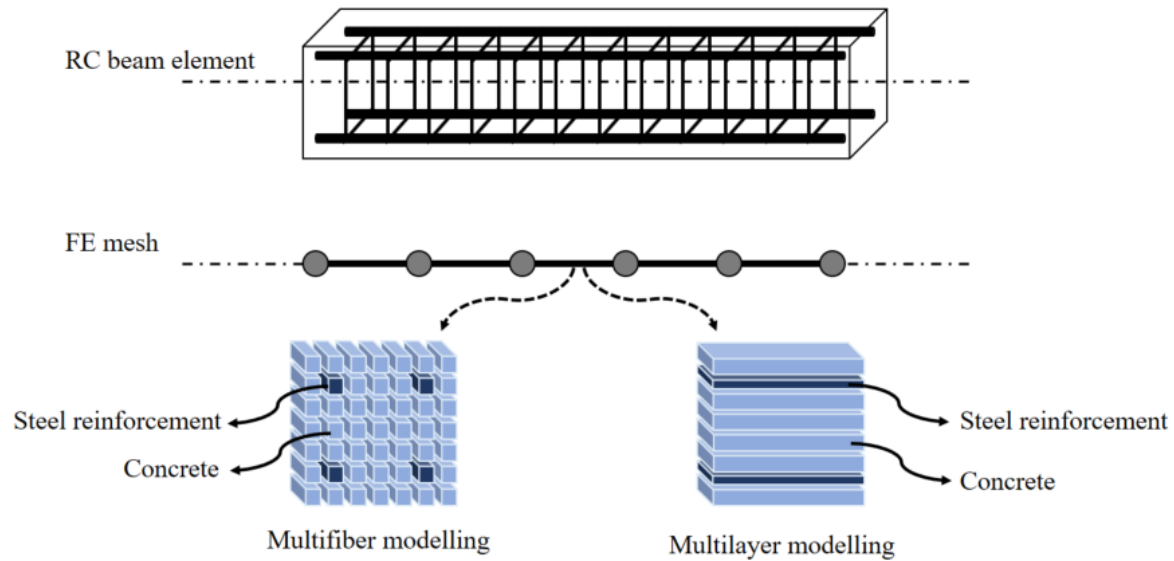


Figure II.19: Modelling with Finite Element Method – Semi-global approach with multifiber and multilayer methods.

This method allows the accessibility to the local information of materials state, and the fields of displacements and forces are calculated by classical beam element formulations, which can be displacement-based or force-based (flexibility-based) (Spacone et al., 1996; Mazars et al., 2006). Furthermore, this approach integrates the benefits of local and global approaches: saving on computation time and ability to describe geometrical and material non-linearities (Franz-Josef, 1996).

The semi-global approach is widely used in the progressive collapse analysis (Adam et al., 2018), where it allows to simulate accurately the response of structure with reasonable computation time comparing to local approach (Sadek et al., 2011; Bao et al., 2014). This method was used to simulate the structural response under column loss (Kazemi-Moghaddam and Sasani, 2015; Y. Li et al., 2016), also it was used to analyse progressive collapse from a threat-dependent scenario such as Liu et al. (2015) and Sun et al. (2012), where they simulate the progressive collapse due to fire action.

The beam-column and slab-beam joints are complex zones, to simulate accurately the behaviour on these points of structure, they can suffer from large rotations and deformations, as well as the interaction of shear and axial and flexural loading, especially to simulate the membrane action (Bao et al., 2014). Therefore, in the aim to model the beam-column joints, several macromodels were proposed (Bao et al., 2008; Sadek et al., 2008; Vlassis et al., 2008; Yu and Tan, 2013; Vidalis, 2014), where the macromodels of joints are formed by a series of springs and rigid elements as shown in Figure II.20.

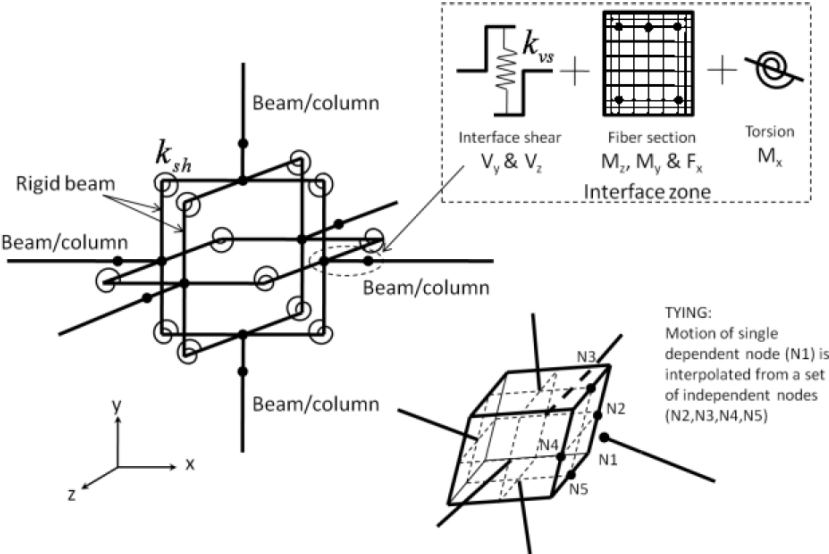


Figure II.20: Macromodel of beam-column joint (Bao et al., 2014).

II.3.3.2 Discrete Element Method (DEM)

The Discrete Element Method (DEM) has been introduced to model the discontinuity of materials such as granular (Cundall and Strack, 1979). However, it was also used to model the continuous materials, where it enables to model the appearance of discontinuities (crack) in these materials, where the discontinuity is easier to implement than Finite Element models (Vu, 2013). The materials are treated as an assembly/collection of mobile and interacting discrete elements, and the behaviour of the material at the macro-length-scale is deduced from the statistical analysis of the (normal, tangential, rolling and twisting) contact-interactions and motions of these elements (Grujicic et al., 2013). The discrete elements can be in different geometric shape like spheres or polyhedral as shown in Figure II.21. The great evolution in the computation capacity of computers allows to apply this method, but the application of this method to large structures usually needs a high computational cost compared to the Finite Element Method (Adam et al., 2018).

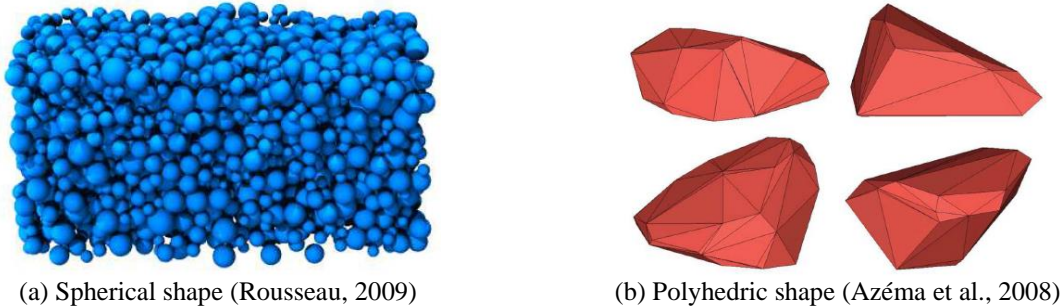


Figure II.21: Geometric shape of discrete elements.

The benefit of this method in the progressive collapse analysis is its ability to simulate the discontinuities associated with the progressive collapse, in the case of cracks and separation of elements. This method was not commonly used to simulate progressive collapse, where the scientific community has so far paid little attention to this technique (Adam et al., 2018). However, there are some studies that applied this method to simulate the progressive collapse like Masoero et al. (2012) and Gu et al. (2014). Furthermore, there are studies that combined the Discrete Element Method with the Finite Element Method, where the results are considered accurate with an acceptable computation cost (Munjiza et al., 2004; Lu et al., 2009).

II.3.3.3 Applied Element Method (AEM)

The Applied Element Method is a relatively recent method, which was developed by Tagel-Din and Meguro (2000) for modelling the entire collapse process. The model consists of an assembly of small rigid elements, connected together by sets of normal and shear springs as shown in Figure II.22, where these springs represent the element deformations and stresses. The comparison between Finite Element Method (FEM) and the Applied Element Method (AEM) demonstrates that they have a reasonable agreement in terms of load displacement and failure pattern (Tagel-Din, 2009).

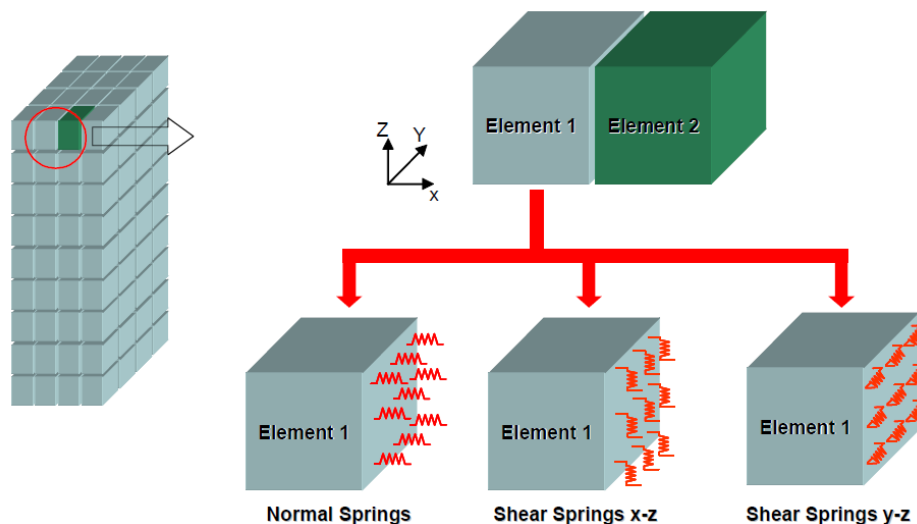
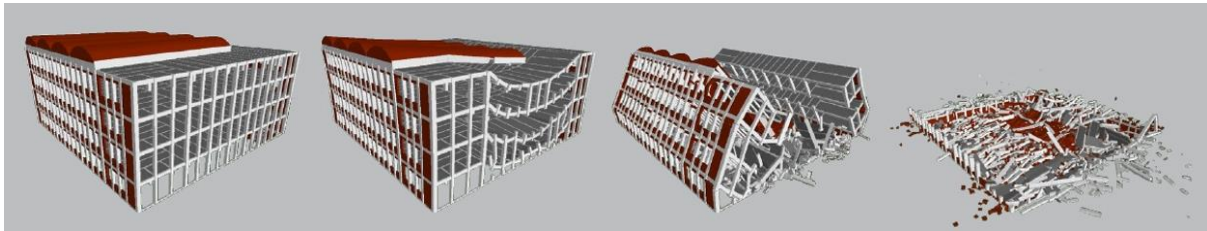


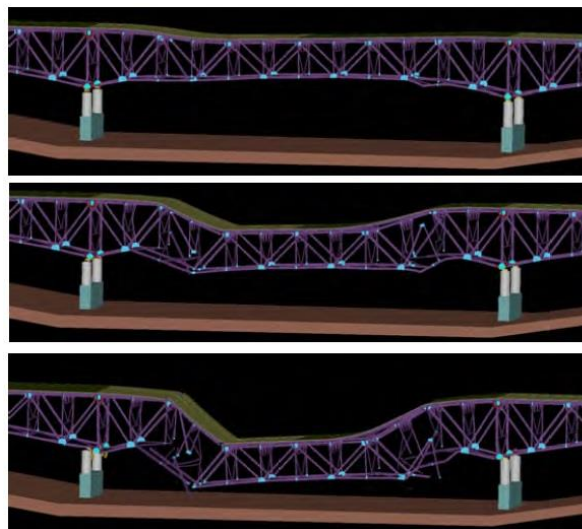
Figure II.22: Applied Element Method - connectivity matrix springs (Tagel-Din, 2009).

The main advantage of this method is its ability to simulate the behaviour of structure under progressive collapse (Figure II.23), and to follow the propagation of failure, starting from crack initiation and propagation, element separation, formation of debris and collision between falling debris and other structural components in reasonable time, until complete collapse. Due to its capacities, this method has been used in recent years to simulate the

progressive collapse of structures in several studies such as Sasani (2008) and Marginean et al. (2018).



(a) Brown Brewery demolition (reinforced concrete structure)



(b) Minnesota I-35W bridge failure (steel structure)

Figure II.23: Structural modelling of the Sheraton Hotel Raleigh NC demolition (source: <https://www.appliedscienceint.com/>).

II.3.3.4 Cohesive Element Method (CEM)

The Cohesive Element Method is widely used to model the material fracture (Le and Xue, 2014). Le and Xue (2014, 2016a, 2016b) developed a numerical model based on the concept of Cohesive Element Method in the aim of modelling the progressive collapse of building structures. The structural elements are modelled by several elastic blocks connected by a set of cohesive elements, which represents the potential damage zones as shown in Figure II.24. Therefore, the simulation of the non-linear behaviour of the structural components is presented by the cohesive elements. Indeed, there are difficulties to accurately simulate the behaviour of materials, where the model calibration is essential on the cohesive constitutive relations of the cohesive elements.

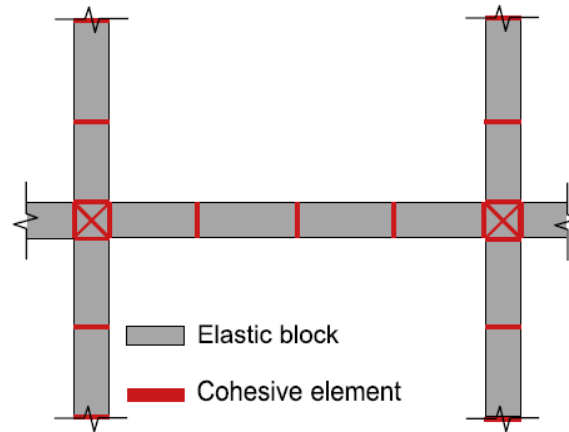


Figure II.24: Cohesive element modelling of a frame subassembly (Le and Xue, 2014).

II.3.4 Experimental testing for building recommendations

Numerous experimental campaigns have been carried out to investigate the progressive collapse in frame building structures. An experimental test has been conducted by Demonceau (2008), where this test aims to simulate the static loss of a column on 2D sub-assembly of a composite frame structure as shown in Figure II.25. The objective was to study the development of the membrane action in the beams, as well as the behaviour of beam-column joints.

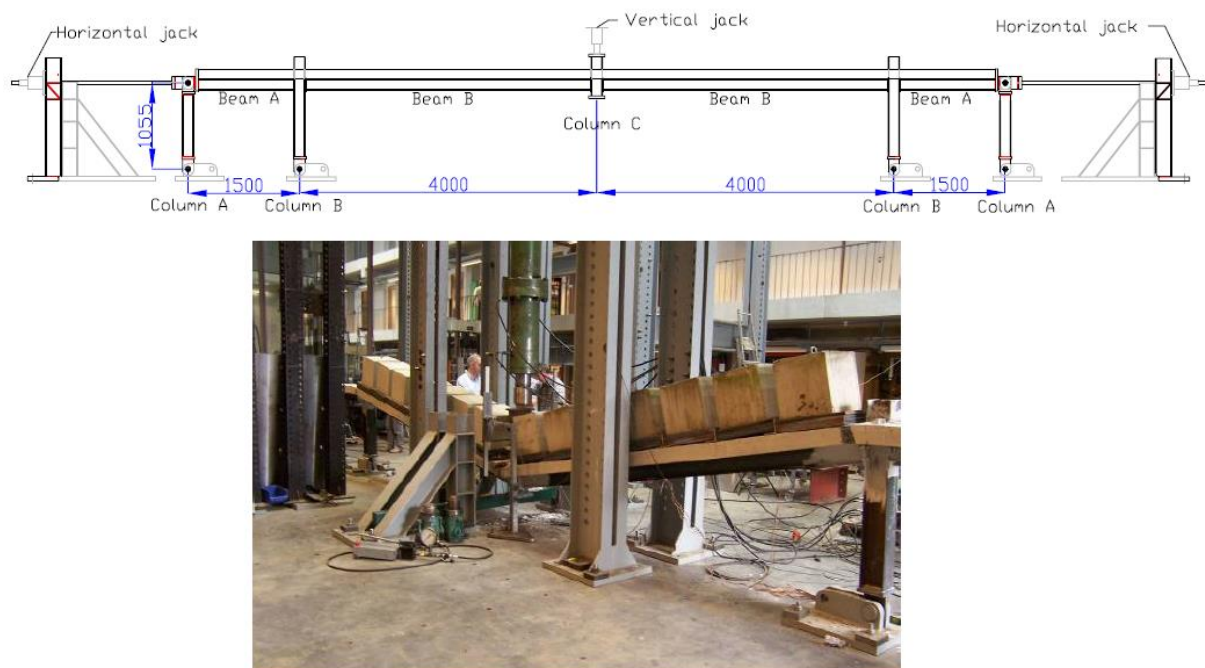


Figure II.25: Experimental test on 2D sub-assembly (Demonceau, 2008).

Other studies on sub-assemblages can be mentioned, where different types of structures were tested as concrete, steel and composite structures (Dinu et al. (2017); Elsanadedy et al. (2017)). Experimental tests were also done on 2D multi-storey frames as shown in Figure II.26, such as the studies performed by Shan et al. (2016) and Qian and Li (2017).

The tests on full-scale building are complex experiments due to the high costs involved, the difficulty of performing the tests in laboratories and the potential dangers of deliberately causing the failure. Nevertheless, some studies were conducted on building structures such as those shown in Figure II.27, or those performed by Sasani et al. (2011).

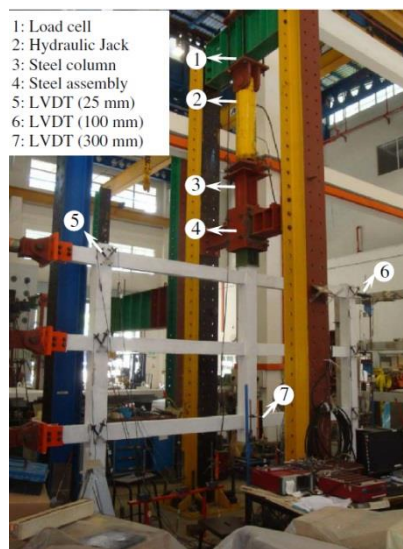


Figure II.26: Experimental test on 2D multi-storey frame structure (Qian and Li, 2017a)



Figure II.27: Experimental test on 3D building frame structure (Zandonini et al., 2014).

II.4 FEEDBACK ON CURRENT APPROACHES AND IDENTIFICATION OF IMPROVEMENT NEEDS

The interest in structural robustness analysis has grown, with a considerable increase in research activity to analyze properties of structural robustness and develop quantitative measures of structural safety against unexpected actions. In this context, there has also been some growing interest to study the progressive collapse, and to model the response of structures under exceptional actions. The motivation behind this growing interest has been the catastrophic collapse of some structures that were severely damaged, or even reached the total collapse, after the failure propagation, resulting from an exceptional event. In particular, the collapse of the World Trade Centre (WTC) Twin Towers in 2001 and the recent collapse of

the cable-stayed Genoa Bridge collapsed in Italy in 2018 are two events that alarmed the public opinion about the required level of structural safety.

The standards and codes of civil engineering can benefit from a quantitative assessment of robustness to verify if the structure has a sufficient level of residual resistance when damaged under an exceptional event. With the aim to quantify structural robustness, the proposed research activity focuses on two main axes: the robustness measures, and the progressive collapse analysis. In the following, one proposes some feedback on the approaches previously presented in this chapter and that motivate further research.

II.4.1 Feedback on robustness measures

With regards to the robustness measures proposed in the literature, the following points can be noted:

- the majority of proposed robustness indices are related to only one scenario that can be threat-dependent or threat-independent, where there is one value of the robustness index for each scenario. Thus, these indices fail to evaluate the structural robustness in a general manner based on several significant scenarios ;
- the magnitude of locale failure or the type of action itself is generally not considered although it is important to characterize the adopted scenarios to evaluate the subsequent structural response ;
- the concept of structural robustness relates to that of disproportionate collapse. Therefore the robustness measure has to consider the comparison between an initial and a final state after failure propagation to estimate if it is acceptable or not ;
- the consideration of some local failure, such as the loss of one column, enables to check the structural capacity to survive to such applied scenarios. However, it does not characterize the magnitude of actions or the extent of initial damage, though it is important to determine the maximum capacity of structure to withstand some local damage. The identification of the maximum extent of some local failure that propagates with an acceptable manner could represent the maximum capacity of the structure to survive to some unexpected actions. The quantification of robustness by the maximum capacity of the structure to withstand some actions can then be a useful measure in structural design. It allows to evaluate the structural safety, and to identify the critical scenarios for which an unacceptable collapse occurs, thus taking the appropriate measures.

Based on the observations above, there is a need for robustness measures that allow a global assessment, with identifying the maximum capacity of structure to withstand some exceptional actions without unacceptable collapse. Besides, the characterization of local failure scenarios is needed to evaluate the maximum magnitude of scenarios for which the structure can survive. Furthermore, the evaluation of the degree of failure propagation is an important information to evaluate whether the damage is disproportionate or not, compared to the initial damage.

II.4.2 Feedback on progressive collapse analysis

Progressive collapse analysis represents an essential tool in the structural robustness assessment. The features needed for progressive collapse modelling are related to the identification of the main aspects in the approach of the structural robustness quantification. These features are described as below:

- to perform an overall assessment of structural robustness, a large number of scenarios have to be considered. Therefore, a simplified structural modelling method is required to model the structural response under the applied scenario with a reasonable computation time;
- in order to assess the degree of failure propagation, the initial and the final states of failure have to be identified. Thus, the structural modelling method has to be able to follow the propagation of failure, starting from the initial failure until the final stage of failure. The methods used to predict whether the local failure will propagate or not, without simulating the propagation of failure may be inappropriate to assess the degree of failure propagation;
- with the view to achieve a simulation of progressive collapse close to reality, the essential aspects of progressive collapse analysis have to be taken into account, which relate to the geometrical and materials non-linearities as well as the dynamic effects.

II.5 CONCLUSIONS

The quantification of structural robustness can be used in different areas of application, with many roles such as: optimisation, regulation, evaluation, design, and updating of system partial safety factors (Starossek and Haberland, 2008). However, the regulation of the structural robustness in the design and construction codes and standards still needs to be

developed by adding quantification approaches, where it can be defined in a general manner, or according to the type of structure.

The evaluation of the structural capacity to withstand accidental actions and the progressive collapse is important to check a required structural safety level, also to identify the critical elements and the most dangerous scenarios that lead to unacceptable consequences. Moreover, the comparison between different structural design variants becomes possible by using some quantitative measures. In structural design, the measures of structural robustness should be decision tools, with a view to assess if the resistance of the structure is sufficient or if there is a need to modify the structural design and provide solutions to improve the structural capacity.

Furthermore, it is important to identify the requirements of the quantification of structural robustness, which contribute to the validity and usefulness of the structural robustness measure. The following general requirements were identified by (Haberland, 2007): expressiveness, objectivity, simplicity, calculability, and generality. The robustness measure should express the capacity of the structure to withstand some accidental actions and help to avoid some disproportionate progressive collapse. Objectivity ensures that the credibility of the robustness measure, the opinions or decisions of users should not affect the result, where it should always present the same value under the same conditions. Usefulness and applicability of the robustness measures depend also on their simplicity. Therefore the measures should be as simple as possible. Calculability is to provide input parameters of the numerical calculation that are quantifiable, and the robustness measures should be sufficiently accurate and easy to carry out. Finally, the structural robustness measures should be developed at a level of generality that allows application to any type of structures. These requirements are partly in conflict with each other, thus making it difficult to fulfill all of them together.

Considering these requirements on robustness measures and the feedback detailed in Section II.4, one identifies three main questions below that will be considered in the following of this dissertation:

- How to propose a simplified modelling of progressive collapse by taking into account the dynamic effects, the geometrical and the material non-linearities? There is a high uncertainty level associated with the type and intensity of exceptional actions, so a large number of scenarios should be investigated and the structural modelling should effectively describe failure propagation.
- How to identify the degree of failure propagation, in order to evaluate and quantify the extent of failure after an initial event? The robustness measure should then compare initial and final (after propagation) structural states;

- How to assess the maximum structural capacity with respect to some performance thresholds? The characterization of some scenarios in the robustness assessment is required to evaluate the corresponding structural response and identify the worst-case scenario;

To provide answers to the first question, Chapter III details the structural modelling strategy used to follow the failure propagation. Chapter IV then addresses the second and third questions by proposing some measures of structural robustness, both to evaluate the capacity of structures to prevent the propagation of failure (with a robustness propagation failure index) and also to identify the maximum magnitude that the structure can resist without unacceptable collapse (with a robustness energy index). It is shown how these measures can be used separately or simultaneously and how the approach can be used for comparison of design options. Finally, the sensitivity of the approach to some input parameters is proposed in Chapter V.

CHAPTER III

MODELLING OF PROGRESSIVE COLLAPSE

III.1 INTRODUCTION

In a context where there is a large number of scenarios to investigate, the simplification of the structural modelling is needed. Hence, the difficulty is to take into account the geometrical and material non-linearities, as well as the dynamic effects within a simplified structural modelling. The yield design approach may be a good compromise, where this approach is a direct method, that enables to determine the ultimate load of a structure, thus avoiding a step-by-step non-linear analysis of the structural response along the full loading path until failure (de Buhan, 2007).

The theory of yield design (a limit analysis in the context of perfectly plastic materials) is based upon the analysis of the conditions ensuring the compatibility between the equilibrium of the structure and the local verification of a criterion of resistance at any point of the structure (Salençon, 2013). This method consists of the application of two approaches, static and kinematic, that enable to approximate and bracket the ultimate load of the structure by lower and upper bounds, respectively. The main benefit of this method is its ability to investigate the ultimate state of the structure with avoiding complex non-linear computations with potential convergence issues, and significantly saving computational costs. Besides, this method provides valuable information such as the failure mechanism and the most critical areas of the structure.

Principles of the yield design theory can be explicitly found in the strut-and-tie modelling (NF EN 1992-1-1, 2005). Strut-and-tie models consist of struts representing compressive stress fields, of ties representing the reinforcement, and of the connecting nodes. The forces in the elements of a strut-and-tie model should be determined by maintaining the equilibrium with the applied loads in the ultimate limit state. In some way, this approach can

be related to the lower bound static approach of yield design (Vincent et al., 2017). Other areas of civil engineering design methods are based on such kind of reasoning, as for instance:

- soil slope stability or bearing capacities of footings in geotechnics,
- yield line theory for plates and slabs,
- rigid blocks mechanism for masonry structures,
- plastic hinges mechanisms for frame structures, etc.

The yield design approach is based on infinitesimal strain assumption, considering that the materials are elastic perfectly plastic. Therefore, the main challenge to use this method for robustness analysis is to take into account the geometrical non-linearities and to iteratively simulate the propagation of the failure. Using a non-linear analysis on the affected part identified by the yield design is proposed herein to offset the limits of the yield design calculation. The principle of coupling a yield design approach with another type of analysis to model the geometrical and material changes was used by Pham (2014) and Bleyer (2015), where they studied the behaviour of a reinforced concrete panel under the fire action. A thermo-elastic analysis was used to identify the geometrical displacements and the materials degradation was integrated in a yield design calculation in order to identify the stability factor of the deformed structure.

In this chapter, one introduces an embedded yield design approach within a non-linear analysis for structural modelling of progressive collapse. Such an iterative procedure aims to check if an alternative load path can be found in the area close to the directly affected part of a structure, and if not, how the failure propagation can be discretized until one reaches a final stage. Concepts of yield design theory are reminded first and associated numerical modelling is presented. Then, the proposed coupling strategy is detailed and applied on a steel frame case study.

III.2 YIELD DESIGN APPROACH

III.2.1 General principles

The essential input data required for a structural yield design analysis are the geometry of the structure, the load acting on the structure, and the resistance criteria of the structural elements. The geometry of the structure is defined by the volume Ω of the system under consideration, and the boundary $\partial\Omega$ (see Figure III.1). As mentioned previously, the infinitesimal strain theory is an essential assumption in the yield design calculation, where the

geometry and the constitutive properties of the material at each point of space can be assumed to be unchanged by the deformation. The system is considered to be subject to a loading mode of n parameters, represented by a vector $\underline{Q} = (Q_i; i = 1, \dots, n)$. The applied load can be related to body forces \underline{F} (such as gravity) or forces applied to the boundary of the system \underline{T} .

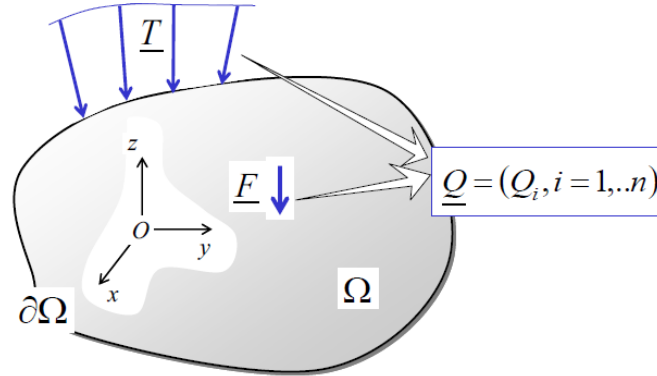


Figure III.1: Data for a structural yield design analysis (de Buhan, 2007).

Each point \underline{x} of the system Ω is defined by a strength domain $G(\underline{x})$ (admissible stress states at point \underline{x}), which is the only knowledge required regarding material properties. Therefore, the stress tensor $\underline{\sigma}(\underline{x})$ at each point \underline{x} in Ω is admissible if in $G(\underline{x})$, in the sense of the criterion of resistance, where the strength condition can be written as follows :

$$\forall \underline{x} \in \Omega, \quad \underline{\sigma}(\underline{x}) \in G(\underline{x}) \quad (\text{III.1})$$

The strength domain $G(\underline{x})$ characterizes the constituent material, and it identifies the local resistance capacity. Usually, it has the following two properties:

- $G(\underline{x})$ includes the origin $\underline{0}$:

$$\forall \underline{x} \in \Omega, \quad \underline{\sigma}(\underline{x}) = \underline{0} \in G(\underline{x}) \quad (\text{III.2})$$

- $G(\underline{x})$ is convex (see Figure III.2):

$$\forall (\underline{\sigma}^{(1)}(\underline{x}), \underline{\sigma}^{(2)}(\underline{x})) \in G(\underline{x}), \forall \lambda \in [0,1] \Rightarrow \lambda \underline{\sigma}^{(1)}(\underline{x}) + (1 - \lambda) \underline{\sigma}^{(2)}(\underline{x}) \in G(\underline{x}) \quad (\text{III.3})$$

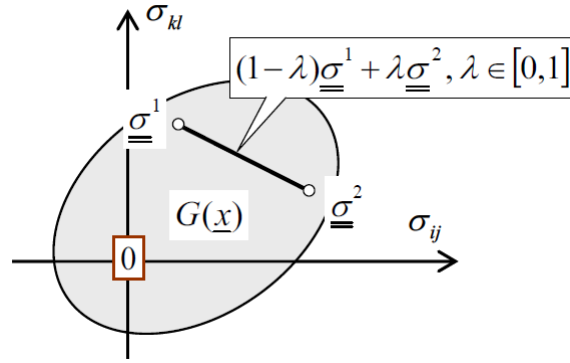


Figure III.2: Convex strength domain $G(\underline{x})$ in the internal forces space (de Buhan, 2007).

Various strength criteria describe the yielding of materials (de Buhan, 2007). For example, Tresca and Von Mises isotropic strength criteria are used to describe coherent materials such as metals and clay soils. Otherwise, the Drucker-Prager and Mohr Coulomb criteria can be used to describe the decohesion of materials such as concrete and rocks. Figure III.3 illustrates the yield surfaces of the criteria described below, in principal stress coordinates:

- Tresca:

$$f(\underline{\sigma}) = \sup\{\sigma_i - \sigma_j - \sigma_0 \mid i, j = I, II, III\} \quad (\text{III.4})$$

- Von Mises:

$$f(\underline{\sigma}) = \sqrt{\frac{1}{6}((\sigma_I - \sigma_{II})^2 + (\sigma_{II} - \sigma_{III})^2 + (\sigma_{III} - \sigma_I)^2)} - k \quad (\text{III.5})$$

- Mohr-Coulomb:

$$f(\underline{\sigma}) = \sup\{\sigma_i(1 + \sin\phi) - \sigma_j(1 - \sin\phi) - 2C\cos\phi \mid i, j = I, II, III\} \quad (\text{III.6})$$

- Drucker-Prager:

$$f(\underline{\sigma}) = \sqrt{\frac{1}{6}((\sigma_I - \sigma_{II})^2 + (\sigma_{II} - \sigma_{III})^2 + (\sigma_{III} - \sigma_I)^2)} - \frac{3\sin\phi}{\sqrt{3(3 + \sin^2\phi)}} \left(\frac{C}{\tan\phi} - \frac{1}{3} \text{tr}\underline{\sigma} \right) \quad (\text{III.7})$$

where σ_I , σ_{II} and σ_{III} are the principal stresses, σ_0 is the resistance of the material under simple tension, k is the resistance of the material under simple shear, ϕ is the friction angle, and C is the cohesion of the material. The strength criterion is given by:

$$G(\underline{x}) = \{ \underline{\sigma}(\underline{x}) \text{ s. t. } f(\underline{\sigma}(\underline{x})) \leq 0 \} \quad (\text{III.8})$$

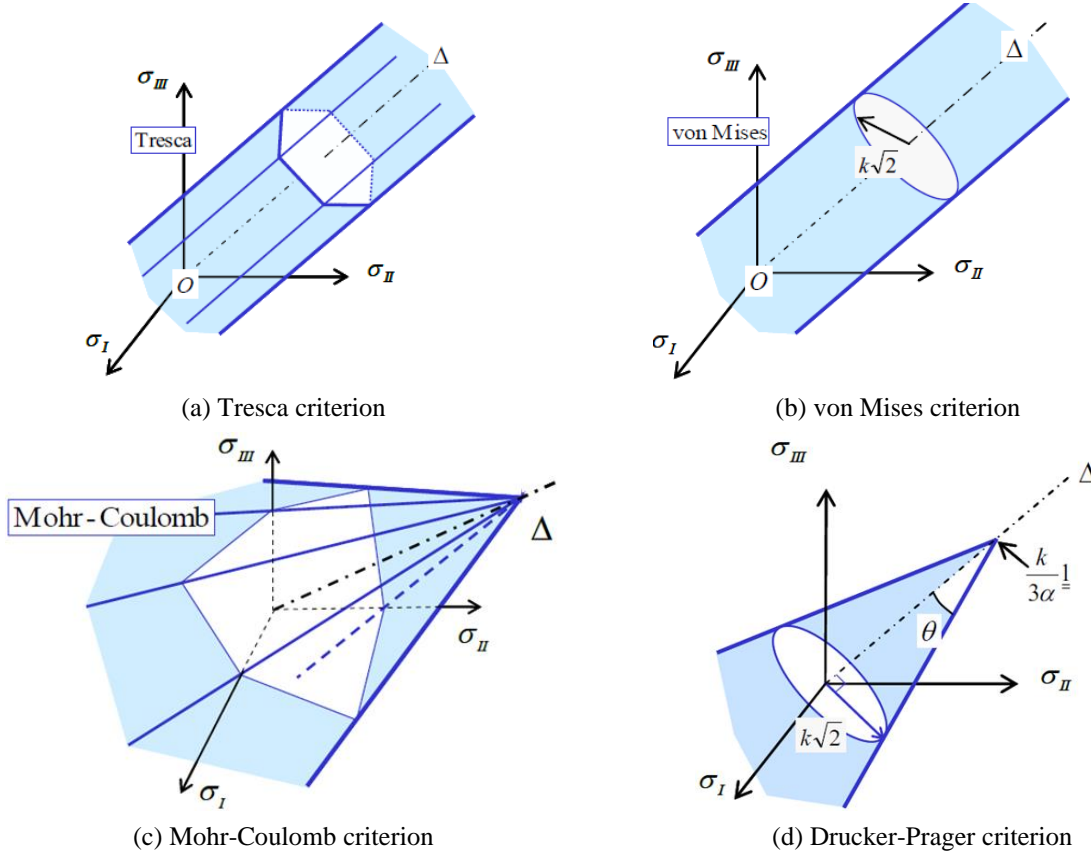


Figure III.3: Usual isotropic strength criteria (de Buhan, 2007).

The yield design approach allows to identify the potential safe loads K based on the compatibility between the equilibrium of the structure and the local resistance at any point of the structure. The domain of potential safe loads K is defined as the set of loads \underline{Q} , where the stress tensor $\underline{\sigma}(\underline{x})$ under the loading mode \underline{Q} must be statically admissible complying with the strength condition at each point of the system by verifying the resistance criteria $G(\underline{x})$. Therefore, the identification of the potential safe loads K can be presented as follows:

$$\underline{Q} \in K \Leftrightarrow \begin{cases} 1. \exists \underline{\sigma}(\underline{x}) \text{ statically admissible in the} & \text{(equilibrium condition)} \\ \text{loading mode with load } \underline{Q} & \\ 2. \underline{\sigma}(\underline{x}) \in G(\underline{x}), \forall \underline{x} \in \Omega & \text{(resistance condition)} \end{cases} \quad (\text{III.9})$$

The properties of strength domain $G(\underline{x})$ imply that the domain of potential safe loads K has the same properties. Thus $\underline{Q} = \underline{0}$ is an element of K , which is also a convex set.

III.2.2 Static approach of the potential safe loads

The static approach directly proceeds from the conditions of Equation (III.1) and provides a lower estimate of the extreme loads (i.e. an interior approximation of the domain of the potential safe loads K).

The equilibrium condition is ensured if the stress tensor $\underline{\underline{\sigma}}(\underline{x})$ is statically admissible, which means that $\underline{\underline{\sigma}}(\underline{x})$ satisfies the equilibrium equations on Ω and the stress boundary conditions on $\partial\Omega$:

$$\forall \underline{x} \in \Omega, \quad \text{div} \underline{\underline{\sigma}}(\underline{x}) + \rho \underline{F}(\underline{x}) = 0 \quad (\text{III.10})$$

where $\rho \underline{F}$ is the body forces in Ω .

Besides, the resistance condition is ensured if the stresses at each point of the system are in the admissible strength domain $G(\underline{x})$:

$$\forall \underline{x} \in \Omega, \quad \underline{\underline{\sigma}}(\underline{x}) \in G(\underline{x}) \quad (\text{III.11})$$

Hence, the static approach enables to identify a set of loads K^{stat} belonging to the domain of potential safe loads K ($K^{stat} \subseteq K$) as shown in Figure III.4.

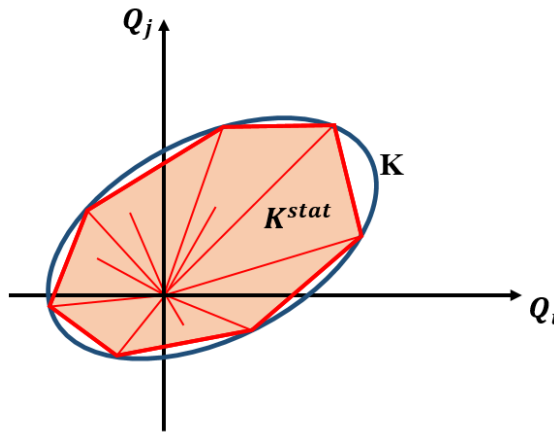


Figure III.4: Potential safe loads domain identified by the static approach.

III.2.3 Kinematic approach of the potential safe loads

The kinematic approach is derived by dualizing the static approach through the principle of virtual work, thus ensuring full mechanical consistency, and leading to upper estimates of the extreme loads. This approach presents an exterior approximation K^{kin} of the domain of the potential safe loads K (see Figure III.5).

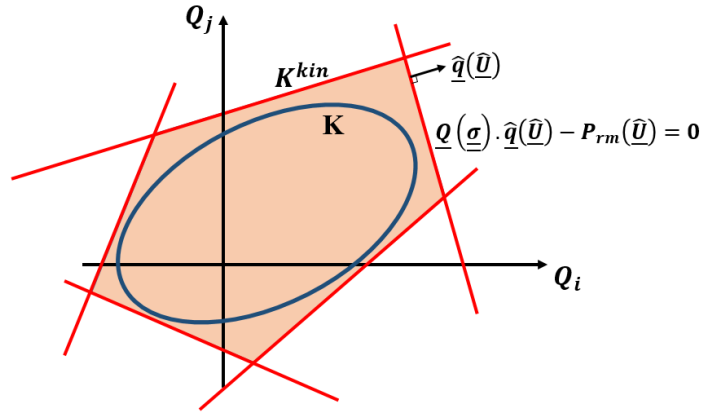


Figure III.5: Potential safe loads domain identified by the kinematic approach.

Based on the principle of virtual work, the virtual velocity field $\underline{\hat{U}}$ on Ω and $\partial\Omega$ has to be piecewise continuous and continuously differentiable. The set of virtual motions of the system is a vector space. Therefore, the strain rate field $\underline{\hat{d}}$ is defined from the gradient of $\underline{\hat{U}}$, as shown below:

$$\underline{\hat{d}}(\underline{x}) = \frac{1}{2} \left(\underline{\underline{grad}} \underline{\hat{U}}(\underline{x}) + {}^t \underline{\underline{grad}} \underline{\hat{U}}(\underline{x}) \right) \quad (\text{III.12})$$

In presence of discontinuities in a surface denoted by Γ (Figure III.6), this surface is a jump surface for the field $\underline{\hat{U}}$, and the discontinuity at point \underline{x} on the surface Γ following the outward normal $\underline{n}(\underline{x})$ is expressed as:

$$\llbracket \underline{\hat{U}}(\underline{x}) \rrbracket = \underline{\hat{U}}^2(\underline{x}) - \underline{\hat{U}}^1(\underline{x}) \quad (\text{III.13})$$

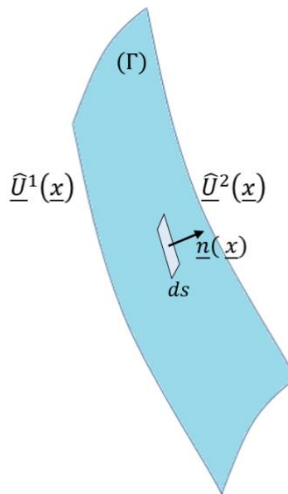


Figure III.6: Discontinuous virtual velocity field.

Under the assumption that the virtual velocity field $\underline{\hat{U}}$ is kinematically admissible with the boundary conditions on $\partial\Omega$, a generalized virtual velocity vector $\underline{\hat{q}}$ of the system can be introduced, which is dually associated with the vector of loading \underline{Q} . Hence, the virtual work by all the external forces developed in the virtual velocity field $\underline{\hat{U}}$ is expressed as:

$$P_{ext}(\underline{\hat{U}}) = \underline{Q} \cdot \underline{\hat{q}} \quad (III.14)$$

The principle of virtual work allows to reformulate the equilibrium equations in a dualised form, by providing the equality of the virtual work of external efforts $P_{ext}(\underline{\hat{U}})$ and the virtual work of deformation $P_d(\underline{\hat{U}})$. It can be expressed as:

$$\left\{ \begin{array}{l} \forall \underline{\underline{\sigma}} \text{ statically admissible with } \underline{Q} \Leftrightarrow \forall \underline{\hat{U}} \text{ kinematically admissible with } \underline{\hat{q}} \\ P_{ext}(\underline{\hat{U}}) = P_d(\underline{\hat{U}}) \Rightarrow \\ \underline{Q}(\underline{\underline{\sigma}}) \cdot \underline{\hat{q}}(\underline{\hat{U}}) = \int_{\Omega} \underline{\underline{\sigma}}(\underline{x}) : \underline{\hat{d}}(\underline{x}) \, d\Omega + \int_{\Gamma} (\underline{\underline{\sigma}}(\underline{x}) \cdot \llbracket \underline{\hat{U}}(\underline{x}) \rrbracket) \underline{n}(\underline{x}) \, ds \end{array} \right. \quad (III.15)$$

The equilibrium Equation (III.15) identifies the maximum resisting work, which is the maximum value of the virtual work of deformation considering the strength criteria of materials at each point of the system. Hence the maximum resisting work $P_{rm}(\underline{\hat{U}})$ can be expressed as:

$$P_{rm}(\underline{\hat{U}}) = \int_{\Omega} \pi(\underline{\hat{d}}(\underline{x}), \underline{x}) \, d\Omega + \int_{\Gamma} \pi(\underline{n}(\underline{x}), \llbracket \underline{\hat{U}}(\underline{x}) \rrbracket) \, ds \quad (III.16)$$

where π is the support function of $G(\underline{x})$, and it is expressed as:

$$\begin{aligned} \pi(\underline{\hat{d}}(\underline{x}), \underline{x}) &= \sup \{ \underline{\underline{\sigma}}(\underline{x}) : \underline{\hat{d}}(\underline{x}) \mid \underline{\underline{\sigma}}(\underline{x}) \in G(\underline{x}) \} \\ \pi(\underline{n}(\underline{x}), \llbracket \underline{\hat{U}}(\underline{x}) \rrbracket) &= \sup \{ \underline{\underline{\sigma}}(\underline{x}) \cdot \underline{n}(\underline{x}) \cdot \llbracket \underline{\hat{U}}(\underline{x}) \rrbracket \mid \underline{\underline{\sigma}}(\underline{x}) \in G(\underline{x}) \} \end{aligned} \quad (III.17)$$

Based on Equations III.9, III.15, III.16 and III.17, the potential safe loads of the kinematic approach K^{kin} can be identified according to the following condition:

$$\underline{Q} \in K^{kin} \Leftrightarrow \forall \underline{\hat{U}} \text{ kinematically admissible with } \underline{\hat{q}}, P_{ext}(\underline{Q}, \underline{\hat{q}}) \leq P_{rm}(\underline{\hat{U}}) \quad (III.18)$$

In practice, the potential safe loads K for a virtual velocity field $\underline{\hat{U}}$ is a subset of the half-space that contains the origin, and delimited by the hyperplane of the equation:

$$\underline{Q}(\underline{\sigma}) \cdot \hat{q}(\hat{U}) - P_{rm}(\hat{U}) = 0 \quad (\text{III.19})$$

By considering different fields of virtual velocity \hat{U} (failure mechanism), a convex domain K^{kin} can be obtained by the intersection of many half-spaces, which is a superset of the domain of the potential safe loads K . Thus, the domain K^{kin} represents an exterior approximation of K as shown in Figure III.5.

III.3 NUMERICAL MODELLING OF YIELD DESIGN APPROACH

III.3.1 Components of the yield design implementation

The numerical implementation of the yield design approach is based on four principal components: the mechanical model, the yield criterion, the discretization model, and some optimization techniques. The mechanical model depends on the structure and its structural components, where the model can consist of bar, beam, or shell elements. The chosen mechanical model influences the numerical equilibrium equations and the yield criteria of elements.

The yield criterion of the constitutive materials represents the resistance capacity at a local scale. Besides, the yield criterion can be generalized to the structural element, which allows to simplify the structural modelling in a global scale. The estimation of the macroscopic yield criterion of an element is based on the microscopic yield criteria of the constitutive materials, and the geometric shape of the element cross-section.

The numerical modelling also depends on the choice of the discretization model, that is related to the method for generating a finite set of statically admissible internal forces, or the kinematically admissible virtual velocity fields.

To approximate the ultimate load by some lower and upper bounds, the choice of the optimization techniques has an essential role in the efficiency of the approximation procedure. Generally, the static approach requires the maximization of a variable parameter with solving a linear optimization problem under non-linear convex constraints. Conversely, the kinematic approach requires the minimization of a variable parameter with solving a non-linear convex optimization problem under linear constraints. These aspects are further described for a beam element and illustrated in the following sections.

III.3.2 Yield criterion characterization for a beam element cross-section

The model proposed by Bleyer and de Buhan (2013) is used herein to identify and calculate the yield criteria for frame members infinitely resistant with respect to shear effects as well as torsion. The model then considers that the element is infinitely resistant with respect to shear and torsion forces. Hence, the yield criterion is identified in the 3D space involving axial force N and the bending moments M_y and M_z . The beam cross-section S consists of several subsections S_i (Figure III.7), where each subsection represents one type of material. Furthermore, the yield criterion for each type of materials is defined through the corresponding strength domain G_i . The bonding between the subsections is considered as perfect.

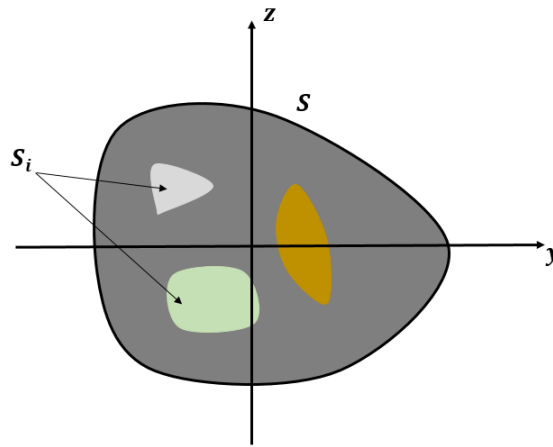


Figure III.7: Different subsections for a beam cross-section.

The aim thereafter is to identify a generalized yield surface G , which represents the potential safe forces of the beam cross-section by taking into account the interaction between axial force and bending moments. In this respect, the auxiliary yield design problem is defined on a representative segment of length L of the composite beam, as shown in Figure III.8. The assumptions of the model are detailed below:

- the body forces are considered null,
- the lateral boundary $\partial\Omega_{lat}$ is stress free,

$$\underline{\underline{\sigma}} \cdot \underline{\underline{n}} = \underline{\underline{0}} \quad \text{on } \partial\Omega_{lat} \quad (\text{III.20})$$

- at $x = 0$, the contact is smooth with a fixed vertical plane,

$$U_x(x = 0, y, z) = 0 \quad (\text{III.21})$$

$$\sigma_{xy}(x = 0, y, z) = \sigma_{xz}(x = 0, y, z) = 0 \quad (\text{III.22})$$

- at $x = L$, the contact is smooth with a plane rotating about $\Delta = \{(y, z) | \delta - z\chi_y - y\chi_z = 0\}$, where δ is the axial extension and χ_y and χ_z are the curvatures around y and z axes, respectively.

$$U_x(x = L, y, z) = \delta - z\chi_y - y\chi_z \quad (\text{III.23})$$

$$\sigma_{xy}(x = L, y, z) = \sigma_{xz}(x = L, y, z) = 0 \quad (\text{III.24})$$

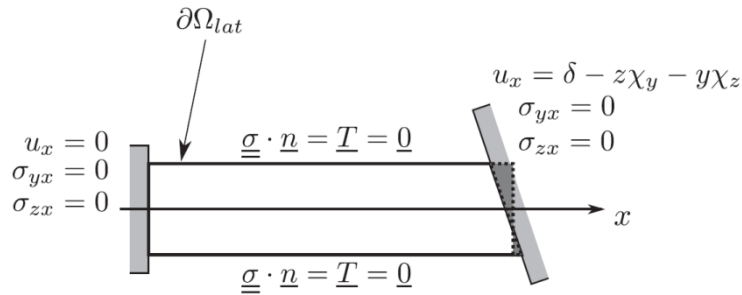


Figure III.8: Auxiliary yield design problem (Bleyer and de Buhan, 2013).

The normal force and bending moments are expressed as:

$$\begin{cases} N = \int_{S(x=L)} \sigma_{xx} dS \\ M_y = - \int_{S(x=L)} z \sigma_{xx} dS \\ M_z = - \int_{S(x=L)} y \sigma_{xx} dS \end{cases} \quad (\text{III.25})$$

The virtual work of external efforts $P_{ext}(\hat{\underline{u}})$ of any virtual kinematically admissible velocity field $\hat{\underline{u}}$ is described below:

$$\begin{cases} P_{ext}(\hat{\underline{u}}) = \int_{\partial\Omega} \underline{n} \cdot \underline{\underline{\sigma}} \cdot \hat{\underline{u}} dS \\ = \delta \int_{S(x=L)} \sigma_{xx} dS + \chi_y \left(- \int_{S(x=L)} z \sigma_{xx} dS \right) \\ + \chi_z \left(- \int_{S(x=L)} y \sigma_{xx} dS \right) \end{cases} \quad (\text{III.26})$$

Based on Equation (III.25), the Equation (III.26) can be expressed as :

$$P_{ext}(\hat{u}) = \delta N + \chi_y M_y + \chi_z M_z \quad (\text{III.27})$$

where, this equation allows to interpret in duality the generalized strain (δ, χ_y, χ_z) and stress (N, M_y, M_z) variables.

One considers herein the case of a steel cross-section IPE360, where the geometric details are described in Figure III.9(a) (ArcelorMittal, 2018). The conditions of the beam are assumed according to the Euler-Bernoulli beam theory, and the materials are described by a uniaxial constitutive law. The cross-section S is subdivided into subsections S_i (see Figure III.9-b) and the local yield criterion G_i , which defines each subsection S_i and corresponds to the material of the subsection, is described by a simple uniaxial condition for the normal force, where the ultimate strength in tension and compression is denoted by σ_t^i and σ_c^i , respectively. Furthermore, the stress field is assumed uniaxial as described below:

$$\underline{\sigma} = \begin{cases} \sigma_t^i \underline{e}_x \otimes \underline{e}_x & \text{if } \delta - z\chi_y - y\chi_z > 0 \text{ and } (y, z) \in S_i \\ -\sigma_c^i \underline{e}_x \otimes \underline{e}_x, & \text{if } \delta - z\chi_y - y\chi_z < 0 \text{ and } (y, z) \in S_i \end{cases} \quad (\text{III.28})$$

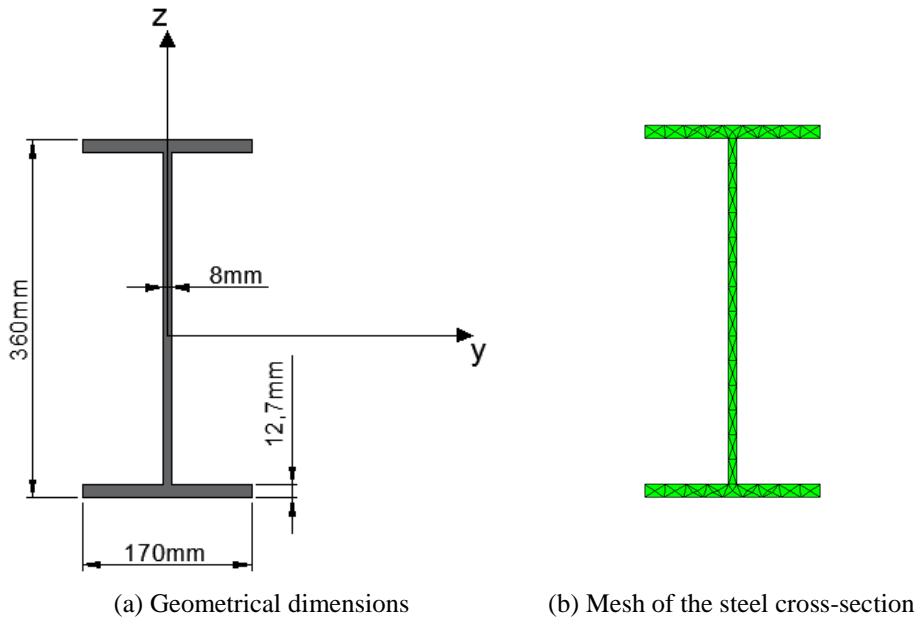


Figure III.9: I-shaped cross-section steel beam IPE360.

The yield surface is identified by considering that the stress field reaches the ultimate strength of the material, either in tension and compression. Then, the yield surface G_u is described as follow:

$$(N, M_y, M_z) \in G_S \Leftrightarrow \exists (\delta, \chi_y, \chi_z) \begin{cases} N = \sum_i \left(\int_{S_i^+} \sigma_t^i dS - \int_{S_i^-} \sigma_c^i dS \right) \\ M_y = \sum_i \left(\int_{S_i^-} z \sigma_c^i dS - \int_{S_i^+} z \sigma_t^i dS \right) \\ M_z = \sum_i \left(\int_{S_i^-} y \sigma_c^i dS - \int_{S_i^+} y \sigma_t^i dS \right) \end{cases} \quad (\text{III.29})$$

where $S_i^+ = S_i \cap \{\delta - z\chi_y - y\chi_z > 0\}$ and $S_i^- = S_i \cap \{\delta - z\chi_y - y\chi_z < 0\}$.

Based on the duality of the generalized strain (δ, χ_y, χ_z) and stress (N, M_y, M_z) in Equation (III.29), the support function of G_u is defined as below:

$$\pi_{G_u}(\delta, \chi_y, \chi_z) = \sup_{(N, M_y, M_z) \in G_u} \{\delta N + \chi_y M_y + \chi_z M_z\} \quad (\text{III.30})$$

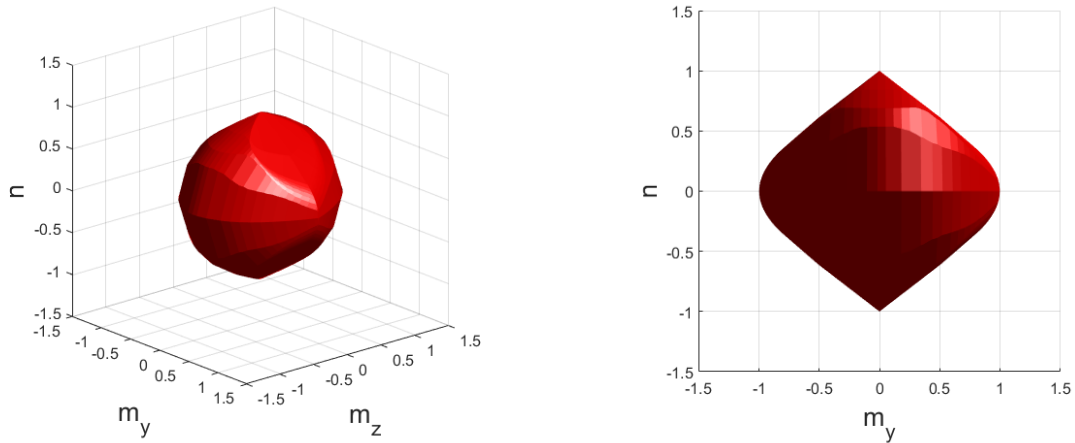
Then, Equation (III.30) can be described as follow:

$$\pi_{G_u}(\delta, \chi_y, \chi_z) = \sum_i \int_{S_i} \sup\{\sigma_t^i(\delta - z\chi_y - y\chi_z); -\sigma_c^i(\delta - z\chi_y - y\chi_z)\} dS \quad (\text{III.31})$$

The dual formulation (III.31) allows the identification of the yield surface by taking into account the interaction between the forces (N, M_y, M_z) , as shown in Figure III.10. For better graphical representation, the yield surface is presented in the non-dimensional space (n, m_y, m_z) defined below:

$$\begin{cases} n = \frac{N}{N_0} ; & N_0 = \frac{|\min(N)| + |\max(N)|}{2} \\ m_y = \frac{M_y}{M_{y0}} ; & M_{y0} = \frac{|\min(M_y)| + |\max(M_y)|}{2} \\ m_z = \frac{M_z}{M_{z0}} ; & M_{z0} = \frac{|\min(M_z)| + |\max(M_z)|}{2} \end{cases} \quad (\text{III.32})$$

In the following of this manuscript, the yield surface is always shown in this way by indicating the values of N_0, M_{y0} and M_{z0} .



(a) View in (n, m_y, m_z) non-dimensional space (b) View in (n, m_y) non-dimensional space

$$\begin{aligned}
 N &= n * N_0; N_0 = 2,483.0 \text{ kN} \\
 M_y &= m_y * M_{y0}; M_{y0} = 346.0 \text{ kN.m} \\
 M_z &= m_z * M_{z0}; M_{z0} = 76.3 \text{ kN.m}
 \end{aligned}$$

Figure III.10: Yield surface of a IPE360 steel beam cross-section.

To check the local resistance of structural components in a global structure, there is a need to describe the yield surface by an analytical formula. Therefore, Bleyer and de Buhan (2013) proposed to use a Minkowski sum of ellipsoids, that enables to obtain a simple description of the yield surface with few parameters, where the sum of two sets A and B is noted $A \oplus B$, and it is defined as:

$$A \oplus B = \{c | \exists (a, b) \in A \times B \text{ such that } c = a + b\} \quad \text{(III.33)}$$

The support function of an ellipsoid $\varepsilon(\underline{\underline{Q}}, \underline{\underline{q}})$ can be described as:

$$\pi_\varepsilon(\underline{\underline{d}}) = \sqrt{{}^T \underline{\underline{d}} \cdot \underline{\underline{Q}} \cdot \underline{\underline{d}}} + {}^T \underline{\underline{q}} \cdot \underline{\underline{d}} \quad \text{(III.34)}$$

where $\underline{\underline{Q}}$ is a symmetric positive semi-definite matrix that defines the orientation of the ellipsoid and the length of its axis, and $\underline{\underline{q}}$ represents the coordinates of the ellipsoid center. The support function $\pi_\varepsilon(\underline{\underline{d}})$ can also be described as follows:

$$\pi_\varepsilon(\underline{\underline{d}}) = \left\| \underline{\underline{J}} \cdot \underline{\underline{d}} \right\| + {}^T \underline{\underline{q}} \cdot \underline{\underline{d}} \quad \text{(III.35)}$$

where $\underline{\underline{J}}$ is the Cholesky factorization of matrix $\underline{\underline{Q}}$ ($\underline{\underline{Q}} = {}^T \underline{\underline{J}} \cdot \underline{\underline{J}}$). In the case of two ellipsoids $\varepsilon_1(\underline{\underline{Q}}_1, \underline{\underline{q}}_1)$ and $\varepsilon_2(\underline{\underline{Q}}_2, \underline{\underline{q}}_2)$, the sum is defined by:

$$\pi_{\varepsilon_1 \oplus \varepsilon_2}(\underline{d}) = \pi_{\varepsilon_1}(\underline{d}) + \pi_{\varepsilon_2}(\underline{d}) = \left\| \underline{J}_1 \cdot \underline{d} \right\| + \left\| \underline{J}_2 \cdot \underline{d} \right\| + {}^T(\underline{q}_1 + \underline{q}_2) \cdot \underline{d} \quad (\text{III.36})$$

The approximation of the yield surface G_u is equivalent to the approximation of its support function π_{G_u} in Equation (III.31), which can be implemented by the support function of a sum of n ellipsoids π_n , as described below:

$$\pi_{G_u}(\underline{d}) \approx \pi_n(\underline{d}) = \sum_{i=1}^n \left\| \underline{J}_i \cdot \underline{d} \right\| + {}^T \underline{q} \cdot \underline{d} \quad \forall \underline{d} = (\delta, \chi_y, \chi_z) \quad (\text{III.37})$$

where \underline{J}_i is the Cholesky factorization of matrix \underline{Q}_i of the ellipsoid $\varepsilon_i(\underline{Q}_i, \underline{q})$.

In order to solve this problem, Bleyer and de Buhan (2013) proposed to minimize the gap between the support functions $\pi_{G_u}(\underline{d})$ and $\pi_n(\underline{d})$ for M points \underline{d}_j belonging to the unit sphere in \mathbb{R}^3 . The coefficients of \underline{J}_i and \underline{q} are considered as an unknown vector $\chi \in \mathbb{R}^{6n+3}$ such that:

$$\underline{J}_i = \begin{bmatrix} \chi_{6i-5} & \chi_{6i-4} & \chi_{6i-3} \\ 0 & \chi_{6i-2} & \chi_{6i-1} \\ 0 & 0 & \chi_{6i} \end{bmatrix}; \underline{q} = \begin{cases} \chi_{6n+1} \\ \chi_{6n+2} \\ \chi_{6n+3} \end{cases} \quad (\text{III.38})$$

Then, the minimization problem is defined as:

$$\min_{\chi \in \mathbb{R}^{6n+3}} \sum_{j=1}^M \left(\pi_{G_u}(\underline{d}_j) - \sum_{i=1}^n \left\| \underline{J}_i \cdot \underline{d}_j \right\| + {}^T \underline{q} \cdot \underline{d}_j \right)^2 \quad (\text{III.39})$$

As Equation (III.39) corresponds to a general nonlinear least-square problem, a sequential quadratic programming (SQP) algorithm is used (Biggs, 1975; Han, 1977; Powell, 1978).

The approximation of yield surface π_{G_u} is realised in two different ways. The first one is an inscribed approximation (see Figure III.11) used for the static approach in the yield design calculation for the global structure (Section III.3.3). The following non-linear constraint is added to Equation (III.39):

$$\pi_{G_u}(\underline{d}_j) - \pi_n(\underline{d}_j) \geq 0 \quad (\text{III.40})$$

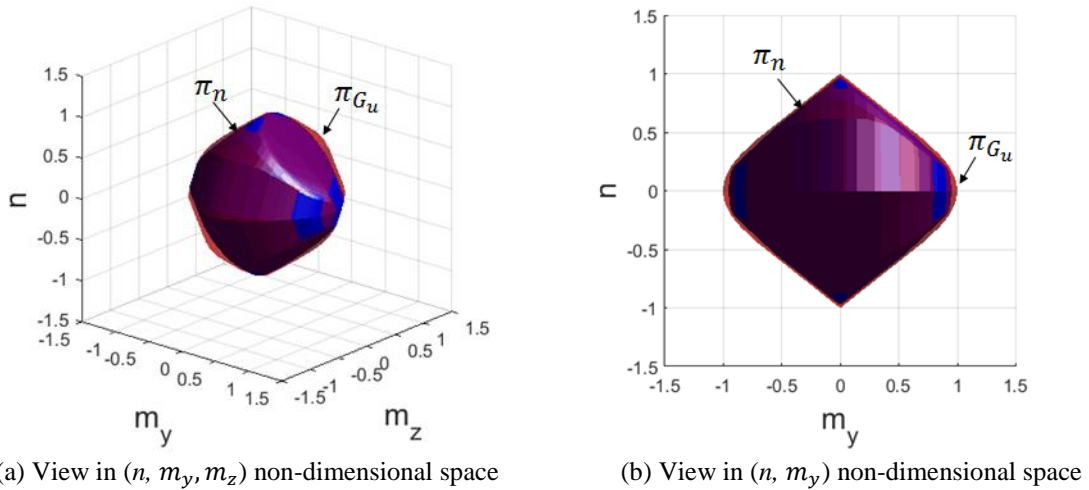


Figure III.11: Inscribed approximation of yield surface π_{G_u} .

The second way is a circumscribed approximation (see Figure III.12) used for the kinematic approach in the yield design calculation for the global structure (Section III.3.4), where the constraint is described as:

$$\pi_{G_u}(d_j) - \pi_n(d_j) \leq 0 \quad (\text{III.41})$$

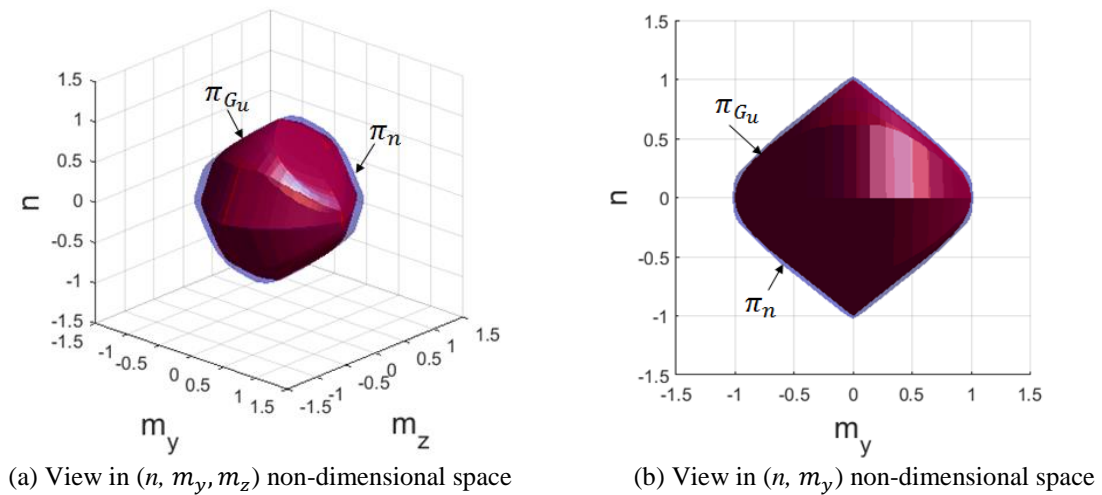


Figure III.12: Circumscribed approximation of yield surface π_{G_u} .

To evaluate the accuracy of the yield surface approximation by using the sum of ellipsoids method, an error index is considered to measure the gap between π_{G_u} and π_n for the M points d_j , as described below:

$$\epsilon(\pi_n)_j = \frac{|\pi_n(d_j) - \pi_{G_u}(d_j)|}{\pi_{G_u}(d_j) - \underline{q} \cdot \underline{d}_j} \quad (\text{III.42})$$

Then, the error index according to the L^∞ norm is defined as:

$$\|\epsilon(\pi_n)\|_\infty = \max_j(\epsilon(\pi_n)_j) \quad (\text{III.43})$$

The minimization problem in Equation (III.39) is solved by using a sequential quadratic programming (SQP), implemented in Matlab, with $M = 10,000$ points on the unit sphere (Byrd et al., 2000; Waltz et al., 2006).

With the aim to evaluate the effect of the number of ellipsoids on the yield surface approximation, a sensitivity analysis is done to study the variation of the error norms with the number of ellipsoids used in the approximation. As shown in Figure III.13, the error decreases with the number of ellipsoids. Error remains quite stable with more than five ellipsoids, and close to 5% with more than 6 ellipsoids. Moreover, the computation time of the yield criterion calculation increases according to the number of ellipsoids (see Figure III.14). In the following of this manuscript, six ellipsoids are systematically used for the yield surface inscribed and circumscribed approximations.

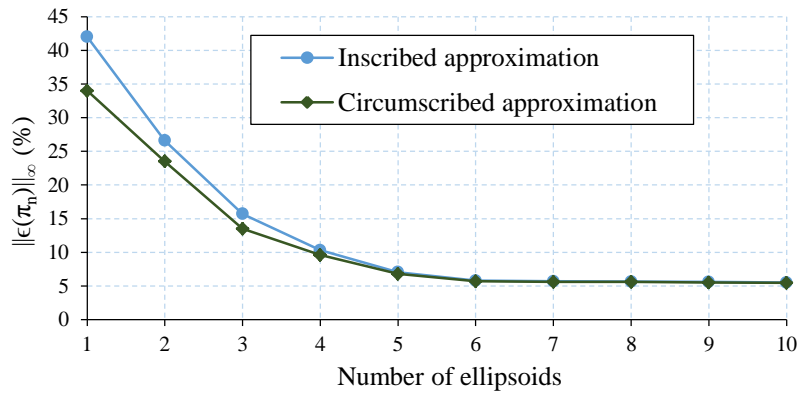


Figure III.13: Sensitivity analysis of the yield surface approximation to the number of ellipsoids for a steel beam cross-section (Figure III.9).

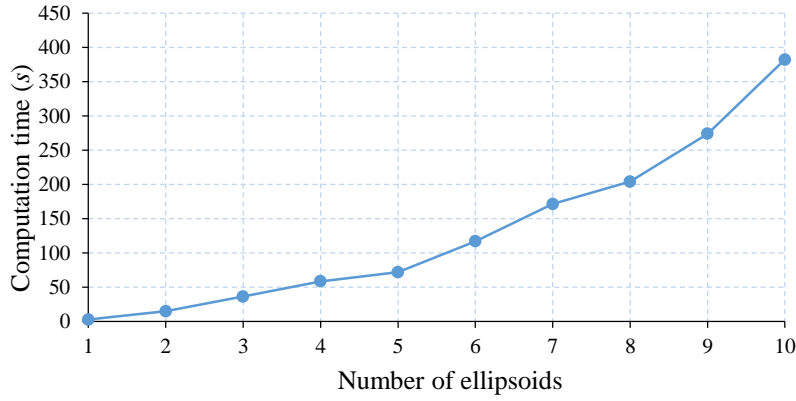


Figure III.14: Computation time of the yield criterion calculation according to the number of ellipsoids for the considered steel beam cross-section (Figure III.9).

III.3.3 Static approach for the global structure

The model of Bleyer and de Buhan (2013) is used to identify the ultimate capacity of the global structure, where the discretization by the 3D beam finite elements is applied on the structure. The classical two noded elements are used, with linear distribution of the bending moments M_y and M_z , the constant normal force N , and the torsional moment M_T . The local equilibrium verification on a finite element "e" is between the nodal stress variables ${}^T\underline{\Sigma}_e = (N, M_T, M_{y1}, M_{z1}, M_{y2}, M_{z2})$ and the forces of the beam element $\underline{f}_e = (f_{e,i})_{i=1,\dots,12}$ (see Figure III.15). The numerical expression of the equilibrium finite element is described below:

$$\underline{f}_e = \underline{h}_e \cdot \underline{\Sigma}_e \quad (\text{III.44})$$

where \underline{h}_e is the elementary equilibrium matrix.

Therefore, the verification of the equilibrium of the global structure is expressed by the following equation:

$$\underline{H} \cdot \underline{\Sigma} = \lambda \cdot \underline{F} + \underline{F}_0 \quad (\text{III.45})$$

where \underline{H} is the global equilibrium matrix, and $\underline{\Sigma}$ is the global vector of stress parameters. The term $\lambda \cdot \underline{F} + \underline{F}_0$ represents the external loads, where \underline{F}_0 is the dead load, and $\lambda \cdot \underline{F}$ is the multiplicative load used to identify the ultimate load.

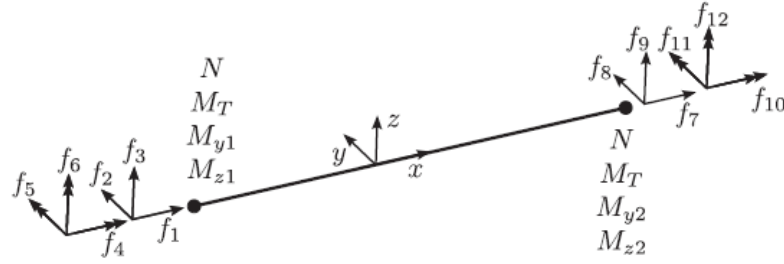


Figure III.15: Nodal stresses and forces of the finite beam element (Bleyer and de Buhan, 2013).

The verification of the yield criterion is processed at the nodes of each element "e" according to the following condition:

$$\underline{\sigma} \in G = \bigoplus_{i=1}^n \varepsilon_i(\underline{\tilde{J}}_i, 0) \oplus \underline{\tilde{q}} \quad (\text{III.46})$$

$$\text{in which } \underline{\tilde{J}}_i = \begin{bmatrix} 0 & 0 & 0 \\ \underline{J}_i & 0 & 0 \\ 0 & 0 & 0 \end{bmatrix}, \quad \underline{\tilde{q}} = \begin{Bmatrix} \underline{q} \\ 0 \end{Bmatrix} \quad (\text{III.47})$$

where ${}^T \underline{\sigma} = (N, M_y, M_z, M_T)$ is the generalized forces vector, and n is the number of ellipsoids. \underline{J}_i matrices and center vector \underline{q} are obtained from the inner approximation of the yield criterion. As torsion is not considered in calculation, the torsion strength has been penalised by the term $T_{pen} = 10^2 \times \max(\underline{J}_i)$.

The previous condition of Equation (III.46) can be numerically implemented using a standard form of a second-order cone programming (SOCP) constraints involving auxiliary variables τ_i (Bleyer and de Buhan, 2013), as expressed below:

$$\underline{\sigma} \in G \Leftrightarrow \exists \tau_1, \dots, \tau_n \quad s. t. \begin{cases} \underline{\sigma} = \underline{\tilde{J}}_1 \cdot \tau_1 + \dots + \underline{\tilde{J}}_n \cdot \tau_n + \underline{\tilde{q}} \\ \|\tau_i\| \leq 1 \quad \forall i = 1, \dots, n \end{cases} \quad (\text{III.48})$$

To identify the ultimate load in the static approach, one finds the maximum value of the load multiplier λ in Equation (III.45), by considering the yield criterion constraints in Equation (III.48). Therefore, the problem can be described as:

$$\lambda_s = \max \lambda; \text{ such that } \begin{cases} \underline{H} \cdot \underline{\Sigma} = \lambda \cdot \underline{F} + \underline{F}_0 \\ \underline{\Sigma} = \underline{J} \cdot \underline{\tau} + \underline{Q} \\ \|\underline{\tau}_{i,e}\| \leq 1 \forall i, e = 1, \dots, 2n \cdot N_e \end{cases} \quad (\text{III.49})$$

Furthermore, the buckling load on beam elements is also verified according to Euler load formulation (NF EN 1992-1-1, 2005), which is expressed as:

$$N_{Euler} = \frac{\pi^2 EI_{min}}{l_f^2} \quad (\text{III.50})$$

where EI_{min} is the minimum bending stiffness, and l_f is the effective length of the beam element. The boundary conditions of the element are considered as fixed. Hence, $l_f = 0.5l$, where l is the element length. It is worth to note that the Euler formula represents the capacity of a perfectly elastic column to resist flexural buckling under compression, as a function of its elastic stiffness (EI) and interaction with yielding (Zhao et al., 2005). This equation is considered in the following as a first approximation and further detailed interaction relationship between axial compression and bending should be used in future studies for beam-column elements.

III.3.4 Kinematic approach for the global structure

Each node of the finite element has 6 degrees of freedom, as shown in Figure III.16. The displacement vector is represented by u, v and w , which are the axial displacements along x , and the transversal displacements in directions y and z , respectively. Besides, the rotations around each axis are noted θ_x, θ_y and θ_z .

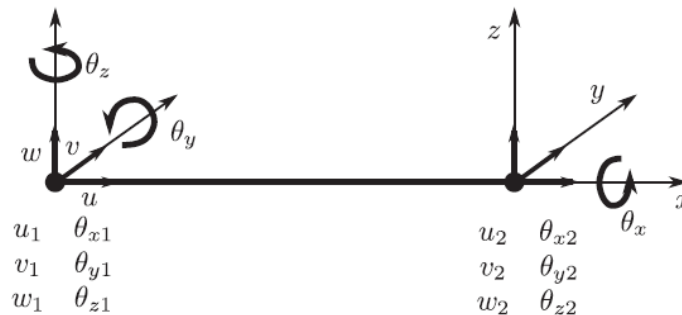


Figure III.16: Displacement finite element (Bleyer and de Buhan, 2013).

Based on the Euler-Bernoulli beam theory, one can identify the following parameters (Bleyer and de Buhan, 2013):

$$\left\{ \begin{array}{l} \text{rotation around y axis: } \theta_y = \frac{dw}{dx} \\ \text{rotation around z axis: } \theta_z = \frac{dv}{dx} \\ \text{curvature around y axis: } \chi_y = \frac{d^2w}{dx^2} \\ \text{curvature around z axis: } \chi_z = \frac{d^2v}{dx^2} \\ \text{axial extension: } \delta = \frac{du}{dx} \\ \text{torsion strain: } \omega = \frac{d\theta_x}{dx} \end{array} \right. \quad (\text{III.51})$$

In the following, the local yield criterion on each element is expressed by the following support function:

$$\pi(\delta, \chi_y, \chi_z, \omega) = \sum_{i=1}^n \left\| \underline{\tilde{J}}_i \cdot \underline{d} \right\| + {}^T \underline{\tilde{q}} \cdot \underline{d} \quad (\text{III.52})$$

The application of the kinematic approach is based on the identification of the work of external loads $P_{ext}(\underline{U})$ for a virtual displacement field \underline{U} kinematically admissible, and of the maximum resisting work $P_{rm}(\underline{U})$. These works are expressed as (Bleyer and de Buhan, 2013) :

$$P_{ext}(\underline{U}) = \lambda^T \underline{F} \cdot \underline{U} + {}^T \underline{F}_0 \cdot \underline{U} \quad (\text{III.53})$$

$$P_{rm}(\underline{U}) = \int_{\Omega} \pi(d[\underline{U}]; x) d\Omega \quad (\text{III.54})$$

where $d[\underline{U}]$ is the strain vector related to \underline{U} at point x . The ultimate load in the kinematic approach is identified according to the following minimization problem:

$$\lambda_k = \min_{\tau_{\underline{F}, \underline{U}}=1} \left(P_{rm}(\underline{U}) - {}^T \underline{F}_0 \cdot \underline{U} \right) \quad (\text{III.55})$$

The kinematic approach is implemented according to a standard SOCP problem. Due to the non-linearity of the local support functions, the integration at the element level has to be performed using a Gaussian quadrature rule with m points $\xi_g \in [-1; 1]$ for $g = 1, \dots, m$. Therefore, the maximum resisting work $P_{rm}(\underline{U})$ is expressed as:

$$P_{rm} = \sum_{e=1}^{N_e} \sum_{g=1}^m c_{e,g} \left(\sum_{i=1}^n \left\| \underline{R}_{i,g,e} \cdot \underline{U}_e \right\| + {}^T \underline{\tilde{q}} \cdot \underline{B}_e(\xi_g) \cdot \underline{U}_e \right) \quad (\text{III.56})$$

where $c_{e,g}$ are some weighting coefficients coming from the quadrature rule, and $\underline{\underline{R}}_{j,g,e} = \underline{\underline{J}}_i \cdot \underline{\underline{B}}_e(\xi_g)$. Furthermore, one introduces the following auxiliary variables $\underline{\underline{r}}_{j,g,e} = \underline{\underline{R}}_{j,g,e} \cdot \underline{\underline{U}}_e$, and $t_{i,g,e} = \|\underline{\underline{r}}_{j,g,e}\|$. Therefore, the minimization problem for the kinematic approach is described as below:

$$\left\{ \begin{array}{l} \lambda_k = \min \sum_{e=1}^{N_e} \sum_{g=1}^m c_{e,g} \left(\sum_{i=1}^n t_{i,g,e} + {}^T \underline{\underline{q}} \cdot \underline{\underline{B}}_e(\xi_g) \cdot \underline{\underline{U}}_e \right) - {}^T \underline{\underline{F}}_D \cdot \underline{\underline{U}} ; \\ \text{such that } \begin{cases} {}^T \underline{\underline{F}} \cdot \underline{\underline{U}} = 1 & \forall i = 1, \dots, n \\ \underline{\underline{r}}_{j,g,e} = \underline{\underline{R}}_{j,g,e} \cdot \underline{\underline{U}}_e & \forall e = 1, \dots, m \\ t_{i,g,e} \geq \|\underline{\underline{r}}_{j,g,e}\| & \forall g = 1, \dots, N_e \end{cases} \end{array} \right. \quad (\text{III.57})$$

III.3.5 Illustration on a simple beam case study and comparison with a non-linear static analysis

In this section, the comparison of the yield design calculation previously introduced with a non-linear static analysis is illustrated on a simple case study which is a steel beam element with different boundary conditions: (i) pinned supports at both ends (B1), (ii) one pinned support and roller support (B2), and (iii) fixed supports at both ends (B3). More precisely, the beam is an I-shaped cross-section steel beam IPE360 where the cross-section details are those of the example considered in Section III.3.2. It is noted that the computations in this dissertation are all performed using a workstation with six cores Intel Xeon processors and 32 GB of RAM.

The MATLAB toolbox FEDEASLab (Filippou and Constantinides, 2004) is used to apply the non-linear static analysis, where the multilayer approach is applied in the structural modelling. The choice of this approach is based on (i) the possibility to take into account the geometrical and material non-linearities with providing local information about the state of section and materials, and (ii) the computation cost of this method which is lower than with a local approach (see Section II.3.3.1.3). FEDEASLab enables to study the response of a 2D beam element with distributed inelasticity under non-linear geometry (Spacone et al., 1996). The essential assumptions are those of the Bernoulli beam theory, where the plan sections remain plane and normal to the longitudinal axis during the element deformation history, which is acceptable for small axial strains. Besides, the shear effects are neglected, which is an acceptable assumption for medium to large span to depth ratios of the member. Moreover, the non-linear analysis in this manuscript is performed by using the imposed displacement method, where the displacement increment enables to control structural behaviour close to the collapse and prevent the frame from drifting apart suddenly in the ultimate state (Natal, 2014).

The numerical solution of geometrically non-linear frame problems is generally based on either a total Lagrangian, an updated Lagrangian, or a corotational formulation. In the total Lagrangian formulation, the reference system is the original undeformed element configuration. In the updated Lagrangian formulation, the last computed deformed configuration is adopted as the reference system. The corotational formulation is in fact a total Lagrangian formulation (Le et al., 2011; Le, 2013; Le et al., 2014) in which one separates rigid-body modes from local deformations, using as reference, a single coordinate system that continuously translates and rotates with the element as the deformation proceeds (Magalhães de Souza, 2000). The concept of corotational approach is then to separate the rigid body modes from element deformations by attaching a reference coordinate system (local system) to the element as it deforms (Le et al., 2014). The beam element potentially does three things: rotation, translation and deformation. During the rigid body motion that concerns the rotation and translation of element, the deformational motion is measured in the local coordinate system (see Figure III.17), where this system is attached to the element and has the same rotation and translation (Alsafadie et al., 2011).

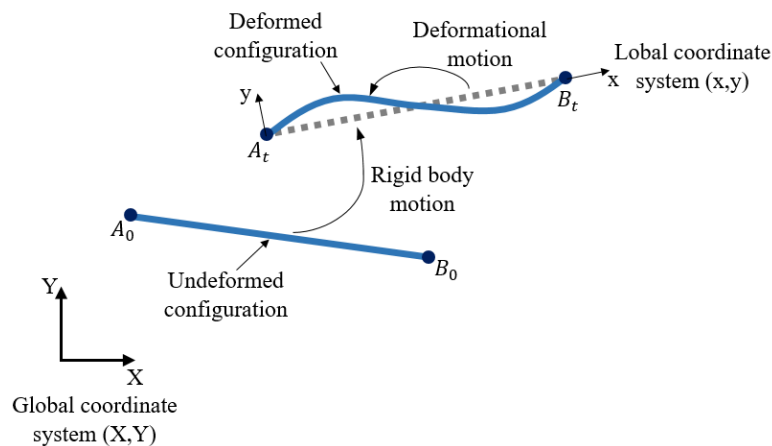


Figure III.17: Corotational kinematics of a beam element.

The corotational formulation, when compared to the Total Lagrangian and Updated formulation, has good convergence properties for large displacement and large rotation, but small strain problems (Li et al., 2008). Such formulation is chosen in this dissertation to take into account the geometrical non-linearities (using the FEDEASLab toolbox that integrates the effect of the large displacements and rotations). For the examples considered in the following, the constitutive law of materials in the non-linear analysis is assumed as elastic-plastic bilinear, and the hardening modulus is zero. Such assumption is considered in the non-linear analysis with a view to be compatible with the yield design calculation. In the steel beam example, the non-linear analysis is performed by considering two different assumptions to show their effects on the structural response. The first case considers that the steel is elastic perfectly plastic without any corotational formulation, so the geometrical non-linearities are

not taken into account (NL1). The assumptions with NL1 are those adopted in the yield design theory. The second case considers the geometrical non-linearities within a corotational formulation (NL2). Figure III.18 describes the constitutive law of steel under assumptions NL1 and NL2, where the structural steel is S355 with Young modulus $E = 210 \text{ GPa}$, and yield strength $f_y = 355 \text{ MPa}$. The material behaviour is elastic for strain value between zero and the yield strain value ($\varepsilon \in [0; \varepsilon_y]$), while it is perfectly plastic when $\varepsilon > \varepsilon_y$, so the yield strength remains unchanged during deformation.

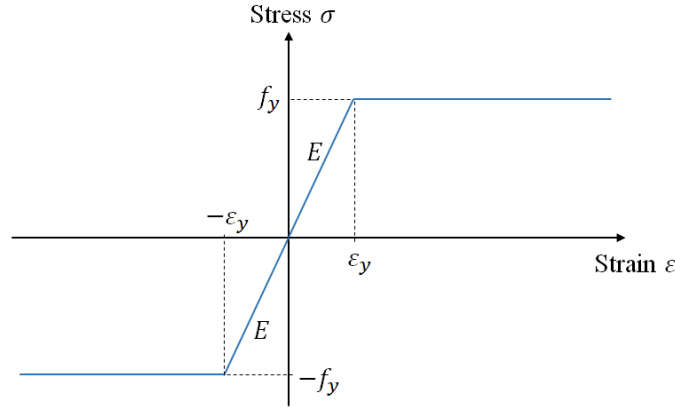


Figure III.18: Constitutive law of steel in the non-linear static approach under the assumptions NL1 and NL2.

III.3.5.1 Configuration B1 with pinned supports at both ends

The 6-meter span is exposed to a uniform load Q (see Figure III.19). In this example, the ultimate load can be calculated analytically. The distribution of the bending moment and shear forces under load Q is shown in Figure III.20 for configuration B1. The maximum bending moment $M_{max}(Q) = 4.5Q \text{ kN.m}$ and shear force $V_{max}(Q) = 3Q \text{ kN}$. Besides, the bending and shear resistance are calculated below (NF EN 1993-1-1, 2005):

$$M_{pl,a} = W_{pl}f_y = (0.9737 * 10^6 \text{ mm}^3) * (355 \text{ MPa}) = 345.7 \text{ kN.m} \quad (\text{III.58})$$

$$V_{pl,a} = A_v \left(\frac{f_y}{\sqrt{3}} \right) = (2.68 * 10^3 \text{ mm}^2) * \left(\frac{355}{\sqrt{3}} \right) = 548.6 \text{ kN} \quad (\text{III.59})$$

where $M_{pl,a}$ = bending resistance, W_{pl} = plastic section modulus, $V_{pl,a}$ = shear resistance, and A_v = shear area. Therefore, the ultimate load (calculated analytically) that the beam can support in configuration B1 is $Q_{u,a}^{B1} = 76.8 \text{ kN/m}$.

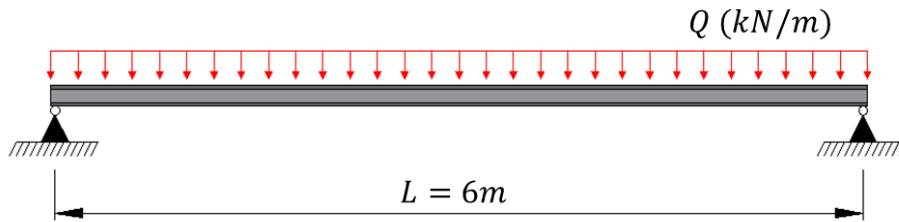


Figure III.19: Steel beam element with pinned supports at the ends (configuration B1).

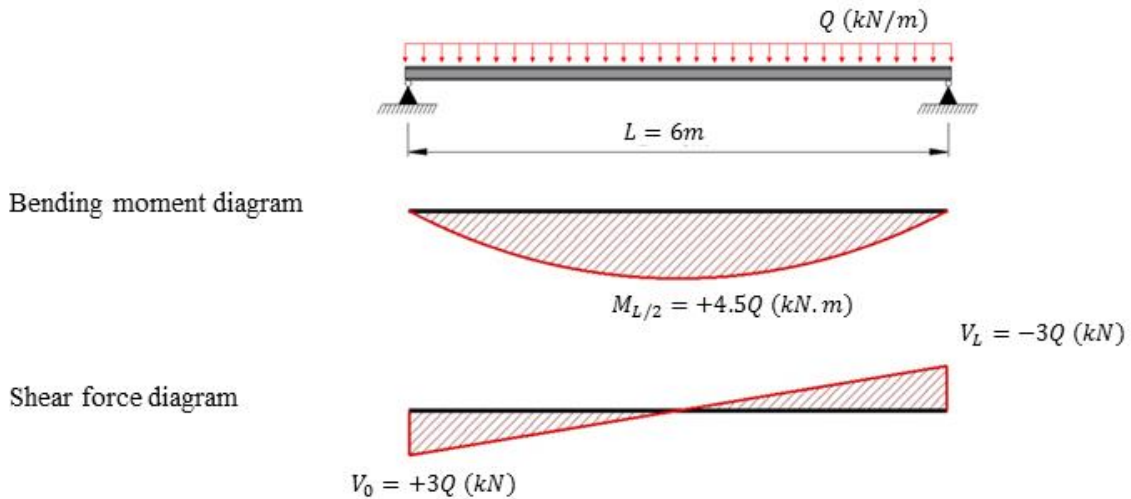


Figure III.20: Shear force and bending moment diagrams of the steel beam element (configuration B1).

The ultimate load is now calculated by the yield design approach. Figure III.10 shows that the bending resistance $M_{pl,yd} = 346.0 \text{ kN.m}$ which is almost equal to the value calculated in Equation (III.58).

The inscribed and circumscribed approximations of the yield criterion are realised by using the sum of 6 ellipsoids as explained in Section III.3.2. The inscribed approximation is used to identify the ultimate load by the static approach, which is denoted $Q_{u,s}$, according to the maximization problem in Equation (III.49). The ultimate load identified by the kinematic approach is denoted $Q_{u,k}$, and it is identified according to the minimization problem in Equation (III.57), with using the circumscribed approximation of the yield criterion. The obtained ultimate loads are $Q_{u,s}^{B1} = 76.5 \text{ kN/m}$ and $Q_{u,k}^{B1} = 76.9 \text{ kN/m}$, respectively, which are lower and upper bounds close to the actual ultimate load.

The static approach allows to identify the distribution of forces, where it indicates that the beam reaches the bending resistance $M_{pl,yd} = 346.0 \text{ kN.m}$ at mid-span under the ultimate load $Q_{u,s}^{B1}$ (Figure III.21). The kinematic approach allows to identify the failure mechanism shown in Figure III.22, exhibiting a plastic hinge at mid-span.



Figure III.21: Bending moment according to the static approach of yield design calculation (configuration B1).

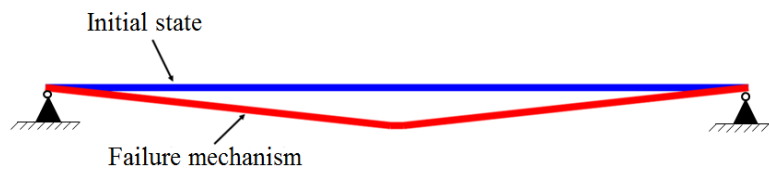


Figure III.22: Failure mechanism according to the kinematic approach of yield design calculation (configuration B1).

The profiles of uniform load, normal force and bending moment at mid-span are now shown in Figure III.23, Figure III.24 and Figure III.25, respectively, each time using the non-linear static analysis with assumption NL1 or NL2.

Under assumption NL1, which corresponds to the assumption of the yield design theory, the ultimate load $Q_{u,NL1}^{B1} = 76.6 \text{ kN/m}$ (Figure III.23-a) is very close to the analytical value and between the two bounds $Q_{u,S}^{B1}$ and $Q_{u,k}^{B1}$. With NL2, the structural response is very similar to the linear response until the deflection at the mid-span $\delta_{L/2} = 0.07 \text{ m}$ (Figure III.23-b). Then the capacity of the beam starts to increase in a remarkable manner when $\delta_{L/2} > 0.07 \text{ m}$, resulting from the developing of the membrane effect. Figure III.24(b) shows the development of the membrane effect in the beam, where the bending moment increases in the elastic domain with a slight increment of the normal force. Then a plastic hinge appears in the middle of the beam under bending moment $M_{y,L/2}^{NL2} = 343 \text{ kN.m}$, which is lower than the one with NL1 ($M_{y,L/2}^{NL1} = 345.8 \text{ kN.m}$), because of the correlation between the normal force and the bending moment. In contrast, Figure III.24(a) shows that there is no increment in the normal force when the corotational formulation is not integrated in the analysis (assumption NL1), and that the bending moment remains stable when $\delta_{L/2} > 0.06 \text{ m}$, as shown in Figure III.25(a). The bending moment $M_{y,L/2}^{NL2}$ under assumption NL2 stabilizes when $0.06 \text{ m} < \delta_{L/2} < 0.12 \text{ m}$ (Figure III.25-b), then it decreases with the development of normal force.

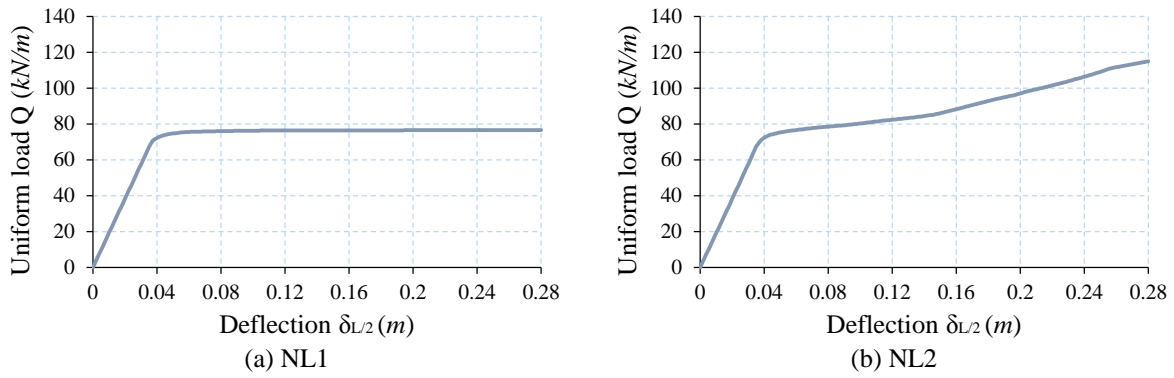


Figure III.23: Load-deflection diagram of non-linear static analysis of the steel beam element (configuration B1).

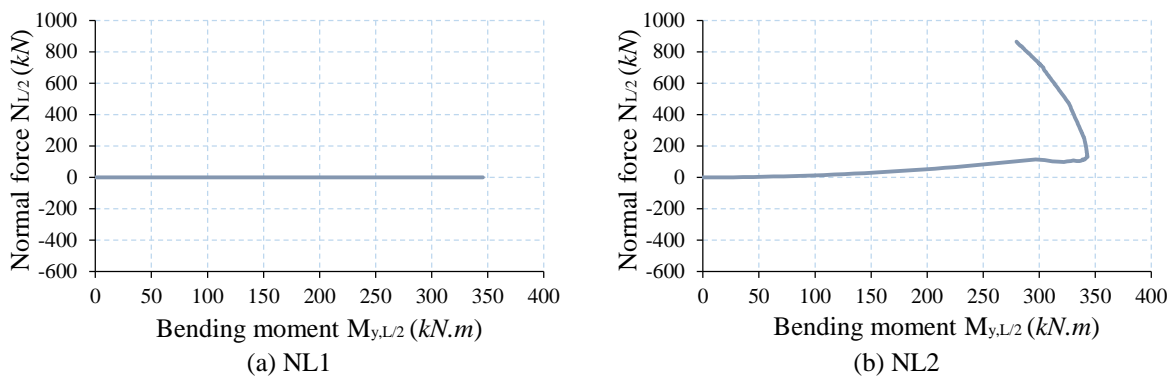


Figure III.24: Bending moment and normal forces diagram at the mid-span of the steel beam element (configuration B1).

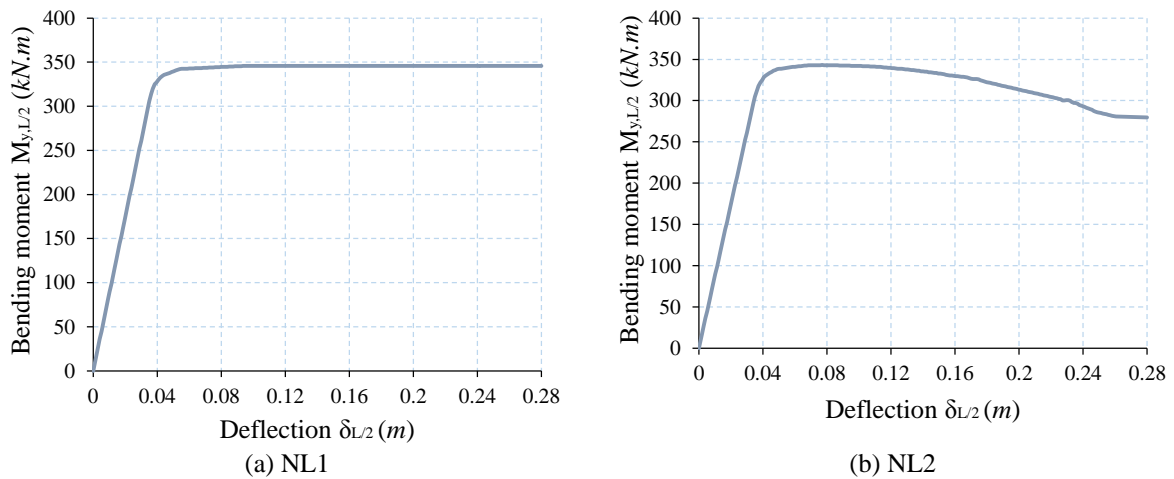


Figure III.25: Bending moment and deflection diagram at the mid-span of the steel beam element (configuration B1).

III.3.5.2 Configuration B2 with one pinned support and one roller support

The second configuration B2 is shown in Figure III.26. As for configuration B1, the ultimate load identified by analytical analysis is $Q_{u,a}^{B2} = 76.8 \text{ kN/m}$, and those identified by

the yield design calculation are $Q_{u,s}^{B2} = 76.5 \text{ kN/m}$ (static approach) and $Q_{u,k}^{B2} = 76.9 \text{ kN/m}$ (kinematic approach).

The non-linear analysis NL1 for configuration B2 is similar to the one with configuration B1 (compare Figure III.27-a with Figure III.23-a). However, the analysis NL2 indicates that the beam cannot develop any tensile membrane action due to the unrestrained support (roller support). In particular, Figure III.27 (b) shows that the capacity of the beam with the corotational formulation (NL2) does not increase after yielding. The ultimate load is equal to $Q_{u,NL1}^{B2} = Q_{u,NL2}^{B2} = 76.7 \text{ kN/m}$, where this value is between $Q_{u,s}^{B2}$ and $Q_{u,k}^{B2}$.

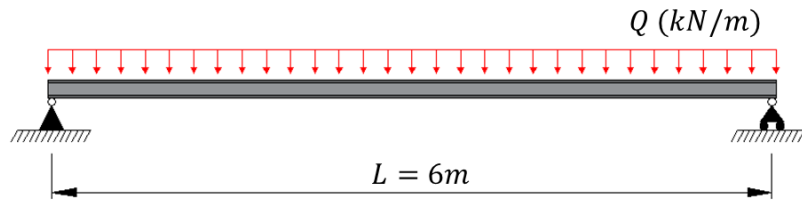


Figure III.26: Steel beam element with pinned and roller supports (configuration B2).

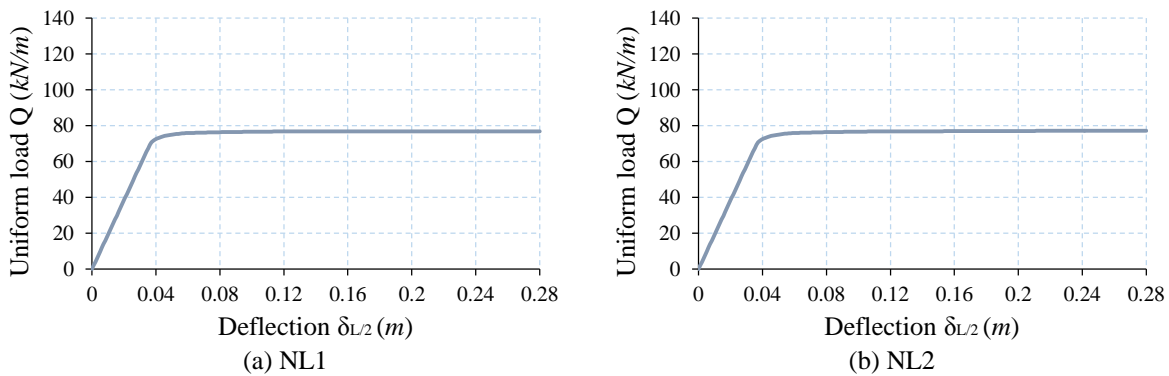


Figure III.27: Load-deflection diagram of non-linear static analysis of the steel beam element (configuration B2).

III.3.5.3 Configuration B3 with fixed supports at both ends

Configuration B3 is shown in Figure III.28. The yield design calculation identifies that $Q_{u,s}^{B3} = 155.3 \text{ kN/m}$ and $Q_{u,k}^{B3} = 156.6 \text{ kN/m}$. Besides, Figure III.29 presents the load-deflection diagram for the two cases NL1 and NL2, where the yielding load $Q_{u,NL1}^{B3} = 156 \text{ kN/m}$ (Figure III.29-a), which is between $Q_{u,s}^{B3}$ and $Q_{u,k}^{B3}$. The load capacity of the beam in NL2 increases to $Q_{NL2}^{B3}(\delta_{L/2} = 0.6 \text{ m}) = 240 \text{ kN/m}$ (see Figure III.29-b).

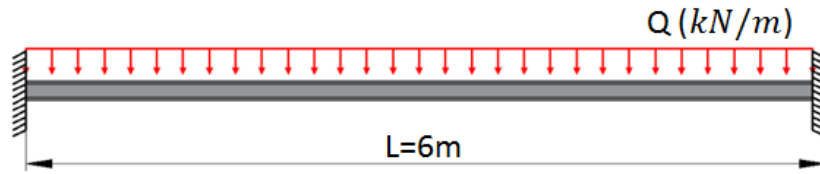


Figure III.28: Steel beam element with fixed supports (configuration B3).

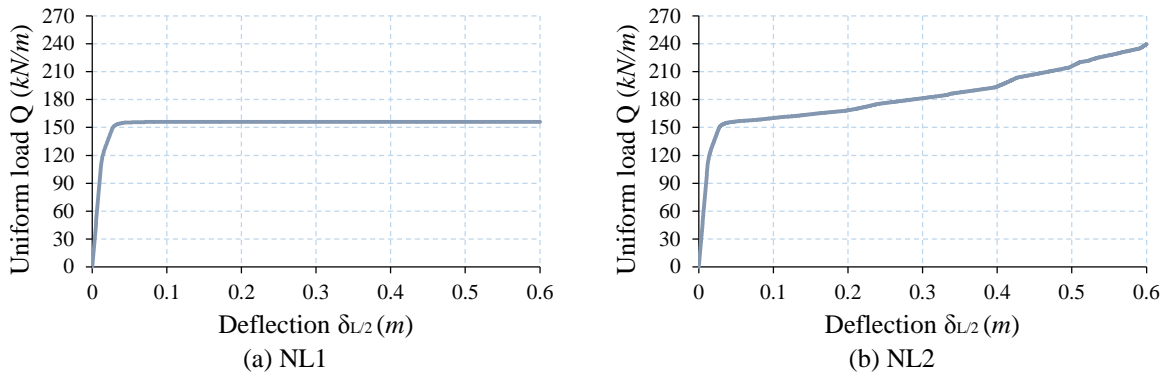


Figure III.29: Load-deflection diagram of non-linear static analysis of the steel beam element (configuration B3).

Figure III.30(a) shows that the tensile membrane action is inactive in NL1, where the normal force is zero. Figure III.30 (b) illustrates the tension force developed under NL2 assumption with $N_{L/2}^{NL2}(\delta_{L/2} = 0.6 \text{ m}) = 763.9 \text{ kN}$ and the decrease of bending moment at the mid-span with $M_{y,L/2}^{NL2}(\delta_{L/2} = 0.6 \text{ m}) = 295.4 \text{ kN.m}$.

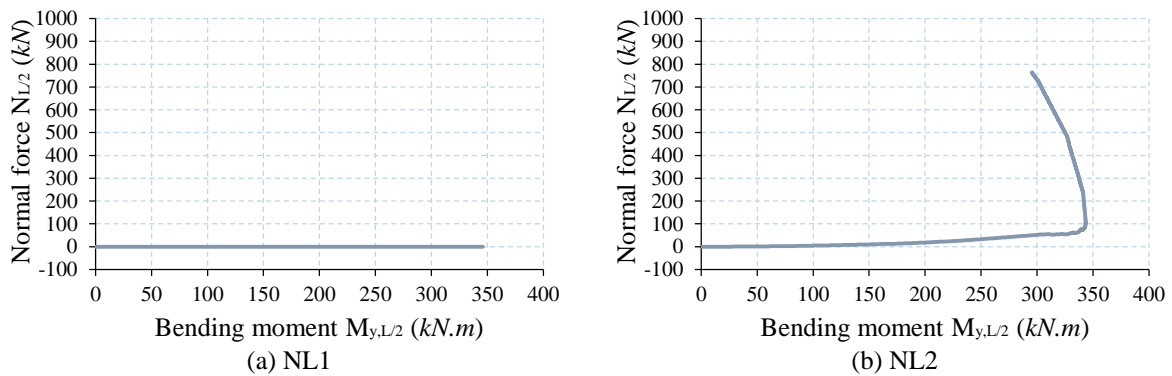


Figure III.30: Bending moment and normal forces diagram at the mid-span of the steel beam element (configuration B3).

III.3.5.4 Comparison of computation cost

In the aim to compare the computation cost of yield design calculation with that of the non-linear analysis, Table III.1 presents the calculation time under each analysis assumption (NL1 and NL2) of the considered beam configurations (B1, B2 and B3). It is clear that the

yield design calculation allows a significant saving in the computational cost, where the percentage of time saved can reach 98.94 % of the non-linear analysis calculation time.

$$\text{Time saving \%} = \frac{T_{NL} - T_{YD}}{T_{NL}} \times 100 \quad (\text{III.60})$$

where T_{NL} and T_{YD} are the maximum values of calculation time for the non-linear analysis (NL1 and NL2), and the yield design calculation, respectively.

Analysis mode	Yield design calculation (static+kinematic approaches)	NL1	NL2
B1	1.21	66.8	83.7
B2	1.20	74.9	89.0
B3	1.24	94.1	117.6

Table III.1: Comparison in the computation cost (in seconds) of yield design calculation with that of the non-linear analysis.

III.3.6 How to use the benefits of the yield design approach for progressive collapse analysis?

The ability of the yield design approach to identify the ultimate load that a structure can withstand allows to verify if the damaged structure, with a local failure scenario, can resist to some applied loads. This method is a good compromise, as it identifies the failure mechanism and limit loads, while saving computing time and avoiding problems of non-convergence compared to a full non-linear analysis.

However, the theory of yield design approach is based on two essential assumptions, which are the infinitesimal strain theory, and the consideration of the constitutive behaviour of materials as elastic perfectly plastic. As the structure may be exposed to excessive geometrical changes and a redistribution of internal forces during the progressive collapse, a first issue is how to take into account the geometrical non-linearities in the yield design approach. Progressive collapse analysis also needs to take into account the propagation of failure. Structural elements initially affected may trigger a failure mechanism at a global scale. Hence, a second issue is how to simulate the successive states of the failure propagation.

In order to combine the benefits of the yield design approach and the non-linear analysis, a coupling between these two approaches is proposed in the next section to lead a progressive collapse analysis.

III.4 COUPLING BETWEEN THE YIELD DESIGN APPROACH AND A NON-LINEAR ANALYSIS

III.4.1 General principles

The yield design approach enables to approximate and surround the ultimate load Q_u of the structure by a lower bound $Q_{u,s}$ with the static approach and upper bound $Q_{u,k}$ with the kinematic approach ($Q_{u,s} < Q_u < Q_{u,k}$), and it also identifies the corresponding failure mechanism. One can then identify the capacity of the structure and estimate if the structure can resist a load Q under an exceptional situation. The structure is assumed to be able to resist an applied load if $Q < Q_{u,s}$, which indicates that the structure can support the applied load without any failure. Conversely, the structure is unable to resist an applied load if $Q > Q_{u,s}$, meaning that the structure fails under the mechanism identified by the kinematic approach of yield design. The applied load Q is compared with $Q_{u,s}$, where the comparison with the lower bound of the ultimate load estimation allows to avoid the overestimation of the structural capacity.

The corresponding failure mechanism identifies the directly affected part, and the critical points of the structure, where the structural element cannot resist the applied forces. Besides, the failure mechanism also allows to estimate if there is either a loss of stability of the directly affected part, or the possibility to develop an alternative functioning. When the failure mechanism indicates the mechanical instability of some elements under the applied load, there is no interest to simulate the geometrical displacements of the affected part after the failure. Conversely, if the failure mechanism reveals a potential alternative equilibrium state, the geometrical displacements might lead to a change in the redistribution of the forces in the elements, and the structure might be able to function in a different manner. Furthermore, this alternative functioning can increase the structural capacity to withstand the applied load. Therefore, there is an interest to simulate the geometrical changes in this case, and to study the evolution of the structural capacity with the geometrical displacements in order to investigate the ability of the structure to resist the applied load. In this respect, as the yield design approach is unable to simulate the geometrical non-linearities, the non-linear analysis can be used as a supplementary method.

In order to follow the propagation of failure and identify the successive structural states, an iterative procedure of yield design calculation is proposed (El Hajj Diab et al., 2019). At each step i of the iterative process, the yield design calculation checks the ability of the structure to resist the applied load Q , and identifies the failure mechanism if $Q > Q_{u,s}^i$. The proposed structural modelling strategy is based on the coupling between the yield design

approach and the non-linear analysis in an iterative procedure. This procedure is illustrated in Figure III.32, with the following steps (each step is identified in Figure III.32):

- 1) The yield design approach is applied to identify the ultimate load $Q_{u,s}$ and the failure mechanism.
- 2) $Q_{u,s}$ and applied loads Q are compared.
- 3) If $Q < Q_{u,s}$, the current structural configuration can support the applied load, and the failure stops at this stage.
- 4) If $Q \geq Q_{u,s}$, a failure mode potentially occurs under the applied loads.
- 5) The failure mechanism identified by the kinematic approach allows to identify the affected part and to estimate if there is either a loss of stability or the possibility to develop an alternative functioning.
- 6) The possibility of developing an alternative functioning by the tensile membrane action is checked by verifying whether the joints on both sides of the directly affected part (see Figure III.31-a) are connected to the indirectly affected part or not.
- 7) If there is no continuity of the directly affected part beams with the indirectly affected parts on both sides, the failure mechanism indicates a mechanical instability of some elements, and the affected part is removed for the next iteration of the yield design calculation. If the entire structure is affected, then the overall structure collapses.
- 8) If the failure mechanism reveals that the directly affected part may develop an alternative functioning after large displacement, a non-linear analysis is applied to this part, in order to calculate the geometric displacements. The effect of the indirectly affected part on the substructure of the directly affected part is taken into account by considering horizontal springs at the extremities N_i of the substructure, as shown in Figure III.31(b). The rotation and the vertical displacement are restrained at N_i with allowing the horizontal displacement, and the springs are attached to fixed supports. In order to characterize these springs, the indirectly affected part is assumed to be perfectly elastic as assumed in Demonceau (2008), and the springs are assumed as fully elastic. The stiffness K_i of each spring is calculated by applying a unitary force (1 kN) at the i^{th} corresponding extremity (see Figure III.31-c), where K_i is described as follow:

$$K_i = \frac{1}{u_{N_i}} \quad (\text{III.61})$$

where u_i is the horizontal displacement of the joint N_i .

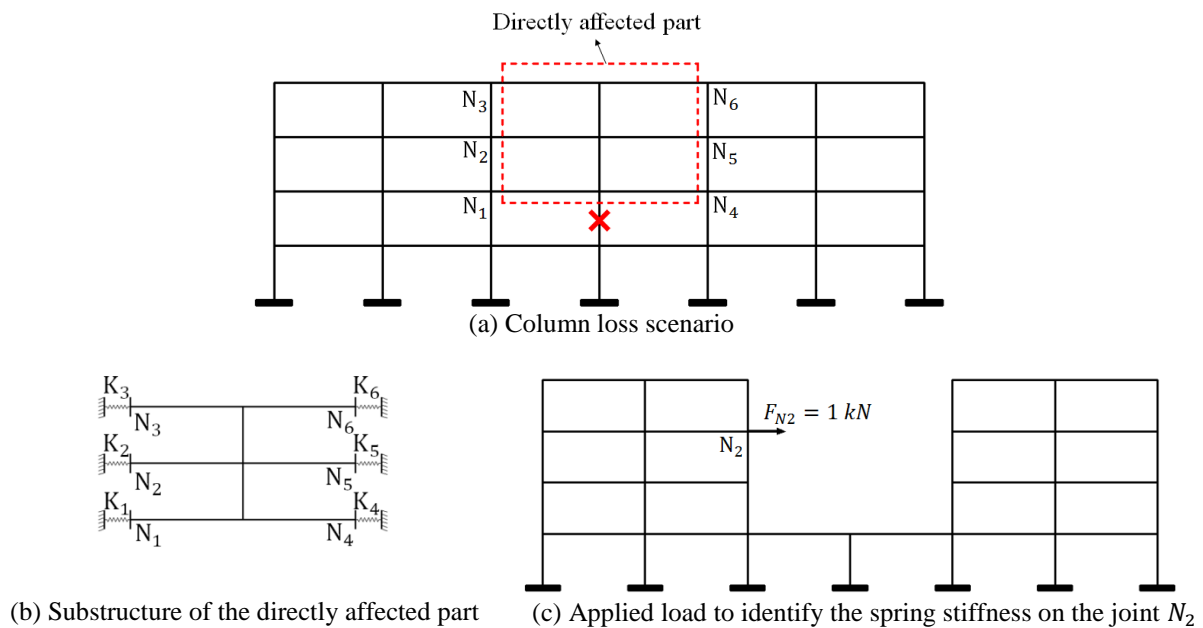


Figure III.31: Characterization of springs of the substructure.

- 9) A non-linear analysis under NL2 assumption is applied on the substructure identified in the previous step with a view to identify the geometrical change under the applied loads Q .
- 10) The geometric changes are integrated in the next iteration of the yield design calculation.
- 11) The iterative procedure continues until the end of collapse, for which the ultimate load on remaining elements is larger than the applied load, or until total collapse of the structure.

In order to take into account the dynamic effects resulting from a geometrical modification after the loss structural component, though preventing the use of a full dynamic analysis, the structural response can be estimated from a non-linear static response under amplified gravity loading using a dynamic amplification factor. This approach is mentioned in many codes and standards, such as EN 1990 (2003), GSA (2003), and UFC 4-023-03 (2009). The recommended value of the dynamic amplification factor is often 2.0, and the load amplification should only be applied over the bays adjacent to the removed elements. Otherwise, Marchand and Alfawakhiri (2005) mentioned that the factor of 2.0 is very conservative, and that a value between 1.3 and 1.5 is more realistic for a non-linear analysis when members achieve significant plastic rotation and displacements. In this chapter and also in Chapter IV, the dynamic amplification factor is fixed at 1.5. In order to study the impact of the assumptions related to the dynamic effect on the structural robustness assessment, a sensitivity of the model to this parameter is further analyzed in Chapter V.

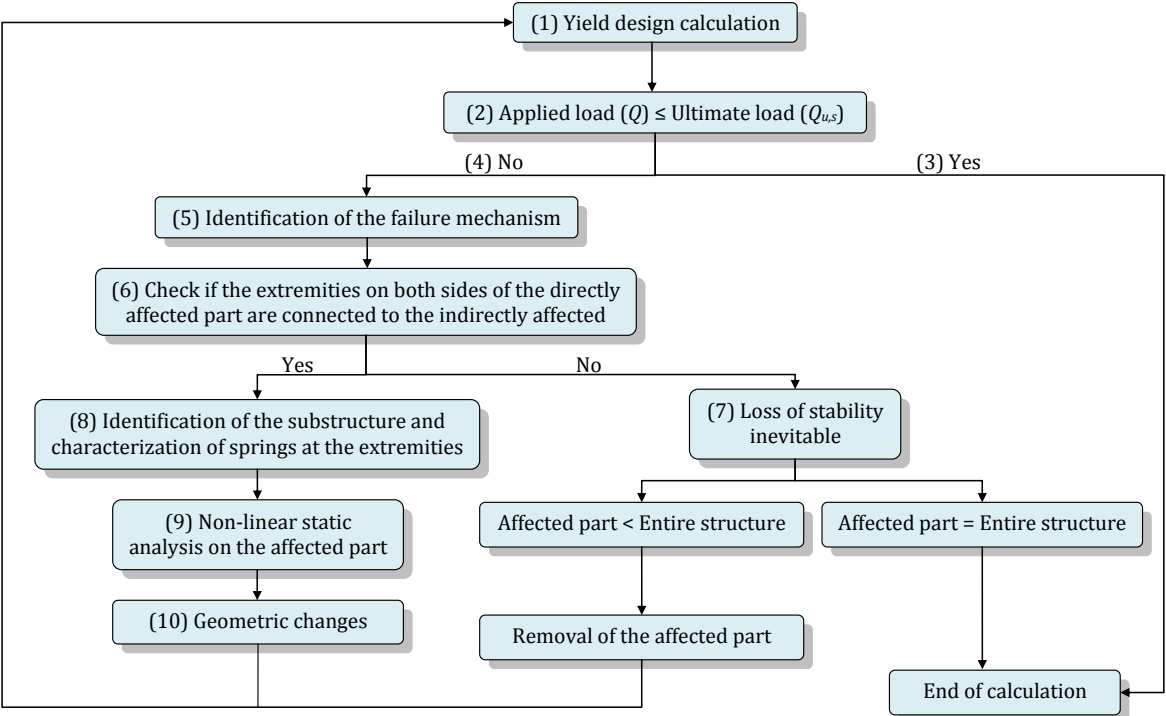


Figure III.32: Proposed structural modelling strategy for progressive collapse analysis.

III.4.2 Application on a beam element

The proposed strategy is illustrated with an application to the different configurations of the steel beam element B1, B2 and B3 of Section III.3.5. The beam is considered to be exposed to a uniform load $Q = 90 \text{ kN/m}$.

For the configuration B1, a first iteration of yield design calculation indicates that $Q_{u,s}^{B1,1} = 76.5 \text{ kN/m} < Q = 90 \text{ kN/m}$. Hence, the structure cannot resist the applied load Q in the current configuration. As the horizontal displacement on the supports of the beam are restrained, the failure mechanism presented in Figure III.22 reveals that the tensile membrane action may develop. Then, a non-linear analysis is applied to identify the geometrical change under the load Q , under assumption NL2, where the corotational formulation is used to take into account the geometrical non-linearities. Figure III.33 presents the load-deflection diagram of the non-linear analysis, where the tensile membrane action developed in the beam allows to support the load Q (90 kN/m) with a mid-span deflection $\delta_{L/2} = 0.17 \text{ m}$. The normal force $N_{L/2}$ developed in the beam at the final stage is equal to 448 kN , and the bending moment $M_{y,L/2}$ reaches 343 kN/m , then decreases to 328 kN/m (see Figure III.34).

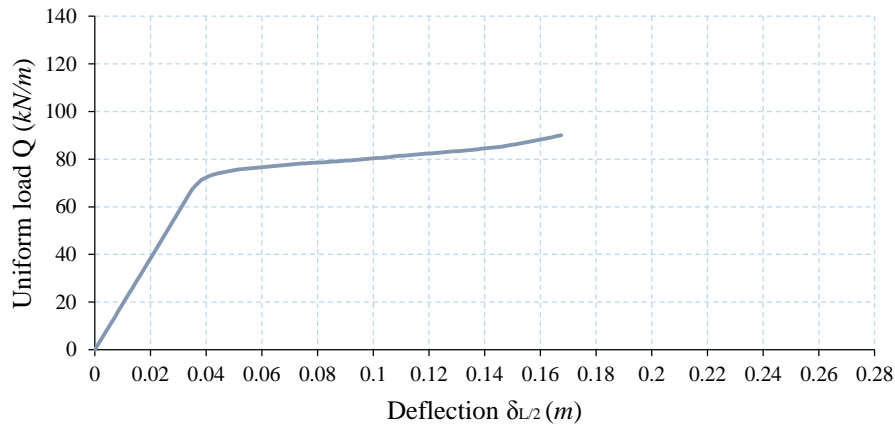


Figure III.33: Load-deflection diagram of non-linear static analysis of the first iteration (configuration: B1).

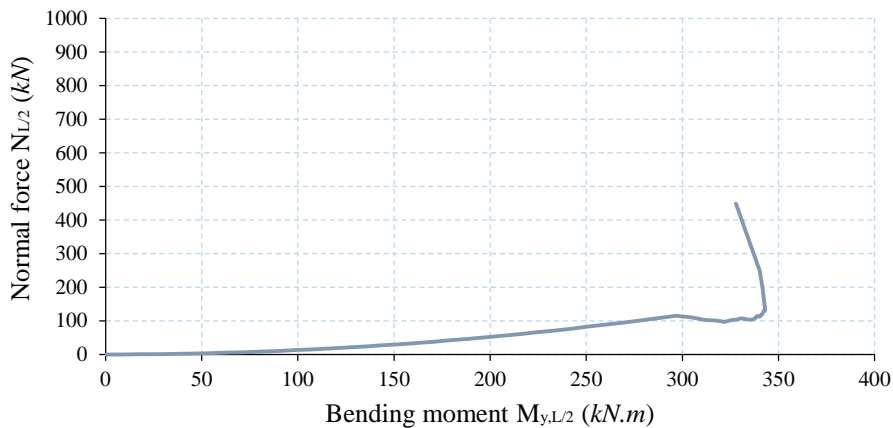


Figure III.34 : Mid-span Bending moment and normal force diagrams (configuration: B1).

Based on this new configuration, a second iteration of yield design calculation is realised with the new geometrical configuration, where $Q_{u,s}^{B1,2} = 94,8 \text{ kN/m}$ and $Q_{u,k}^{B1,2} = 96,2 \text{ kN/m}$. The yield design calculation indicates that the geometrical deformation increases the structural capacity ($Q_{ultimate}$), and it becomes larger than the applied load Q (90 kN/m), so the calculation stops at this stage.

The results for the second configuration B2 in the first iteration of yield design calculation are similar to those with configuration B1. As one of the supports is a roller support, there is no possibility to develop a tensile membrane action, so the beam has a mechanical instability according to the failure mechanism (see Figure III.22), which leads to the total collapse of the system.

Finally, for the third configuration B3, $Q_{u,s}^{B3,1} = 155.3 \text{ kN/m}$ and $Q_{u,k}^{B3,1} = 156.6 \text{ kN/m}$. These two bounds are larger than the applied load $Q = 90 \text{ kN/m}$, and the structure is able to resist Q without any damage in the structure.

III.4.3 Application on a steel-framed building

III.4.3.1 Presentation of the case study

The structure considered herein and as a common thread in the following of this dissertation is a 2D typical five-storey steel-framed building with ten bays. The geometric layout of the structure is presented in Figure III.35. The constitutive structural elements are beams with cross-section IPE360 shown in Figure III.9(a), and columns with cross-section HE500B. The geometric details of the H-shaped cross-section steel element HE500B are described in Figure III.36, and the corresponding surface criterion is given in Figure III.37.

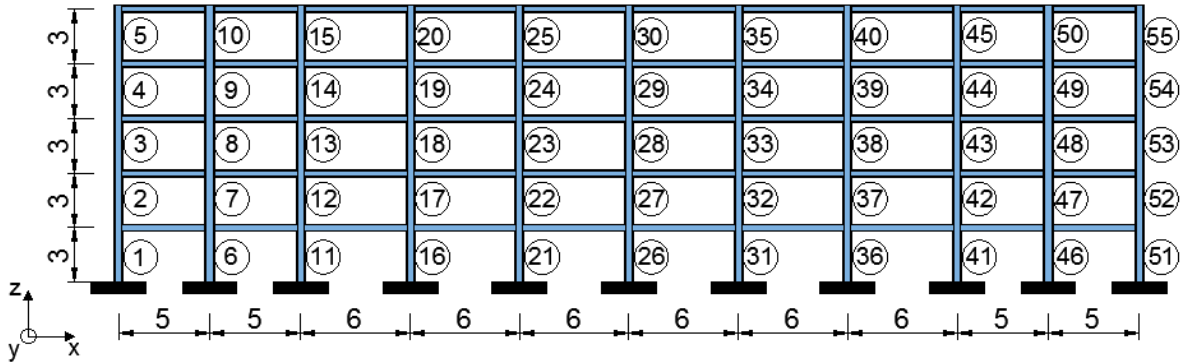


Figure III.35: Layout of steel-frame building (dimensions in meter).

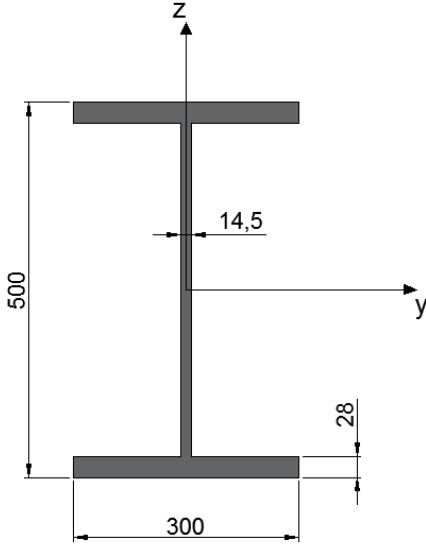
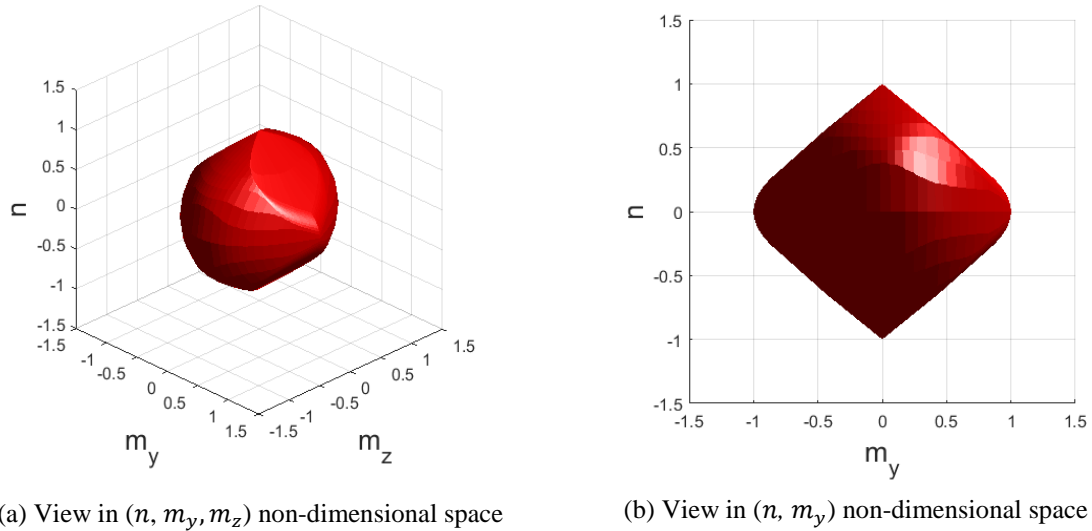


Figure III.36: H-shaped cross-section steel element HE500B.



$$N = n * N_0; N_0 = 8,250.0 \text{ kN}$$

$$M_y = m_y * M_{y0}; M_{y0} = 1,662.0 \text{ kN.m}$$

$$M_z = m_z * M_{z0}; M_{z0} = 474.0 \text{ kN.m}$$

Figure III.37: Yield surface of HE500B beam section.

Structural steel is S355, where the Young modulus $E = 210 \text{ GPa}$ and the yield strength $f_y = 355 \text{ MPa}$. The connections column/beam and column/footing are considered as rigid joints. Besides, the local failure scenarios adopted in this example are limited to the notional total loss of one or several adjacent column(s), which is assumed to represent the occurrence of an exceptional event.

The bay dimensions are considered 6 m or 5 m in the x direction and 4 m in the y direction, and the floors consist of reinforced concrete slabs carried by the principal steel beams. The thickness of the slab is considered 25 cm , with density 25 kN/m^3 , and the density of the steel structural elements is $7,850 \text{ kg/m}^3$. Besides, the imposed loads on floors are equal to 3 kN/m^2 according to the Eurocodes NF EN 1991-1-1 (2003), where the structure is considered as an administration building. The beams are exposed to uniform loads, where the values of dead loads (DL) and live loads (LL) are 25.6 kN/m and 12 kN/m , respectively. The combination of actions DL and LL refers to an ultimate state as recommended in the Eurocodes NF EN 1990 (2003) for an accidental situation, for which one can mitigate the reserve on the applied loads by using smaller partial factors than those with a persistent situation, as follows:

- persistent situation: $W_p = 1.35 DL + 1.5 LL$
 - accidental situation: $W_a = DL + 0.5 LL$
- (III.62)

This design configuration respects the Eurocodes serviceability and ultimate limit states. Moreover, the load capacity of the intact structure is verified under the combination of

loads in the persistent situation $W_p = 52.5 \text{ kN/m}$. A yield design calculation identifies that the ultimate capacity of the structure is between $Q_{u,s}^{intact} = 152 \text{ kN/m}$ and $Q_{u,k}^{intact} = 159.2 \text{ kN/m}$. As $W_p < Q_{u,s}^{intact}$, the structure in the intact situation can support the combination of loads in the ultimate state W_p .

In the structural robustness assessment, the combination of loads used under the local failure scenarios is that of the accidental situation $W_a = 31.6 \text{ kN/m}$. Further, the dynamic amplification factor used in this example is 1.5. The load amplification is applied only on the directly affected part, which normally contains all the beams, columns and beam-to-column joints located just above lost column(s). Table III.2 summarizes the input data of the structural system.

Material properties			
Type	Young modulus E	Yield strength f_y	
S355	210 GPa	355 MPa	
Applied loads			
Dead load DL	Live load LL	Combination of loads	
		Persistent situation $W_p = 1.35 DL + 1.5 LL$	Accidental situation $W_a = DL + 0.5 LL$
25.6 kN/m	12 kN/m	52.5 kN/m	31.6 kN/m

Table III.2: Input data of the steel-framed building.

The structural response under the applied local failure scenarios can be classified into four categories, as described below:

- C1 without consequences: the local failure does not lead to any failure mechanism,
- C2 without collapse of the directly affected part: a failure mechanism is initiated according to the yield design theory. For a frame structure, the directly damaged part contains beams, columns and beam-to-column joints located just above lost column(s). However, the structure succeeds to find a second line of defence (i.e. by the catenary action developed in the directly affected part),
- C3 with collapse of the directly affected part: the structure does not succeed to find a second line of defence, and the failure mechanism leads to a partial collapse without further propagation beyond the first failure mechanism,

- C4 expanded collapse: the indirectly affected part of the structure cannot support the redistribution of loads in the new structural configuration and the collapse propagates out of the directly affected part.

The affected or the collapsed parts are quantified by the length of associated beams, where this value represents the consequences and the part of a structure that becomes out of service. The following sections present examples of local failure scenarios that correspond to each type of the categories described above. Results are provided each time both considering the proposed coupling strategy and using a full non-linear analysis, to compare numerical results as well as computation times. The ultimate loads identified by the yield design calculation are noted as $Q_{u,s}^{C_i,j}$ and $Q_{u,k}^{C_i,j}$ for static and kinematic approaches, respectively, where i represents the category of the local failure scenario C_i , and j is the iteration number of yield design calculation. As explained previously, the identification of the ultimate load $Q_{u,s}^{C_i,j}$ of the static approach is according to the maximization problem in Equation (III.49), and the ultimate load $Q_{u,k}^{C_i,j}$ of the kinematic approach is identified according to the minimization problem in Equation (III.57).

III.4.3.2 Illustration of local failure scenario C1

III.4.3.2.a Coupling strategy

The first scenario of local failure is the notional loss of column # 6. Figure III.38 shows the loading mode of the structure under this local failure scenario. The first iteration of the yield design calculation indicates that $Q_{u,s}^{C1,1} = 37.7 \text{ kN/m}$ and $Q_{u,k}^{C1,1} = 39.2 \text{ kN/m}$. The failure mechanism under the ultimate load is presented in Figure III.39. The distribution of bending moments and normal forces are shown in Figure III.40 and Figure III.41, respectively, which shows that the failure is identified at the joints of the directly affected part, by the creation of plastic hinges in these joints, where the bending moments reach the bending resistance limit of the beams ($M_{y0}^{IPE360} = 346.0 \text{ kN.m}$, see Figure III.10).

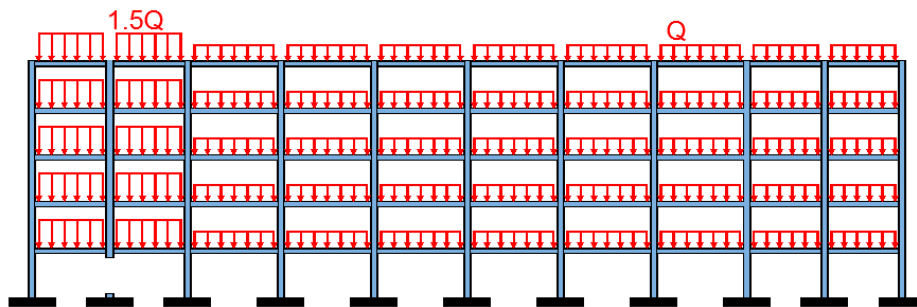


Figure III.38: Notional loss of column # 6.

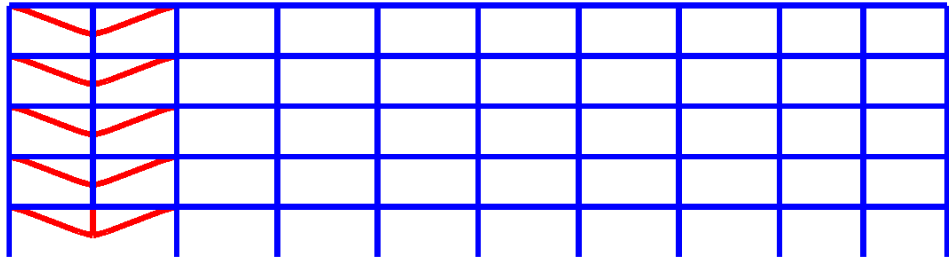


Figure III.39: Failure mechanism identified by to first iteration of the yield design calculation after the loss of column # 6 (the displacement are not representative).

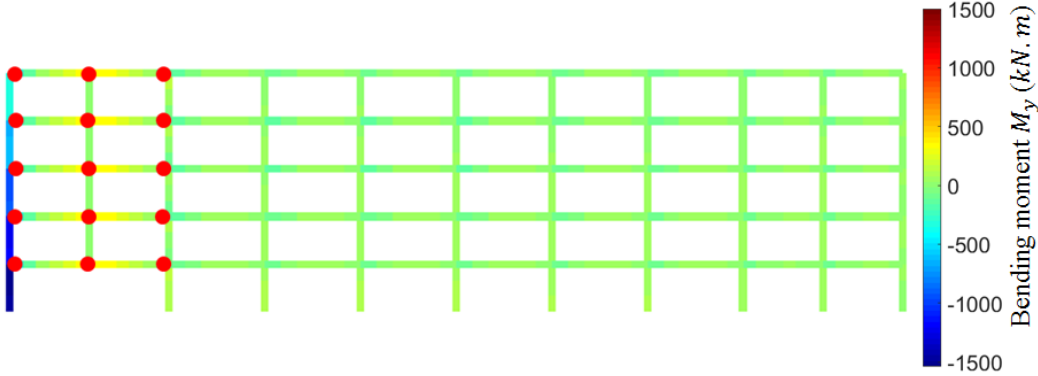


Figure III.40: Bending moment M_y diagram according to the first iteration of the yield design calculation after the loss of column # 6 ($M_{y0}^{IPE360} = 346.0 \text{ kN.m}$ and $M_{y0}^{HE500B} = 1,662.0 \text{ kN}$, see Figure III.10 and Figure III.37).

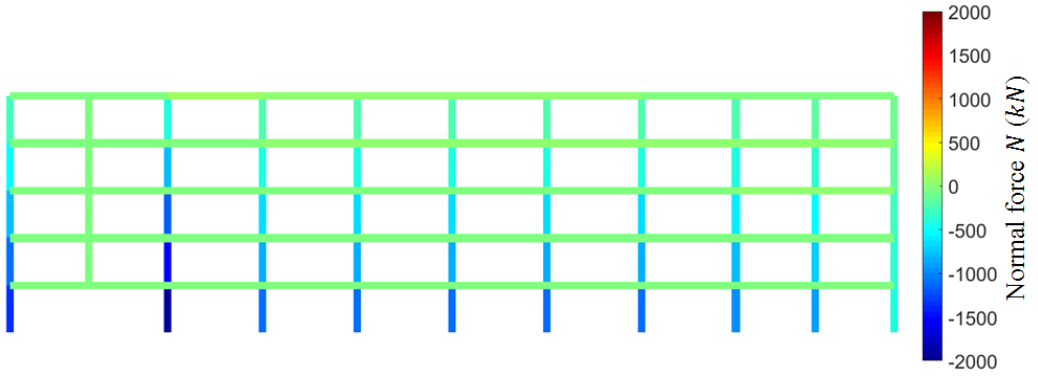


Figure III.41: Normal force diagram according to the first iteration of the yield design calculation after the loss of column # 6 ($N_0^{IPE360} = 2,840.0 \text{ kN}$ and $N_0^{HE500B} = 8,250.0 \text{ kN}$, see Figure III.10 and Figure III.37).

As $W_a(31.6 \text{ kN/m}) < Q_{u,s}^{C1,1}(36.7 \text{ kN/m})$, the structure can resist the loss of the column # 6 without initiation of any failure mechanism (category C1).

III.4.3.2.b Non-linear static analysis on the whole structure

The non-linear static analysis on the whole structure with the assumption NL2 indicates that the ultimate load is $Q_{u,NL2}^{C1} = 38.8 \text{ kN/m}$ (see Figure III.42), where $Q_{u,s}^{C1,1} <$

$Q_{u,NL}^{C1} < Q_{u,k}^{C1,1}$. Figure III.43 shows the deflection δ_6 on the top of the removed column # 6 according to the uniform load Q , where the bending moment on the joints of the directly affected part (N1, N2, N3, N4, N5, N6, N7, N8, N9, N10, N11, N12, N13, N14 and N15) reaches the bending resistance limit when $\delta_6 > 0.1 m$, which indicates the release of the failure mechanism that corresponds to the ultimate load $Q_{u,NL2}^{C1}$ in Figure III.42. The computation cost with the non-linear static analysis is $t_{C1}^{NL2} = 1,230.0 s$, while it can decrease by using the proposed coupling strategy to $t_{C1}^{CS} = 14 s$ with one iteration of yield design calculation (see Table III.3).

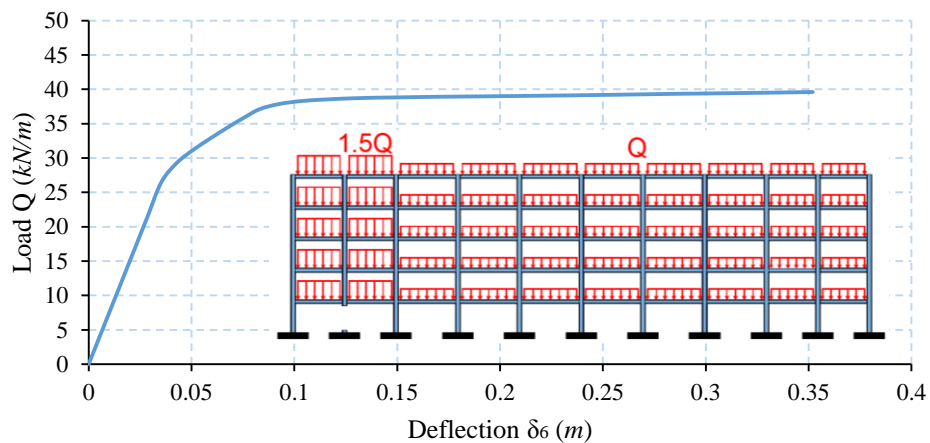


Figure III.42: Deflection δ_6 -load diagram of non-linear static analysis on the whole structure after the loss of column # 6.

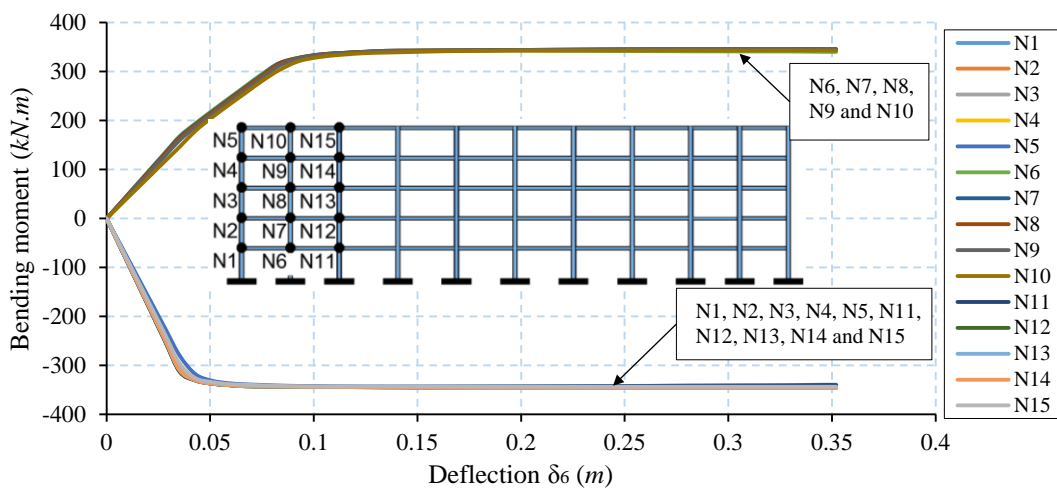


Figure III.43: Deflection δ_6 -bending moment diagram at the joints of the directly affected part after the loss of column # 6.

	Coupling Strategy t_{C1}^{CS}	Non-linear analysis on the whole structure t_{C1}^{NL2}	Gain
	1 st iteration of yield design calculation		
Computation cost (s)	14.0	1,230.0	98.8 %

Table III.3: Comparison of the computation cost for the proposed coupling strategy with that of the non-linear analysis under the loss of column # 6.

III.4.3.3 Illustration of local failure scenario C2

III.4.3.3.a Coupling strategy

The second scenario is the notional loss of column # 26, as shown in Figure III.44 with the loading mode of the structure. The first iteration of the yield design calculation indicates that $Q_{u,s}^{C2,1} = 23.8 \text{ kN/m}$ and $Q_{u,k}^{C2,1} = 25.1 \text{ kN/m}$. As $Q_{u,s}^{C2,1} < W_a = 31.6 \text{ kN/m}$, the structure cannot resist the applied load W_a , where the failure (see Figure III.45) is localized at the joints of the directly affected part due to the bending moments that reach the bending resistance limit (see Figure III.46). The normal force on the columns does not reach the yield limit $N_0 = 8,250.0 \text{ kN}$, as shown in Figure III.47. The failure mechanism shown in Figure III.45 indicates the possibility of developing an alternative functioning, where the continuity of the beams in both sides of the affected part allows the development of tensile membrane action. Therefore, a non-linear analysis is performed on the affected part to identify the geometric changes under the amplified loads ($1.5W_a$). The damaged part of the first iteration is considered as the initial damaged part (*IDP*), which is equal to 60 m in this case (sum of beam length in this part of the structure). This indicator allows to evaluate the size of the part directly affected after the initial local failure.

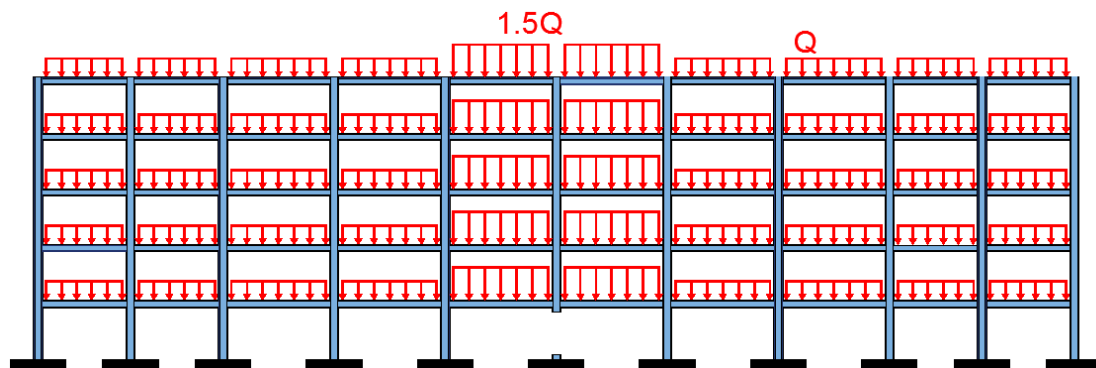


Figure III.44: Notional loss of column # 26.

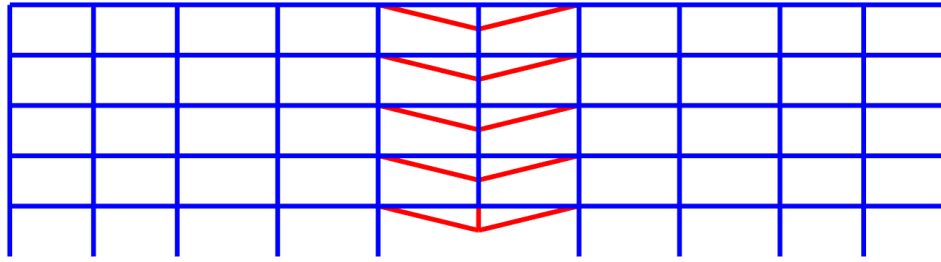


Figure III.45: Failure mechanism identified by the first iteration of the yield design calculation after the loss of column # 26.

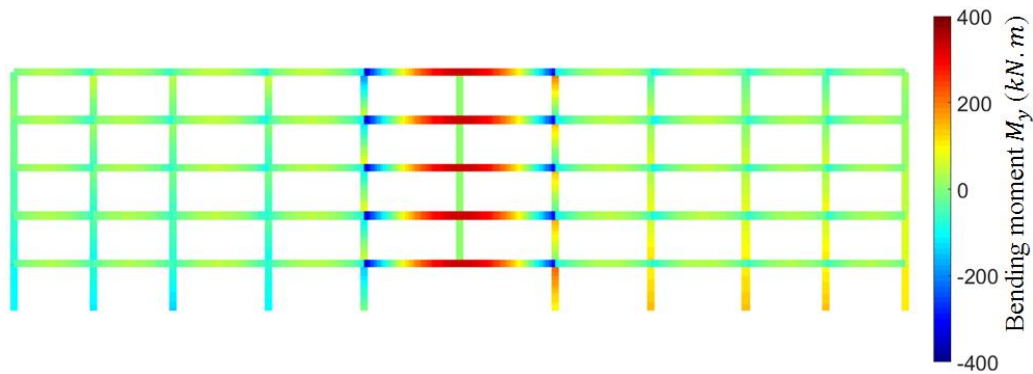


Figure III.46: Bending moment M_y diagram according to the first iteration of the yield design calculation after the loss of column # 26 ($M_{y0}^{IPE360} = 346.0 \text{ kN.m}$ and $M_{y0}^{HE500B} = 1,662.0 \text{ kN}$, see Figure III.10 and Figure III.37).

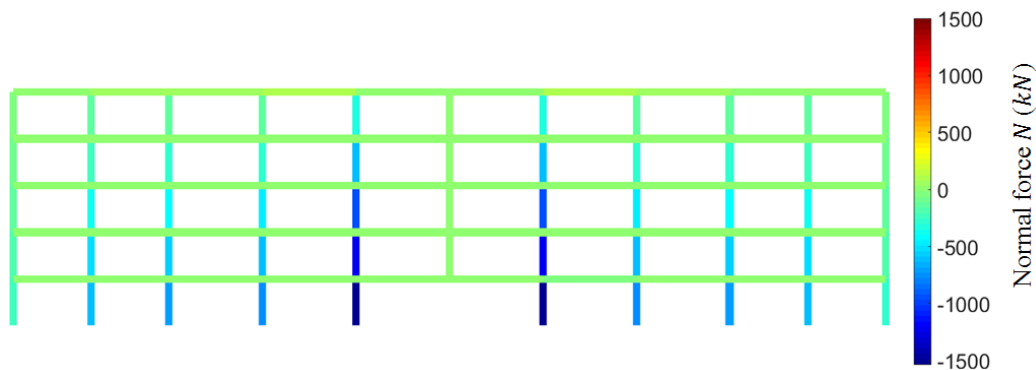


Figure III.47: Normal force diagram according to the first iteration of the yield design calculation after the loss of column # 26 ($N_0^{IPE360} = 2,840.0 \text{ kN}$ and $N_0^{HE500B} = 8,250.0 \text{ kN}$, see Figure III.10 and Figure III.37).

The substructure corresponding to the initial damaged part is presented in Figure III.48. The stiffness of the spring at each extremity of the substructure is identified according to Equation (III.61). As the indirectly affected part is symmetric for both sides of the directly affected part, the stiffness of springs are similar for both sides of each story, as shown in Table III.4.

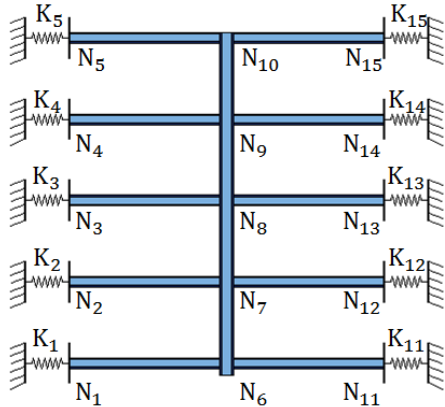


Figure III.48: Substructure of the initial damaged part after the loss of column # 26.

K_1	K_2	K_3	K_4	K_5
143,033.2 kN/m	39,917.3 kN/m	19,547.4 kN/m	12,129.2 kN/m	8,143.5 kN/m
K_{11}	K_{12}	K_{13}	K_{14}	K_{15}
143,033.2 kN/m	39,917.3 kN/m	19,547.4 kN/m	12,129.2 kN/m	8,143.5 kN/m

Table III.4: Stiffness of springs at each extremity of the substructure after the loss of column # 26.

The non-linear analysis with the assumption NL2 of the substructure corresponding to the initial damaged part (Figure III.48) indicates that it achieves to support the applied loads after a certain deflection, where Figure III.49 presents the deflection δ_{N_6} at Joint N_6 and the load (Q) diagram, which shows the increment of the substructure capacity due to the development of the tensile membrane action. The substructure achieves to find an alternative equilibrium state under $W_a = 31.6 \text{ kN/m}$ with $\delta_{N_6} = 0.63 \text{ m}$.

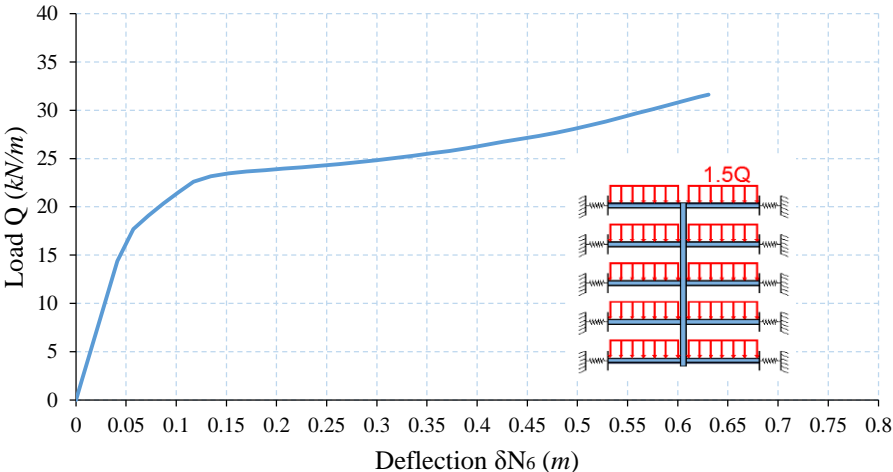


Figure III.49: Deflection-load diagram of non-linear static analysis of the initial damaged part after the loss of column # 26.

Figure III.50 shows the bending moment in the joints according to the deflection δ_{N6} (see Figure III.48). The bending moment at all joints (N_1, \dots, N_{15}) reaches the bending resistance limit ($M_{pl}^{IPE360} = 346.0 \text{ kN.m}$), when the deflection $\delta_{N6} = 0.2 \text{ m}$ (see Figure III.50), with an applied load $Q_{YL}^{NL2} = 24 \text{ kN/m}$ (see Figure III.49). It is highlighted that $Q_{u,s}^{C2,1} = 23.8 \text{ kN/m} < Q_{YL}^{NL2} < Q_{u,k}^{C2,1} = 25.1 \text{ kN/m}$, which shows the consistency of the two methods to identify the yielding load. One notes that the bending moment is similar at the supports ($N_1, N_2, N_3, N_4, N_5, N_{11}, N_{12}, N_{13}, N_{14}$ and N_{15}), also at the joints in the middle of the substructure (N_6, N_7, N_8, N_9 and N_{10}) until $\delta_{N6} = 0.2 \text{ m}$. After yielding, the curves start to diverge, and the decrease of bending moment is different between the different stories, which indicates that the development of the tensile membrane action is not identical on the five stories.

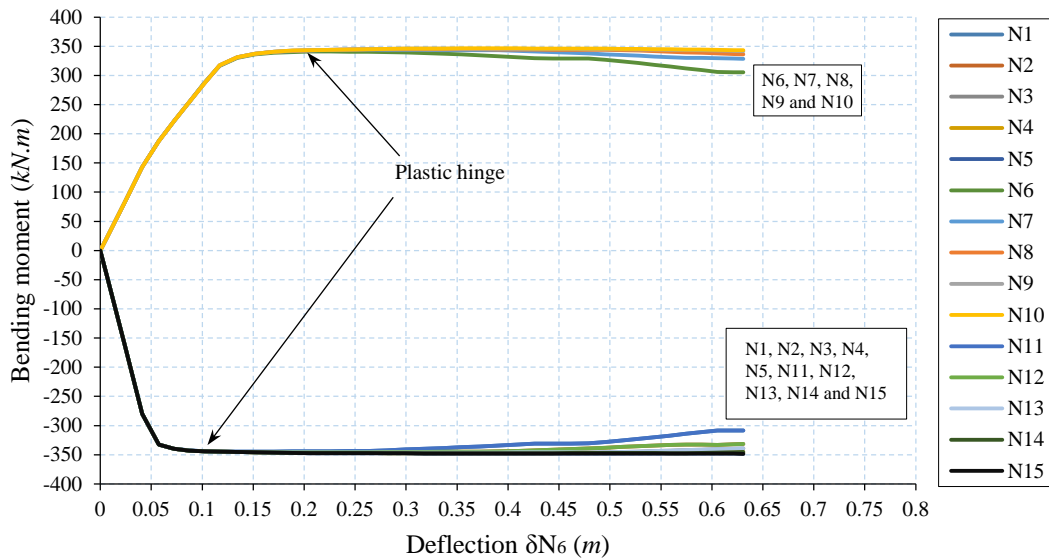


Figure III.50: Deflection δ_{N6} -bending moment diagram at the joints after the loss of column # 26.

The tensile membrane action is revealed by the normal force and bending moment diagrams at the joints. Figure III.51(a) shows the effect of large deflections at the joint N_1 , where after the bending resistance limit is reached, there is an increase of tensile stress in beams and decrease of bending moment effort, which helps the structure to reach an alternative equilibrium configuration. Besides, the normal force and bending moment diagram at joint N_5 on the fifth floor (see Figure III.51-b) indicates that the tension force developed in the beams of this floor is lower than that of the first floor. Hence, the effect of the tensile membrane action is more important in the first floor than that of the top floor.

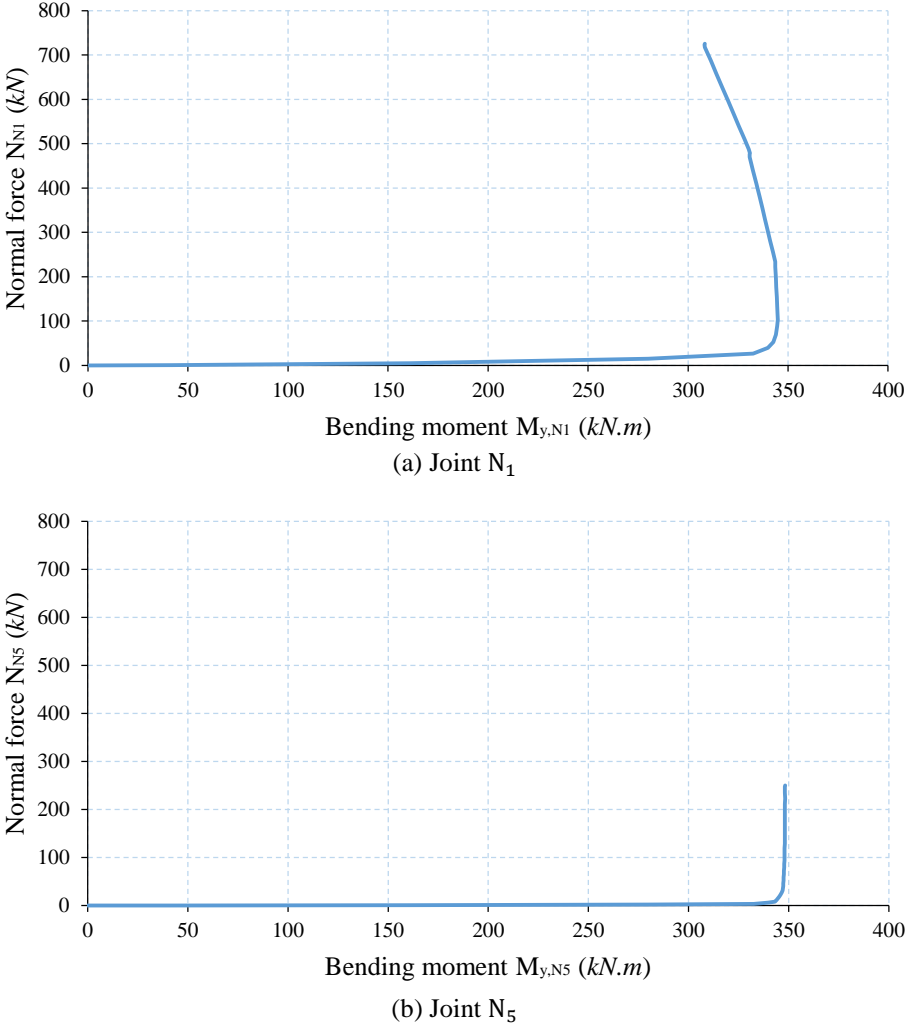


Figure III.51: Normal force – Bending moment curve at the joints N_1 and N_5 after the loss of column # 26.

Figure III.52 shows the axial stress on each layer of the cross-section at joint N_6 . When the deflection $\delta_{N_6} \leq 0.15 \text{ m}$, the number of layers under tension force (L1, L2, L3, L4, L5 and L6) is equivalent to those under compression (L7, L8, L9, L10, L11 and L12). The layers in tension and compression zones start to reach the yield strength of steel ($f_y = 355 \text{ MPa}$) with $\delta_{N_6} \geq 0.12 \text{ m}$. When $\delta_{N_6} \geq 0.15 \text{ m}$, some of compression zone layers become in tension such as L7 and L8. These aspects are due to the development of a tension force in the beam elements (see Figure III.51) that modifies the distribution of stresses in the beam cross-section.

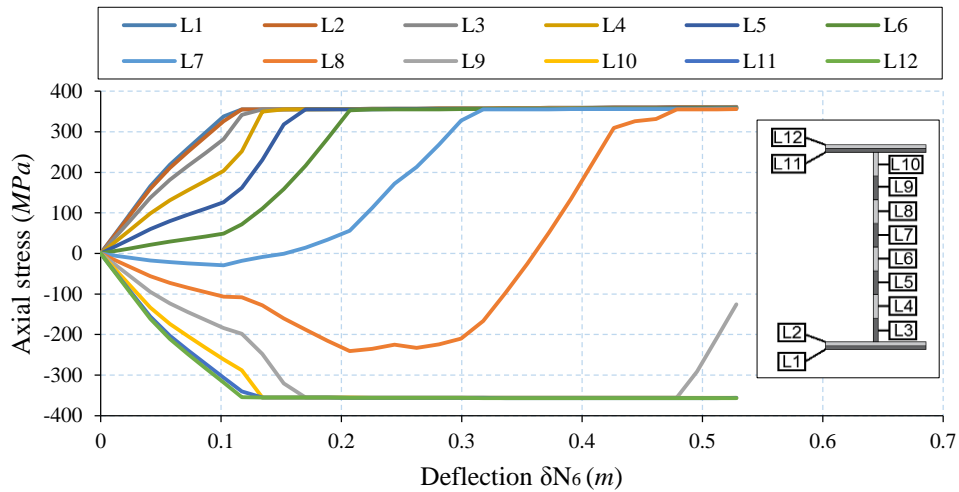


Figure III.52: Load - axial stress of cross-section layers at joint N_6 after the loss of column # 26.

The non-linear analysis identifies if the substructure can develop an alternating functioning, and it identifies the geometrical changes that correspond to the new equilibrium state. However, the development of a second line of defence in the substructure does not mean that the indirectly affected part of the structure can resist the horizontal forces developed at the joints. Here, the second iteration of the yield design calculation allows to verify if the structure can resist these forces. The geometrical deformation of the substructure identified in the non-linear analysis is integrated in the model for the next iteration of yield calculation, as shown in Figure III.53.

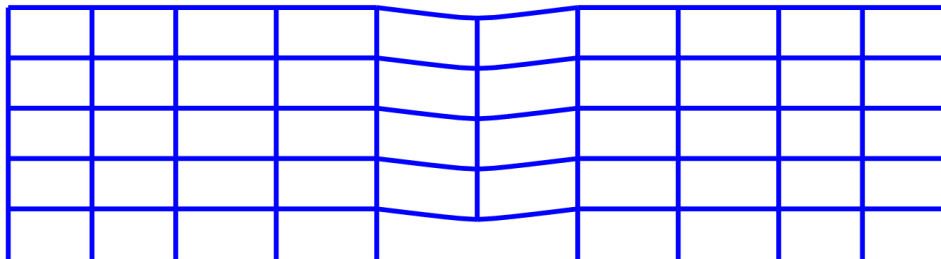


Figure III.53: Deformed model of the structure for the 2nd iteration of yield design calculation after the loss of column # 26.

The ultimate loads found in 2nd iteration of the yield design calculation are $Q_{u,s}^{C2,2} = 32.7 \text{ kN/m}$ and $Q_{u,k}^{C2,2} = 33.1 \text{ kN/m}$. As $W_a(31.6 \text{ kN/m}) < Q_{u,s}^{C2,2}$, the failure of the structure stops in this stage, where there is no collapse of structural elements and the structure manages to develop an alternative functioning to resist the propagation of the applied local failure scenario (category C2).

III.4.3.3.b Non-linear static analysis on the whole structure

In order to evaluate the assumption to calculate the deformation of the damaged structure by isolating the affected part with considering horizontal springs at the extremities of the substructure, as explained in Section III.4.1, a non-linear static analysis with the assumption NL2 is also performed on the whole structure to identify the margin of error. Figure III.54 shows that the maximum vertical deflection on the top of the removed column $\delta_{26} = 0.67 \text{ m}$. As $\delta_{26}(0.67\text{m}) > \delta_{N_6}(0.63 \text{ m})$, the deflection identified in the analysis of the whole structure is larger than that of the substructure, the deflection value in the two cases corresponding to the joint on the top of removed column, so the relative error is around $6\% \left(\frac{\delta_{26} - \delta_{N_6}}{\delta_{26}} \times 100 \right)$. It is worth to note that the stiffnesses of the horizontal springs at the extremities of the substructure are calculated by a simplified method to represent the response of the indirectly affected part. The rotations of the supports in the substructure are omitted, which may explain the difference in the obtained deflection.

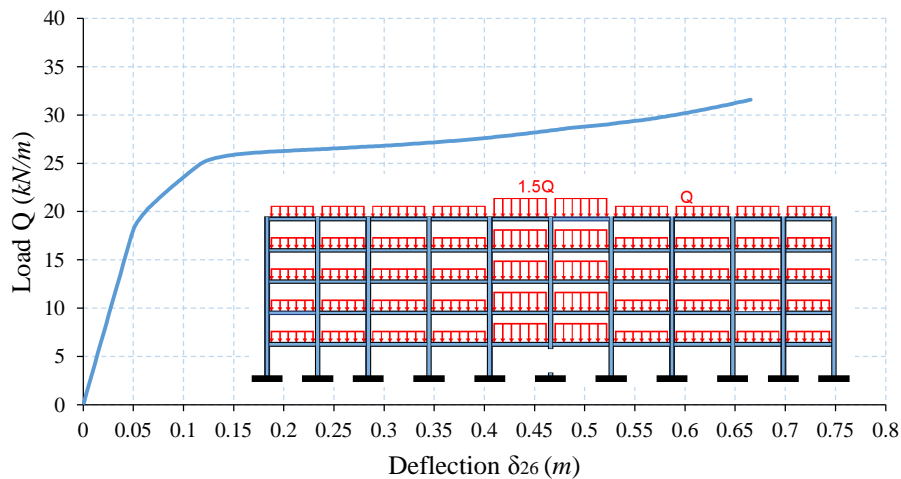


Figure III.54: Deflection-load diagram of non-linear static analysis on the whole structure after the loss of column # 26.

Ignoring the horizontal displacement of the indirectly affected part in the 2nd iteration of the yield design calculation leads to ignoring the P-delta effect that may develop. The horizontal displacement δ_{h,N_5} on the top floor at node N_5 (Figure III.48) is presented in Figure III.55, where the maximum displacement is $\max\{\delta_{h,N_5}\} = 42.7 \text{ mm}$. Further, the horizontal displacement on the left edges of the directly affected part of each level (N_1, N_2, N_3, N_4 and N_5) is presented in Table III.5. The load on these joints is 378.6 kN , so the maximum moment caused by the P-delta effect is 55.1 kN.m , which is 3.3% of the bending moment resistance (1662 kN.m). In this case, the effect of P-delta has a relatively low influence, while this effect could be larger for taller structures.

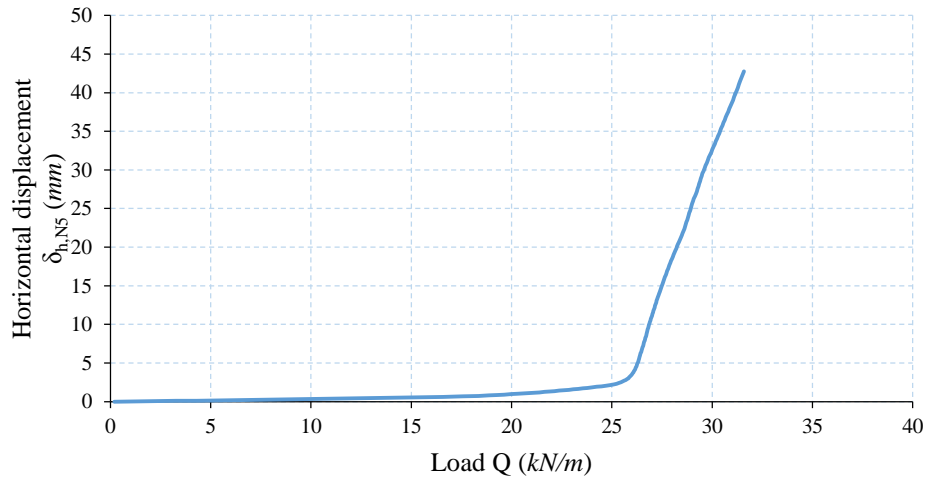


Figure III.55: Load-horizontal displacement diagram at joint N15 after the loss of column # 26.

Joint	N3	N6	N9	N12	N15
Horizontal displacement (mm)	10.8	23.2	31.7	37.3	42.7

Table III.5: Horizontal displacement on the left edges of the directly affected part after the loss of column # 26.

Two iterations of yield design calculation and one iteration of non-linear analysis are performed in the proposed coupling strategy with a total computation time $t_{26}^{CS} = 697.0$ s (see Table III.6), while the non-linear analysis on the whole structure requires $t_{26}^{NL2} = 8,620.0$ s. Hence, one can decrease the computation cost 91.9 % by using the coupling approach.

	Coupling Strategy t_{C2}^{CS}			Non-linear analysis on the whole structure t_{C2}^{NL2}	Gain
	1 st iteration of yield design calculation	Non-linear analysis	2 nd iteration of yield design calculation		
Computation cost (s)	15.0	667.0	15.0	8,620.0	91.9 %
	Total = 697.0				

Table III.6: Comparison in the computation cost of the proposed coupling strategy with that of the non-linear analysis under the loss of column # 26.

III.4.3.4 Illustration of local failure scenario C3

III.4.3.4.a Coupling strategy

The third scenario is the notional loss of the columns # 1 and 6 (see Figure III.56). The ultimate loads of the static and kinematic approaches of the first iteration of the yield design calculation are $Q_{u,s}^{C3,1} = 11.9 \text{ kN/m}$ and $Q_{u,k}^{C3,1} = 12.5 \text{ kN/m}$. As $Q_{u,s}^{C3,1} < W_a(31.6 \text{ kN/m})$, the structure cannot resist the gravity loads, where the failure mechanism presented in Figure III.57 occurs when the bending moment reaches the bending resistance limit of the beams ($M_{y0}^{IPE360} = 346.0 \text{ kN.m}$, see Figure III.10), as shown in Figure III.58. The distribution of normal forces in Figure III.59 indicates that the beam on the bottom of the directly affected part is in compression, while the one on the top is in tension due to the rotation of the damaged part.

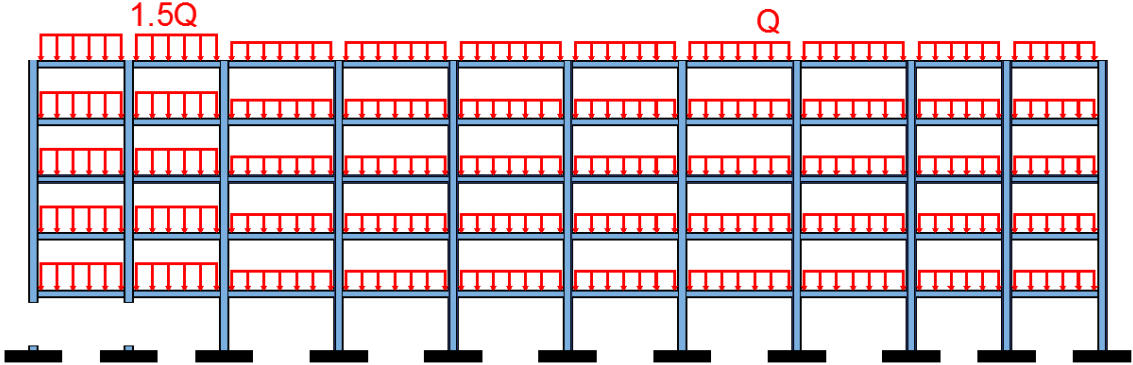


Figure III.56: Notional loss of columns # 1 and 6.

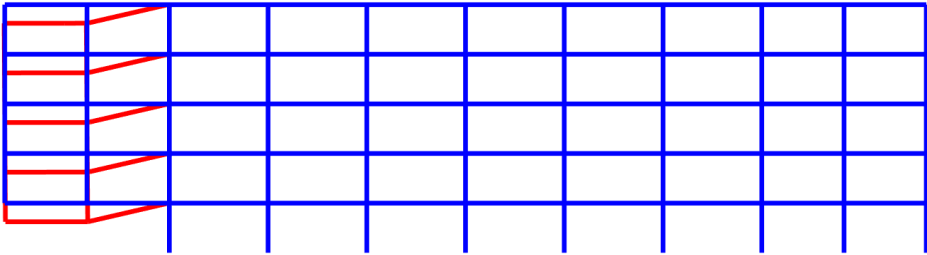


Figure III.57: Failure mechanism identified by to first iteration of the yield design calculation after the loss of columns # 1 and 6 (the displacement are not representative).

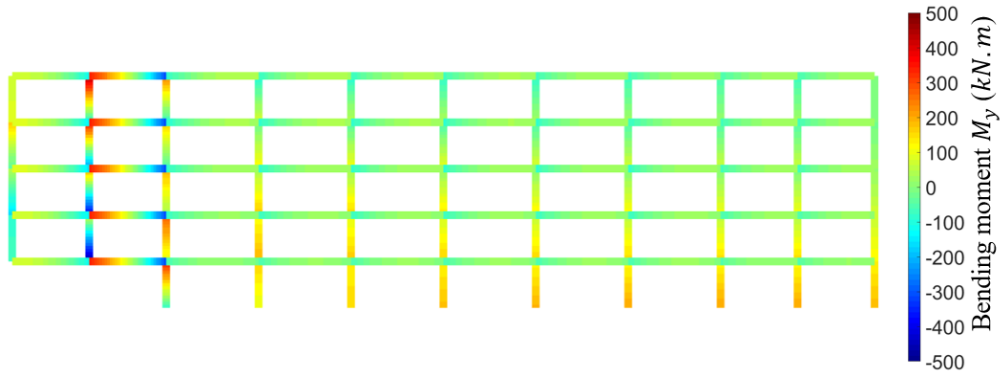


Figure III.58: Bending moment M_y diagram according to the first iteration of the yield design calculation after the loss of columns # 1 and 6 ($M_{y0}^{IPE360} = 346.0 \text{ kN.m}$ and $M_{y0}^{HE500B} = 1,662.0 \text{ kN}$, see Figure III.10 and Figure III.37).

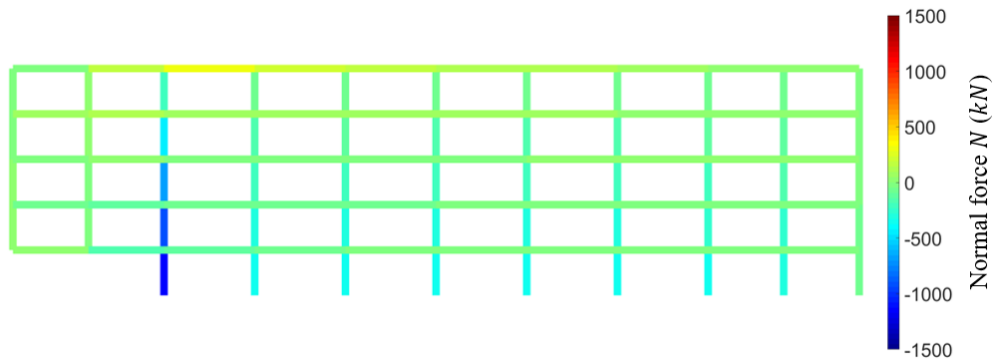


Figure III.59: Normal force diagram according to the first iteration of the yield design calculation after the loss of columns # 1 and 6 ($N_0^{IPE360} = 2,840.0 \text{ kN}$ and $N_0^{HE500B} = 8,250.0 \text{ kN}$, see Figure III.10 and Figure III.37).

Furthermore, the failure mechanism identified in Figure III.57 indicates the loss of stability of the directly affected part, where there is no possibility of an alternative functioning. Therefore, the affected part is removed for the next iteration of the yield design calculation (see Figure III.60). Then, the next iteration indicates that the ultimate loads with the new structural configuration are $Q_{u,s}^{C3,2} = 152 \text{ kN/m}$ and $Q_{u,k}^{C3,2} = 159.2 \text{ kN/m}$. Hence, $W_a = 31.6 \text{ kN/m} < Q_{u,s}^{C3,2}$, and the propagation of the failure stops at this stage with a collapsed part (sum of beams length) equal to 50 m , which is equal to the initial affected part. Therefore, this scenario corresponds to the category C3 of scenarios that have a collapse of the directly affected part.

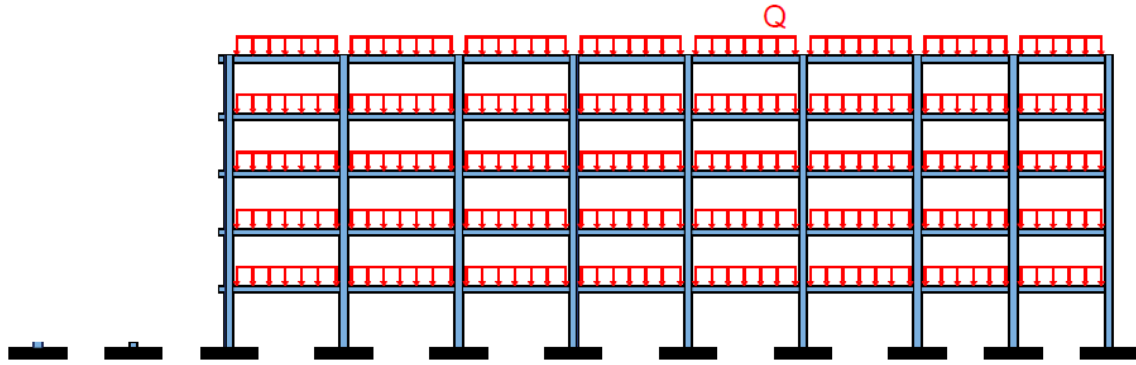


Figure III.60: Layout of the structure for the second iteration of the yield design calculation after the loss of columns # 1 and 6.

III.4.3.4.b Non-linear static analysis on the whole structure

A non-linear static analysis is applied on the whole structure with the assumption NL2, where Figure III.61 shows the maximum vertical deflection δ_1 on the top of the removed column # 1 according to the uniform load Q . As no alternative function can be developed, the load capacity of the structure remains stable when $\delta_1 > 0.13 \text{ m}$. Hence, the ultimate load is $Q_{u,NL2}^{C3} = 12 \text{ kN/m}$, where $Q_{u,s}^{C3,1} < Q_{u,NL2}^{C3} < Q_{u,k}^{C3,1}$.

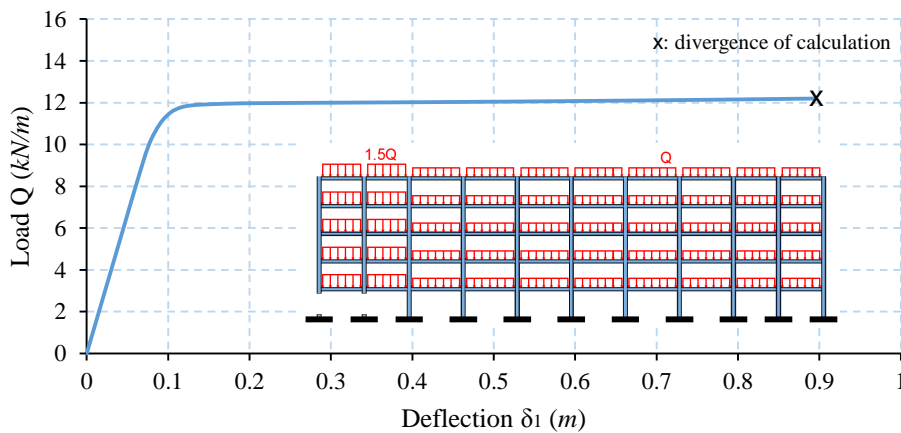


Figure III.61: Deflection δ_1 -load diagram of non-linear static analysis on the whole structure after the loss of columns # 1 and 6.

Table III.7 presents a comparison in the computation cost of the proposed coupling strategy with that of the non-linear analysis on the whole structure. Two iterations of yield design calculation are performed when using the proposed strategy with computation time $t_{C3}^{CS} = 22 \text{ s}$, while the non-linear analysis on the whole structure requires $t_{C3}^{NL2} = 1,157.0 \text{ s}$.

	Coupling Strategy t_{C3}^{CS}		Non-linear analysis on the whole structure t_{C3}^{NL2}	Gain
	1 st iteration of yield design calculation	2 nd iteration of yield design calculation		
Computation cost (s)	13.0	9.0	1,157.0	98.1 %
	Total = 22.0			

Table III.7: Comparison of the computation cost of the proposed coupling strategy with that of the non-linear analysis under the loss of columns # 1 and 6.

III.4.3.5 Illustration of local failure scenario C4

III.4.3.5.a Coupling strategy

The fourth scenario is the notional loss of the columns # 11 and 16 (see Figure III.62). The 1st iteration of the yield design calculation indicates that $Q_{u,s}^{C4,1} = 14.2 \text{ kN/m}$ and $Q_{u,k}^{C4,1} = 15 \text{ kN/m}$. As $Q_{u,s}^{C4,1} < W_a = 31.6 \text{ kN/m}$, the failure propagates according to the failure mechanism presented in Figure III.63. The bending moment and normal force diagrams (see Figure III.64 and Figure III.65, respectively) indicate that the failure is due to the bending moment on the joints of the directly affected that reaches the bending resistance limit of the beams ($M_{y0}^{IPE360} = 346.0 \text{ kN.m}$, see Figure III.10).

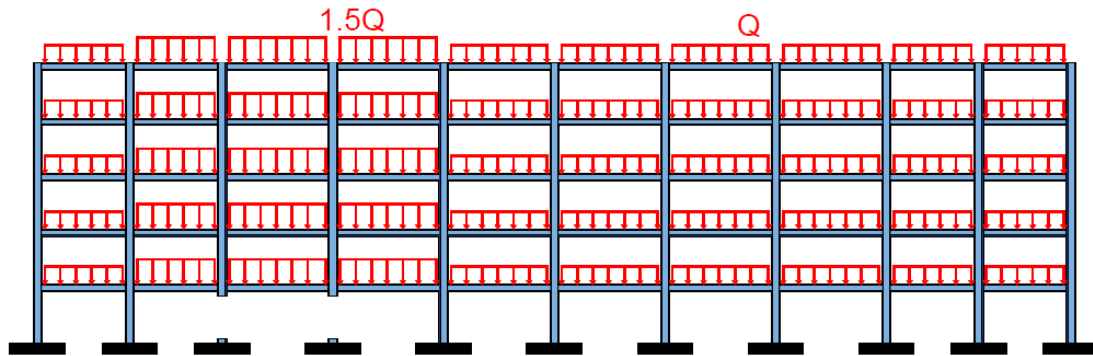


Figure III.62: Notional loss of columns # 11 and 16.

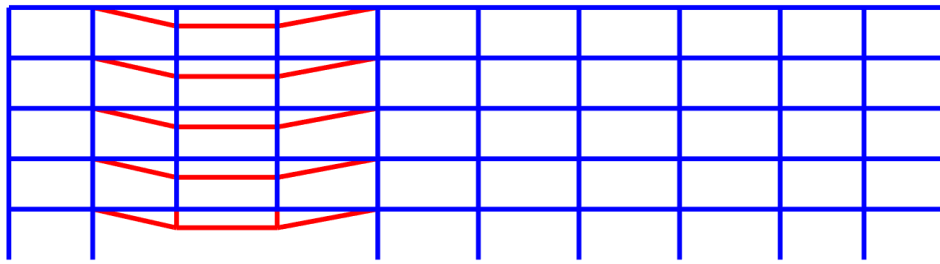


Figure III.63: Failure mechanism identified by the first iteration of the yield design calculation after the loss of columns # 11 and 16.

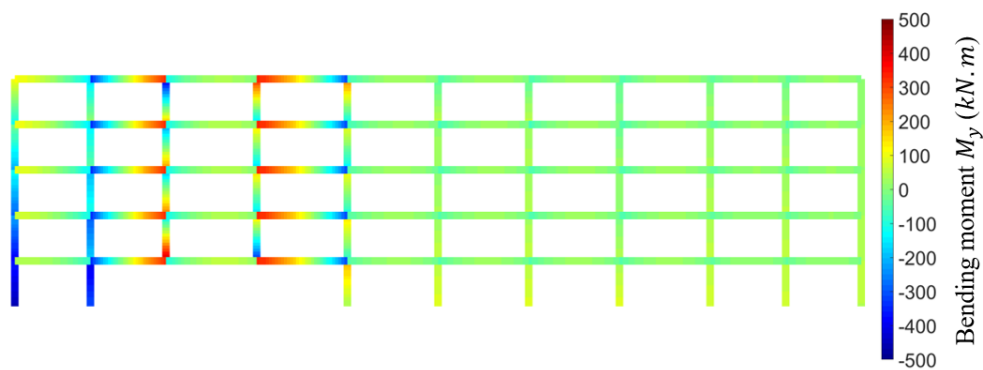


Figure III.64: Bending moment M_y diagram according to the first iteration of the yield design calculation after the loss of columns # 11 and 16 ($M_{y0}^{IPE360} = 346.0 \text{ kN.m}$ and $M_{y0}^{HE500B} = 1,662.0 \text{ kN}$, see Figure III.10 and Figure III.37).

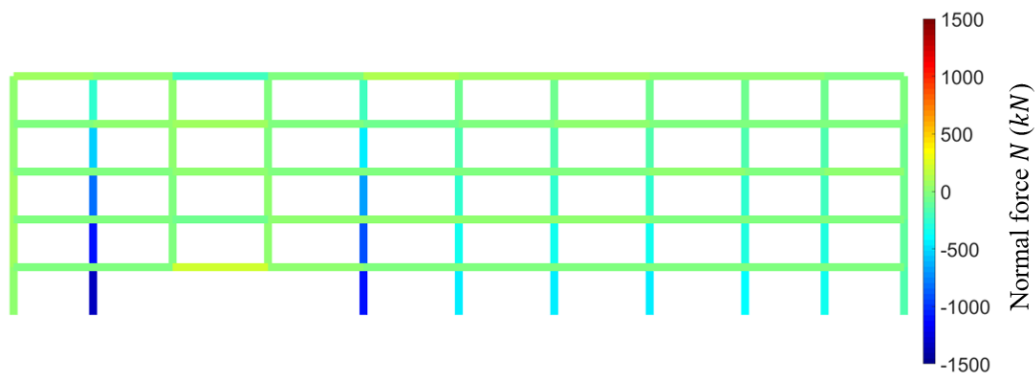


Figure III.65: Normal force diagram according to the first iteration of the yield design calculation after the loss of columns # 11 and 16 ($N_0^{IPE360} = 2,840.0 \text{ kN}$ and $N_0^{HE500B} = 8,250.0 \text{ kN}$, see Figure III.10 and Figure III.37).

The failure mechanism (Figure III.63) indicates that there is a possibility of developing an alternative functioning by the tensile membrane action due to the continuity of the beams on both sides of the affected part. Therefore, a non-linear analysis with the assumption NL2 (using corotational formulation) is performed on the substructure of the affected part (see Figure III.66). The stiffness of each spring is presented in Table III.8.

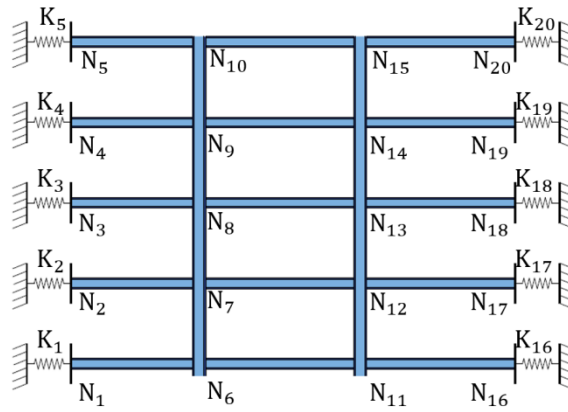


Figure III.66: Substructure of the initial damaged part after the loss of columns # 11 and 16.

K_1	K_2	K_3	K_4	K_5
76,726.0 kN/m	15,401.3 kN/m	6,673.7 kN/m	3,852.4 kN/m	2,478.0 kN/m
K_{16}	K_{17}	K_{18}	K_{19}	K_{20}
159,317.8 kN/m	50,690.2 kN/m	26,347.9 kN/m	16,781.2 kN/m	11,277.4 kN/m

Table III.8: Stiffness of springs at each extremity of the substructure after the loss of columns # 11 and 16.

Figure III.67 presents the diagram of the deflection δ_{N11} on the top of the removed column # 11 and the applied load Q . The load capacity of the structure increases until one reaches the applied load ($W_a = 31.6 \text{ kN/m}$), when $\delta_{N11} = 1.13 \text{ m}$. The normal force and bending moment diagram at the joint N_1 (see Figure III.68) shows the development of the tensile membrane action on the first floor, where the bending moment significantly decreases after the bending resistance limit ($M_{pl}^{IPE360} = 346.0 \text{ kN.m}$) is reached, and the tension force simultaneously increases until 2,179.0 kN.

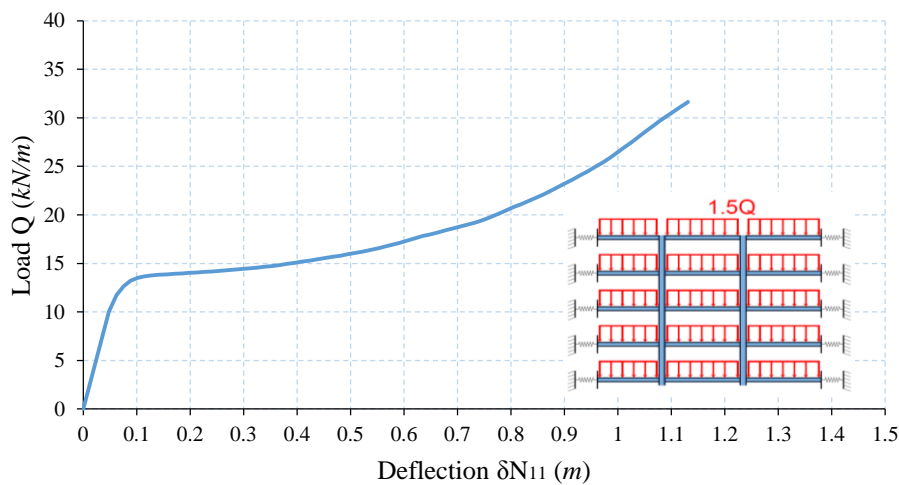


Figure III.67: Deflection-load diagram of non-linear static analysis of the initial damaged part after the loss of columns # 11 and 16.

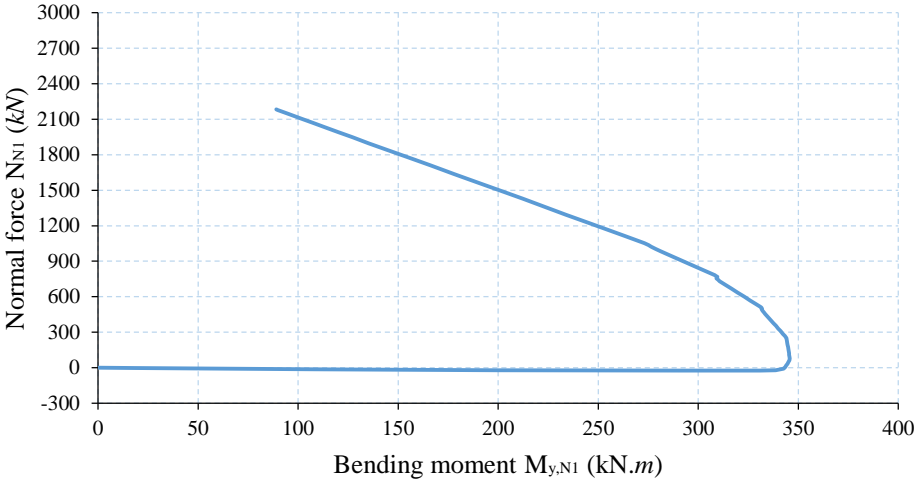


Figure III.68: Normal force – Bending moment curve at the joint N_1 after the loss of columns # 11 and 16.

The second iteration of yield design calculation indicates that $Q_{u,s}^{C4,2} = 21.3 \text{ kN/m}$ and $Q_{u,k}^{C4,2} = 22.4 \text{ kN/m}$. After the large displacement, the ultimate loads of the structure increase compared to the first iteration ($Q_{u,s}^{C4,2} > Q_{u,s}^{C4,1}$ and $Q_{u,k}^{C4,2} > Q_{u,k}^{C4,1}$), while $Q_{u,s}^{C4,2} < W_a = 31.6 \text{ kN/m}$. Hence, the indirectly affected part of the structure is not able to resist the forces developed during the development of the tensile membrane action. Figure III.69 shows the failure mechanism, which reveals that the part on the left side of the initial affected part cannot support the forces developed after the geometrical deformation. The normal forces that developed in the initial affected part lead to an increment in the bending moment at the bottom of columns in the indirectly affected part, as shown in Figure III.70, where the bending moment at b1 and b2 reaches the bending limit of the column element.

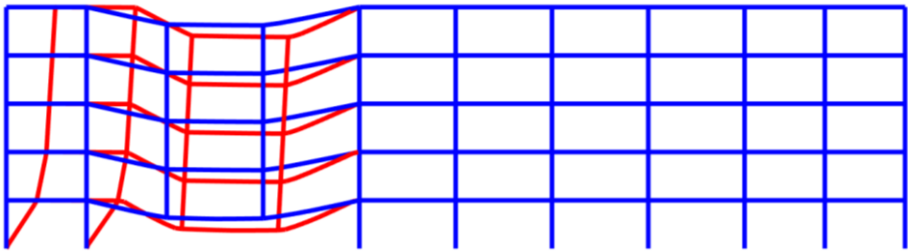


Figure III.69: Failure mechanism identified by the second iteration of the yield design calculation after the loss of columns # 11 and 16.

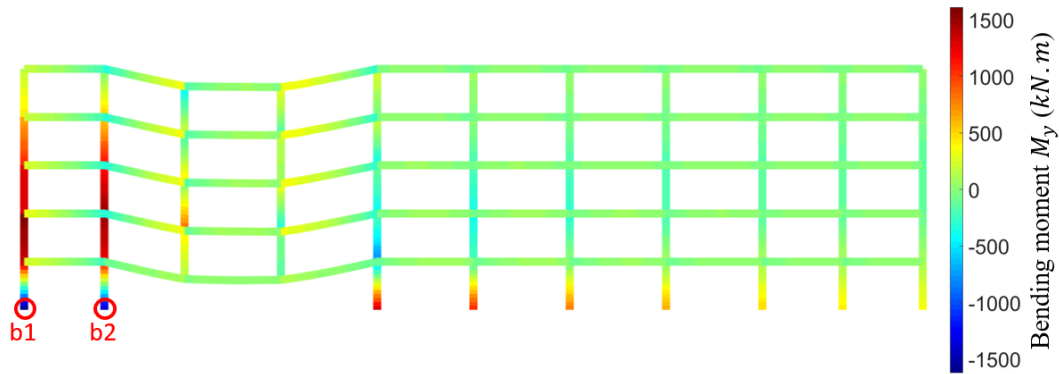


Figure III.70: Bending moment diagram according to the second iteration of the yield design calculation after the loss of columns # 11 and 16 ($M_{y0}^{IPE360} = 346.0 \text{ kN.m}$ and $M_{y0}^{HE500B} = 1,662.0 \text{ kN}$, see Figure III.10 and Figure III.36).

The failure mechanism indicates the loss of stability of the affected part, where it is removed for the next iteration of the yield design calculation, as shown in Figure III.71. Finally, the ultimate loads identified are $Q_{u,s}^{C4,3} = 152 \text{ kN/m}$ and $Q_{u,k}^{C4,3} = 159.2 \text{ kN/m}$, which means that the collapse stops at this stage as $W_a = 31.6 \text{ kN/m} < Q_{u,s}^{C4,3}$. The beam lengths of the initially affected and the collapsed parts for this scenario are equal to 85 m and 110 m, respectively. Therefore, the collapse expands out of the directly affected part and this scenario falls in category C4.

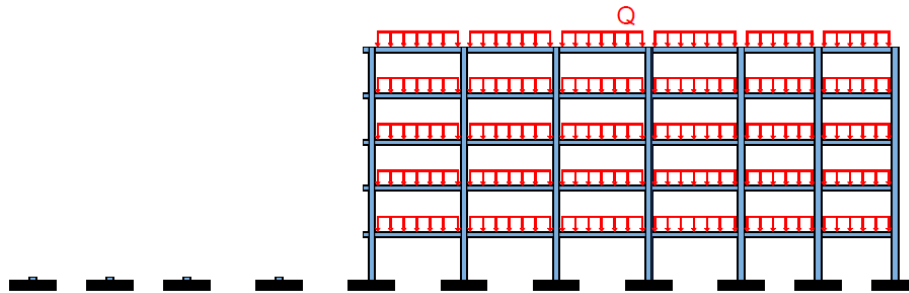


Figure III.71: Layout of the structure for the third iteration of the yield design calculation after the loss of columns # 11 and 16.

III.4.3.5.b Non-linear static analysis on the whole structure

As for previous illustrative examples in categories C1, C2, and C3, a non-linear static analysis with the assumption NL2 is applied on the whole structure. The divergence of calculation occurs when the deflection $\delta_{16} = 1.46 \text{ m}$ on the top of removed column # 16 (see Figure III.72), where the load capacity of the structure increases until $Q_{u,NL2}^{C4} = 25.4 \text{ kN/m}$. Plastic hinges are developed at the base supports b1 and b2, as shown in Figure III.73, which indicates the development of a failure mechanism on the indirectly affected part. The bending moment at b2 is lower than that of b1 due to the high compression force developed in the

column # 6 (see Figure III.74), while a tension force is developed in the column # 1, where the rotation of the indirectly affected on the left side leads to this aspect.

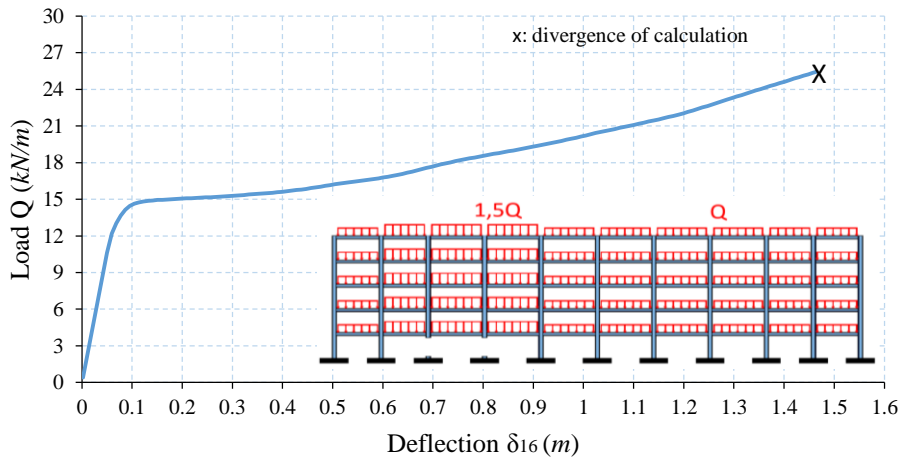


Figure III.72: Deflection δ_{11} -load diagram of non-linear static analysis on the whole structure after the loss of columns # 11 and 16.

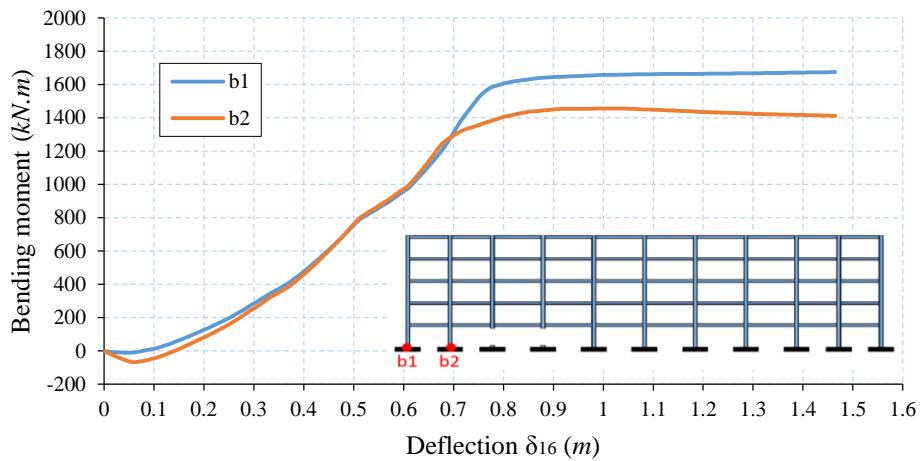


Figure III.73: Deflection δ_{16} -bending moment diagram at base supports after the loss of columns # 11 and 16.

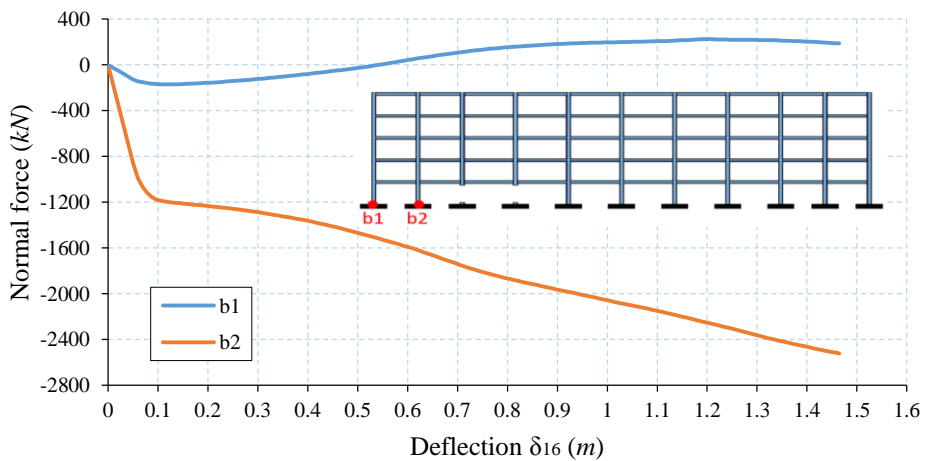


Figure III.74: Deflection δ_{16} -normal force diagram at base supports after the loss of columns # 11 and 16.

The computation time of the non-linear analysis on the whole structure is $t_{C4}^{NL2} = 12,351.0$ s. The use of the proposed coupling strategy indicates that three iterations of yield design calculation and one iteration of non-linear analysis (see Table III.9) on the substructure of the directly affected part are performed, where the total computation cost is $t_{C4}^{CS} = 1,105.0$ s.

	Coupling Strategy t_{C4}^{CS}				Non-linear analysis on the whole structure t_{C4}^{NL2}	Gain
	1 st iteration of yield design calculation	Non-linear analysis	2 nd iteration of yield design calculation	3 rd iteration of yield design calculation		
Computation cost (s)	15	1,067.0	15	8	12,351.0	91%
	Total = 1,105.0					

Table III.9: Comparison in the computation cost of the proposed coupling strategy with that of the non-linear analysis under the loss of columns # 11 and 16.

III.4.4 General discussion

The framework proposed in Section III.4.1 and in particular in Figure III.32 has been applied for illustration to a steel beam element with different boundary conditions (Section III.4.2) and to a steel-framed building (Section III.4.3).

For the beam case study, it is shown how the boundary conditions can change the yield design conclusions, and then the development of a tensile membrane action. For the frame building, the structural response can be classified in four categories (C1, C2, C3 and C4) based on the level of failure propagation. An example of each category is presented to illustrate the different cases of structural response and to compare results with a non-linear analysis applied on the whole structure. These examples show the capacity of the proposed coupling strategy to model the failure propagation with identifying the initial and the final states of collapse. Besides, the comparison of the computation time shows the capacity of this strategy to decrease this time compared to a full non-linear analysis on the whole structure. The iteration of the non-linear analysis in the proposed strategy aims to identify the geometric changes of the structure when there is a possibility to develop an alternative functioning. In order to reduce the computation time, the non-linear analysis is performed only on the directly affected part with taking into account the effect of the indirectly affected part by considering horizontal springs at the extremities of the substructure. The stiffness of the springs are calculated by a simplified method that does not represent the performance of the indirectly affected part with high accuracy. However, the relative error of the deflection results obtained under this assumption compared to those of the whole structure is relatively acceptable. Also,

the omission of the rotations of the supports in the substructure can influence the prediction of the deflection. Through the iterative procedure, the geometric changes are integrated in the model for a next iteration of the yield design calculation to verify if either the indirectly affected part can resist the forces developed in the directly affected part during the development of the tensile membrane action or not. In this iteration the ignoring of the horizontal displacements of the indirectly affected part causes the elimination of some P-delta effect. In the proposed case study, this effect was found to be less significant when compared to the bending resistance of the column. As the objective of this work is not to develop a macro-model of connections (as detailed in Section II.3.2) but rather to focus on a strategy to iteratively follow the failure propagation, this assumption was adopted in this dissertation. However, this effect can have more influence when dealing with taller structures. Such discussions are further proposed in the general conclusions of the manuscript.

III.5 CONCLUSIONS

An original structural modelling strategy is proposed in this chapter to simulate progressive collapse, where this method is based on an iterative coupling between the yield design approach and a non-linear analysis. The adoption of the yield design theory allows a simplification in the analysis of the structural response, where it is a direct approach that offers saving in computation time and mitigating convergence issues. Moreover, the use of a non-linear analysis aims to study the development of an alternative functioning in the directly affected part, and it allows to simulate the geometrical and the material non-linearities. The numerical modelling of the yield design calculation is presented, and a comparison with the non-linear analysis is performed with a view to verify the consistency of the results.

The proposed method is able to identify the initial failure mechanism that occurs due to the local failure scenario, and it allows to follow the propagation of failure, where the final stage of failure can be identified. One can investigate in a reasonable computation time a large number of local failure scenarios, so a general assessment of structural robustness can be performed. The identification of the initial and the final states of failure aims to evaluate and to quantify the propagation, which in the end should help identify the structural capacity to prevent the propagation of local failure.

The proposed strategy will be used in Chapter IV to investigate the structural response under several local failure scenarios and in the end calculate some indices for structural robustness quantification.

CHAPTER IV

QUANTIFICATION OF STRUCTURAL ROBUSTNESS

IV.1 INTRODUCTION

One major goal of this work is the quantification of structural robustness against exceptional events. The concept of exceptional event presents a high level of uncertainty either by the type or the intensity of the action, thus leading to significant uncertainties on the local failure itself. Event-dependent and independent scenarios have been presented in Section II.1.1 by distinguishing the cases when the hazard event (or the abnormal condition) is fully identified and when only a local failure scenario is considered, respectively. The former category appears an adapted option for the engineering community when designing for robustness, in order to avoid the study of a large number of event-dependent scenarios with different types, intensities, locations and configurations of actions. Further, referring to event-independent scenarios allows one to avoid the explicit simulation of the actions and their effects on the structure.

In particular, Eurocodes (NF EN 1991-1-7, 2007) provide some guidelines to mitigate progressive collapse. Depending on the consequence class of a structure, one can use the tying force method (to enhance ductility, continuity and to guarantee structural redundancy), or the alternative load path approach to check that a structure can resist the loss of one structural component (independent scenario). Some previous studies (Izzuddin et al., 2007; Jaspert et al., 2011; Botte et al., 2014) in the scientific community have focused on the alternative load path approach to investigate whether the damage of some components with large displacements can lead to an alternative functioning and eventually prevent the cascading collapse of other elements in the structure.

With respect to the structural robustness definition that is the ability of a structure to avoid disproportionate consequences in relation to some initial damage (NF EN 1991-1-7,

2007), an analysis limited to the notional loss of only one structural component may fail to fully capture the concept of disproportionate consequences. Indeed, the term "disproportionate" relates to some comparison between the local failure and a final state after failure propagation. Hence, event-independent scenarios could include the loss or severe damage of several structural components, such as columns, and not only one element as it is currently considered. This last point is highlighted as it is one major ambition of this research work to provide a framework that (i) opens the set of potential local failures as initial starting point, (ii) follows failure propagation and characterizes progressive collapse, and (iii) gives some direction to avoid considering an infinity of initial local failures.

It has been identified in Section III.4.3.1 that the structure response under a local failure scenario falls into the four following categories:

- the structure resists the local failure without major consequences, and the local failure does not lead to a failure mechanism in any part of the structure (category C1);
- some structural components are damaged due to a large displacement, but the structure manages to develop an alternative equilibrium state. The failure does not propagate and there is no partial collapse of the structure (category C2);
- the structure locally fails and collapses though without propagation out of the directly affected part (category C3);
- the structure locally fails and failure propagates out of the directly affected part (category C4).

In the first two cases, the structure clearly resists the local failure, thus allowing to consider that it is robust against the local failure scenario. While in the third and fourth cases, some questions arise: how can the propagation of failure be described as disproportionate? Does the propagation of failure out of the directly affected part mean that the structure is not robust? Should the robustness concept be a combined metric of the initially affected part and failure propagation extent? One can expect that there will always be a level of local failure scenario for which a progressive collapse initiates. It should then be acknowledged that a structure cannot be designed to resist any local failure scenarios with any level of initial damage. Conceptually, the propagation of failure does not necessarily mean that the structure is not robust until one defines a metric for assessment of a disproportionate failure propagation. In fact, to decide whether some propagation extent is unacceptable, one need first to provide a model that quantifies the failure propagation itself through the structure in relation to some initial local failure scenario. This chapter proposes to investigate this aspect, using the iterative progressive collapse modelling introduced in Chapter III. The

quantification of structural robustness includes the analysis of a set of local failure scenarios applied to the structure, and some robustness indices are proposed, based on the corresponding structural response. In particular, the objective is to assess structural robustness by considering local failure scenarios and introducing a proportional index between the initial and final (after propagation) structural states. A first robustness index is proposed in this direction. Besides, the characterization of the maximum magnitude of local scenarios that the structure can withstand, using an energy-based approach, leads to a second robustness index. The identification of the maximum allowable capacity of the structure to face some exceptional events can be an indication of the structural robustness. The propagation is then considered as unacceptable when a threshold identified beforehand and based on some exploitation criterion is reached. Finally, one discusses how the two metrics on failure propagation and energy needed for initial failure can be combined to simultaneously characterize the concept of robustness.

To detail the proposed strategy, this chapter is organized as follows:

First, one details how local failure scenarios are characterized. The approach considers independent scenarios in the sense that the local failure is not linked to an identified event or action. However, one introduces a set of virtual actions, representative of exceptional events, which enables to identify an energy level required to cause the local failure.

Second, one introduces some robustness indices and details the philosophy between each of these indices.

Third, one illustrates the proposed strategy on the steel frame building introduced in Chapter III. The aim here is to extend the concept of local failure scenarios to several components and to investigate failure propagation to characterize the concept of disproportionate extent in failure propagation. Several strengthening options are then considered for this building and the proposed approach is used to compare structural robustness levels among these options.

IV.2 CHARACTERIZATION OF LOCAL FAILURE SCENARIOS

The characterization of a local failure scenario aims to provide a quantitative indication of its magnitude. The assessment should not be limited to the number of affected structural elements. It should also include the resistance capacity of these elements to withstand an action. As the associated hazard is not considered in an event-independent scenario, it is assumed that the failure of the structural element occurs under a virtual loading action, representative of a potential exceptional event (explosion or impact).

Introducing a load scenario on the structure, the associated energy required to cause the local failure is an indicator to characterize the local failure scenario itself. In order to calculate the energy of local failure scenario, the following points have to be specified:

- type of loading: uniform, concentrated,...
- other existing loads on the structural element,
- location of loading,
- affected elements: beams, columns,...
- type of damage: total loss, cracking, corrosion,...
- boundary conditions of affected elements.

This method is applied for illustration to the steel-framed building of Section III.4.3, and the considered local failure scenario consists of the notional total loss of the column # 26 (see Figure III.35), which is an H-shaped cross-section steel element HE500B. The end of the column on the bottom is considered as fixed support, while the support on the top restrains the rotation and the horizontal displacement with allowing the vertical displacement, as shown in Figure IV.1. Further, the column is subject to a vertical concentrated load P on the top of the column, which represents the gravity load supported by the column. In this example, the gravity load supported by column # 26 is equal to 948 kN.

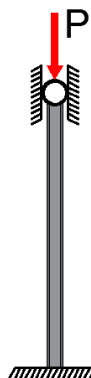


Figure IV.1: Boundary conditions to characterize the loss of a column.

The required energy to cause the failure of a column is expressed in terms of the action load on the structural element and the element deformation, as described below (Izzuddin et al., 2007):

$$E = \int \underline{Q} d\underline{u} \quad (\text{IV.1})$$

where E is the failure energy of the structural element according to the applied action, \underline{Q} is the action load, and \underline{u} is the displacement vector of the structural element. The displacement vector \underline{u} is assumed to correspond to the element failure when the material strains reach the ultimate strain ε_u which corresponds to the ultimate strength f_u of steel material, as shown in Figure IV.2(a). As the constitutive law used in the numerical simulation is elastic-perfectly plastic, the ultimate strength f_u corresponds to the yield strength f_y (see Figure IV.2-b). However, an ultimate strain ε_u is considered with a view to calculate the failure energy with considering the strain of materials. Brozzetti (1996) recommends that the ultimate strain should be $\varepsilon_u \geq 20\varepsilon_y$, where ε_y is the yield strain. Hence, the ultimate strain $\varepsilon_u = 20\varepsilon_y = 34\%$ is adopted in the following to calculate the failure energy E .

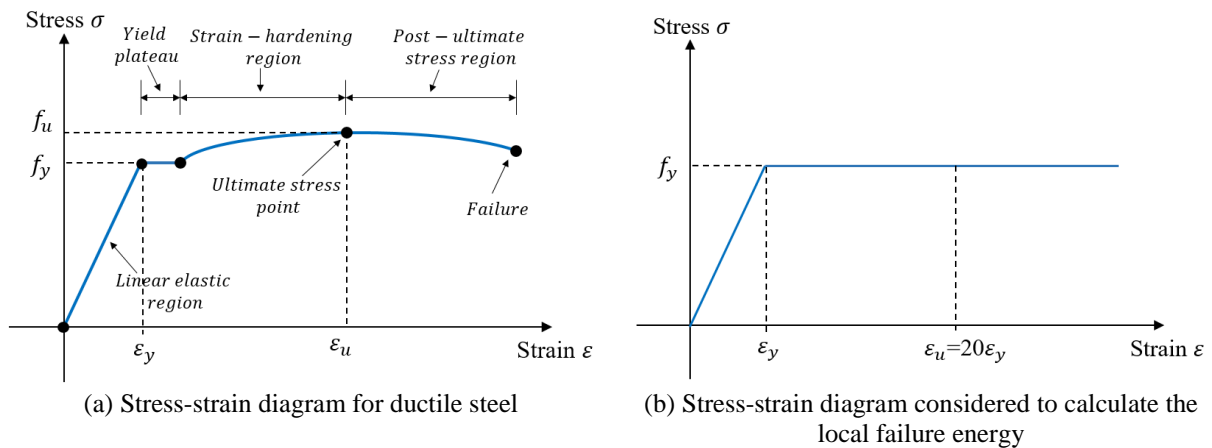


Figure IV.2: Constitutive law of steel.

A non-linear static analysis is performed to calculate the energy of the local failure scenario. Moreover, the energy is calculated according to different types of loading, as shown in Figure IV.3, such as distributed loads (A_1 , A_3 , and A_4) that can represent the effect of an explosion action, or a concentrated load (A_2), in this case in the middle of the column, that can represent the effect of an impact. Including different types of loads enables to evaluate the structural element resistance against different scenarios, and to identify if there is a possibility to consider only one load type for the characterization of the local failure scenarios.

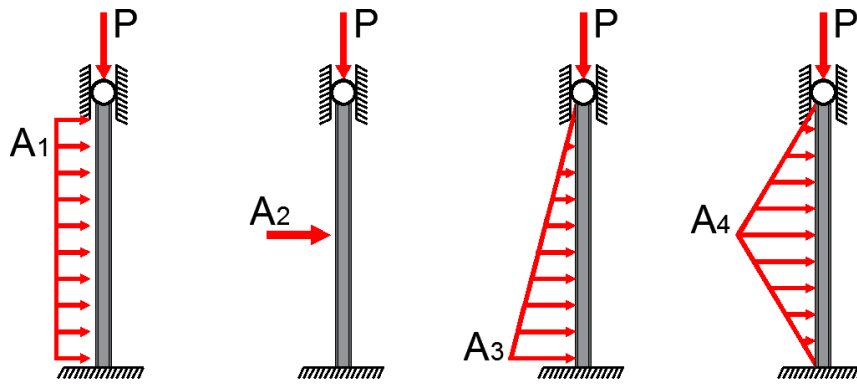


Figure IV.3: Applied loads to characterize the loss of a column.

Figure IV.4(a, b, c and d) shows the deflection δ_c at the middle point of column for each applied load action, until the axial strain of material reaches the ultimate strain ϵ_u (34‰). The maximal deflection at failure is different for each type of load, which relates to the deformation modes of the element in each case. Figure IV.5 presents the axial strain at the critical points, where the material reaches the ultimate strain limit. The material strain reaches the ultimate strain ϵ_u in the compression zone for the four types of loading, and the case of A2 has the maximum horizontal displacement. Moreover, the energy values that correspond to the failure of the columns are presented in Table IV.1, where these values depend on the load type. The failures under loads A2 and A3 require the highest and lowest values of energy, respectively. One observes that the ascending order of the load types is the same when considering the energy and the deflection.

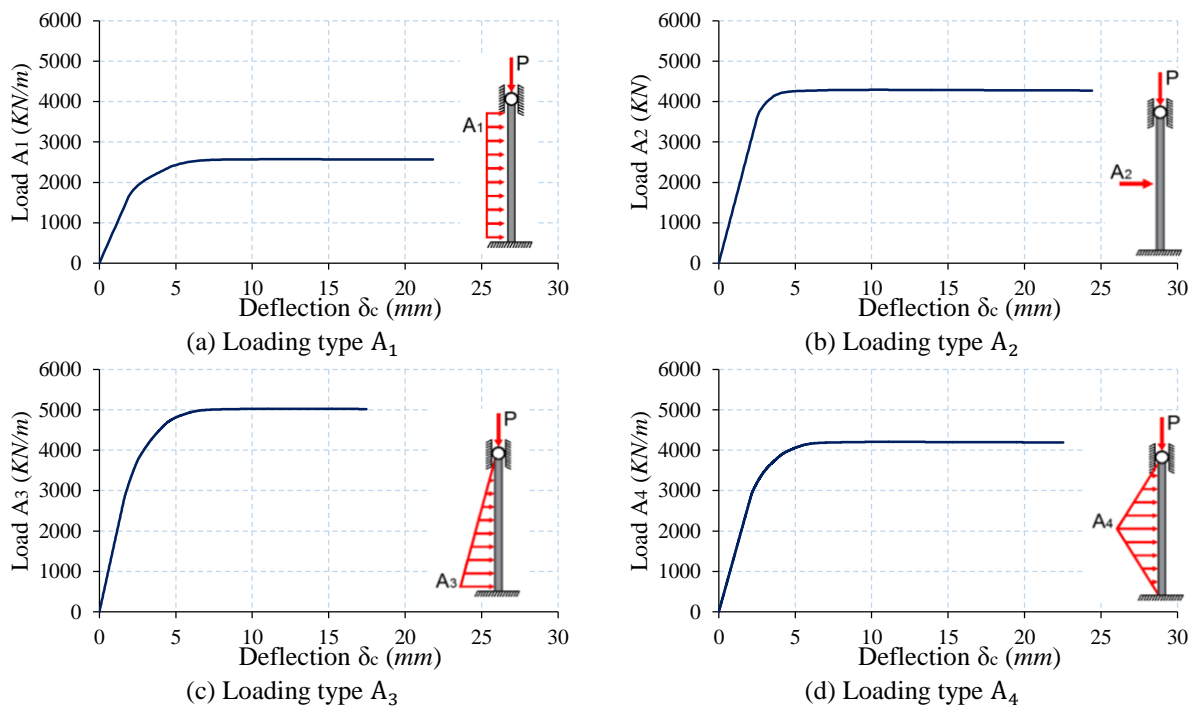


Figure IV.4: Applied load and deflection δ_c diagram of column # 26 with cross-section HE500B under the loading types A₁, A₂, A₃ and A₄.

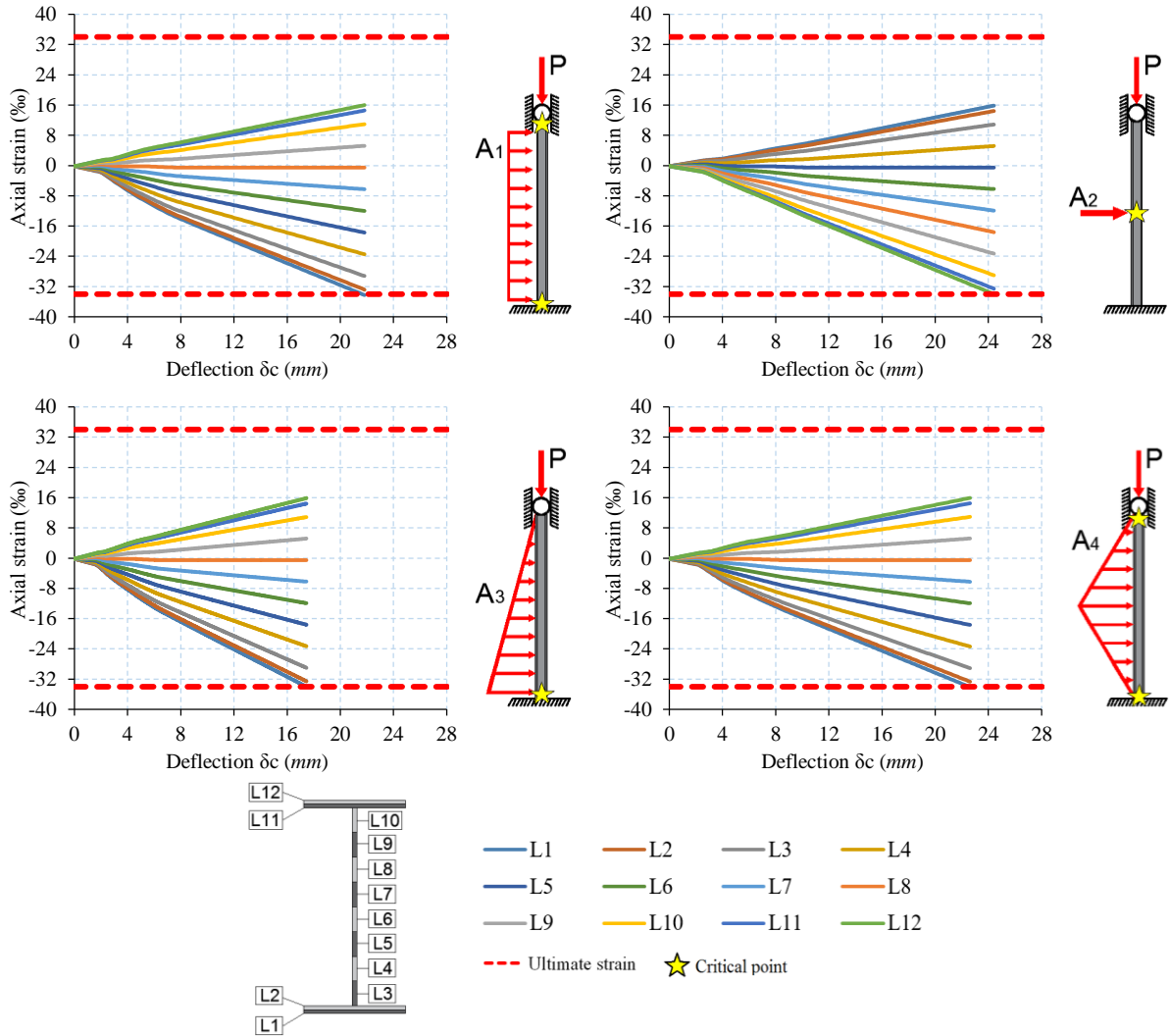
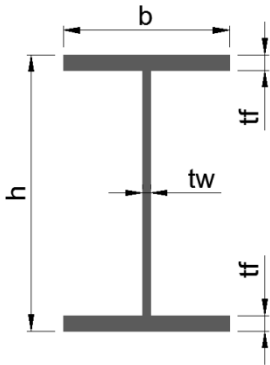


Figure IV.5: Deflection and axial strain at critical points diagram.

Loading type	A ₁	A ₂	A ₃	A ₄
Energy (kJ)	80.6	97.9	66.2	91.3
Deflection δ_c (mm)	21.8	24.4	17.5	22.6

Table IV.1: Failure energy and deflection of column # 26 under the loading types A₁, A₂, A₃ and A₄.

In order to simplify the analysis of local failure scenarios, one investigates if there is a possibility to characterize the local failure scenario by using only one type of action that can be representative of the different load events that may happen when using an energy-based approach. Several cross-sections are considered with the geometric details summarized in Table IV.2.



	Cross-section element l	h (mm)	b (mm)	t_w (mm)	t_f (mm)
HE200B	1	200	200	9	15
HE300B	2	300	300	11	19
HE400B	3	400	300	13.5	24
HE500B	4	500	300	14.5	28
HE600B	5	600	300	15.5	30
HE700B	6	700	300	17	32
HE800B	7	800	300	17.5	33
HE900B	8	900	300	18.5	35
HE1000B	9	1000	300	19	36

Table IV.2: Geometric details of H-shaped cross-section steel elements.

The structural responses for the different elements and actions are shown in Figure IV.6, Figure IV.7, Figure IV.8 and Figure IV.9. These figures show the increment of the resistance capacity against the applied loads with the increment of the element dimensions. Further, the curves that correspond to the same type of loading have the same shape. However, the maximum deflection of the elements δ_c decreases with the increment of element dimensions, where the increment of the element depth causes a larger axial strain according to the deflection δ_c (the material reaches the ultimate strain with a lower value of deflection).

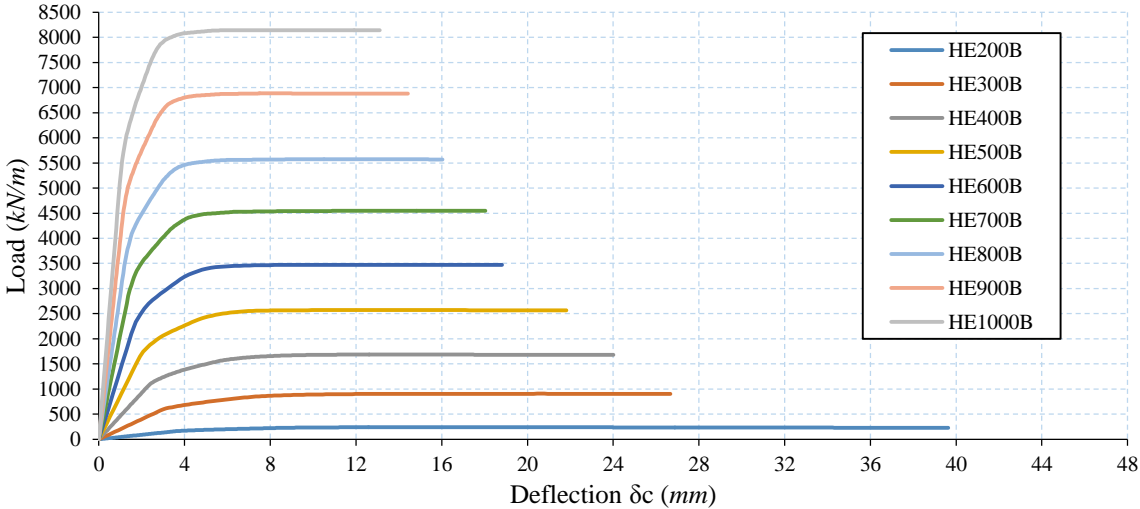


Figure IV.6: Applied load and deflection diagram for load type A₁.

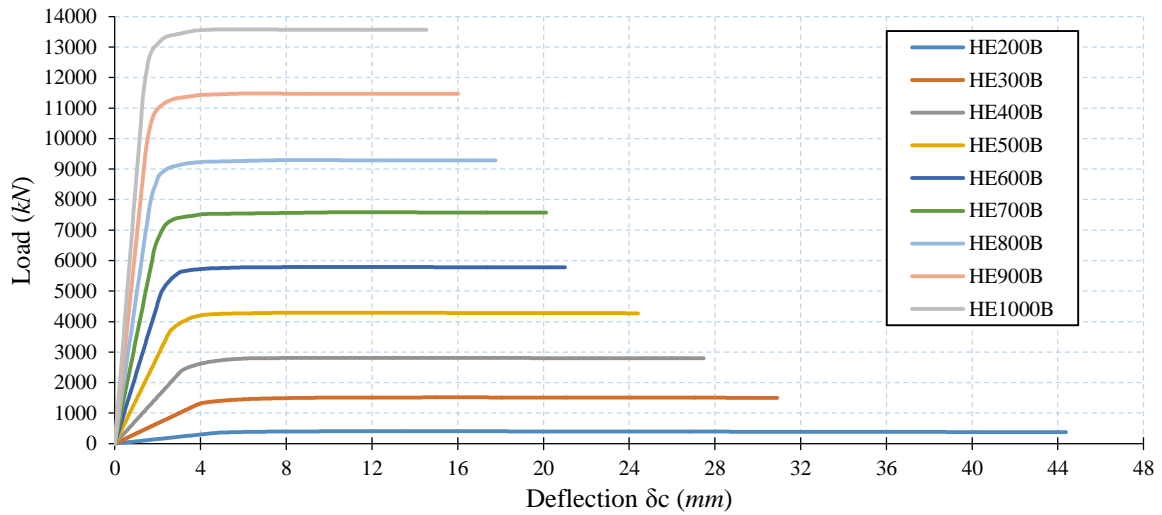


Figure IV.7: Applied load and deflection diagram for load type A₂.

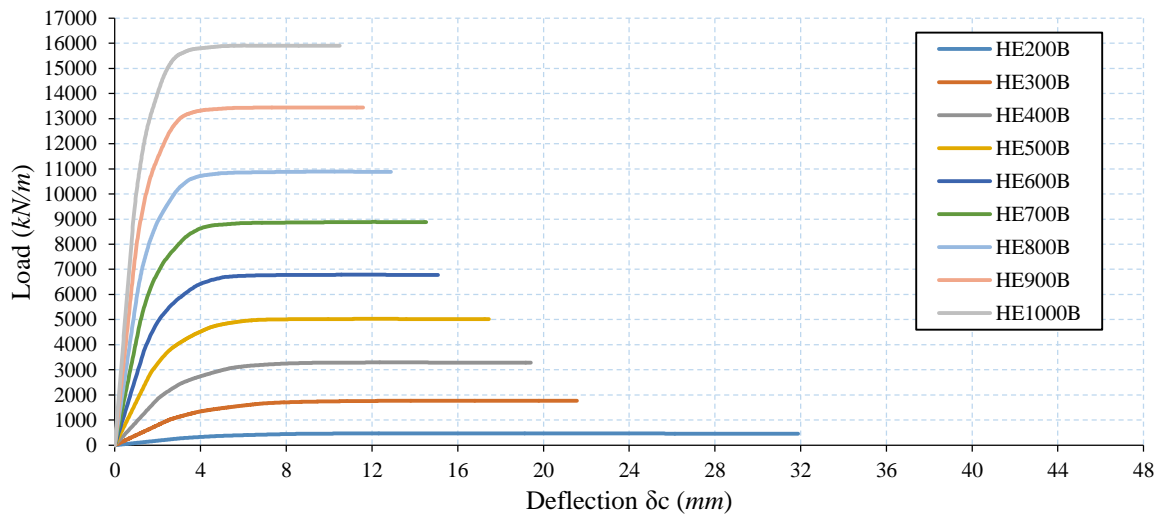


Figure IV.8: Applied load and deflection diagram for load type A₃.

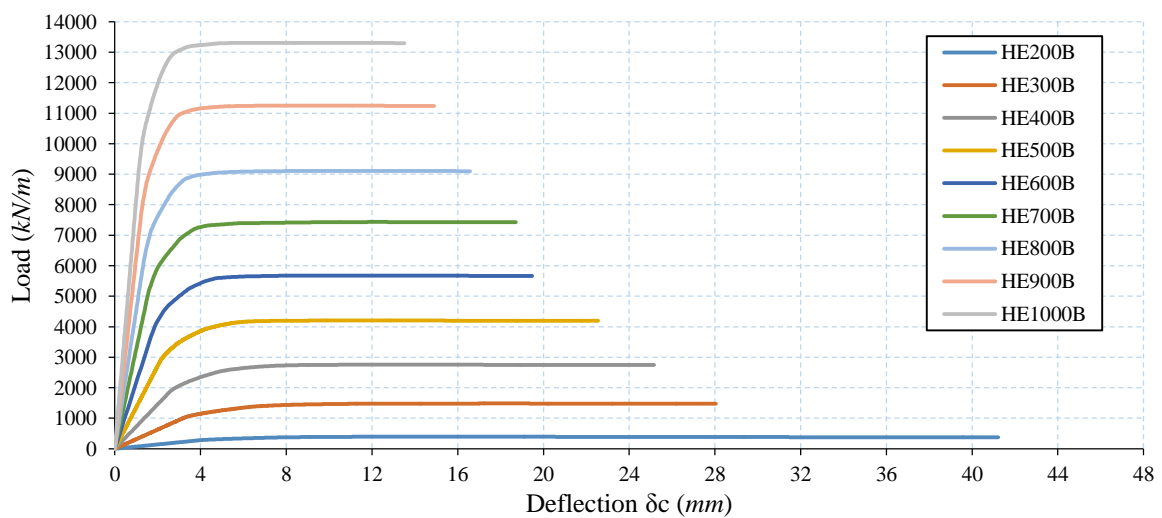


Figure IV.9: Applied load and deflection diagram for load type A₄.

Figure IV.10 shows the increment of failure energy $E_{i,k}$ with the element dimension of cross-section i and under each load type k , which indicates that the evaluation of the resistance capacity of a structural element by the failure energy can be an efficient tool to characterize and quantify the local failure scenario.

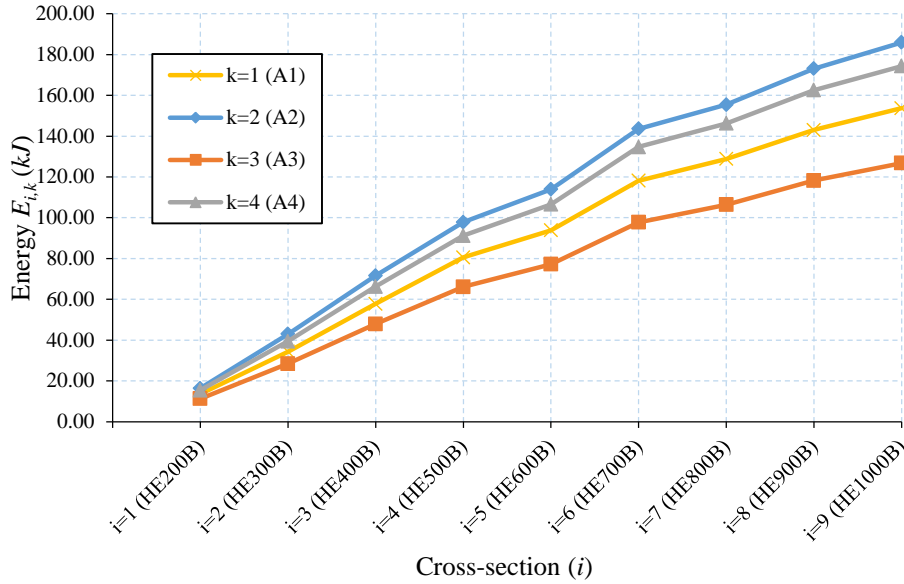


Figure IV.10: Failure energy of a column element with different dimensions of H-shaped steel cross-section.

With a view to evaluate the increment of failure energy according to the structural element dimension, the index $\delta E_{i,k}$ is defined:

$$\delta E_{i,k} = \frac{E_{i,k}}{\bar{E}_k} ; \quad \bar{E}_k = \frac{1}{n_{CS}} \sum_{i=1}^{n_{CS}} E_{i,k} \quad (\text{IV.2})$$

where $E_{i,k}$ is the failure energy for cross-section i and load type k , and \bar{E}_k is the average failure energy for load type k among the n_{CS} cross-sections investigated ($n_{CS} = 9$ in this example). Figure IV.11 shows that when comparing two different cross-sections, the increment of energy is the same for all load types, which shows that the use of the four load types relates to the resistance capacity in a homogeneous manner. Moreover, in order to evaluate the ratio of failure energy according to the load type for each cross-section i , the energy ratio $\rho E_{i,k}$ is calculated as follows:

$$\rho E_{i,k} = \frac{E_{i,k}}{\bar{E}_i} ; \quad \bar{E}_i = \frac{1}{n_l} \sum_{k=1}^{n_l} E_{i,k} \quad (\text{IV.3})$$

where \bar{E}_i is the average energy for element cross-section i among the n_l load types investigated ($n_l = 4$ in this example). Figure IV.12 shows that this energy ratio is similar for

all the different cross-section dimensions. If one compares two different cross-sections in Figure IV.12, the order of energy ratio ($\rho E_{i,k}$) among load types does not change, where they are classified in ascending order as follow: A_3 , A_1 , A_4 and A_2 . Therefore, using only one load type for failure energy calculation is sufficient to lead a relative comparison of cross-sections, when relying on an energy-based approach.

In this dissertation, the uniformly distributed load A_1 is chosen to characterize local failure scenarios, where the energy of a scenario with the notional loss of several structural elements is equal to the sum of the failure energy of each element.

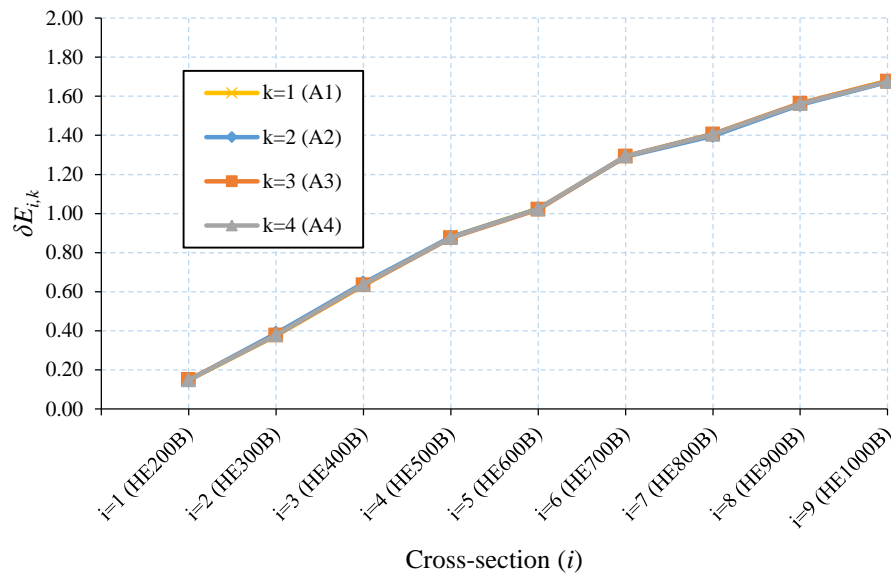


Figure IV.11: Failure energy increment with the structural element dimension.

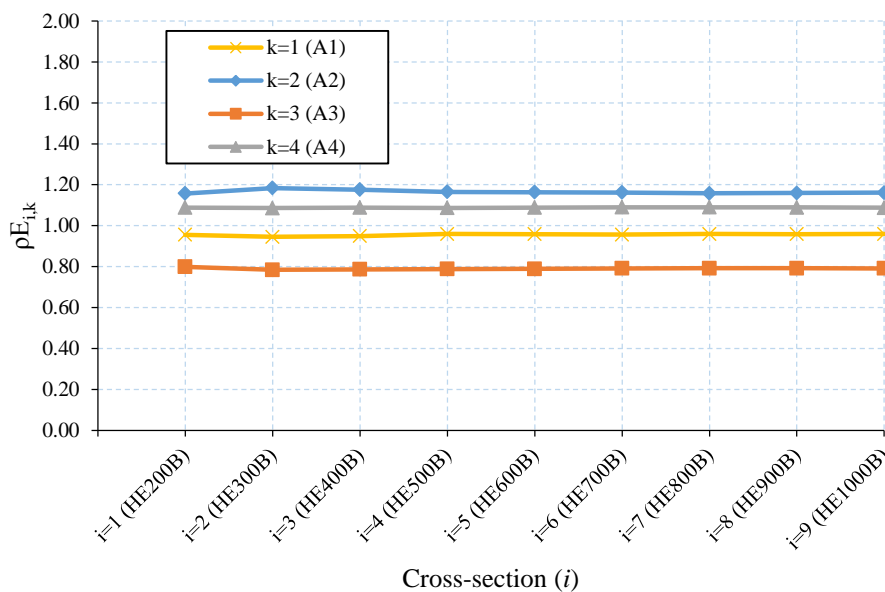


Figure IV.12: Ratio of energy for different types of loading for each cross-section i .

IV.3 PROPOSED STRUCTURAL ROBUSTNESS INDICES

In order to quantify the structural robustness, some indices are introduced thereafter, based on the investigation of some significant local failure scenarios, which allows a global assessment of the structural capacity. These indices aim to provide practical information about the resistance of a structure against some local failure scenarios (El Hajj Diab et al., 2019). In this regard, two main performance assessments are identified:

- the extent to which cascade failure propagates,
- the maximum allowable capacity of the structure to face exceptional events.

IV.3.1 Robustness Propagation Failure Index (*RPMI*)

The first index is the Robustness Propagation Failure Index (*RPMI*), which aims to quantify the structural capacity to prevent the propagation of a local failure. The first step is to identify the degree of failure propagation (DFP_i) for each applied scenario i , which is obtained by dividing a metric $\mathcal{M}(\cdot)$ of the collapsed part after propagation of failure (CP_i) by the same metric for the initially damaged part (IDP_i), as described below:

$$\begin{cases} DFP_i = \frac{\mathcal{M}(CP_i)}{\mathcal{M}(IDP_i)} & \text{if } \mathcal{M}(IDP_i) \neq 0 \\ DFP_i = 0 & \text{if } \mathcal{M}(IDP_i) = 0 \end{cases} \quad (IV.4)$$

The collapsed part (CP_i) and the initially damaged part (IDP_i) can be practically quantified by the length of beams in a 2D structure, or the area of slabs in a 3D structure. The value of initial damaged part allows to identify if the local failure leads to any direct consequences. In case the length of beams in initially damaged part is equal to zero, the structure is insensitive to the local failure, where there is no failure mechanism that initiates. Conversely, if it is positive, the structure cannot remain within the initial configuration and a failure mechanism initiates. The initial damaged part IDP_i under scenario i is then identified by the first iteration of the yield design calculation in which one identifies the failure mechanism that occurs (see Section III.4). Identifying a failure mechanism does not necessarily mean that there is some collapse, as an alternative functioning may develop to resist the applied loads, which is investigated herein by an iterative coupling with a non-linear modelling of the directly affected part. The collapsed part is identified by the last iteration of the proposed modelling strategy (see Figure IV.13), which represents the total part of the structure that has lost the mechanical stability under the applied loads. Hence, the degree of failure propagation described in Equation (IV.4) enables to quantify the propagation of a local failure, and the Robustness Propagation Failure Index (*RPMI*), expressed as:

$$RPF_i = \max \{DFP_i, i = 1, \dots, N\} \quad (IV.5)$$

is equal to the maximum degree of failure propagation among the N applied scenarios.

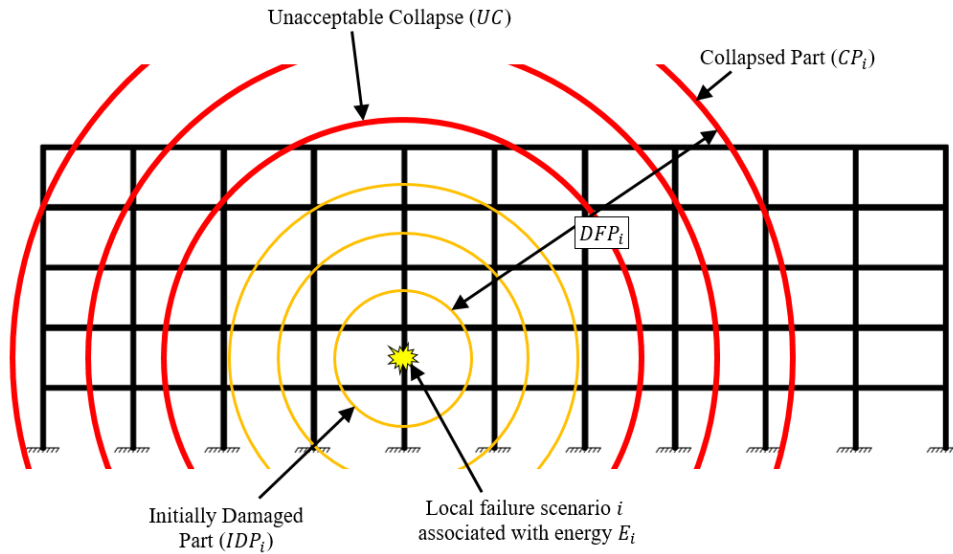


Figure IV.13: Characterization of the progressive collapse for scenario i .

This index represents the worst case of failure propagation that may occur in the structure for the set of considered local failure scenarios. Based on the RPF_i value, one can identify whether the structure undergoes progressive collapse. The local failure scenarios with the largest propagation extent can be identified, as well as the way failure propagates, which allows to identify the critical zones of the structure that should be strengthened.

IV.3.2 Robustness Energy Index (REI)

In order to quantify the maximum capacity of structure to face exceptional events, a second index is proposed, which is the Robustness Energy Index (REI). In this regard, the characterization of applied scenarios by the energy required to cause the local failure allows to quantify the magnitude of the local failure scenario. Further, based on a threshold of unacceptable collapse, the applied scenarios can be characterized as either acceptable or unacceptable. To calculate this index, the first step is to identify the set of critical scenarios leading to an unacceptable collapse, as follows :

$$\forall i \in [1, N], \quad \text{if } \mathcal{M}(CP_i) \geq UC \Rightarrow i \in CS \quad (IV.6)$$

where UC is a threshold for unacceptable collapse and CS is the corresponding set of critical scenarios.

The Robustness Energy Index $REI(UC)$ is equal to the minimum energy value of the critical scenarios belonging to CS :

$$REI(UC) = \min\{E_j, j \in CS\} \quad (IV.7)$$

where E_j is the energy required to cause the j^{th} local failure scenario belonging to CS .

This index identifies the minimum magnitude of local failure scenarios that lead to an unacceptable collapse, based on the threshold UC defined beforehand (see Figure IV.13). It indicates the maximum capacity of a structure to withstand exceptional events and can help to reveal a potential lack of resistance in some critical elements, for which the failure under events that are relatively not significant in magnitude leads to an unacceptable collapse. This index identifies some weak points of a structure that could be strengthened.

IV.3.3 Discussion on the most critical scenarios

The two indices RPM and $REI(UC)$ can be considered separately as they capture different aspects of structural robustness. Identifying the largest degree of failure propagation DFP_i among each applied scenario i enables to quantify the largest extent to which failure may propagate in cascading events. Minimizing the energy required to cause the j^{th} local failure scenario such that one reaches an unacceptable failure extent (threshold) is more focused on the initial scenario. However, using this second index means that the end user is able to identify such threshold UC and to fix it beforehand (for example by the client or some standards). If one refers to the definition of robustness in the Eurocodes, one should design a structure so that it is not damaged to an extent disproportionate to the original cause. One could then consider as the most critical scenarios those with both minimal energy required to cause the local failure and maximal extent of failure propagation. This sorting process among N initial failure scenarios can be formulated as below and does not lead to only one value but to a set of non-dominated solutions known as a Pareto front, which represents the most critical scenarios, for the considered objective functions:

$$\left\{ \begin{array}{l} \text{Find } i = 1, \dots, N \\ \min\{E_i\} \\ \max\{DFP_i\} \end{array} \right. \quad (IV.8)$$

In Equation (IV.8), the two objective functions can be conflicting objectives and this problem corresponds to a bi-objective formulation in which one aims to classify dominated and non-dominated solutions. In mathematical terms, if one denotes X the set of feasible decision vectors of the following optimization problem:

$$\left\{ \begin{array}{l} \text{Min} (f_1(\underline{x}), f_2(\underline{x}), \dots, f_k(\underline{x})) \\ \text{such that } \underline{x} \in X \end{array} \right. \quad (IV.9)$$

there does not typically exist a feasible solution that minimizes all objective functions simultaneously and one looks for non-dominated solutions. A feasible solution $\underline{x}^1 \in X$ is said to (Pareto) dominate another solution $\underline{x}^2 \in X$, if

$$\begin{cases} f_i(\underline{x}^1) \leq f_i(\underline{x}^2) \text{ for all indices } i \in \{1, 2, \dots, k\} \\ f_j(\underline{x}^1) < f_j(\underline{x}^2) \text{ for at least one index } j \in \{1, 2, \dots, k\} \end{cases} \quad (\text{IV.10})$$

One should also mention that if some objective function is to be maximized, it is equivalent to minimize its negative. In Equation (IV.8), as the set of solutions is already fixed, solving this problem corresponds to one iteration of a non dominating sorted process. The fast non-dominated sorting process proposed by Deb et al. (2002) detailed in Equation (IV.11) can be used to successively identify the first non-dominated front (Pareto front), then the second front, the third one and so on.

$$\left\{ \begin{array}{l} \text{fast non dominated sort } (P) \\ \text{for each } p \in P \\ \quad S_p = \emptyset \\ \quad n_p = 0 \\ \quad \text{for each } q \in P \\ \quad \quad \text{if } (p < q) \text{ then} \\ \quad \quad \quad S_p = S_p \cup \{q\} \\ \quad \quad \text{else if } (q < p) \text{ then} \\ \quad \quad \quad n_p = n_p + 1 \\ \quad \text{if } n_p = 0 \text{ then} \\ \quad \quad p_{rank} = 1 \\ \quad \quad F_1 = F_1 \cup \{p\} \\ i = 1 \\ \text{while } F_i \neq \emptyset \\ \quad Q = \emptyset \\ \quad \text{for each } p \in F_i \\ \quad \quad \text{for each } q \in S_p \\ \quad \quad \quad n_q = n_q - 1 \\ \quad \quad \quad \text{if } n_q = 0 \text{ then} \\ \quad \quad \quad \quad q_{rank} = i + 1 \\ \quad \quad \quad \quad Q = Q \cup \{q\} \\ \quad i = i + 1 \\ \quad F_i = Q \end{array} \right. \quad (\text{IV.11})$$

where:

n_p : the number of solutions which dominate the solution p

S_p : set of solutions that the solution p dominates

Q : non-dominated fronts

One could mention other bi-optimization problems such as:

$$\begin{cases} \text{Find } i = 1, \dots, N \\ \min\{\mathcal{M}(IDP_i)\} \\ \max\{DFP_i\} \end{cases} \quad (\text{IV.12})$$

or

$$\begin{cases} \text{Find } i = 1, \dots, N \\ \min\{\mathcal{M}(IDP_i)\} \\ \max\{\mathcal{M}(CP_i)\} \end{cases} \quad (\text{IV.13})$$

where the goal is each time to look for scenarios with minimal initially affected part and maximal extent (based on failure propagation in Equation (IV.12), or part of the structure that failed at the end in Equation (IV.13)).

The philosophy behind each proposed index is illustrated in Figure IV.13. Minimization of initial damage could relate to E_i or $\mathcal{M}(IDP_i)$ and maximization of consequences corresponds to DFP_i or $\mathcal{M}(CP_i)$. In the following section, one illustrates how structural robustness can be quantified, using the approaches presented in Sections IV.3.1, IV.3.2 and IV.3.3.

IV.4 STRUCTURAL ROBUSTNESS ASSESSMENT OF A STEEL-FRAMED BUILDING STRUCTURE

IV.4.1 Identification and characterization of the applied local failure scenarios

The proposed approach is applied on the steel-framed building structure presented in Section III.4.3 (the combination of dead loads and live loads corresponds to the accidental situation presented in Table III.2). The first step in the assessment procedure is to identify the local failure scenarios that represent the exceptional aspect of the events. The scenarios adopted in this example are limited to the notional total loss of one or several column(s), where the damaged columns are always adjacent, and the maximum extent of local failure is in three bays, so the maximum number of damaged columns is four adjacent columns. There are consequently 190 scenarios to be investigated, which are presented in Table IV.3.

1	1	33	33	65	10 - 15	97	42 - 47	129	24-29-34	161	11-16-21-26
2	2	34	34	66	11-16	98	43-48	130	25-30-35	162	12-17-22-27
3	3	35	35	67	12-17	99	44-49	131	26-31-36	163	13-18-23-28
4	4	36	36	68	13-18	100	45-50	132	27-32-37	164	14-19-24-29
5	5	37	37	69	14-19	101	46-51	133	28-33-38	165	15-20-25-30
6	6	38	38	70	15-20	102	47-52	134	29-34-39	166	16-21-26-31
7	7	39	39	71	16-21	103	48-53	135	30-35-40	167	17-22-27-32

8	8	40	40	72	17-22	104	49-54	136	31-36-41	168	18-23-28-33
9	9	41	41	73	18-23	105	50-55	137	32-37-42	169	19-24-29-34
10	10	42	42	74	19-24	106	1-6-11	138	33-38-43	170	20-25-30-35
11	11	43	43	75	20-25	107	2-7-12	139	34-39-44	171	21-26-31-36
12	12	44	44	76	21-26	108	3-8-13	140	35-40-45	172	22-27-32-37
13	13	45	45	77	22-27	109	4-9-14	141	36-41-46	173	23-28-33-38
14	14	46	46	78	23-28	110	5-10-15	142	37-42-47	174	24-29-34-39
15	15	47	47	79	24-29	111	6-11-16	143	38-43-48	175	25-30-35-40
16	16	48	48	80	25-30	112	7-12-17	144	39-44-49	176	26-31-36-41
17	17	49	49	81	26-31	113	8-13-18	145	40-45-50	177	27-32-37-42
18	18	50	50	82	27-32	114	9-14-19	146	41-46-51	178	28-33-38-43
19	19	51	51	83	28-33	115	10-15-20	147	42-47-52	179	29-34-39-44
20	20	52	52	84	29-34	116	11-16-21	148	43-48-53	180	30-35-40-45
21	21	53	53	85	30-35	117	12-17-22	149	44-49-54	181	31-36-41-46
22	22	54	54	86	31-36	118	13-18-23	150	45-50-55	182	32-37-42-47
23	23	55	55	87	32-37	119	14-19-24	151	1-6-11-16	183	33-38-43-48
24	24	56	1-6	88	33-38	120	15-20-25	152	2-7-12-17	184	34-39-44-49
25	25	57	2-7	89	34-39	121	16-21-26	153	3-8-13-18	185	35-40-45-50
26	26	58	3-8	90	35-40	122	17-22-27	154	4-9-14-19	186	36-41-46-51
27	27	59	4-9	91	36-41	123	18-23-28	155	5-10-15-20	187	37-42-47-52
28	28	60	5-10	92	37-42	124	19-24-29	156	6-11-16-21	188	38-43-48-53
29	29	61	6-11	93	38-43	125	20-25-30	157	7-12-17-22	189	39-44-49-54
30	30	62	7-12	94	39-44	126	21-26-31	158	8-13-18-23	190	40-45-50-55
31	31	63	8-13	95	40-45	127	22-27-32	159	9-14-19-24		
32	32	64	9-14	96	41-46	128	23-28-33	160	10-15-20-25		

Table IV.3: Local failure scenarios for the steel-framed building structure (scenario # on blue background, and corresponding removed column(s) on white background).

The second step is to characterize the failure of each column by the relevant energy. In this respect, the vertical concentrated load P on the top of each column that represents the gravity load supported by the column is identified and presented in Table IV.4. As indicated in Section IV.2, the failure energy is calculated according to a uniform load (see Figure IV.14), where it is applied in y direction. In this example, the discretization of each cross-section in the non-linear analysis is the one shown in Figure IV.5.

The values of failure energy for each column are presented in Table IV.4. The failure energy depends on the vertical load applied on the column, where the energy increases as the concentrated load P decreases. As explained in Section IV.2, the material reaches the ultimate strain ε_u at the edges of the column (top and bottom areas) in the compression zone of the cross-section (see Figure IV.5). Under a larger value of P , the column reaches the ultimate strain ε_u with a lower energy associated with the applied uniform load.

Column #	Vertical load (P) [kN]	Energy [kJ]
1; 51	395.0	100.4
2; 52	316.0	102.1
3; 53	237.0	103.8
4; 54	158.0	105.4
5; 55	79.0	108.6
6; 46	790.0	84.2
7; 47	632.0	87.8
8; 48	474.0	98.8
9; 49	316.0	102.1
10; 50	158.0	105.4
11; 41	869.0	82.5
12; 42	695.2	86.1
13; 43	521.4	98.6
14; 44	347.6	102.0
15; 45	173.8	105.4
16; 21; 26; 31; 36	948.0	80.6
17; 22; 27; 32; 37	758.4	84.4
18; 23; 28; 33; 38	568.8	97.0
19; 24; 29; 34; 39	379.2	101.9
20; 25; 30; 35; 40	189.6	105.4

Table IV.4: Vertical load P and failure energy of each column.

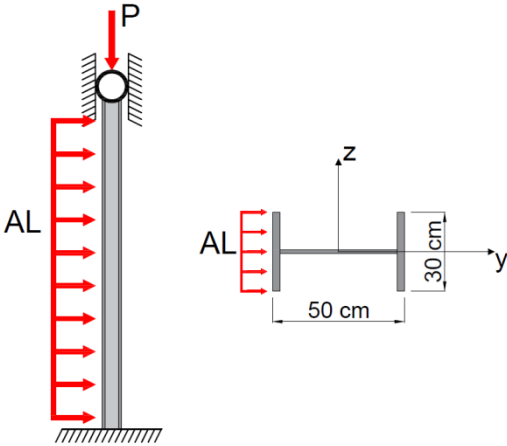


Figure IV.14 : Loading mode of failure energy calculation for the steel columns.

In the following, the failure energy E_i is calculated for each adopted local failure scenario i , where the energy of scenarios with several failed elements is assumed equal to the sum of energy required to the failure of each element. This is a strong assumption in the model where one does not focus on a particular hazard that could damage several elements simultaneously, but rather on the energy needed to damage each element considered in the exceptional scenario until failure. For example, the scenario # 76 is the loss of two columns #

21 and 26 (Figure IV.15), and as the vertical load $P = 948 \text{ kN}$ is similar for both columns, the failure energy is similar $E_{21} = E_{26} = 80.6 \text{ kJ}$. Hence, the failure energy relevant to the scenario # 76 is $E_{76} = E_{21} + E_{26} = 161.2 \text{ kJ}$ (see Figure IV.15). The failure energy values for each adopted local failure scenarios are presented in Table IV.5.

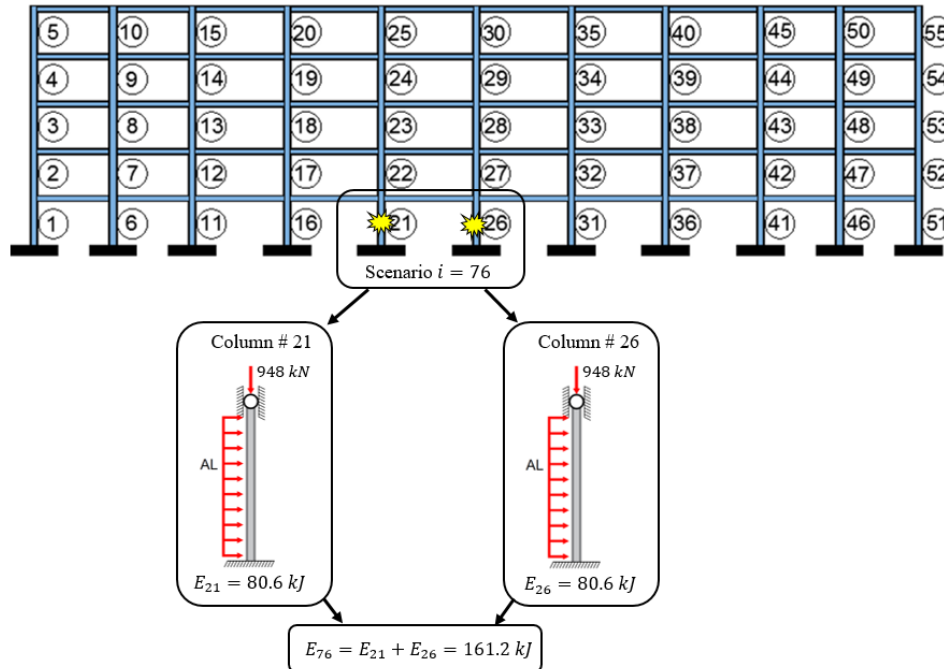


Figure IV.15: Characterization of scenario # 76.

i	E_i												
1	100.4	29	101.9	57	190.0	85	210.8	113	294.4	141	247.3	169	407.8
2	102.1	30	105.4	58	202.6	86	161.2	114	306.1	142	258.3	170	421.5
3	103.8	31	80.6	59	207.6	87	168.7	115	316.2	143	294.4	171	322.5
4	105.4	32	84.4	60	214.0	88	194.0	116	243.7	144	306.1	172	337.5
5	108.6	33	97.0	61	166.7	89	203.9	117	254.8	145	316.2	173	388.1
6	84.2	34	101.9	62	173.9	90	210.8	118	292.7	146	267.1	174	407.8
7	87.8	35	105.4	63	197.4	91	163.1	119	305.9	147	276.0	175	421.5
8	98.8	36	80.6	64	204.2	92	170.4	120	316.2	148	301.2	176	324.3
9	102.1	37	84.4	65	210.8	93	195.7	121	241.9	149	309.6	177	339.2
10	105.4	38	97.0	66	163.1	94	204.0	122	253.1	150	319.4	178	389.7
11	82.5	39	101.9	67	170.4	95	210.8	123	291.0	151	347.7	179	407.9
12	86.1	40	105.4	68	195.7	96	166.7	124	305.8	152	360.4	180	421.6
13	98.6	41	82.5	69	204.0	97	173.9	125	316.1	153	398.2	181	327.9
14	102.0	42	86.1	70	210.8	98	197.4	126	241.9	154	411.6	182	342.6
15	105.4	43	98.6	71	161.2	99	204.2	127	253.1	155	424.8	183	391.4
16	80.6	44	102.0	72	168.7	100	210.8	128	291.0	156	327.9	184	408.1
17	84.4	45	105.4	73	194.0	101	184.7	129	305.8	157	342.6	185	421.6
18	97.0	46	84.2	74	203.9	102	190.0	130	316.1	158	391.4	186	347.7
19	101.9	47	87.8	75	210.8	103	202.6	131	241.9	159	408.1	187	360.4

20	105.4	48	98.8	76	161.2	104	207.6	132	253.1	160	421.6	188	398.2
21	80.6	49	102.1	77	168.7	105	214.0	133	291.0	161	324.3	189	411.6
22	84.4	50	105.4	78	194.0	106	267.1	134	305.8	162	339.2	190	424.8
23	97.0	51	100.4	79	203.9	107	276.0	135	316.1	163	389.7		
24	101.9	52	102.1	80	210.8	108	301.2	136	243.7	164	407.9		
25	105.4	53	103.8	81	161.2	109	309.6	137	254.8	165	421.6		
26	80.6	54	105.4	82	168.7	110	319.4	138	292.7	166	322.5		
27	84.4	55	108.6	83	194.0	111	247.3	139	305.9	167	337.5		
28	97.0	56	184.7	84	203.9	112	258.3	140	316.2	168	388.1		

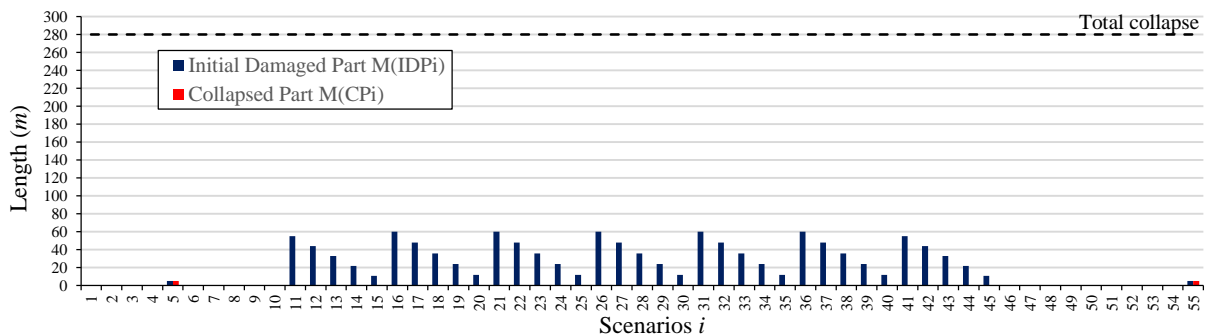
Table IV.5: Energy E_i required to cause the local failure of scenario i (see Table IV.3 for identification of removed columns).

IV.4.2 Structural response under the local failure scenarios

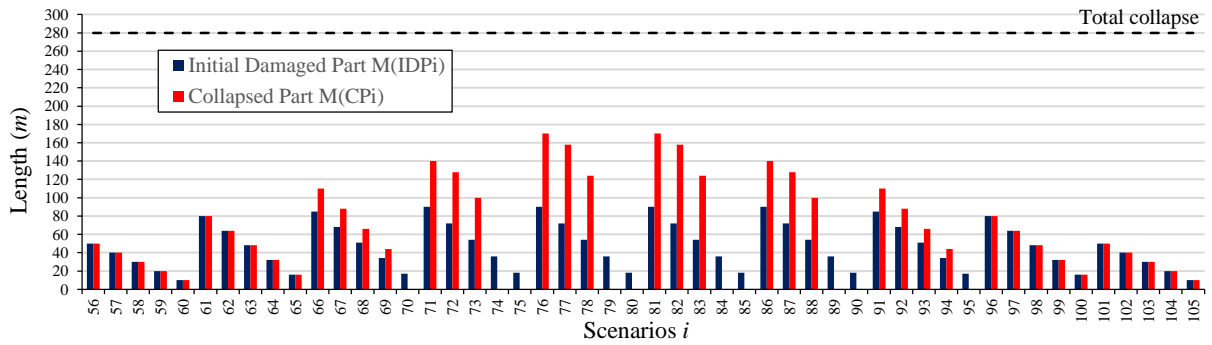
With a view to evaluate the propagation of the failure and quantify the structural robustness, the structural response is presented by two main values:

- a metric of the Initial Damaged Part $\mathcal{M}(IDP_i)$: length of the beams within the area directly affected under the scenario i . The value $\mathcal{M}(IDP_i)$ is identified by the first iteration of yield design calculation in the proposed strategy of progressive collapse modelling ;
- a metric of the Collapsed Part $\mathcal{M}(CP_i)$: length of the beams within the area that collapsed under the scenario i . The value of $\mathcal{M}(CP_i)$ is identified by the last iteration of the yield design calculation in the proposed modelling strategy, where it is equal to the length of the beams that collapse.

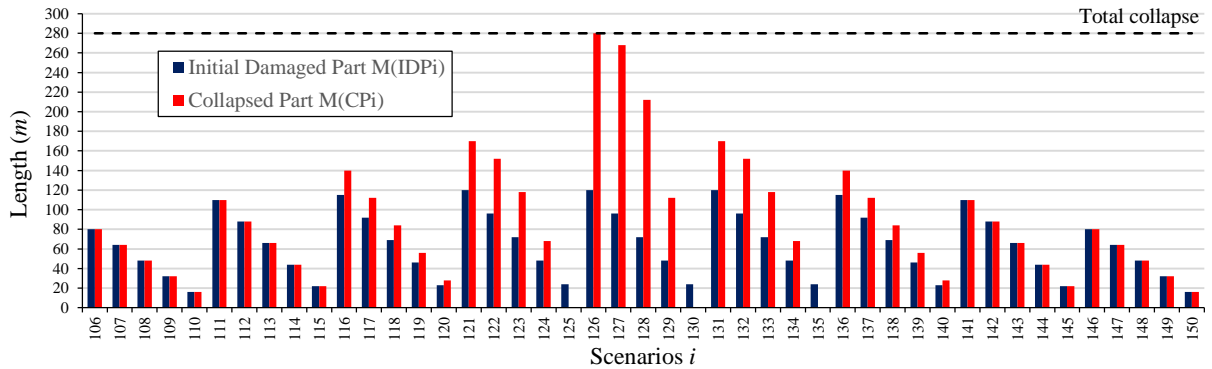
The structural response under each scenario i in Table IV.3 is investigated with the proposed coupling strategy, and the results are summarized in Figure IV.16.



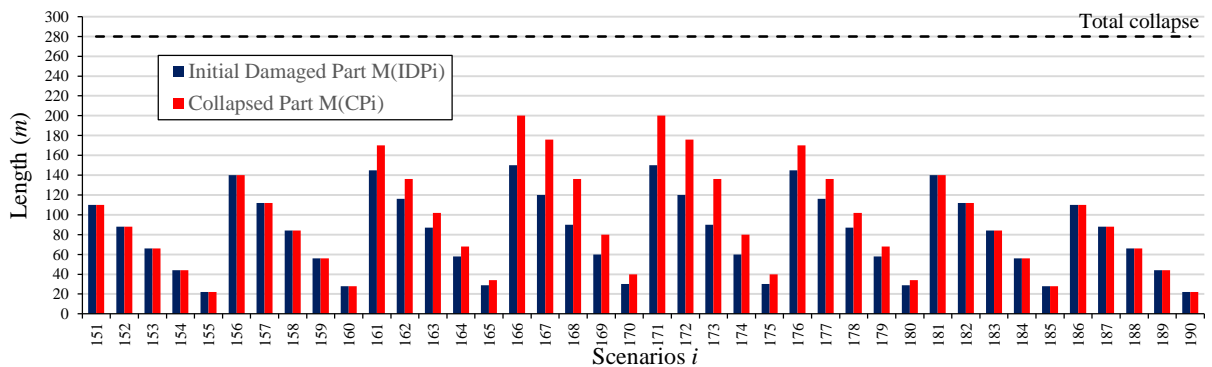
(a) Scenarios i with the loss of one column



(b) Scenarios i with the loss of two columns



(c) Scenarios i with the loss of three columns



(d) Scenarios i with the loss of four columns

Figure IV.16: Measure of IDP_i and CP_i for each scenario i of local failure (see Table IV.3).

According to the values of $\mathcal{M}(IDP_i)$ and $\mathcal{M}(CP_i)$ in Figure IV.16, one can note the presence of scenarios that correspond to the four categories identified previously:

- without consequences (C1),
- without collapse of the directly affected part (C2),
- with collapse of the directly affected part (C3),
- with collapse out of the directly affected part (C4).

Table IV.6 shows the number of scenarios that corresponds to each category. The structure can resist under most of the scenarios with the loss of one column, where it can perfectly resist without any consequences (C1) or it can resist by developing the tensile membrane action (C2). However, the loss of column # 5 or 55 makes the beam located just above the lost column as a cantilever beam (see Figure III.35) that cannot resist the applied loads, which leads to the collapse of the directly affected part. Therefore, these two scenarios fall in category C3. At this stage, one should note that the considered case study is not representative of a building effectively built according to some standards. Rather, it is a virtual example, where some accidental ultimate limit state is checked for design and which is used to illustrate the proposed framework for robustness assessment.

The structure achieves to resist ten scenarios with the loss of two columns ($i = 70, 74, 75, 79, 80, 84, 85, 89, 90$ or 95) by developing a second line of defence with the tensile membrane action (category C2). Moreover, the scenarios $i = 125, 130$ or 135 with the loss of three columns of the top floor also fall in the category C2 where the structure achieves to sustain these scenarios.

Apart from these scenarios, the loss of more than one column always leads to some collapse in the structure, where all scenarios fall in the categories C3 and C4. In particular, the total collapse of the structure can occur with the scenario # 126 with the loss of columns # 21, 26 and 31. It is interesting to note that the scenarios # 166 and 171 do not lead to a total collapse, even if they both include columns 21, 26 and 31. One can explain this result by the redistribution of efforts which is different and dependent on all the elements that are removed (all at the same time in this approach).

Categories	C1	C2	C3	C4
Loss of 1 column	18	35	2	0
Loss of 2 columns	0	10	20	20
Loss of 3 columns	0	3	20	22
Loss of 4 columns	0	0	20	20
Total	18	48	62	62

Table IV.6: Number of local failure scenarios within categories C1 to C4.

For each scenario i of Table IV.3, Table IV.7 shows the number of iterations for both yield design calculation ($n_{YD,i}$) and non-linear analysis ($n_{NL,i}$) realised to model the structural response of each scenario. The scenarios C1 have the lowest computation time ($14 s < T_i^{C1} <$

15 s), where only one iteration of yield design calculation is needed ($n_{YD,i}^{C1} = 1, n_{NL,i}^{C1} = 0$). For category C2, there are two iterations of yield design and one for non-linear analysis ($n_{YD,i}^{C2} = 2, n_{NL,i}^{C2} = 1$) and the computation time is $132 s < T_i^{C2} < 746 s$. One can distinguish two types of scenarios within category C3. In the first type (C3,1), the initially affected part has no possibility to develop an alternative functioning, so the non-linear analysis is not used in this case, and two iterations of yield design calculation are realised ($n_{YD,i}^{C3,1} = 2, n_{NL,i}^{C3,1} = 0$): one for the initially affected part, and another one to check if another failure mode develops in the rest of the structure. The computation time is $20 s < T_i^{C3,1} < 29 s$, which is reasonable since the non-linear analysis is not used. In the second type (C3,2), a non-linear analysis is performed to test the effect of the catenary action, while the structure does not resist, so $n_{YD,i}^{C3,2} = 3$ and $n_{NL,i}^{C3,2} = 1$. These scenarios have a higher computation cost, where $118 s < T_i^{C3,2} < 2156 s$. For category C4, all the scenarios have $n_{YD,i}^{C4} = 3$, and $n_{NL,i}^{C4} = 1$, where the computation cost is $141 s < T_i^{C4} < 1894 s$. These values are illustrated in Table IV.8. The total computation cost to study these 190 scenarios is 29.5 hours.

i	$n_{YD,i}$	$n_{NL,i}$	Cat	$T_i(s)$	i	$n_{YD,i}$	$n_{NL,i}$	Cat	$T_i(s)$	i	$n_{YD,i}$	$n_{NL,i}$	Cat	$T_i(s)$
1	1	0	C1	15	65	3	1	C3	173	129	3	1	C4	567
2	1	0	C1	14	66	3	1	C4	1105	130	2	1	C2	197
3	1	0	C1	14	67	3	1	C4	1237	131	3	1	C4	1294
4	1	0	C1	14	68	3	1	C4	912	132	3	1	C4	1037
5	2	0	C3	28	69	3	1	C4	591	133	3	1	C4	781
6	1	0	C1	14	70	2	1	C2	162	134	3	1	C4	518
7	1	0	C1	14	71	3	1	C4	1273	135	2	1	C2	179
8	1	0	C1	14	72	3	1	C4	1058	136	3	1	C4	1515
9	1	0	C1	14	73	3	1	C4	806	137	3	1	C4	1222
10	1	0	C1	14	74	2	1	C2	541	138	3	1	C4	903
11	2	1	C2	627	75	2	1	C2	156	139	3	1	C4	583
12	2	1	C2	520	76	3	1	C4	1276	140	3	1	C4	141
13	2	1	C2	403	77	3	1	C4	1047	141	3	1	C3	1725
14	2	1	C2	269	78	3	1	C4	811	142	3	1	C3	1355
15	2	1	C2	132	79	2	1	C2	506	143	3	1	C3	988
16	2	1	C2	681	80	2	1	C2	154	144	3	1	C3	628
17	2	1	C2	621	81	3	1	C4	1276	145	3	1	C3	146
18	2	1	C2	458	82	3	1	C4	1047	146	2	0	C3	20
19	2	1	C2	297	83	3	1	C4	811	147	2	0	C3	22
20	2	1	C2	162	84	2	1	C2	506	148	2	0	C3	24
21	2	1	C2	746	85	2	1	C2	154	149	2	0	C3	27
22	2	1	C2	590	86	3	1	C4	1273	150	2	0	C3	29
23	2	1	C2	426	87	3	1	C4	1058	151	2	0	C3	21
24	2	1	C2	300	88	3	1	C4	806	152	2	0	C3	21
25	2	1	C2	157	89	2	1	C2	541	153	2	0	C3	23
26	2	1	C2	697	90	2	1	C2	156	154	2	0	C3	26
27	2	1	C2	575	91	3	1	C4	1105	155	2	0	C3	29
28	2	1	C2	443	92	3	1	C4	1237	156	3	1	C3	2156
29	2	1	C2	300	93	3	1	C4	912	157	3	1	C3	1653
30	2	1	C2	153	94	3	1	C4	591	158	3	1	C3	1196
31	2	1	C2	746	95	2	1	C2	162	159	3	1	C3	754
32	2	1	C2	590	96	3	1	C3	118	160	3	1	C3	263
33	2	1	C2	426	97	3	1	C3	1066	161	3	1	C4	1894

34	2	1	C2	300	98	3	1	C3	756	162	3	1	C4	1491
35	2	1	C2	157	99	3	1	C3	474	163	3	1	C4	1093
36	2	1	C2	681	100	3	1	C3	173	164	3	1	C4	700
37	2	1	C2	621	101	2	0	C3	22	165	3	1	C4	254
38	2	1	C2	458	102	2	0	C3	24	166	3	1	C4	1618
39	2	1	C2	297	103	2	0	C3	26	167	3	1	C4	1266
40	2	1	C2	162	104	2	0	C3	26	168	3	1	C4	945
41	2	1	C2	627	105	2	0	C3	28	169	3	1	C4	621
42	2	1	C2	520	106	2	0	C3	20	170	3	1	C3	323
43	2	1	C2	403	107	2	0	C3	22	171	3	1	C4	1753
44	2	1	C2	269	108	2	0	C3	24	172	3	1	C4	1418
45	2	1	C2	132	109	2	0	C3	27	173	3	1	C4	1054
46	1	0	C1	14	110	2	0	C3	29	174	3	1	C4	680
47	1	0	C1	14	111	3	1	C3	1725	175	3	1	C3	354
48	1	0	C1	14	112	3	1	C3	1355	176	3	1	C4	1618
49	1	0	C1	14	113	3	1	C3	988	177	3	1	C4	1266
50	1	0	C1	14	114	3	1	C3	628	178	3	1	C4	945
51	1	0	C1	15	115	3	1	C3	146	179	3	1	C4	621
52	1	0	C1	14	116	3	1	C4	1515	180	3	1	C4	323
53	1	0	C1	14	117	3	1	C4	1222	181	3	1	C3	1894
54	1	0	C1	14	118	3	1	C4	903	182	3	1	C3	1491
55	2	0	C3	28	119	3	1	C4	583	183	3	1	C3	1093
56	2	0	C3	22	120	3	1	C4	141	184	3	1	C3	700
57	2	0	C3	24	121	3	1	C4	1294	185	3	1	C3	254
58	2	0	C3	26	122	3	1	C4	1037	186	2	0	C3	21
59	2	0	C3	26	123	3	1	C4	781	187	2	0	C3	21
60	2	0	C3	28	124	3	1	C4	518	188	2	0	C3	23
61	3	1	C3	118	125	2	1	C2	179	189	2	0	C3	26
62	3	1	C3	1066	126	3	1	C4	1402	190	2	0	C3	29
63	3	1	C3	756	127	3	1	C4	1162					
64	3	1	C3	474	128	3	1	C4	871					

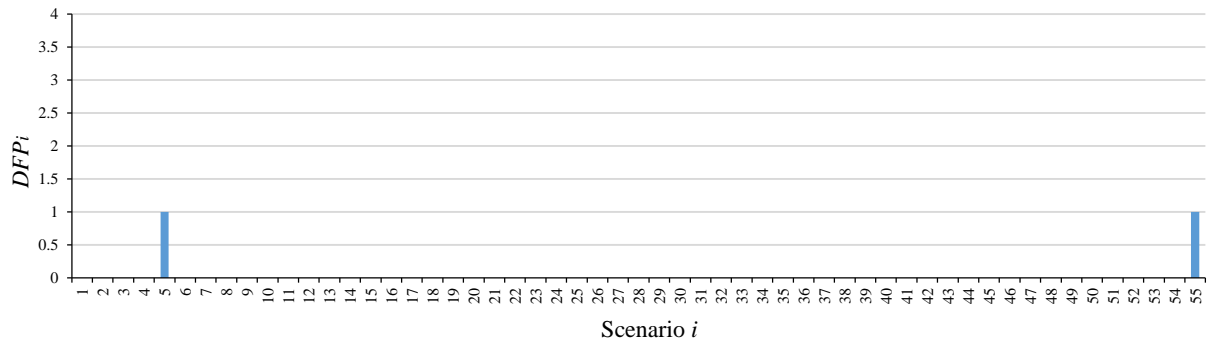
Table IV.7: Number of iterations realised for each scenario i with the computation cost ($n_{YD,i}$ = number of iteration of yield design calculation, $n_{NL,i}$ = number of iteration of non-linear analysis, Cat = category of scenario, T_i =computation cost).

Category		$n_{YD,i}$	$n_{NL,i}$	T_i
C1		1	0	$14 s < T_i^{C1} < 15 s$
C2		2	1	$132 s < T_i^{C2} < 746 s$
C3	C3,1	2	0	$20 s < T_i^{C3,1} < 29 s$
	C3,2	3	1	$118 s < T_i^{C3,2} < 2156 s$
C4		3	1	$141 s < T_i^{C4} < 1894 s$

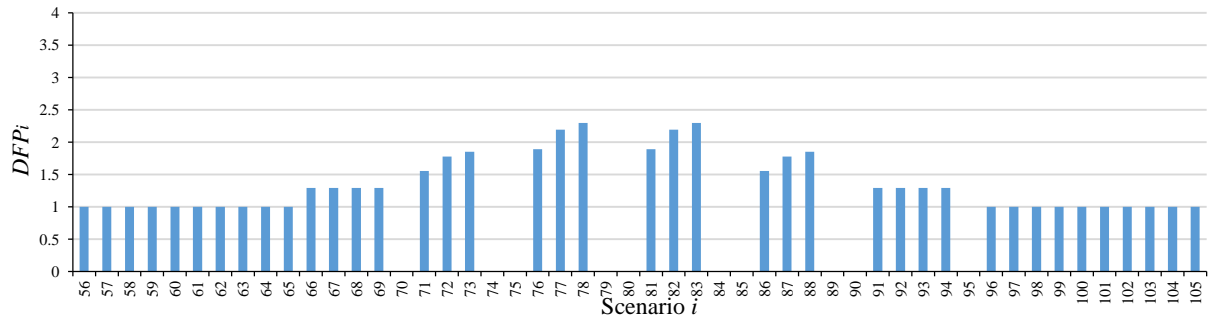
Table IV.8: Number of iterations realised for each category of scenarios with the interval of computation cost.

IV.4.3 Calculation of robustness indices

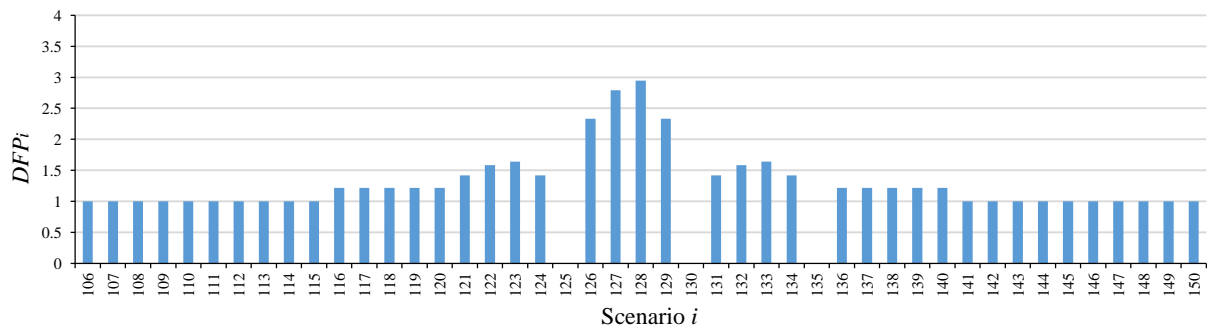
The final step in the proposed structural robustness assessment is to calculate some robustness indices. The degree of failure propagation for each applied local failure scenarios is presented in Figure IV.17. The values quantify the extent of failure propagation from an initial point to the final stage.



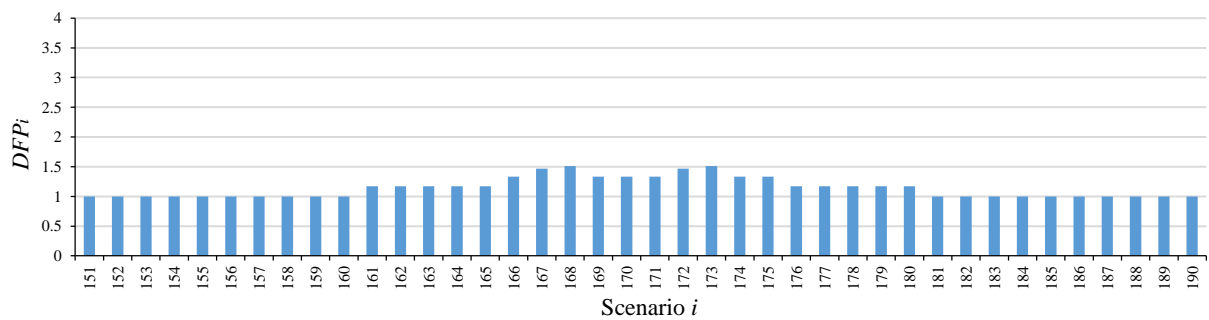
(a) Scenarios i with the loss of one column



(b) Scenarios i with the loss of two columns



(c) Scenarios i with the loss of three columns



(d) Scenarios i with the loss of four columns

Figure IV.17: Degree of failure propagation for the applied local failure scenarios detailed in Table IV.3.

The maximum degree of failure propagation according to the number of removed columns is presented in Table IV.9. The highest value (2.9) corresponds to the loss of three columns. It is interesting to see that removing four columns, which corresponds to the largest initially affected part of the structure leads to a low failure propagation. There are two reasons for this result. First, the more columns one removes in a scenario i , the larger the initially affected part IDP_i , that mathematically decreases the degree of failure extent. Second, one

observes that removing three elements can lead to worst propagation extent than when removing four (compare Figure IV.17 c and d). Indeed, the loss of three elements can lead to situations where indirectly affected part finally collapses on both sides of the directly affected part, due to symmetries of the indirectly affected part in the overall structures. Furthermore, as the Robustness Propagation Failure Index (RPF_i) is equal to the maximum degree of failure propagation among the applied scenarios, $RPF_i=2.9$ in this example. The scenario with the largest propagation is scenario # 128 with the loss of columns 23, 28 and 33.

	Loss of 1 column	Loss of 2 columns	Loss of 3 columns	Loss of 4 columns
Max (DFP_i)	1	2.3	2.9	1.5

Table IV.9: Maximum value of degree of failure propagation according to the number of removed columns.

Figure IV.18 shows the local failure energy E_i and the measure $\mathcal{M}(CP_i)$ of the collapsed part for each applied scenario i . In this example, the threshold used to determine an unacceptable collapse in Equation (IV.6) is fixed at 90 m . Hence, the Robustness Energy Index $REI(UC = 90\text{m}) = 161.2\text{ kJ}$ represents the minimum value of local failure energy that leads to such unacceptable collapse. This index identifies the scenario with the lowest magnitude in energy E_i that leads to an unacceptable failure. In this example, it refers to the scenarios with the loss of two columns: 71, 76, 81 or 86 (see Figure IV.18).

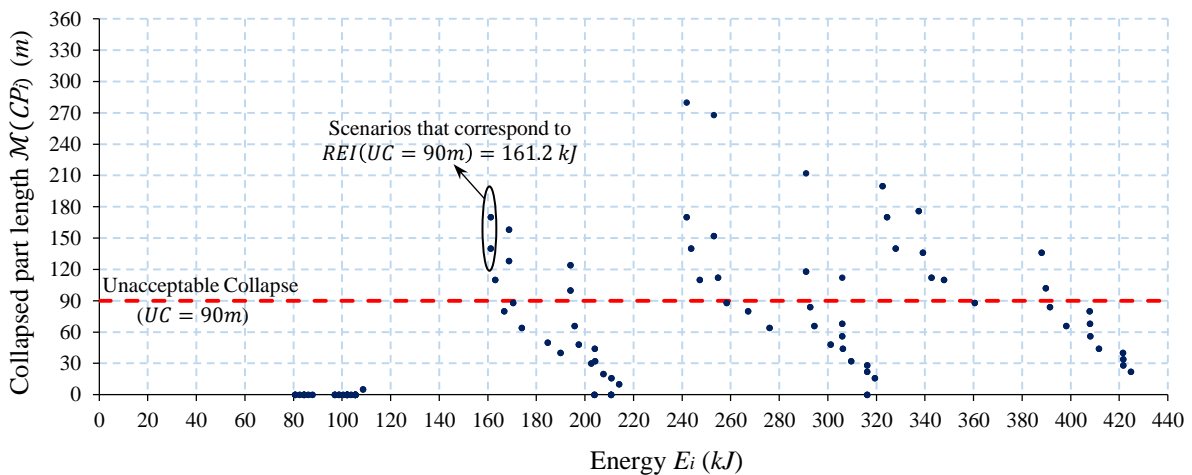


Figure IV.18: Local failure energy – collapsed part length diagram.

To study how the robustness index REI varies with UC , Figure IV.19 presents the REI value if $UC \in [10\text{ m}; 280\text{m}]$. The results indicate that $REI(UC) = 161.2\text{ kJ}$ when $10\text{ m} < UC < 170\text{ m}$, then the highest value is $REI(UC) = 241.9\text{ kJ}$ when $180\text{ m} < UC < 280\text{ m}$. As the maximal collapsed part under the scenarios with the loss of one column is 5 m (see Figure IV.16), these scenarios are not critical if $UC \in [10\text{ m}; 280\text{ m}]$. The scenario 76 (loss

of columns # 21 and 26) and 81 (loss of columns # 26 and 31) have $E_{76} = E_{81} = 161.2 \text{ kJ}$, which is the lowest failure energy for the scenarios with the loss of two columns, and they have a collapsed part $\mathcal{M}(CP_{76}) = \mathcal{M}(CP_{81}) = 170 \text{ m}$. Hence, these two scenarios are the most critical when $UC \in [10 \text{ m}; 170 \text{ m}]$. Then for $UC \in [180 \text{ m}; 280 \text{ m}]$, the scenario 126 ($E_{126} = 241.9 \text{ kJ}$) is the most critical with the loss of columns # 21, 26 and 31 that leads to the total collapse of the structure.

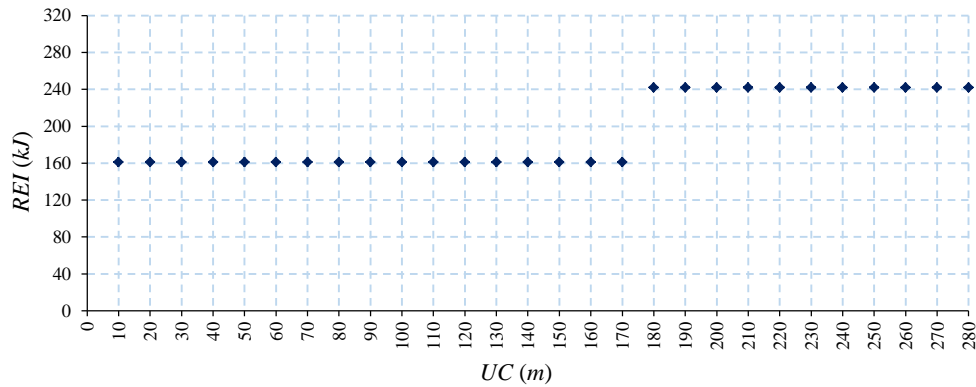


Figure IV.19: Sensitivity of REI index according to UC .

The two indices RPM and $REI(UC)$ measure two different aspects of structural robustness, where RPM focuses on the largest degree of failure propagation, and $REI(UC)$ on the identification of the weakest point of the structure that can lead to an unacceptable collapse. Failure propagation and energy needed for initial failure are two aspects that can be analyzed together. Figure IV.20 presents the diagram of energy (E_i) and the degree of failure propagation (DFP_i) for each scenario i .

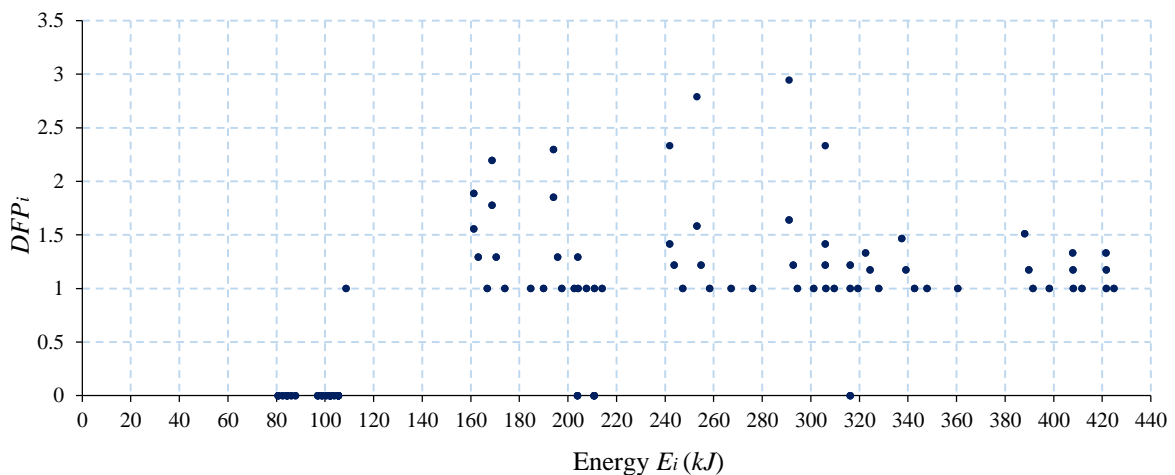


Figure IV.20: E_i - DFP_i diagram.

Based on Equation (IV.8), one can classify the adopted scenarios according to two parameters: (i) maximizing DFP_i , which refers to the largest collapse propagation, and (ii)

minimizing E_i , which refers to the scenario with lowest magnitude of local failure. In this case, minimizing E_i is not associated to any threshold UC fixed beforehand. This bi-objective problem is solved with the fast non-dominated sorting process proposed by Deb et al. (2002) and reminded in Equation (IV.11). The classification of the applied scenarios are presented in a bubble diagram, as shown in Figure IV.21, where the diameter of the bubbles refers to the successive number of non-dominated fronts (largest diameter is for the Pareto front).

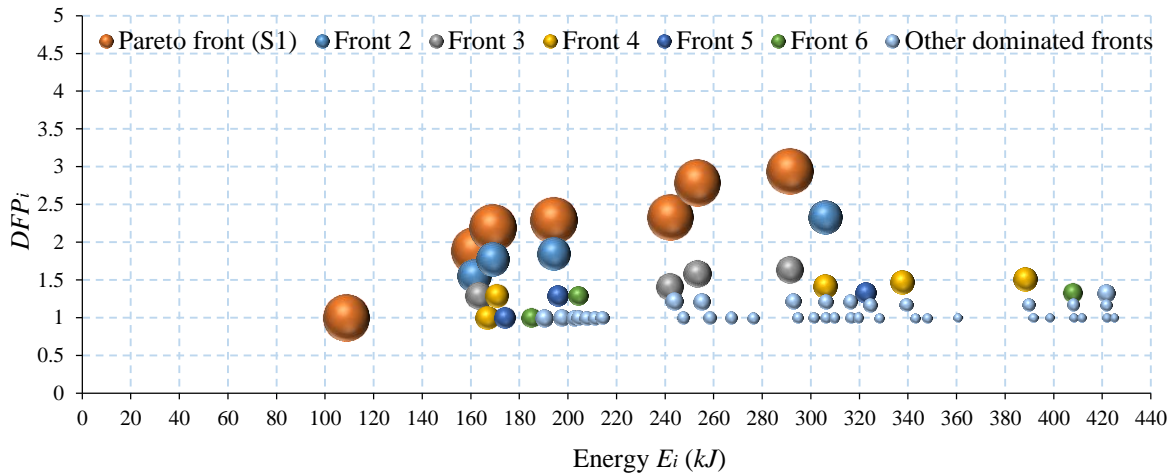


Figure IV.21: Identification of non-dominated scenarios when simultaneously minimizing E_i and maximizing DFP_i (Equation IV.8).

These results identify that eleven scenarios (Pareto front S1) are non-dominated (the ones with the largest diameter in Figure IV.21). These scenarios described in Table IV.10 simultaneously maximize propagation and minimize energy associated with local failure. In this sense, all other scenarios in Figure IV.21 are dominated by the Pareto front scenarios of that appear as the most critical ones, when Equation (IV.8) is considered.

Scenario i	Column #	E_i (kJ)	DFP_i
5	5	108.6	1.0
55	55	108.6	1.0
76	21-26	161.2	1.9
81	26-31	161.2	1.9
77	22-27	168.7	2.2
82	27-32	168.7	2.2
78	23-28	194.0	2.3
83	28-33	194.0	2.3
126	21-26-31	241.9	2.3
127	22-27-32	253.1	2.8
128	23-28-33	291.0	2.9

Table IV.10: Non-dominated scenarios (Pareto front S1) related to Equation (IV.8).

The structural robustness analysis can also be studied by identifying the worst collapse propagation DFP_i with the minimal initial damaged part $\mathcal{M}(IDP_i)$, as described in Equation (IV.12). Figure IV.22 presents the diagram of initial damaged part $\mathcal{M}(IDP_i)$ and the degree of failure propagation (DFP_i) for each scenario i . The classification of these scenarios according to the bi-objective problem of Equation (IV.12) leads to the Pareto front S2 in Figure IV.23 (unlike what was shown in Figure IV.21, one only shows the Pareto front and not the dominated scenarios). Eight non-dominated scenarios are identified and described in Table IV.11. These scenarios simultaneously maximize DFP_i and minimize the level of initial damaged part $\mathcal{M}(IDP_i)$. They are the most critical scenarios, according to Equation (IV.12).

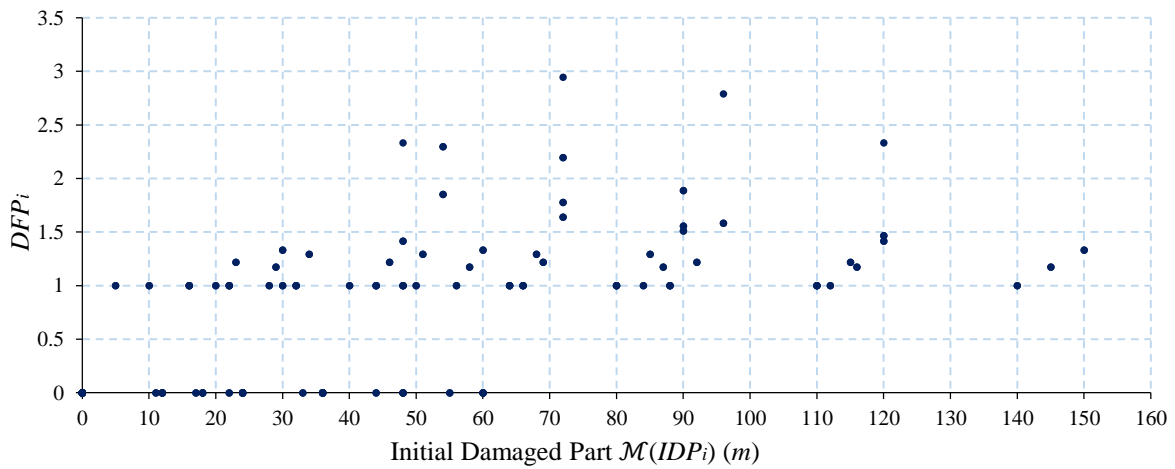


Figure IV.22: $\mathcal{M}(IDP_i)$ - DFP_i diagram.

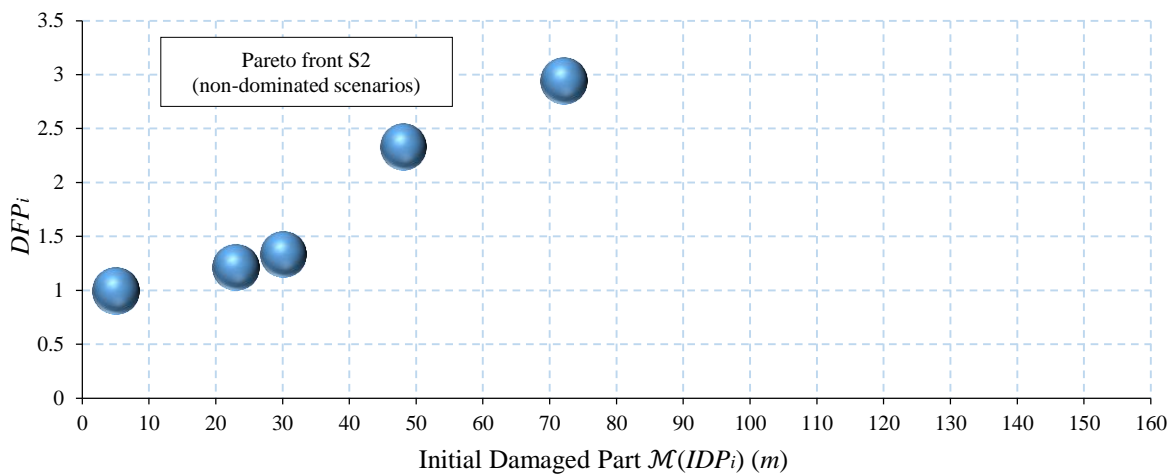


Figure IV.23: Identification of non-dominated solutions (Pareto front S2) when simultaneously minimizing $\mathcal{M}(IDP_i)$ and maximizing DFP_i (Equation IV.12).

Scenario i	Column #	$\mathcal{M}(IDP_i) (m)$	DFP_i
5	5	5	1.0
55	55	5	1.0
120	15-20-25	23	1.2
140	35-40-45	23	1.2
170	20-25-30-35	30	1.3
175	25-30-35-40	30	1.3
129	24-29-34	48	2.3
128	23-28-33	72	2.9

Table IV.11: Non-dominated scenarios (Pareto front S2) related to Equation (IV.12).

Figure IV.24 presents the diagram of initial damaged part $\mathcal{M}(IDP_i)$ and the collapsed part $\mathcal{M}(CP_i)$ for each scenario i . Based on the bi-objective sorting of Equation (IV.13), one can identify the non-dominated scenarios that maximize $\mathcal{M}(CP_i)$ and minimize initial damaged part $\mathcal{M}(IDP_i)$. Figure IV.25 shows the classification among scenarios, where 30 non-dominated scenarios are identified (Pareto front S3) and described in Table IV.12. These solutions are the most critical according to Equation (IV.13).

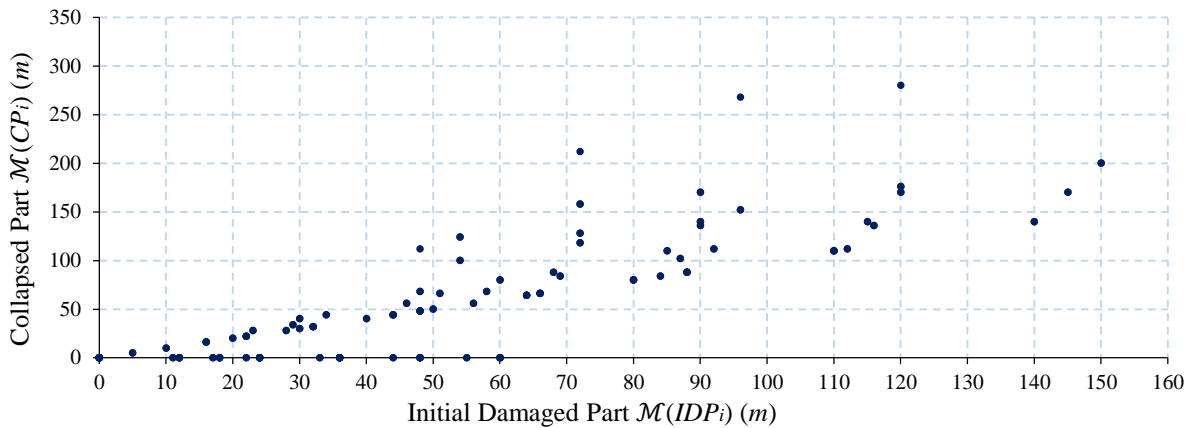


Figure IV.24: $\mathcal{M}(IDP_i)$ - $\mathcal{M}(CP_i)$ diagram for local scenarios of Table IV.3.

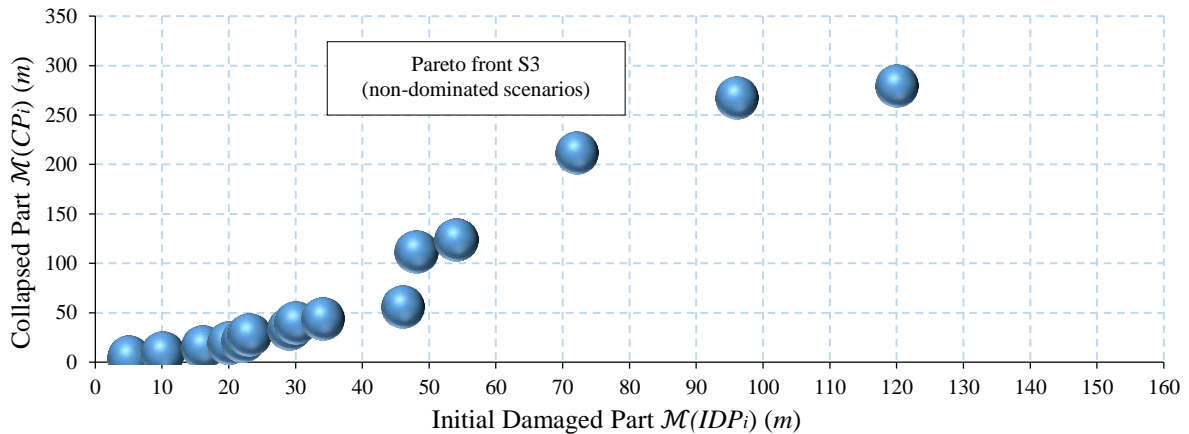


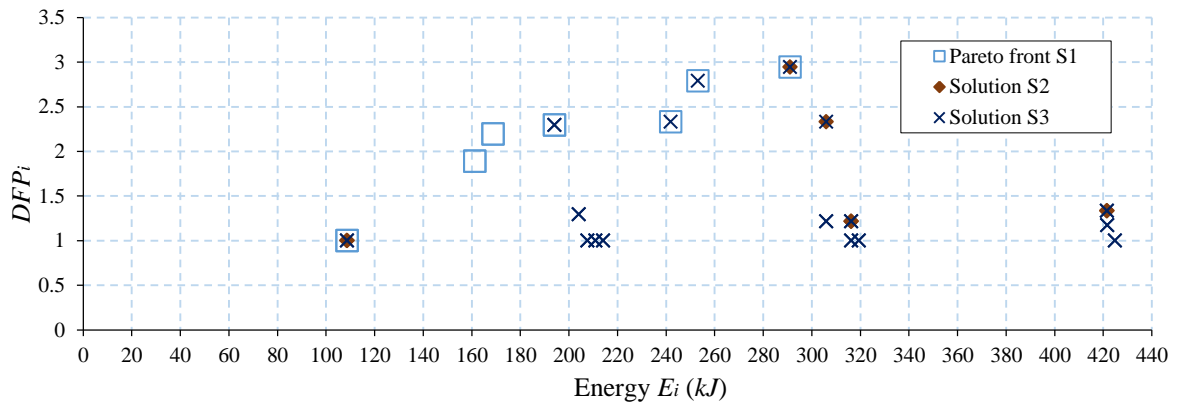
Figure IV.25: Identification of non-dominated scenarios (Pareto front S3) when simultaneously minimizing $\mathcal{M}(IDP_i)$ and maximizing $\mathcal{M}(CP_i)$.

Scenario # i	Column #	$M(IDP_i)$ (m)	$M(CP_i)$ (m)
5	5	5	5
55	55	5	5
60	5-10	10	10
105	50-55	10	10
65	10-15	16	16
100	45-50	16	16
110	5-10-15	16	16
150	45-50-55	16	16
59	4-9	20	20
104	49-54	20	20
115	10-15-20	22	22
145	40-45-50	22	22
155	5-10-15-20	22	22
190	40-45-50-55	22	22
120	15-20-25	23	28
140	35-40-45	23	28
165	15-20-25-30	29	34
180	30-35-40-45	29	34
170	20-25-30-35	30	40
175	25-30-35-40	30	40
69	14-19	34	44
94	39-44	34	44
119	14-19-24	46	56
139	34-39-44	46	56
129	24-29-34	48	112
78	23-28	54	124
83	28-33	54	124
128	23-28-33	72	212
127	22-27-32	96	268
126	21-26-31	120	280

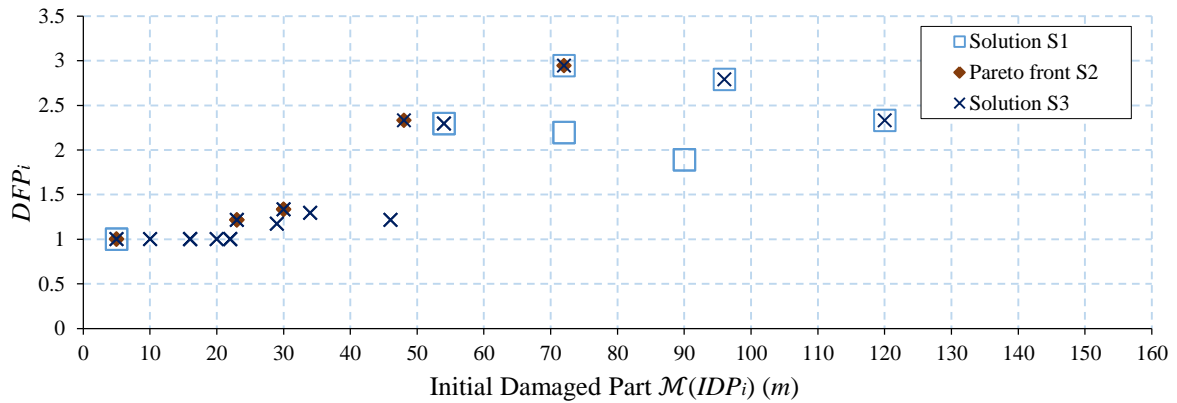
Table IV.12: Non-dominated scenarios (Pareto front S3) related to Equation (IV.13).

To illustrate the fact that the non-dominated status of scenarios strongly depends on the choice of the bi-objective problem in Equations (IV.8), (IV.12) or (IV.13), one represents the solutions S1, S2 and S3 in the diagrams $E_i - DFP_i$, $\mathcal{M}(IDP_i) - DFP_i$, and $\mathcal{M}(IDP_i) - \mathcal{M}(CP_i)$ in Figure IV.26 a, b and c, respectively. First, one can easily identify the critical scenarios if one aims to find those with the lowest initial magnitude (E_i or $\mathcal{M}(IDP_i)$ in x axis) or those with the largest extent (DFP_i or $\mathcal{M}(CP_i)$ in y axis). Second, one can see how far some critical scenarios can be from the Pareto front obtained with some specific objective functions. In Figure IV.26(a), one observes that some solutions of S2 and S3 have a relatively low DFP_i index, when compared to solutions S1. One can explain this result as minimizing $\mathcal{M}(IDP_i)$ does not necessarily correspond to the solutions with lowest energy level. In fact minimizing local failure energy leads to scenarios of column loss in the lower stories of the structure (as the failure energy increases when the concentrated load decreases, see Table IV.4). Conversely, minimizing $\mathcal{M}(IDP_i)$ leads to scenarios of column loss in the upper stories of the structure where the directly affected part is smaller. Such consideration explains why the majority of S1 solutions in Figure IV.26(b) and Figure IV.26(c) are on the right side of the

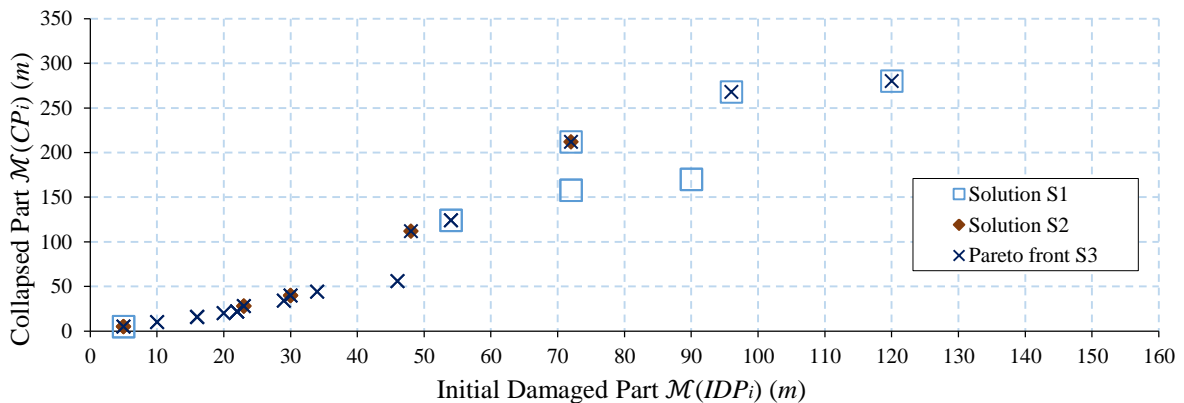
x axis. Solutions S2 and S3 are more grouped in these two figures. Besides, in Figure IV.26(b), the critical scenarios identified when maximizing DFP_i (Pareto front S2) are among the set of scenarios of solution S3 (see Table IV.11 and Table IV.12) when maximizing $\mathcal{M}(CP_i)$. Indeed, simultaneously minimizing $\mathcal{M}(IDP_i)$ and maximizing $\mathcal{M}(CP_i)$ is close to minimizing $\mathcal{M}(IDP_i)$ and maximizing DFP_i . However, the results of these problems are different due the fact that the DFP_i is a relative difference between the directly affected part and the one at the end of the failure propagation. It is noted that the scenarios 5, 55 and 128 belong to S1, S2, and S3 simultaneously (which makes these scenarios particularly critical).



(a) $E_i - DFP_i$ diagram



(b) $M(IDP_i) - DFP_i$ diagram



(c) $\mathcal{M}(IDP_i) - \mathcal{M}(CP_i)$ diagram

Figure IV.26: Pareto fronts S1, S2 and S3.

IV.5 COMPARISON WITH DIFFERENT STRUCTURAL CONFIGURATIONS OF STEEL-FRAMED STRUCTURE

IV.5.1 Presentation of design configurations

The steel-framed building of Section IV.4 is now considered with different design configurations. In order to identify how the structural strengthening can influence the structural robustness, five design configurations are considered as described below:

- D0: it corresponds to the initial configuration in Section III.4.3 (cross-section IPE360 for beams, and cross-section HE500B for columns) with detailed results provided in Section IV.4.
- D1: the beams in configuration D0 are strengthened by using cross-section IPE550 (see the yield surface in Figure IV.27).

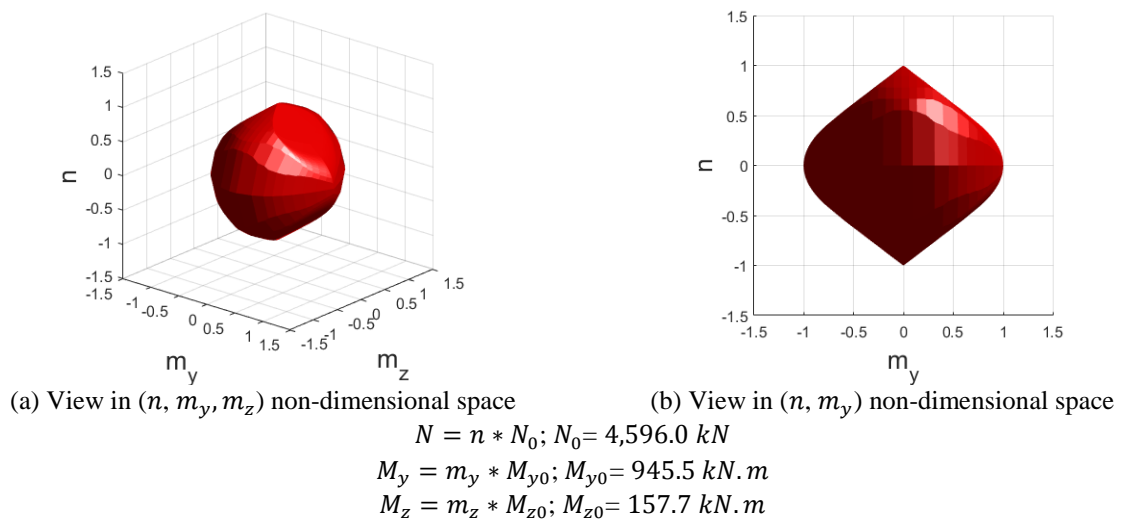


Figure IV.27: Yield surface of IPE550 cross-section.

- D2: the columns in configuration D0 are strengthened by using cross-section HE800B (see the yield surface in Figure IV.28).

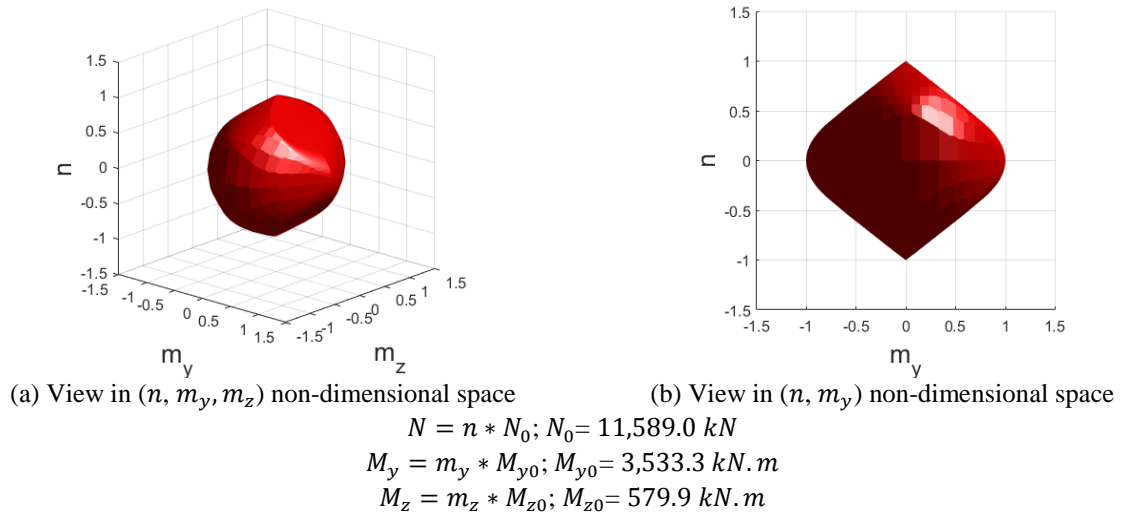


Figure IV.28: Yield surface of HE800B cross-section.

- D3: both beams and columns in configuration D0 are strengthened by using cross-sections IPE550 and HE800B, respectively.
- D4: the redundancy in configuration D0 is improved by adding braces for the bays on the edges of the structure, as shown in Figure IV.29. The braces $Br150 \times 150 \times 6$ have a square hollow cross-section, as shown in Figure IV.30 (corresponding yield surface is shown in Figure IV.31). The connections between the braces and the other structural elements are considered as rigid joints.

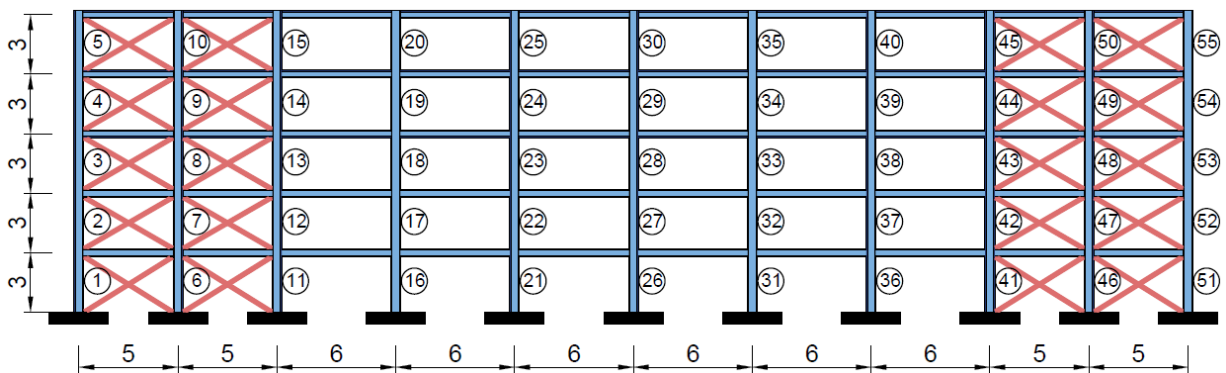


Figure IV.29: Layout of design configuration D4 (dimensions in meter).

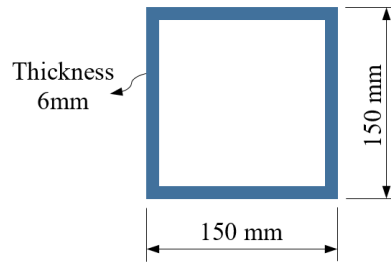


Figure IV.30: Cross-section of braces $Br150 \times 150 \times 6$ (ArcelorMittal, 2018).

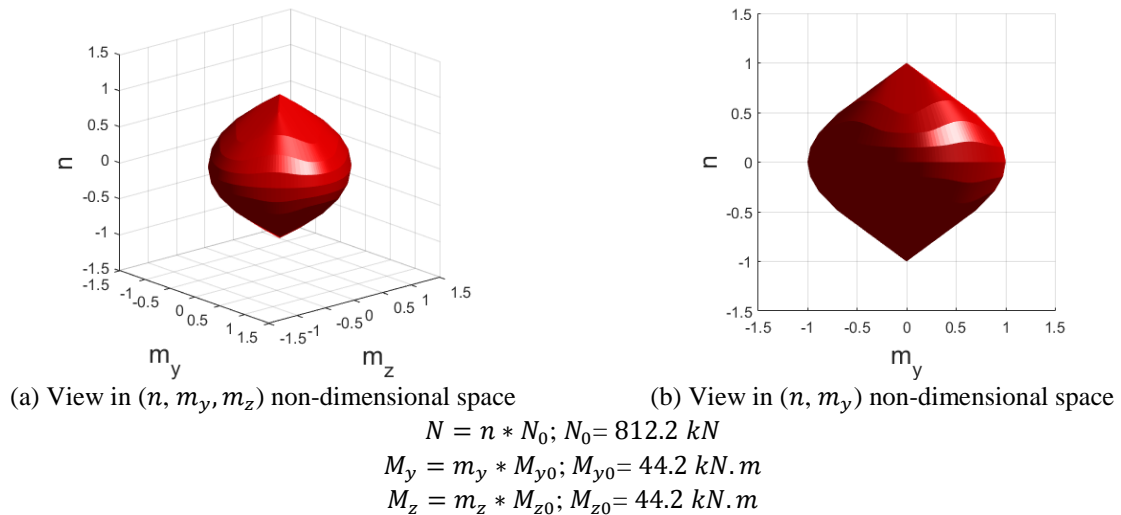


Figure IV.31: Yield surface of square hollow cross-section $Br150 \times 150 \times 6$.

Table IV.13 provides the element characteristics and the applied loads under the local failure scenarios for each configuration, and the steel material properties are presented in Table IV.14.

Design configuration	Beams	Columns	Braces	Dead load DL (kN/m)	Live load LL (kN/m)	Combination of loads $W_a = DL + 0.5 LL$ (kN/m)
D0	IPE360	HE500B	-	25.6	12	31.6
D1	IPE550	HE500B	-	26	12	32
D2	IPE360	HE800B	-	25.6	12	31.6
D3	IPE550	HE800B	-	26	12	32
D4	IPE360	HE500B	$Br150 \times 150 \times 6$	25.6	12	31.6

Table IV.13: Characteristics of structural elements and applied loads for each design configuration D0, D1, D2, D3 and D4.

Cross-section element	Type	Young modulus E	Yield strength f_y
IPE360, IPE550, HE500B, HE800B	S355	210 GPa	355 MPa
Braces $Br150 \times 150 \times 6$	S235	210 GPa	235 MPa

Table IV.14: Steel material properties for structural elements.

IV.5.2 Analysis of structural response

The applied local failure scenarios are those presented in Table IV.3. In configuration D4, it is assumed that the column loss also leads to the loss of its connections with braces. The failure energy E_i relevant to each scenario i for the design configurations D0, D1, D2, D3 and D4 are presented in Table A.1 (Annex A), where the energy levels are quite similar for D0, D1 and D4 that have column cross-section HE500B (see Figure IV.32). They are also quite similar for D2 and D3 with a column cross-section HE800B, where the strengthening of structural column elements requires a larger magnitude of energy to cause their failure when compared to those of D0, D1 and D4.

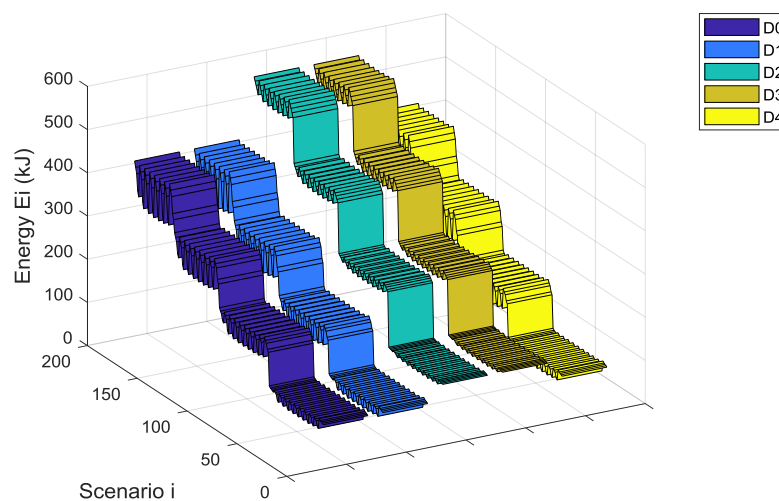


Figure IV.32: Energy E_i required to cause the local failure of scenario i for design configurations D0, D1, D2, D3 and D4.

The structural response under each local failure scenario i for design configurations D0, D1, D2, D3 and D4 is presented in Table A.2 (Annex A) by giving the metrics of Initial Damaged Part $\mathcal{M}(IDP_i)$ and Collapsed Part $\mathcal{M}(CP_i)$. Figure IV.33(a, b, c, d and e) presents the number of local failure scenarios within categories C1 to C4 for each design configuration when one column is lost. The strengthening of structural beam elements in D1 and D3 improves the structural capacity to withstand these scenarios, where all of them correspond to

category C1, meaning that the structure achieves to resist these scenarios without any further damage, as shown in Figure IV.33(b and d).

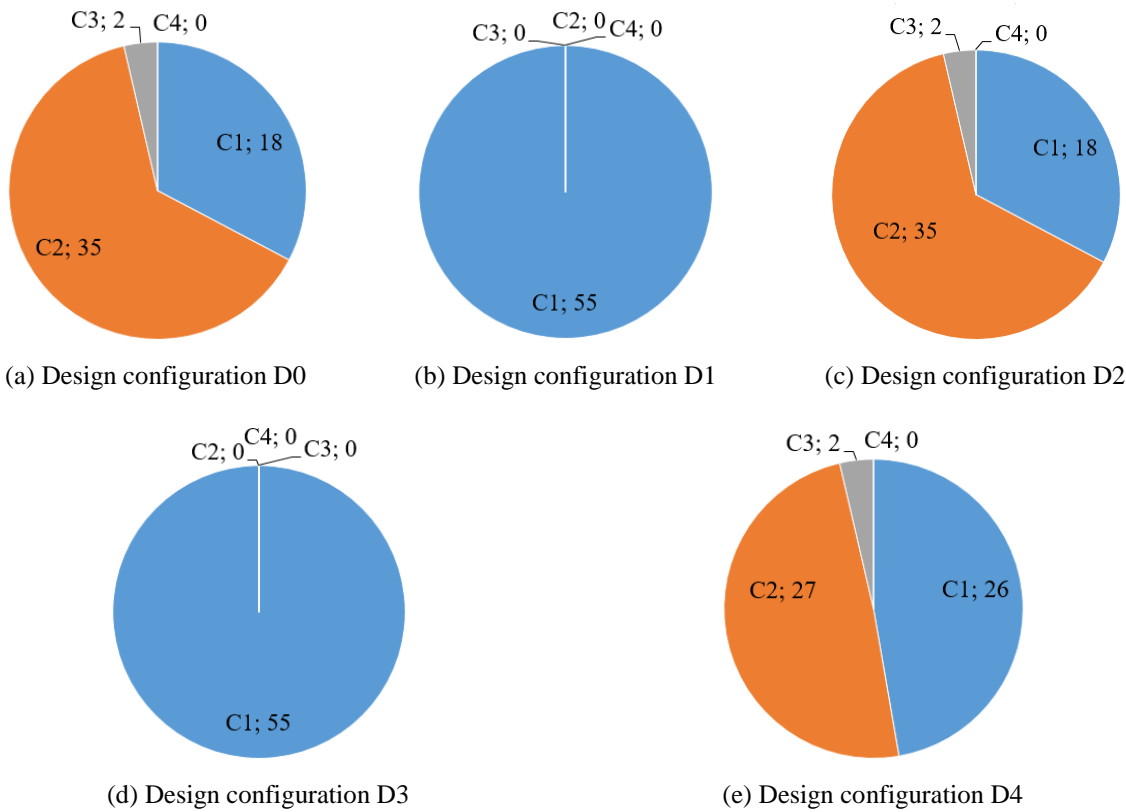


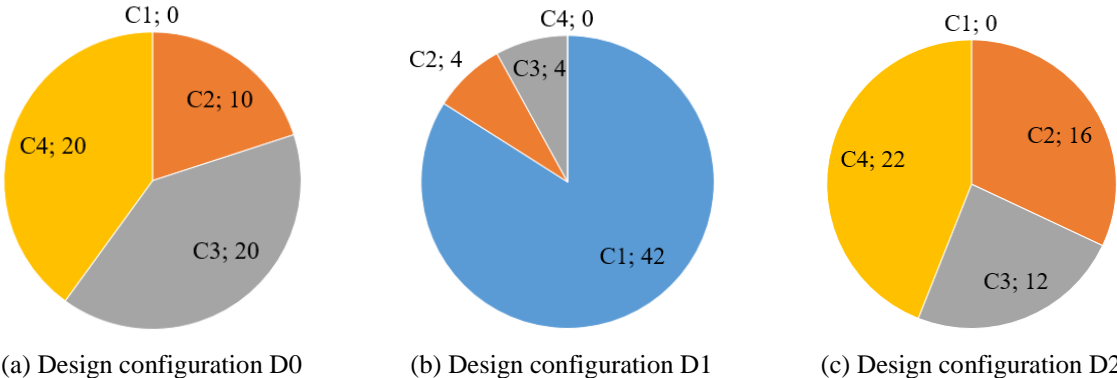
Figure IV.33: Number of local failure scenarios within categories C1 to C4 for design configurations D0, D1, D2, D3 and D4, when one column is lost.

One can note that the strengthening of structure by the reinforcement of column elements in configuration D2 does not change the number of scenarios within categories C1 to C4 compared to D0, as shown in Figure IV.33(c). The scenarios of category C1 depend on the capacity of beams to resist the applied loads without developing a failure mechanism, and as the beams cross-section (IPE360) are similar in the configurations D0 and D2, they have a similar number of scenarios in category C1 ($n_{C1}^{D0, \text{loss of 1 column}} = n_{C1}^{D2, \text{loss of 1 column}} = 18$). Two scenarios with the loss of column # 5 or 55 make the beam located just above the lost column as a cantilever beam (see Figure III.35), which cannot resist the applied loads in configuration D0, and then these scenarios lead to the collapse of these beams, where they correspond to category C3 (see Figure IV.33a). The strengthening of the indirectly affected part in D2 and D4 does not have any influence on the structural response under these scenarios, and they are always in category C3 (see Figure IV.33 c and e). As the structure with configuration D0 achieves to resist all other scenarios with the loss of one column ($n_{C2}^{D0, \text{loss of 1 column}} = 35$) by developing the tensile membrane action, structural

configuration D2 also resists the local failure under these scenarios, and therefore $n_{C2}^{D0, loss of 1 column} = n_{C2}^{D2, loss of 1 column} = 35$.

The strengthening by adding braces in D4 increases the number of scenarios in category C1 compared to configuration D0, where the structure can resist some additional scenarios ($i = 11, 12, 13, 14, 41, 42, 43$ or 44) without any consequence.

For the local failure scenarios with the loss of two columns, the strengthening of beam elements in the configurations D1 and D3 helps the structure to resist 42 scenarios (see Figure IV.34 b and d) without any consequences (category C1), while for the configurations D0 and D2 there is no scenario in category C1. The strengthening of the indirectly affected part in D2 and D4 improves the structural capacity to develop a sufficient tensile membrane action and to prevent the propagation of failure out of the directly affected part. Hence, the number of scenarios corresponding to category C2 increases for the configurations D2 and D4 compared to D0. One can note that $n_{C1}^{D2, loss of 2 columns} = 0 < n_{C1}^{D4, loss of 2 columns} = 16$ and $n_{C2}^{D2, loss of 2 columns} = 16 < n_{C2}^{D4, loss of 2 columns} = 20$, which indicates that adding braces (D4) is more efficient than strengthening columns (D2) to prevent a collapse in the structure. Surprisingly, the strengthening of column elements in configuration D2 can increase the propagation of failure under some scenarios, where the strengthening of the indirectly affected part causes the collapse of some beam elements below the lost columns under the compression force, which is larger than that of the configuration D0 as the ultimate load is increased. Hence, the configuration D2 has the highest number of scenarios in category C4. This aspect can also be found under the scenarios with the loss of three or four columns.



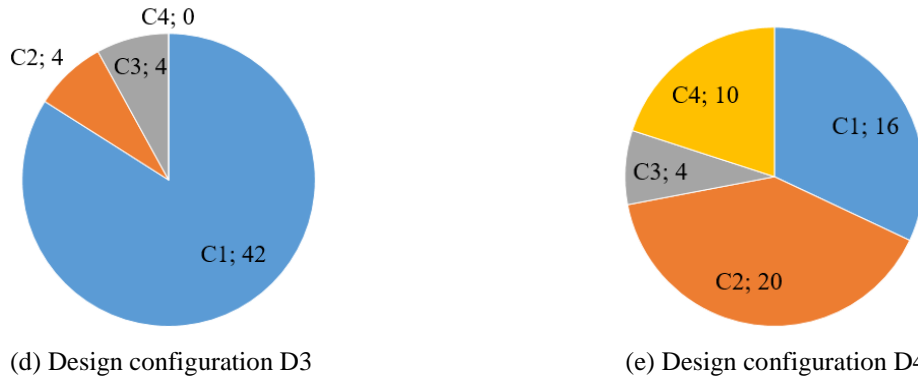


Figure IV.34: Number of local failure scenarios within categories C1 to C4 for design configurations D0, D1, D2, D3 and D4, when two columns are lost.

Following the loss of three columns, the structure cannot resist the local failure scenarios without consequences for the various design configurations (no scenario in category C1), as shown in Figure IV.35(a, b, c, d and e). The strengthening of the structure helps to prevent the progressive collapse under some scenarios, where the number of scenarios in the category C2 increases for the configurations D1, D2, D3 and D4 compared to D0. One can note that the strengthening of beams and columns in configuration D3 has the highest number of scenarios in category C2, which makes this configuration the most efficient in this example.

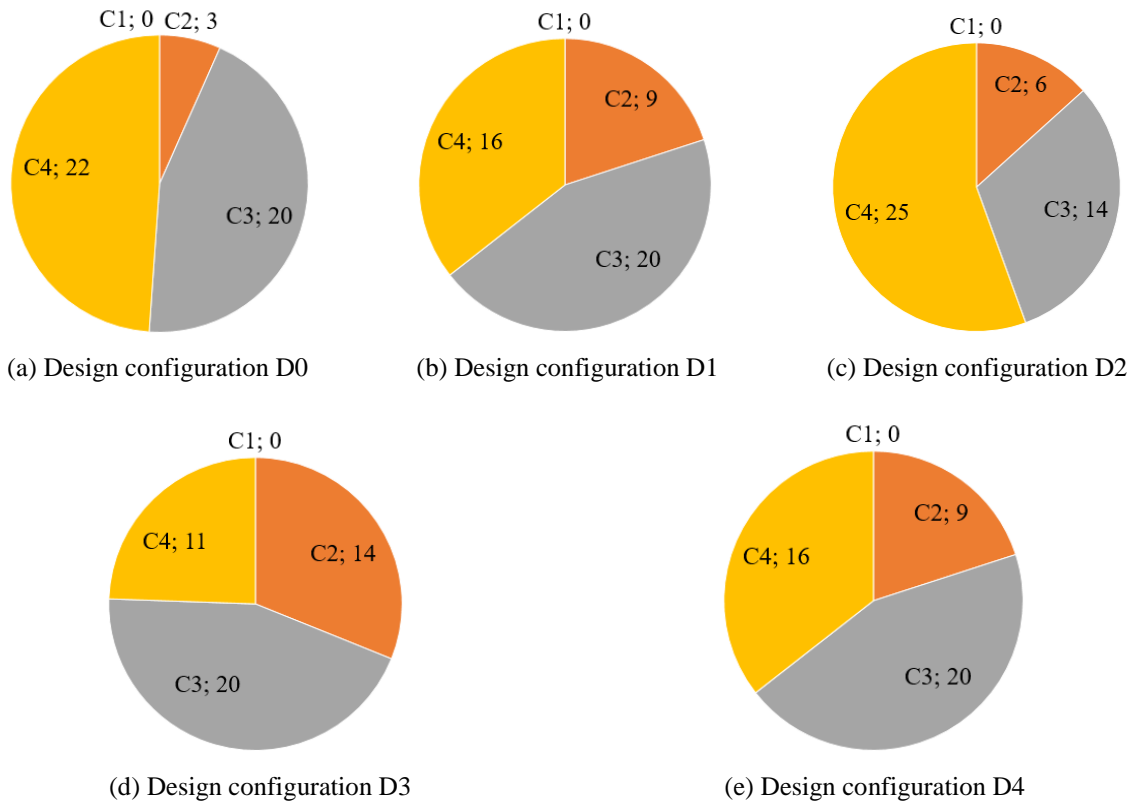


Figure IV.35: Number of local failure scenarios within categories C1 to C4 for design configurations D0, D1, D2, D3 and D4, when three columns are lost.

Following the loss of four columns, a partial/total collapse in the structure is observed for the configuration D0 for all the scenarios, where they all fall in the categories C3 and C4, as shown in Figure IV.36(a). For the configurations D1, D2, D3 and D4, the majority of the local failure scenarios fall in the categories C3 and C4, where the structure systematically undergoes some collapse (see Figure IV.36 b, c, d and e). However, the structure achieves to resist some scenarios by developing the tensile membrane action (category C2) for configurations D1, D2, D3 and D4. Similarly to the scenarios with the loss of three columns, the configuration D3 has the highest number of scenarios in category C2.

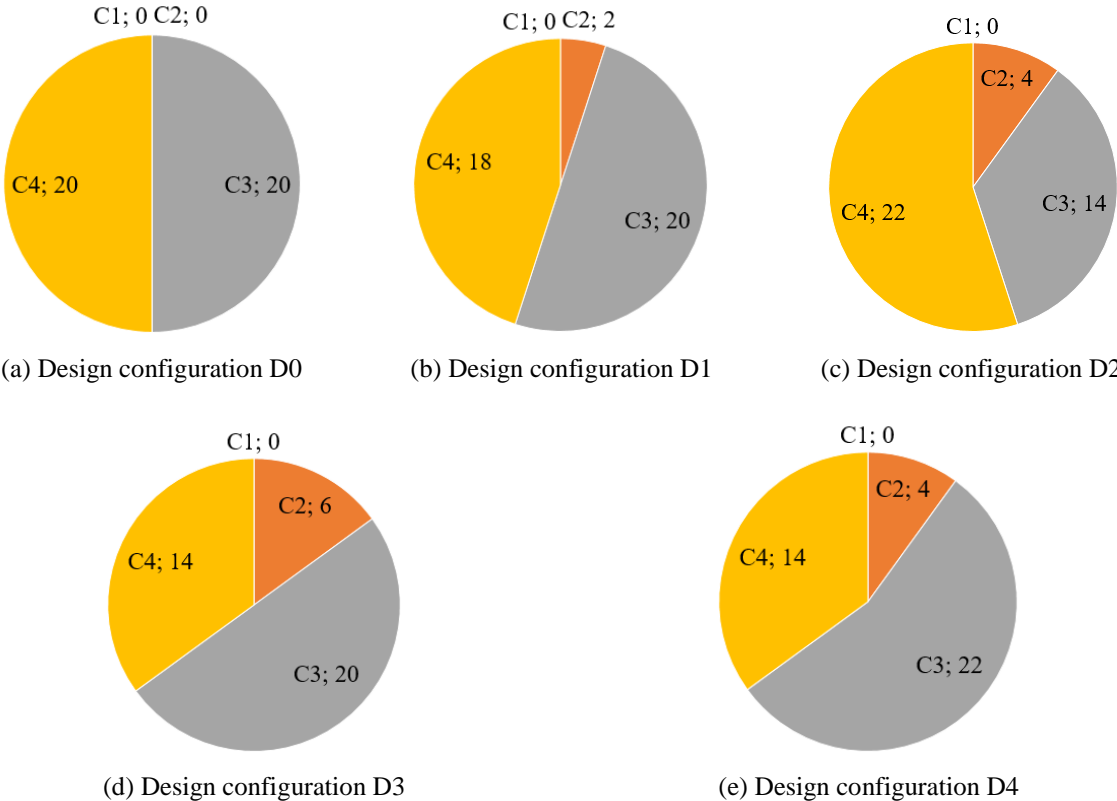


Figure IV.36: Number of local failure scenarios within categories C1 to C4 for design configurations D0, D1, D2, D3 and D4, when four columns are lost.

Figure IV.37(a, b, c, d and e) gives a general overview of the number of local failure scenarios within categories C1 to C4 for the 190 applied local failure scenarios (loss of one, two, three, or four columns in Table IV.3). One also represents in Figure IV.38 the breakdown of the numbers of scenarios without (C1 + C2) or with (C3 + C4) partial/total collapse. Such figure clearly reveals how each design option performs related to the initiation of progressive collapse. The design configuration D3 has the highest number of scenarios in the categories C1 and C2. D3 is the design configuration that can resist to the highest number of the applied local failure scenarios without collapse in the structure. Conversely, the design configuration D0 has the highest number of scenarios in the categories C3 and C4, that lead to a partial/total collapse in the structure.

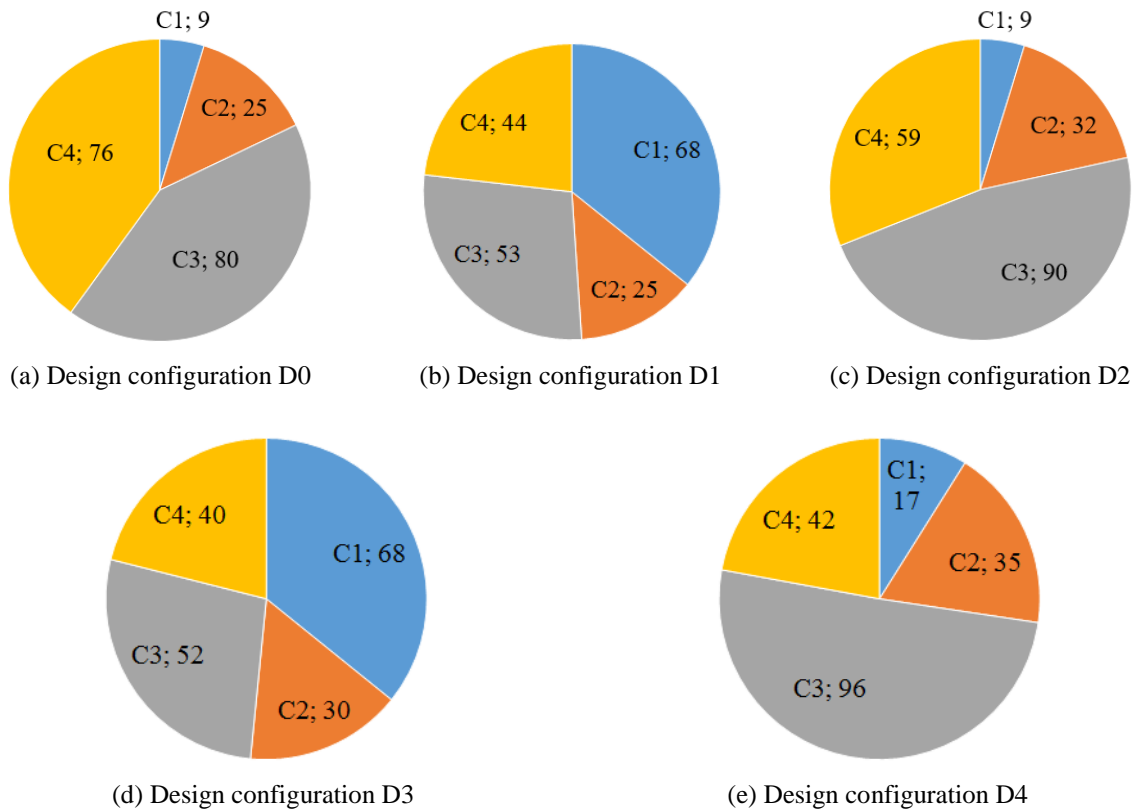


Figure IV.37: Number of local failure scenarios within categories C1 to C4 for design configurations D0, D1, D2, D3 and D4.

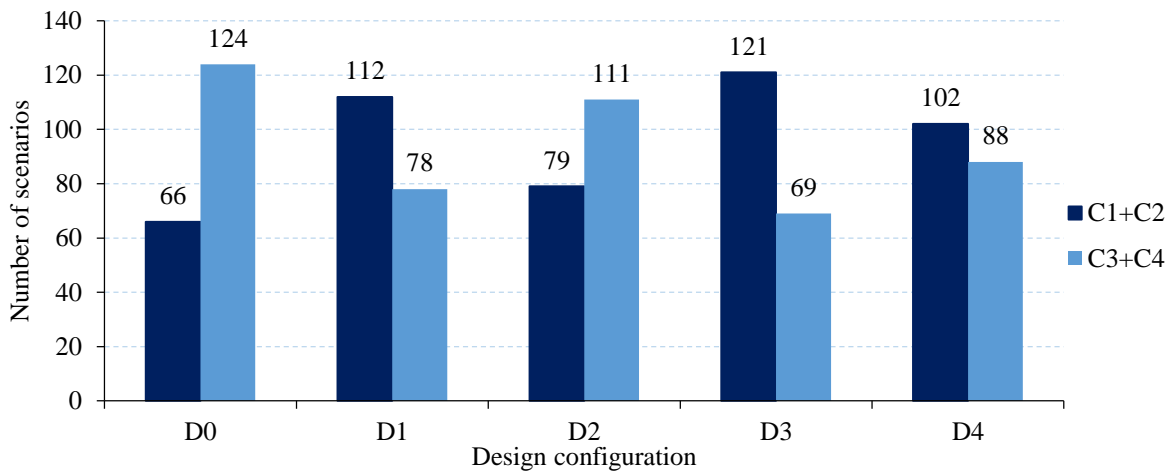


Figure IV.38: Number of local failure scenarios without (C1 + C2) or with (C3 + C4) partial/total collapse for design configurations D0, D1, D2, D3 and D4.

IV.5.3 Assessment of structural robustness with *RPMI*

Figure IV.39 presents the degree of failure propagation DFP_i for each scenario i presented in Table IV.3 with a view to compare the failure propagation for each design configuration D0, D1, D2, D3 and D4. As already explained, for the scenarios with the loss of

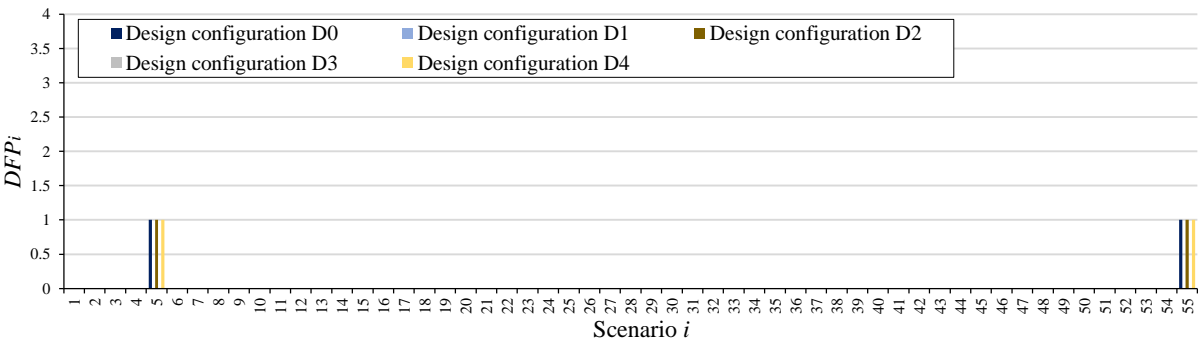
one column (Figure IV.39-a), a collapse is detected under the scenarios 5 and 55 for the configurations D0, D2 and D4, while the strengthening of beams in D1 and D3 helps to resist these scenarios without collapse.

Configurations D1 and D3 have the lowest number of scenarios that lead to a collapse under the loss of two columns (collapse occurs under the scenarios $i = 59, 60, 104$ and 105 , see Figure IV.39-b). The strengthening of the structure in the configurations D2 and D4 also avoids the propagation of some scenarios such as $i = 69, 78, 83$ and 94 .

The failure propagation under the loss of three columns (Figure IV.39-c) is quite similar for the different configurations for most of the scenarios. Strengthened configurations prevent the propagation of failure under the scenarios $i = 120, 129$ and 140 . Some differences exist through as under some scenarios ($i = 124, 128$ and 134), the configurations D1, D3 and D4 resist the local failure, while the strengthening of columns in D2 is not sufficient to avoid the collapse.

Under the loss of four columns, the failure propagation is also quite similar for the considered configurations. One improves the structural capacity to resist some scenarios ($i = 170$ and 175), as shown in Figure IV.39(d). A collapse is detected under the scenarios $i = 165$ and 180 for configuration D1, while the structure achieves to resist the local failure of these scenarios with the configurations D2, D3 and D4, which have a higher structural capacity to resist lateral force than the other configurations. Hence, the strengthening of columns or the adding of braces helps the indirectly affected part to resist the tension forces developed in the beams of the directly affected part.

As mentioned previously in Section IV.5.2, the degree of failure propagation DFP_i under some scenarios (e.g. scenarios $i = 62, 63, 64, 67, 68$, etc.) increases after the strengthening of columns in D2 configuration ($DFP_i^{D2} > DFP_i^{D0}$). As the columns in D2 configuration fail under a load larger than that for D0 configuration, the compression force in the beams below the lost columns is larger for D2 than for D0, which leads in some cases to the failure of these beam elements, and to an increased collapsed part when compared to D0 configuration ($CP_i^{D2} > CP_i^{D0}$).



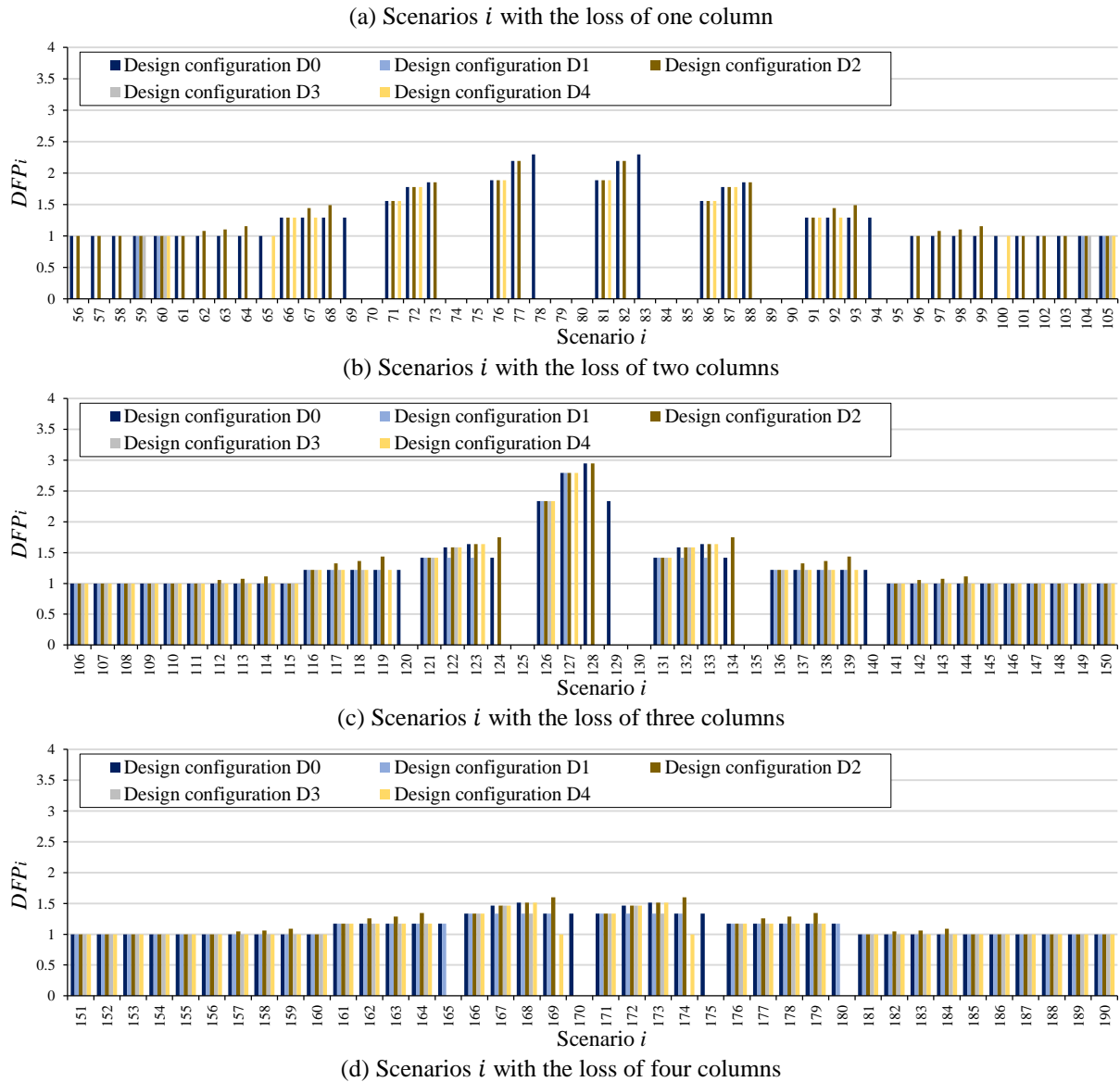


Figure IV.39: Comparison of the degree of failure propagation between the design configurations D0, D1, D2, D3 and D4.

The analysis of the maximum degree of failure propagation according to the number of removed columns is now proposed. The collapse under the loss of one column only occurs for the scenarios 5 and 55 ($DFP_{5 \text{ or } 55}^{D0, D2 \text{ or } D4} = 1$), as shown in Table IV.15. For the configurations D1 and D3, the strengthening of beams avoids the collapse under all the scenarios with the loss of one column.

	D0	D1	D2	D3	D4
Loss of 1 column	1.0	0.0	1.0	0.0	1.0
Loss of 2 columns	2.3	1.0	2.2	1.0	1.9
Loss of 3 columns	2.9	2.8	2.9	2.3	2.8
Loss of 4 columns	1.5	1.3	1.6	1.5	1.5

Table IV.15: Maximum degree of failure propagation $\max(DFP_i)$ according to the number of removed columns for the design configurations D0, D1, D2, D3 and D4.

Table IV.15 shows that the highest value of DFP_i under the loss of two columns is for the configuration D0, for scenario 78 ($DFP_{78}^{D0} = 2.3$), whereas the strengthened configurations D1, D2, D3 and D4 resist this scenario without collapse. The worst two-column removal scenario for D2 is # 77 ($DFP_{77}^{D2} = 2.2$), whereas the configuration D4 resists to this scenario. For configuration D4, the worst case is under scenarios 76 and 81 with $DFP_{76 \text{ or } 81}^{D4} = 1.9$. Finally, the worst two-column removal scenario for configurations D1 and D3 corresponds to the collapse of the directly affected part only (category C3 with $\max\{DFP_i^{D1 \text{ or } D3} | \text{loss of 2 columns}\} = 1$).

For the loss of three columns, the configurations D0 and D2 have the highest degree of failure propagation for the scenario 128 (loss of columns # 23, 28 and 33). Strengthening configurations D1, D3 and D4 help the structure to resist the scenario 128, which is no longer critical. However, the most critical scenario for D1 and D4 becomes the scenario 127 ($DFP_{127}^{D1 \text{ or } D4} = 2.8$). For D3, the worst scenario is # 126 ($\max\{DFP_i^{D3} | \text{loss of 3 columns}\} = 2.3$).

With the loss of four columns, the configuration D2 has the highest degree of failure propagation under the scenarios 169 or 174. The worst degree of failure propagation is similar for the configurations D0, D3 and D4 under the scenarios $i = 127, 128, 172$ and 173. These scenarios are also the most critical for configuration D1, but with a lower degree of failure propagation, where the strengthening of beam elements helps to resist the compression forces developed in the beams below the removed columns. Therefore, the propagation of collapse is lower than that with the three other configurations above mentioned.

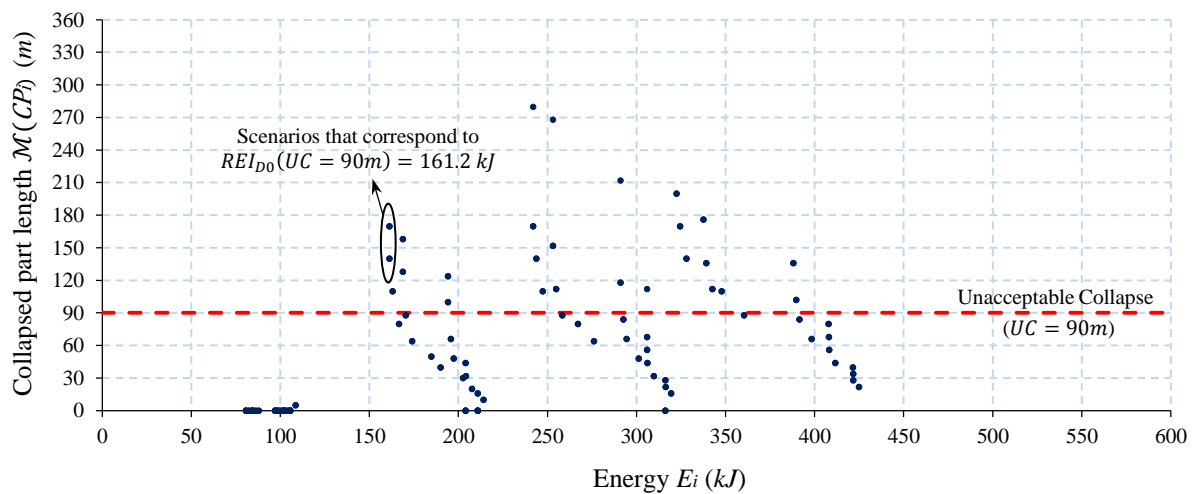
Table IV.16 finally presents the Robustness Propagation Failure Index ($RPMI$) for each design configuration, which is the worst case of failure propagation under the applied scenarios of Table IV.3. The configurations D0 and D2 have the lowest level of robustness with the highest robustness index $RPMI_{D0 \text{ or } D2} = 2.9$. Despite the fact that the strengthening of columns in D2 configuration decreases the number of scenarios that lead to a collapse (see Figure IV.38), the scenario 128 remains the worst scenario and then $RPMI$ is the same for D0 and D2. Configurations D1 and D4 lead to a decrease of $RPMI$ when compared to D0 ($RPMI_{D1 \text{ or } D4} = 2.8$). In this example, the configuration D3 has the best overall performance in terms of failure propagation with the lowest $RPMI$ index ($RPMI_{D3} = 2.3$). It is noted that the ranking order between configurations might change depending on the number of removed columns. However, the three-column loss scenarios dominate all other scenarios in terms of failure propagation for all configurations, which orientate the final ranking based on $RPMI$.

	D0	D1	D2	D3	D4
<i>RPM</i>	2.9	2.8	2.9	2.3	2.8

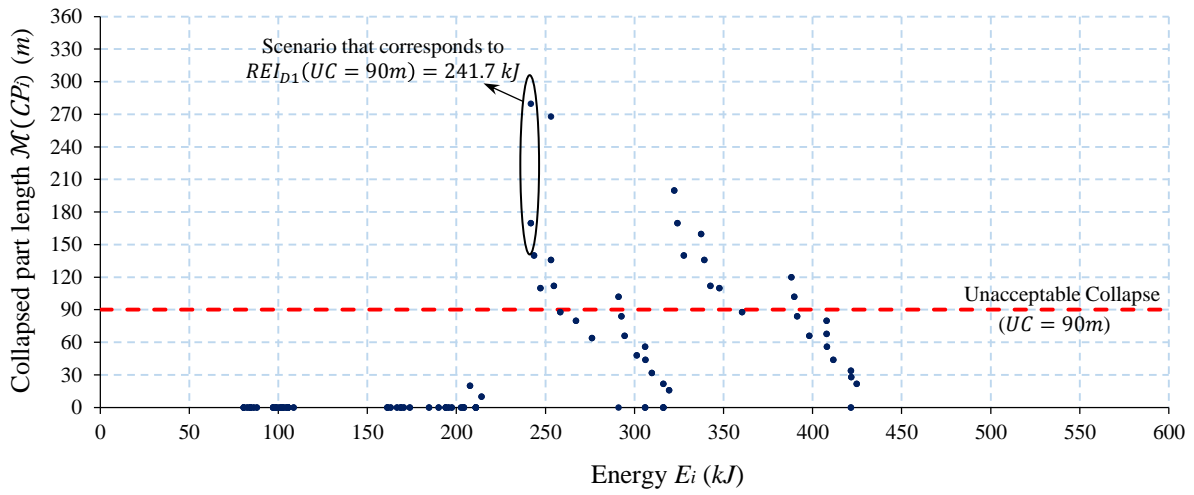
Table IV.16: Robustness Propagation Failure Index (*RPM*) for the design configurations D0, D1, D2, D3 and D4.

IV.5.4 Assessment of structural robustness with *REI(UC)*

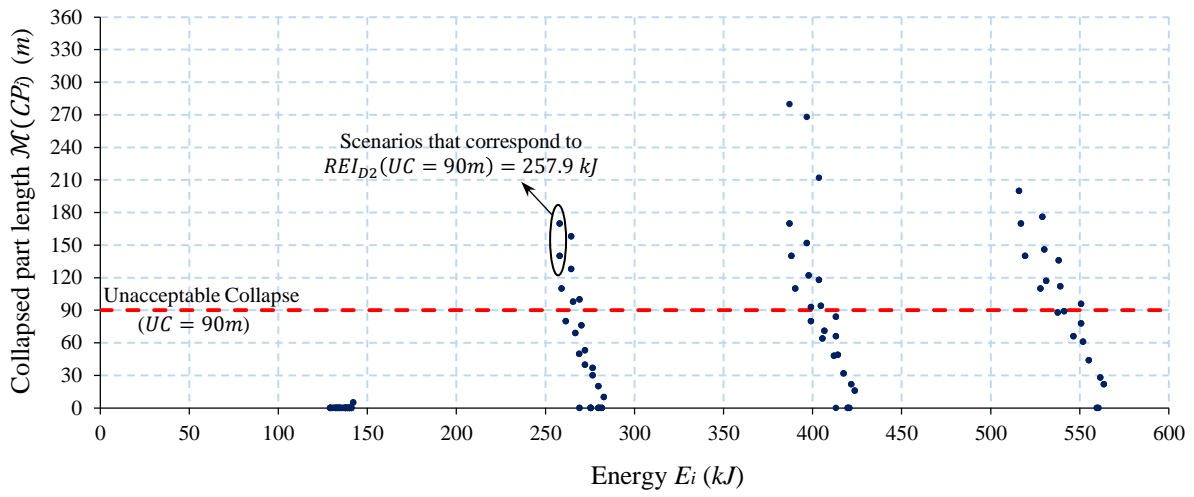
For each design configuration, in order to identify the magnitude of local failure that leads to an unacceptable collapse, Figure IV.40(a, b, c, d and e) shows the diagrams of local failure energy E_i and the measure $\mathcal{M}(CP_i)$ of the collapsed part for each applied scenario i . In this example, the threshold UC defined in Equation (IV.6) is fixed at $90m$. Strengthening column elements in configurations D2 and D3 leads to an increment of the local failure energy, where a higher magnitude of accidental action is required to cause the failure of columns (see Figure IV.40 c and d). Based on these results, one notes that there is a difference between the different design configurations on the scenarios that lead to an unacceptable collapse with the lowest energy (principle of Robustness Energy Index *REI* in Equation (IV.7)).



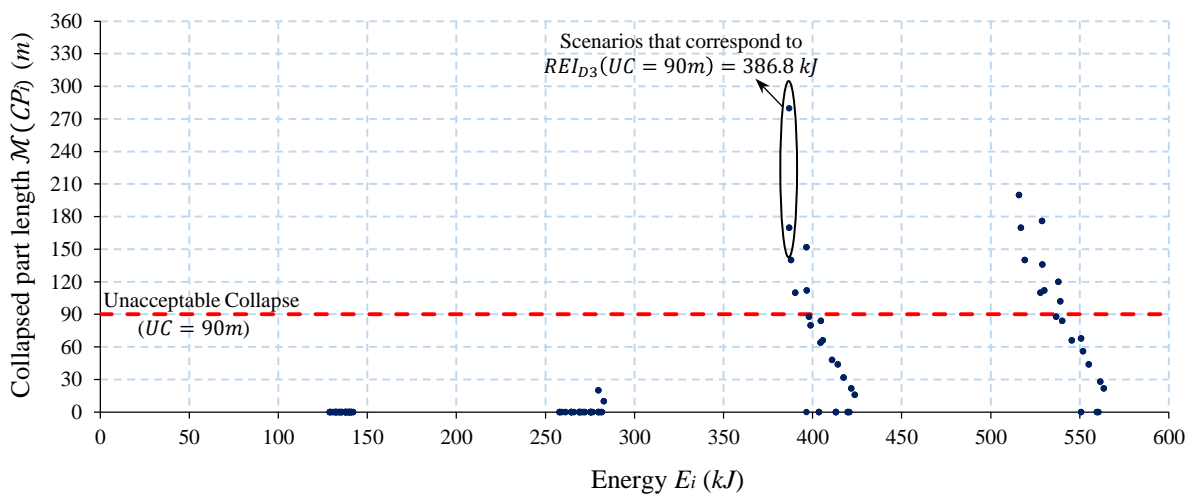
(a) Design configuration D0



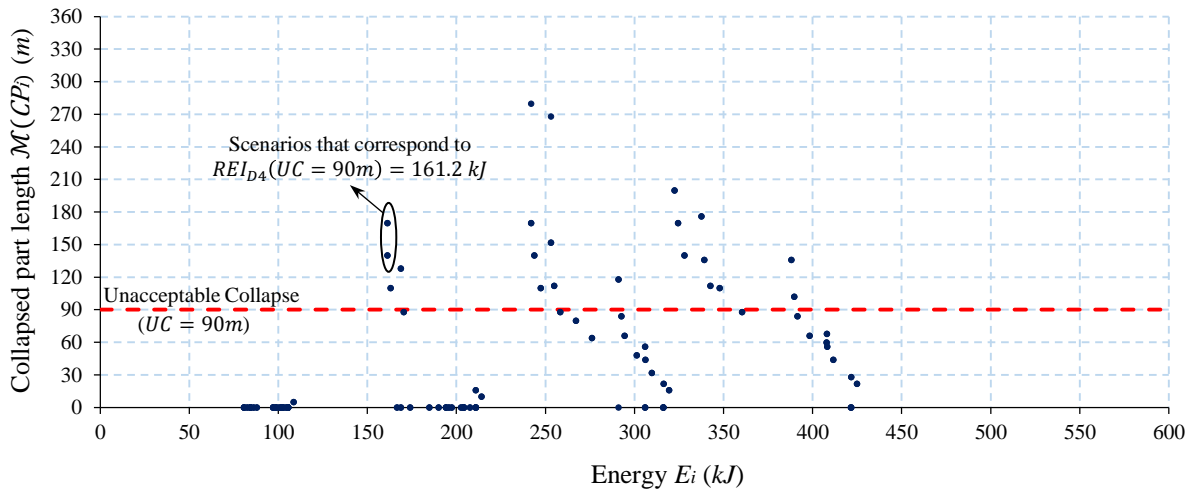
(b) Design configuration D1



(c) Design configuration D2



(d) Design configuration D3



(e) Design configuration D4

Figure IV.40: Local failure energy – collapsed part length diagrams for the design configurations D0, D1, D2, D3 and D4.

Table IV.17 shows $REI(UC = 90m)$ for each design configuration as well as the associated scenarios. The critical scenarios leading to an unacceptable collapse are similar for design configurations D0, D2 and D4 ($i = 71, 76, 81$ and 86 with the loss of two columns). The index $REI_{D2}(UC = 90m) = 257.9 kJ$ for configuration D2 is larger than those of D0 and D4 ($REI_{D0 \text{ or } D4}(UC = 90m) = 161.2 kJ$), due to the fact that the column elements in D2 are strengthened.

The strengthening of beams in the configurations D1 and D3 avoids the unacceptable collapse under the scenarios with the loss of one or two columns, where some unacceptable collapse is detected only under the loss of three columns. The critical scenarios ($i = 121, 126$ and 131) are also similar for D1 and D3. As the column elements are strengthened in the configuration D3, $REI_{D3}(UC = 90m) = 386.8 kJ > REI_{D1}(UC = 90m) = 241.7 kJ$.

In this example, the design configuration D3 is the most robust configuration in terms of Robustness Energy Index $REI(UC = 90m)$, where it requires the highest value of failure energy to cause an unacceptable collapse ($UC = 90m$).

Design configuration	$REI(UC = 90m)$ [kJ]	i	Columns #	CP_i (m)
D0	161.2	71	16-21	140
		76	21-26	170
		81	26-31	170
		86	31-36	140
D1	241.7	121	16-21-26	170
		126	21-26-31	280
		131	26-31-36	170
D2	257.9	71	16-21	140
		76	21-26	170
		81	26-31	170

		86	31-36	140
D3	386.8	121	16-21-26	170
		126	21-26-31	280
		131	26-31-36	170
		71	16-21	140
D4	161.2	76	21-26	170
		81	26-31	170
		86	31-36	140

Table IV.17: Robustness Energy Index REI with unacceptable collapse threshold $UC = 90\text{ m}$ for the design configurations D0, D1, D2, D3 and D4.

In order to study the sensitivity of the Robustness Energy Index $REI(UC)$ to the threshold UC , Figure IV.41 presents $REI(UC)$ for each design configuration D0, D1, D2, D3 and D4 if $UC \in [10\text{ m}; 280\text{ m}]$. Based on these results, one can conclude that the design configurations with the lowest $REI(UC)$ can change according to the threshold of the unacceptable collapse UC (D0 and D4 for $UC \leq 170\text{ m}$, then D0, D1 and D4 for $UC > 170\text{ m}$). One observes similar changes for the highest value $REI(UC)$ (configuration D3 for $UC \leq 170\text{ m}$, then D2 and D3 for $UC > 170\text{ m}$). The reason is the critical scenario that can be different or the same between configurations depending on UC . Also critical scenarios are sometimes the same between configurations, but $REI(UC)$ is different due to the dimensions of the columns. This is the case when comparing configurations D1 and D3. Table IV.18 and Table IV.19 summarize the lowest and highest values of $REI(UC)$ with the associated configurations. It confirms that D0 and D4 have the lowest robustness level based on $REI(UC)$ (also D1 when UC is important) and that D3 performs the best (also D2 when UC is important).

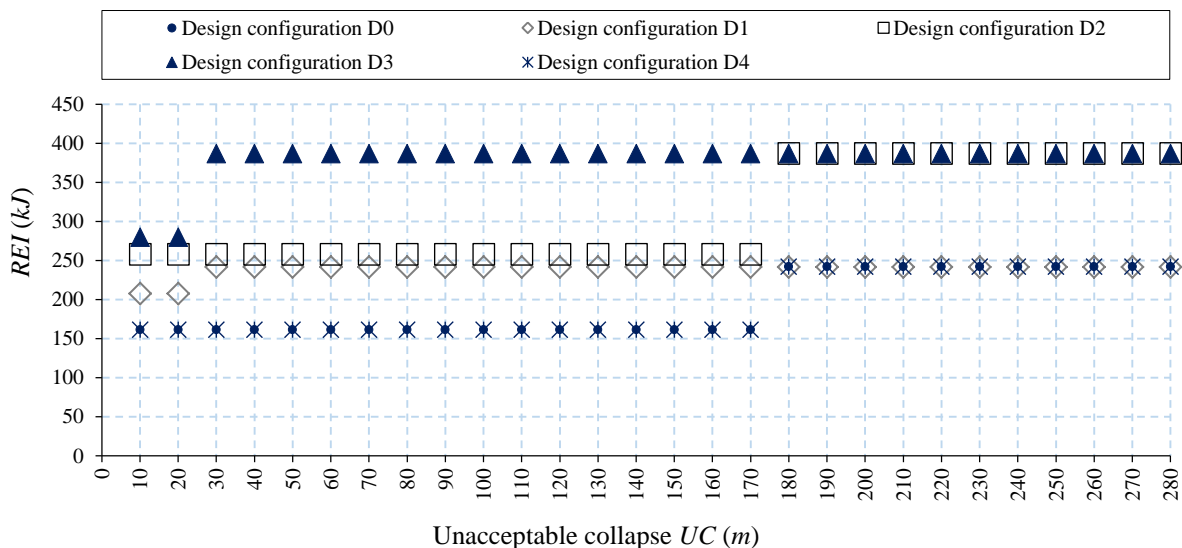


Figure IV.41: Sensitivity of REI index according to the threshold of the unacceptable collapse UC for the design configurations D0, D1, D2, D3 and D4.

UC	$\min\{REI(UC)\} (kJ)$	Design configuration	Critical scenarios
[10 m; 170 m]	161	D0; D4	76; 81
[180 m; 280m]	242	D0; D1; D4	126

Table IV.18: Minimal value of $REI(UC)$ between the design configurations D0, D1, D2, D3 and D4.

UC	$\max\{REI(UC)\} (kJ)$	Design configuration	Critical scenarios
[10 m; 20 m]	280	D3	59; 104
[30 m; 280 m]	387	D2; D3	126

Table IV.19: Maximal value of $REI(UC)$ between the design configurations D0, D1, D2, D3 and D4.

IV.5.5 Assessment of structural robustness with several criteria

In this section, one considers several criteria to identify scenarios that minimize initial failure magnitude and maximize propagation extent as introduced in Equations (IV.8), (IV.12) and (IV.13). Figure IV.42 shows the non-dominated solutions (Pareto front) for the design configurations D0, D1, D2, D3 and D4 based on the bi-objective problem of Equation (IV.8) when simultaneously minimizing E_i and maximizing DFP_i .

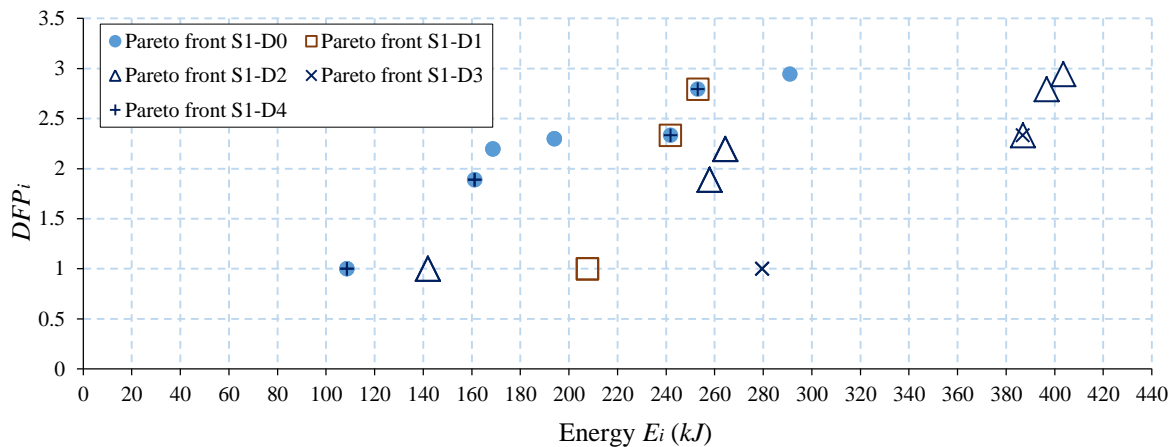


Figure IV.42: Identification of non-dominated solutions for the design configurations D0, D1, D2, D3 and D4 when simultaneously minimizing E_i and maximizing DFP_i (Equation IV.8).

The scenarios of Pareto front for each design configuration are described in Table IV.20. One observes that the non-dominated scenarios of S1-D4 belong to the Pareto fronts of D0 and D2 (S1-D0 and S1-D2, respectively). In fact, configuration D4 enables to remove some of the critical scenarios present for D0 and D2. In this sense, it represents an improvement for robustness. Besides, the failure energy values for D3 are larger than those of D0 and D4 due the fact that the column elements are strengthened. Moreover, the scenarios of

S1-D3 belong to the Pareto front S1-D1 (one removes critical scenario 127), and as the columns are strengthened in D3, the failure energy values for D3 is larger than those of D1.

Pareto front	Scenario i	Column #	E_i (kJ)	DFP_i
S1-D0	5	5	108.6	1.0
	55	55	108.6	1.0
	76	21-26	161.2	1.9
	81	26-31	161.2	1.9
	77	22-27	168.7	2.2
	82	27-32	168.7	2.2
	78	23-28	194.0	2.3
	83	28-33	194.0	2.3
	126	21-26-31	241.9	2.3
	127	22-27-32	253.1	2.8
S1-D1	59	4-9	207.5	1.0
	104	49-54	207.5	1.0
	126	21-26-31	241.7	2.3
	127	22-27-32	253.0	2.8
S1-D2	5	5	141.9	1.0
	55	55	141.9	1.0
	76	21-26	257.9	1.9
	81	26-31	257.9	1.9
	77	22-27	264.4	2.2
	82	27-32	264.4	2.2
	126	21-26-31	386.9	2.3
	127	22-27-32	396.6	2.8
S1-D3	59	4-9	279.6	1.0
	104	49-54	279.6	1.0
	126	21-26-31	386.8	2.3
S1-D4	5	5	108.6	1.0
	55	55	108.6	1.0
	76	21-26	161.2	1.9
	81	26-31	161.2	1.9
	126	21-26-31	241.9	2.3
	127	22-27-32	253.1	2.8

Table IV.20: Non-dominated scenarios for the design configurations D0, D1, D2, D3 and D4 related to Equation (IV.8).

The application of the bi-objective problem of Equation (IV.8) on the set of non-dominated scenarios of Table IV.20 identified for each design configuration (S1-D0, S1-D1, S1-D2, S1-D3 and S1-D4) allows to identify which are non-dominated (and then most critical) scenarios when comparing all configurations, as shown in Figure IV.43. 11 non-dominated scenarios are identified for the Pareto front Pf-S1, and they are described in Table IV.21. One can note that S1-D0 has the highest percentage of scenarios that correspond to Pf-S1 (see Table IV.22), which indicates that the design configuration D0 has the most critical set of scenarios, according to Equation (IV.8). Conversely, S1-D3 has the highest percentage of scenarios that correspond to the front 4 of the dominated scenarios (see Table IV.22), and

therefore the scenarios of S1-D3 have the lowest level of criticality compared to the other scenarios, which indicates that D3 configuration is the most robust.

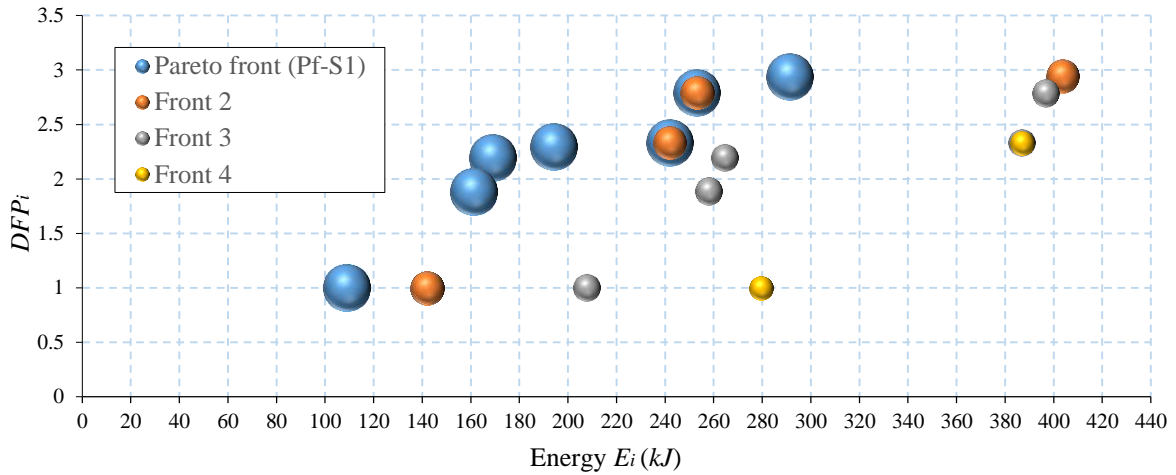


Figure IV.43: Identification of non-dominated scenarios of the Pareto fronts S1-D0, S1-D1, S1-D2, S1-D3 and S1-D4 according to Equation (IV.8).

Front	Scenario i	Column #	E_i (kJ)	DFP_i	Pareto front
Pf-S1	5	5	108.6	1.0	S1-D0; S1-D4
	55	55	108.6	1.0	S1-D0; S1-D4
	76	21-26	161.2	1.9	S1-D0; S1-D4
	81	26-31	161.2	1.9	S1-D0; S1-D4
	77	22-27	168.7	2.2	S1-D0
	82	27-32	168.7	2.2	S1-D0
	78	23-28	194.0	2.3	S1-D0
	83	28-33	194.0	2.3	S1-D0
	126	21-26-31	241.7	2.3	S1-D1
	127	22-27-32	253.0	2.8	S1-D1
	128	23-28-33	291.0	2.9	S1-D0
Front 4	126	21-26-31	386.9	2.3	S1-D2
	59	4-9	279.6	1.0	S1-D3
	104	49-54	279.6	1.0	S1-D3

Table IV.21: Scenarios of Pareto front Pf-S1 and front 4 according to Equation (IV.8).

	Pareto front Pf-S1	Front 2	Front 3	Front 4
S1-D0	82 %	18 %	0 %	0 %
S1-D1	50 %	0 %	50 %	0 %
S1-D2	0 %	33 %	56 %	11 %
S1-D3	0 %	0 %	33 %	67 %
S1-D4	67 %	33 %	0 %	0 %

Table IV.22: Distribution of S1-D0, S1-D1, S1-D2, S1-D3 and S1-D4 scenarios in the different fronts.

The comparison between the design configurations is now considered by identifying the Pareto fronts S2-D0, S2-D1, S2-D2, S2-D3 and S2-D4 according to the bi-objective problem of Equation (IV.12) when simultaneously minimizing $\mathcal{M}(IDP_i)$ and maximizing DFP_i . Figure IV.44 presents the Pareto fronts for each design configuration, and the non-dominated scenarios are identified and described in Table IV.23.

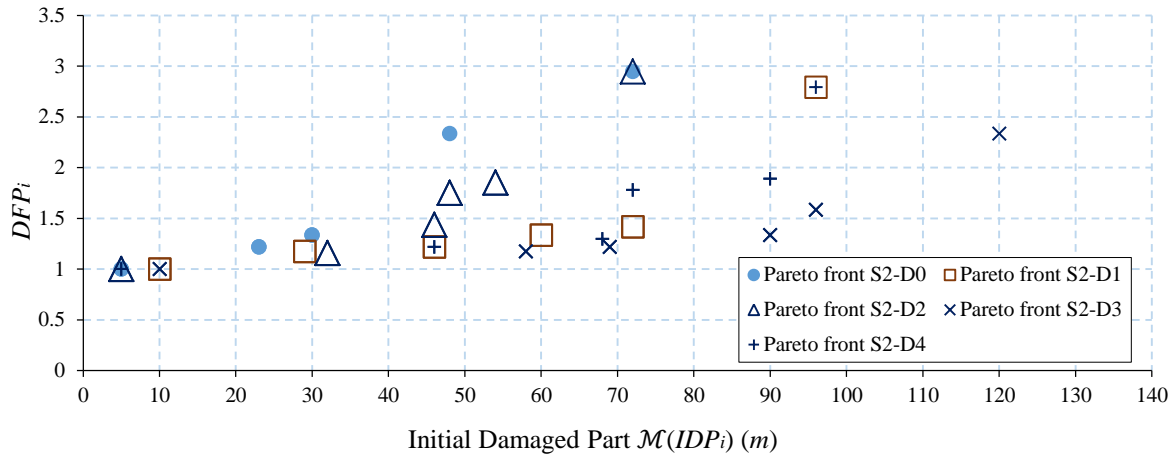


Figure IV.44: Identification of non-dominated solutions for the design configurations D0, D1, D2, D3 and D4 when simultaneously minimizing $\mathcal{M}(IDP_i)$ and maximizing DFP_i (Equation IV.12).

Pareto front	Scenario i	Column #	$\mathcal{M}(IDP_i)$ (m)	DFP_i
S2-D0	5	5	5	1.0
	55	55	5	1.0
	120	15-20-25	23	1.2
	140	35-40-45	23	1.2
	170	20-25-30-35	30	1.3
	175	25-30-35-40	30	1.3
	129	24-29-34	48	2.3
	128	23-28-33	72	2.9
S2-D1	60	5-10	10	1.0
	105	50-55	10	1.0
	165	15-20-25-30	29	1.2
	180	30-35-40-45	29	1.2
	119	14-19-24	46	1.2
	139	34-39-44	46	1.2
	169	19-24-29-34	60	1.3
	174	24-29-34-39	60	1.3
	123	18-23-28	72	1.4
	133	28-33-38	72	1.4
	127	22-27-32	96	2.8
S2-D2	5	5	5	1.0
	55	55	5	1.0
	64	9-14	32	1.2
	99	44-49	32	1.2
	119	14-19-24	46	1.4
	139	34-39-44	46	1.4
	124	19-24-29	48	1.8
	134	29-34-39	48	1.8
	73	18-23	54	1.9

	88	33-38	54	1.9
	128	23-28-33	72	2.9
S2-D3	60	5-10	10	1.0
	105	50-55	10	1.0
	164	14-19-24-29	58	1.2
	179	29-34-39-44	58	1.2
	118	13-18-23	69	1.2
	138	33-38-43	69	1.2
	168	18-23-28-33	90	1.3
	173	23-28-33-38	90	1.3
	122	17-22-27	96	1.6
	132	27-32-37	96	1.6
	126	21-26-31	120	2.3
S2-D4	5	5	5	1.0
	55	55	5	1.0
	119	14-19-24	46	1.2
	139	34-39-44	46	1.2
	67	12-17	68	1.3
	92	37-42	68	1.3
	72	17-22	72	1.8
	87	32-37	72	1.8
	76	21-26	90	1.9
	81	26-31	90	1.9
	127	22-27-32	96	2.8

Table IV.23: Non-dominated scenarios for the design configurations D0, D1, D2, D3 and D4 related to Equation (IV.12).

In order to compare the Pareto fronts S2-D0, S2-D1, S2-D2, S2-D3 and S2-D4, the bi-objective problem of Equation (IV.12) is applied on the scenarios of Table IV.23. Figure IV.45 shows that these scenarios are classified into five fronts, and the non-dominated scenarios of Pareto front Pf-S2 are described in Table IV.24. All the scenarios of S2-D0 (Table IV.23) are among Pf-S2, which is the highest percentage compared to the others configurations (see Table IV.25). Hence, the design configuration D0 has the most critical scenarios according to Equation (IV.12). Moreover, the scenarios of front 5 (see Table IV.24) correspond to the Pareto front S2-D3, and these scenarios include 36% of S2-D3 scenarios, as shown in Table IV.25. As S2-D3 has the highest percentage of the dominated scenarios (Front 5) that are less critical than the others scenarios, the design configuration D3 is also the most robust when considering the bi-objective problem of Equation (IV.12).

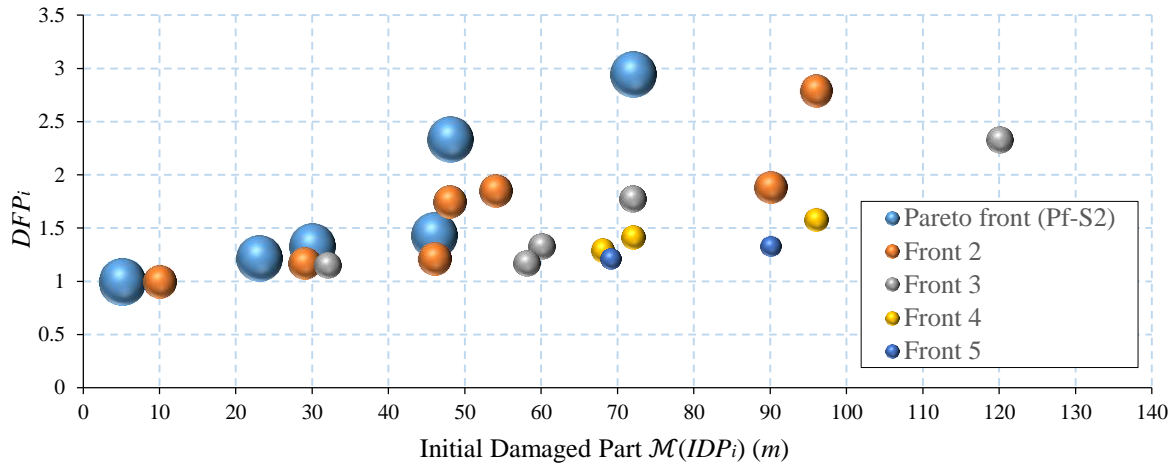


Figure IV.45: Identification of non-dominated scenarios of the Pareto fronts S2-D0, S2-D1, S2-D2, S2-D3 and S2-D4 according to Equation (IV.12).

Front	Scenario i	Column #	$\mathcal{M}(IDP_i) (m)$	DFP_i	Pareto front
Pf-S2	5	5	5	1.0	S2-D0; S2-D2; S2-D4
	55	55	5	1.0	S2-D0; S2-D2; S2-D4
	120	15-20-25	23	1.2	S2-D0
	140	35-40-45	23	1.2	S2-D0
	170	20-25-30-35	30	1.3	S2-D0
	175	25-30-35-40	30	1.3	S2-D0
	119	14-19-24	46	1.4	S2-D2
	139	34-39-44	46	1.4	S2-D2
	129	24-29-34	48	2.3	S2-D0
	128	23-28-33	72	2.9	S2-D0; S2-D2
Front 5	118	13-18-23	69	1.2	S2-D3
	138	33-38-43	69	1.2	S2-D3
	168	18-23-28-33	90	1.3	S2-D3
	173	23-28-33-38	90	1.3	S2-D3

Table IV.24: Scenarios of Pareto front Pf-S2 and front 5 according to Equation (IV.12).

	Pareto front Pf-S2	Front 2	Front 3	Front 4	Front 5
S2-D0	100 %	0 %	0 %	0 %	0 %
S2-D1	0 %	64 %	18 %	18 %	0 %
S2-D2	45 %	36 %	18 %	0 %	0 %
S2-D3	0 %	18 %	27 %	18 %	36 %
S2-D4	18 %	45 %	18 %	18 %	0 %

Table IV.25: Distribution of S2-D0, S2-D1, S2-D2, S2-D3 and S2-D4 scenarios on the different fronts.

The non-dominated scenarios that maximize $\mathcal{M}(CP_i)$ and minimize initial damaged part $\mathcal{M}(IDP_i)$ according to Equation (IV.13) are presented in Figure IV.46, where the Pareto

fronts of the design configurations D0, D1, D2, D3 and D4 are noted S3-D0, S3-D1, S3-D2, S3-D3 and S3-D4, and described in Table IV.26. The scenarios $i = 60, 105, 110, 115, 126, 145, 150, 155$ and 190 are common in the Pareto fronts of the five different configurations. Hence, these scenarios are critical for the different configurations D0, D1, D2, D3 and D4 according to the bi-objective sorting of Equation (IV.13).

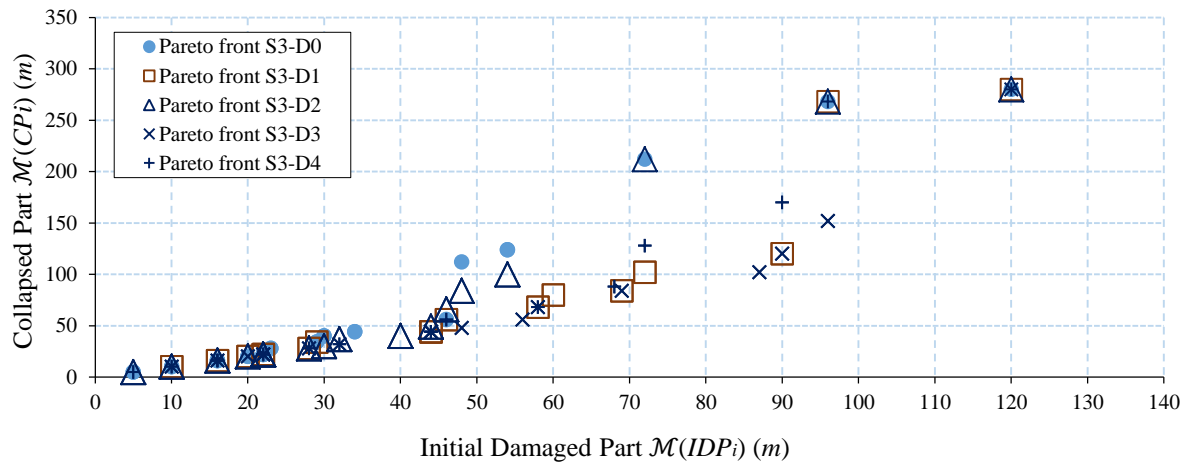


Figure IV.46: Identification of non-dominated solutions for the design configurations D0, D1, D2, D3 and D4 when simultaneously minimizing $\mathcal{M}(IDP_i)$ and maximizing $\mathcal{M}(CP_i)$ (Equation IV.13).

Pareto front	i	Column #	$\mathcal{M}(IDP_i)$ (m)	$\mathcal{M}(CP_i)$ (m)	Pareto front	i	Column #	$\mathcal{M}(IDP_i)$ (m)	$\mathcal{M}(CP_i)$ (m)
S3-D0	5	5	5	5	S3-D2	99	44-49	32	37
	55	55	5	5		57	2-7	40	40
	60	5-10	10	10		102	47-52	40	40
	105	50-55	10	10		114	9-14-19	44	49
	65	10-15	16	16		144	39-44-49	44	49
	100	45-50	16	16		119	14-19-24	46	66
	110	5-10-15	16	16		139	34-39-44	46	66
	150	45-50-55	16	16		124	19-24-29	48	84
	59	4-9	20	20		134	29-34-39	48	84
	104	49-54	20	20		73	18-23	54	100
	115	10-15-20	22	22	88	33-38	54	100	
	145	40-45-50	22	22	128	23-28-33	72	212	
	155	5-10-15-20	22	22	127	22-27-32	96	268	
	190	40-45-50-55	22	22	126	21-26-31	120	280	
	120	15-20-25	23	28	S3-D3	60	5-10	10	10
	140	35-40-45	23	28		105	50-55	10	10
	165	15-20-25-30	29	34		110	5-10-15	16	16
	180	30-35-40-45	29	34		150	45-50-55	16	16
	170	20-25-30-35	30	40		59	4-9	20	20
	175	25-30-35-40	30	40		104	49-54	20	20
69	14-19	34	44	115		10-15-20	22	22	
94	39-44	34	44	145		40-45-50	22	22	
119	14-19-24	46	56	155		5-10-15-20	22	22	
139	34-39-44	46	56	190		40-45-50-55	22	22	
129	24-29-34	48	112	160	10-15-20-25	28	28		
78	23-28	54	124	185	35-40-45-50	28	28		

	83	28-33	54	124		109	4-9-14	32	32	
	128	23-28-33	72	212		149	44-49-54	32	32	
	127	22-27-32	96	268		114	9-14-19	44	44	
	126	21-26-31	120	280		144	39-44-49	44	44	
S3-D1	60	5-10	10	10		154	4-9-14-19	44	44	
	105	50-55	10	10		189	39-44-49-54	44	44	
	110	5-10-15	16	16		108	3-8-13	48	48	
	150	45-50-55	16	16		148	43-48-53	48	48	
	59	4-9	20	20		159	9-14-19-24	56	56	
	104	49-54	20	20		184	34-39-44-49	56	56	
	115	10-15-20	22	22		164	14-19-24-29	58	68	
	145	40-45-50	22	22		179	29-34-39-44	58	68	
	155	5-10-15-20	22	22		118	13-18-23	69	84	
	190	40-45-50-55	22	22		138	33-38-43	69	84	
	160	10-15-20-25	28	28		163	13 18 23 28	87	102	
	185	35-40-45-50	28	28		178	28-33-38-43	87	102	
	165	15-20-25-30	29	34		168	18-23-28-33	90	120	
	180	30-35-40-45	29	34		173	23-28-33-38	90	120	
	114	9-14-19	44	44		122	17-22-27	96	152	
	144	39-44-49	44	44		132	27-32-37	96	152	
	154	4-9-14-19	44	44		126	21-26-31	120	280	
	189	39-44-49-54	44	44		S3-D4	5	5	5	5
	119	14-19-24	46	56			55	55	5	5
	139	34-39-44	46	56			60	5-10	10	10
	164	14-19-24-29	58	68			105	50-55	10	10
	179	29-34-39-44	58	68			65	10-15	16	16
	169	19-24-29-34	60	80			100	45-50	16	16
	174	24-29-34-39	60	80			110	5-10-15	16	16
	118	13-18-23	69	84			150	45-50-55	16	16
	138	33-38-43	69	84			115	10-15-20	22	22
	123	18-23-28	72	102			145	40-45-50	22	22
	133	28-33-38	72	102			155	5-10-15-20	22	22
	168	18-23-28-33	90	120			190	40-45-50-55	22	22
	173	23-28-33-38	90	120			160	10-15-20-25	28	28
	127	22-27-32	96	268			185	35-40-45-50	28	28
	126	21-26-31	120	280			109	4-9-14	32	32
S3-D2	5	5	5	5	149		44-49-54	32	32	
	55	55	5	5	114		9-14-19	44	44	
	60	5-10	10	10	144		39-44-49	44	44	
	105	50-55	10	10	154		4-9-14-19	44	44	
	110	5-10-15	16	16	189		39-44-49-54	44	44	
	150	45-50-55	16	16	119		14-19-24	46	56	
	59	4-9	20	20	139		34-39-44	46	56	
	104	49-54	20	20	164		14-19-24-29	58	68	
	115	10-15-20	22	22	179		29-34-39-44	58	68	
	145	40-45-50	22	22	67		12-17	68	88	
	155	5-10-15-20	22	22	92		37-42	68	88	
	190	40-45-50-55	22	22	72		17-22	72	128	
	160	10-15-20-25	28	28	87		32-37	72	128	
	185	35-40-45-50	28	28	76		21-26	90	170	
	58	3-8	30	30	81		26-31	90	170	
	103	48-53	30	30	127		22-27-32	96	268	
64	9-14	32	37	126	21-26-31		120	280		

Table IV.26: Non-dominated scenarios for the design configurations D0, D1, D2, D3 and D4 related to Equation (IV.13).

The bi-objective problem of Equation (IV.13) is applied on the set of scenarios in Table IV.26. The Pareto front Pf-S3 is shown in Figure IV.47, and the non-dominated scenarios are described in Table IV.27. As it was previously observed in Figure IV.43 and Figure IV.45 for the bi-objective problems of Equations (IV.8) and (IV.12), the majority of S3-D0 scenarios (93%) correspond to the Pareto front Pf-S3 (see Table IV.28), which means that the non-dominated scenarios of the design configuration D0 (S3-D0) are also non-dominated compared to the Pareto fronts of the other configurations according to Equation (IV.13). Moreover, S3-D3 has the lowest percentage of scenarios that correspond to Pf-S3, while it has the highest percentage for front 4, as shown in Table IV.28. Hence, the scenarios of S3-D3 are less critical than the others scenarios, which also indicates that the design configuration D3 has the highest level of structural robustness compared to the configurations when considering the bi-objective problem of Equation (IV.13).

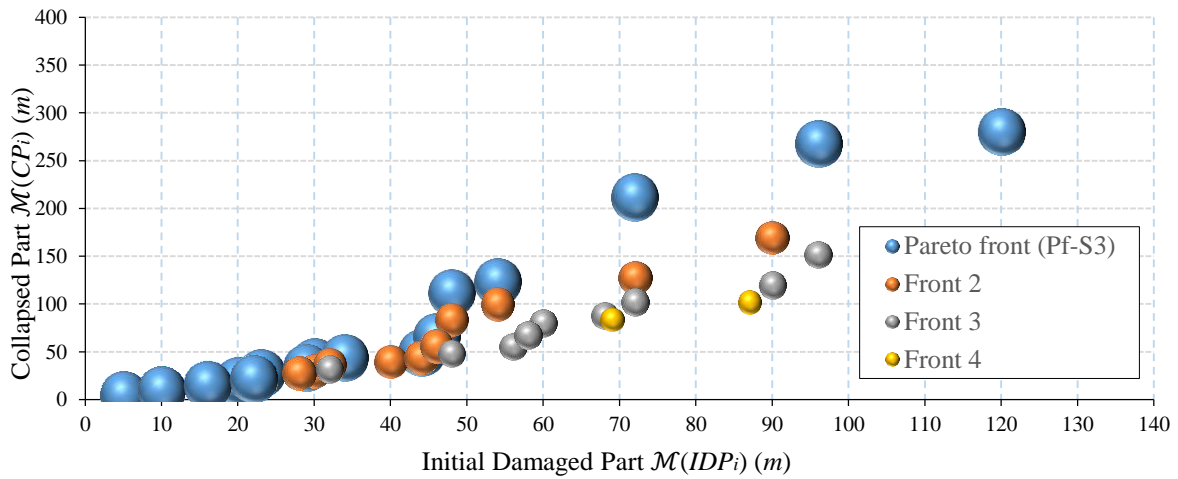


Figure IV.47: Identification of non-dominated scenarios of the Pareto fronts S3-D0, S3-D1, S3-D2, S3-D3 and S3-D4 according to Equation (IV.13).

Front	Scenario i	Column #	$\mathcal{M}(IDP_i)$ (m)	$\mathcal{M}(CP_i)$ (m)	Pareto front
Pf-S3	5	5	5	5	S3-D0; S3-D2; S3-D4
	55	55	5	5	S3-D0; S3-D2; S3-D4
	60	5-10	10	10	S3-D0; S3-D1; S3-D2; S3-D3; S3-D4
	105	50-55	10	10	S3-D0; S3-D1; S3-D2; S3-D3; S3-D4
	65	10-15	16	16	S3-D0; S3-D4
	100	45-50	16	16	S3-D0; S3-D4
	110	5-10-15	16	16	S3-D0; S3-D1; S3-D2; S3-D3; S3-D4
	150	45-50-55	16	16	S3-D0; S3-D1; S3-D2; S3-D3; S3-D4
	59	4-9	20	20	S3-D0; S3-D1; S3-D2; S3-D3
	104	49-54	20	20	S3-D0; S3-D1; S3-D2; S3-D3
	115	10-15-20	22	22	S3-D0; S3-D1; S3-D2; S3-D3; S3-D4
	145	40-45-50	22	22	S3-D0; S3-D1; S3-D2; S3-D3; S3-D4
	155	5-10-15-20	22	22	S3-D0; S3-D1; S3-D2; S3-D3; S3-D4
	190	40-45-50-55	22	22	S3-D0; S3-D1; S3-D2; S3-D3; S3-D4
	120	15-20-25	23	28	S3-D0
140	35-40-45	23	28	S3-D0	

	165	15-20-25-30	29	34	S3-D0; S3-D1
	180	30-35-40-45	29	34	S3-D0; S3-D1
	170	20-25-30-35	30	40	S3-D0
	175	25-30-35-40	30	40	S3-D0
	69	14-19	34	44	S3-D0
	94	39-44	34	44	S3-D0
	114	9-14-19	44	49	S3-D2
	144	39-44-49	44	49	S3-D2
	119	14-19-24	46	66	S3-D2
	139	34-39-44	46	66	S3-D2
	129	24-29-34	48	112	S3-D0
	78	23-28	54	124	S3-D0
	83	28-33	54	124	S3-D0
	128	23-28-33	72	212	S3-D0; S3-D2
	127	22-27-32	96	268	S3-D0; S3-D1; S3-D2; S3-D4
126	21-26-31	120	280	S3-D0; S3-D1; S3-D2; S3-D3; S3-D4	
Front 4	118	13-18-23	69	84	S3-D1; S3-D3
	138	33-38-43	69	84	S3-D1; S3-D3
	118	13-18-23	69	84	S3-D1; S3-D3
	138	33-38-43	69	84	S3-D1; S3-D3
	163	13-18-23-28	87	102	S3-D3
	178	28-33-38-43	87	102	S3-D3

Table IV.27: Scenarios of Pareto front Pf-S2 and front 4 according to Equation (IV.13).

	Pareto front Pf-S3	Front 2	Front 3	Front 4
S3-D0	93 %	7 %	0 %	0 %
S3-D1	44 %	25 %	25 %	6 %
S3-D2	61 %	39 %	0 %	0 %
S3-D3	33 %	18 %	36 %	12 %
S3-D4	44 %	38 %	19 %	0 %

Table IV.28: Distribution of S3-D0, S3-D1, S3-D2, S3-D3 and S3-D4 scenarios on the different fronts.

IV.5.6 General discussion

The proposed robustness indices have been used in the previous section to compare several design configurations. It has been shown how the ranking order among configurations based on the degree of failure propagation is influenced by the number of columns lost and also that *RPMI* is determined by the scenarios with the loss of three columns. The configurations D0 and D2 have the highest *RPMI*, which means that the worst failure propagation under the applied scenarios (Table IV.3) corresponds to D0 and D2. As the configuration D3 has the lowest *RPMI*, it can be considered as the best design configuration to limit the failure propagation.

The ranking order between design configurations when using the Robustness Energy Index *REI(UC)* depends on the unacceptable collapse threshold *UC*. In particular, the configurations D0 and D4 always have the lowest *REI(UC)*. Conversely, the configuration D3 always has the highest value of *REI(UC)*. Increasing of the threshold *UC* changes the

ranking order of the configurations based on this index, due mainly to two reasons: the change of critical scenarios, and the strengthening of columns that increases energy requested for the initial failure event.

Furthermore, one observes that in the three bi-objective problems (Equations (IV.8), (IV.12) and (IV.13)), the non-dominated scenarios of the Pareto fronts of the configuration D0 (S1-D0, S2-D0 and S3-D0) are non-dominated compared to the Pareto fronts of the other configurations, which is coherent. Therefore, according to the different ways of analysis, one shows the increase of structural robustness from design configuration D0 to the strengthened configurations (D1, D2, D3 and D4). Besides, the Pareto fronts S1-D3, S2-D3 and S3-D3 for the design configuration D3 always have the lowest percentage of the non-dominated scenarios and the highest percentage of the dominated percentage. Hence in this example, the configuration D3 has a high level of structural robustness compared to the other configurations when considering the different bi-objective problems.

IV.6 CONCLUSIONS

Progressive collapse modelling is used in this chapter for investigating the disproportionate aspect of failure propagation. Under occurrence of some local failure, the structure is modelled to take into account the redistribution of efforts and identify if a failure mode occurs in the directly affected part of the structure. The iterative coupling with a non-linear analysis that was detailed in Chapter III is used to investigate if a second line of defence can be found and how the failure propagates in cascading events to the rest of the structure.

The illustrative case study shows the ability of the proposed strategy to study a large number of local failure scenarios. With the aim to characterize the event-independent scenarios, this chapter presents an approach to characterize the local failure scenarios by the associated energy required to cause the failure of the structural elements according to an applied loading mode. Several loading modes are studied with different element dimensions with a view to check the efficiency of using only one load type to characterize the resistance capacity of the structural elements. The results show that one load type can be sufficient to perform a relative comparison of cross-sections, based on an energy-based approach, as there is some proportional ratio among energy levels. In this chapter, the uniformly distributed load is chosen to characterize local failure scenarios.

Then, one quantifies the level of robustness through the introduction of two robustness metrics: (i) the Robustness Propagation Failure Index (*RPMI*), that quantifies the propagation extent after a local failure occurrence, and (ii) the Robustness Energy Index (*REI*) equal to the minimum energy value of the critical scenarios (based on a threshold fixed in advance on

some unacceptable extent of failure). These two indices can be used separately or both together to provide a combined measure of the initial scenario and the extent of failure propagation through the structure. To illustrate the proposed indices, an application to a steel framed-building is considered.

The investigation of structural robustness using the proposed indices shows their ability to identify some critical scenarios, where the structural engineer can improve the structural design to avoid these scenarios by increasing the resistance of the structural elements or the redundancy of the structure. Besides, some bi-objective problems are proposed to identify some critical scenarios with minimal magnitude of local failure and with maximal extent of failure, which is quite interesting to capture the concept of robustness and disproportionate collapse.

If the proposed approach can be used as a decision making tool to discriminate different design options, it might be sensitive to several criteria in the analysis. In the next chapter, one investigates the sensitivity of the approach to some key parameters to see how the results can be influenced by some adopted choices.

CHAPTER V

ANALYSIS OF FACTORS INFLUENCING THE STRUCTURAL ROBUSTNESS ASSESSMENT

V.1 INTRODUCTION

The framework proposed in Chapter IV is based on an alternative load path analysis in which one compares an initial structural state after the occurrence of an exceptional event with a final structural state after progressive collapse. Some indices have been introduced to quantify the level of structural robustness, with an illustration on some case studies. These indices can be associated with various characteristics such as the parts of the structure initially and finally affected, the energy needed for the initial failure scenario, or the extent of failure propagation through the structure. It was shown how the most critical scenarios can be identified when considering these characteristics separately or simultaneously.

Chapter V aims to go a step further by focusing on the sensitivity of the approach to several parameters on which the proposed strategy is based. As one aims to capture the concept of progressive and then disproportionate collapse, the idea is to analyze how some variations on the model inputs might change the conclusions on the ability of the structure to survive the applied initial damage scenarios.

This chapter is organized as follows. First, one studies the effect of the combination of action loads to be considered when an exceptional event occurs. This is related to the choice of the accidental load combination, according to Eurocodes limit state and also to some US standards. The use of various dynamic amplification factors is tested in each case to take into account dynamic effects without conducting a full dynamic analysis. Second, a change in the geometrical configuration is analyzed by modifying the bay dimensions of the steel framed case study, in particular with considering a larger span between columns. Finally, an intrinsic

characteristic of the structure such as materials ductility is looked at. More precisely, the ductility of the steel is restrained by adding a fracture strain on the constitutive law. After having analyzed these additional configurations, a last section summarizes and discusses the various assumptions introduced throughout this dissertation, and the necessary needs for further research work that also limit the conclusions of the model in its current form.

V.2 EFFECT OF LOADS COMBINATION AND DYNAMIC AMPLIFICATION FACTOR

V.2.1 Presentation of case studies

The combinations of loads and the dynamic amplification factor have an essential effect on the structural robustness assessment, as it can highly change the structural response under the local failure scenarios. As explained in Section III.4.3.1, the Eurocodes NF EN 1990 (2003) recommend to use for an accidental situation a combination of actions with smaller partial factors than those with a persistent situation. Equation III.62 provides the combination of actions for dead loads and live loads under an accidental situation that was considered so far when removing one (several) column(s) in the structure. Moreover, ASCE Standard 7-10 (ASCE, 2010) indicates to check the residual load-carrying capacity of a structure or structural element following the occurrence of a damaging event by notionally removing some selected load-bearing elements identified by the Responsible Design Professional. The capacity of the damaged structure shall be evaluated using the following gravity load combination:

$$(0.9 \text{ or } 1.2)DL + 0.5LL + 0.2(L_R \text{ or } S \text{ or } R) \quad (\text{V.1})$$

where DL = dead load, LL = live load, L_R = roof live load, S = snow load, R = rain load. Such combination is considered in the following to compare results between different standards. Furthermore, in this dissertation the dynamic effect that can be produced after the loss of structural components is taken into account by amplifying the gravity load. As mentioned previously in Section III.4.1, several values of dynamic amplification factor (DAF) are recommended in some design standards and publications.

This section aims to study the influence of the applied load assumptions on the structural robustness assessment. In this respect, several case studies are selected and presented in Table V.1. On the one hand, three combinations of dead loads (DL) and live loads (LL) are studied, where $W1$ is the load combination in accidental situation mentioned in the Eurocodes NF EN 1990 (2003), and where $W2$ and $W3$ are the combinations mentioned in ASCE Standard 7-10. On the other hand, four dynamic amplification factor (DAF) values

are applied, where $DAF = 2.0$ is mentioned in some standards such as UFC 4-023-03 (2009), and GSA (2013). The lower and upper bounds $1.3 \leq DAF \leq 1.5$ are recommended by Marchand and Alfawakhiri (2005), and finally one also tests $DAF = 1.0$ to check the case when fully ignoring the dynamic effects.

	$W1 = DL + 0.5 LL$	$W2 = 0.9 DL + 0.5 LL$	$W3 = 1.2 DL + 0.5 LL$
$DAF = 1$	W1-DAF1	W2-DAF1	W3-DAF1
$DAF = 1.3$	W1-DAF1.3	W2-DAF1.3	W3-DAF1.3
$DAF = 1.5$	W1-DAF1.5	W2-DAF1.5	W3-DAF1.5
$DAF = 2$	W1-DAF2	W2-DAF2	W3-DAF2

Table V.1: Case studies to study the effect of loads combination and dynamic amplification factor.

One considers in the following the steel-framed building structure introduced in Section III.4.3. The values of dead loads (DL) and live loads (LL) are similar to those used in this section, where $DL = 25.6 \text{ kN/m}$ and $LL = 12 \text{ kN/m}$. Hence, the applied loads on the directly and indirectly affected parts are described in Table V.2 for each case study.

Case study	Applied loads on the indirectly affected part $W_{ind} \text{ (kN/m)}$	Applied loads on the directly affected part $W_d \text{ (kN/m)}$
W1-DAF1	31.6	31.6
W1-DAF1.3		41.1
W1-DAF1.5		47.4
W1-DAF2		63.2
W2-DAF1	29.0	29.0
W2-DAF1.3		37.7
W2-DAF1.5		43.5
W2-DAF2		58.0
W3-DAF1	36.7	36.7
W3-DAF1.3		47.7
W3-DAF1.5		55.1
W3-DAF2		73.4

Table V.2: Applied loads on the directly affected and the indirectly affected parts.

V.2.2 Structural response under the local failure scenarios

It is highlighted that the failure energy associated with the removal of columns depends on the combination of loads, but not on the dynamic amplification factor (*DAF*). Hence, the characterization of the local failure scenarios described in Table IV.3 is presented in Figure V.1 corresponding to the combinations W1, W2 and W3. As mentioned in Section IV.4.1, the failure energy of the columns with a similar cross-section dimension depends on the concentrated vertical load supported by the column element, where the energy decreases when the concentrated vertical load increases. The failure energy under the combinations W1, W2 and W3 slightly changes, and the ascending order of the failure energy is $E_i^{W3} < E_i^{W1} < E_i^{W2}$ for each local failure scenario i , as shown in Figure V.1. A detailed table of the failure energy for each scenario is presented in Table B.1 (Annex B). In order to evaluate the variation of the failure energy under the combinations W2 and W3 for each scenario i compared to that under W1, two relative difference indices are calculated as described below:

$$\rho E_i^{W21} = \frac{E_i^{W2} - E_i^{W1}}{E_i^{W1}} \times 100 \quad (\text{V.2})$$

$$\rho E_i^{W31} = \frac{E_i^{W3} - E_i^{W1}}{E_i^{W1}} \times 100 \quad (\text{V.3})$$

where ρE_i^{W21} and ρE_i^{W31} represent the relative difference of failure energy under the combinations W2 and W3 compared to that under W1, respectively. Figure V.2 shows that ρE_i^{W21} (respectively ρE_i^{W31}) is positive (respectively negative) for all considered scenarios.

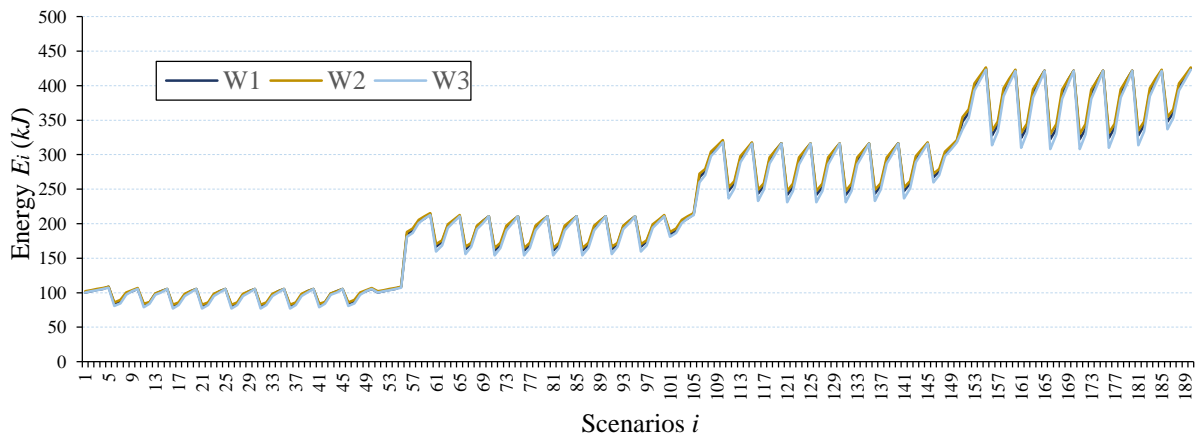


Figure V.1: Energy E_i required to cause the local failure of scenario i under the combinations of actions W1, W2 and W3 (see Table IV.3 for identification of removed column(s)).

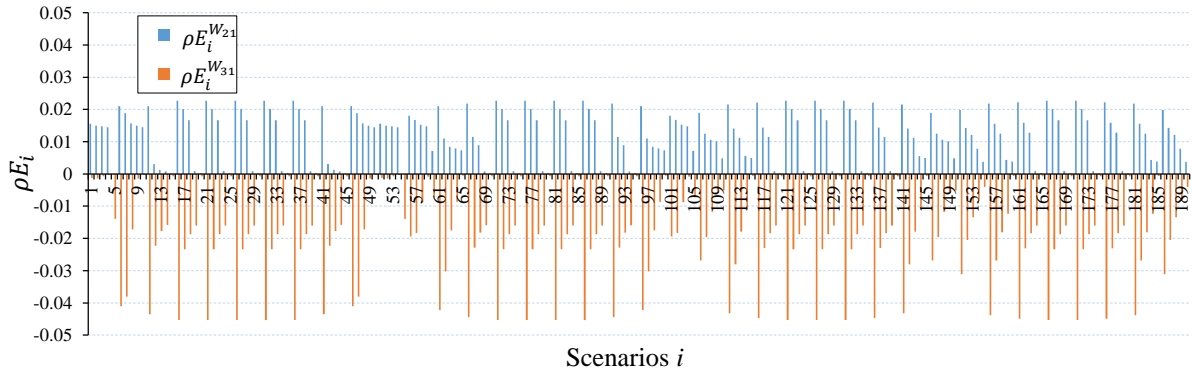


Figure V.2: Ratio of failure energy $\rho E_i^{W_{21}}$ and $\rho E_i^{W_{31}}$ for scenario i (see Table IV.3 for identification of removed column(s)).

The structural response under each local failure scenario i when applying the combinations of actions W1, W2 and W3 is detailed in Table B.2, Table B.3 and Table B.3 (Annex B), respectively. Under the loss of one column ($i \in [1; 55]$), Figure V.3 indicates that the number of scenarios in category C1 decreases when the dynamic amplification factor (DAF) increases for each combination of actions. Also, it decreases for each value of DAF when the combination of actions increases. Conversely, the number of scenarios of C3 and C4 categories increases when the combination of actions or the dynamic amplification factor (DAF) increases.

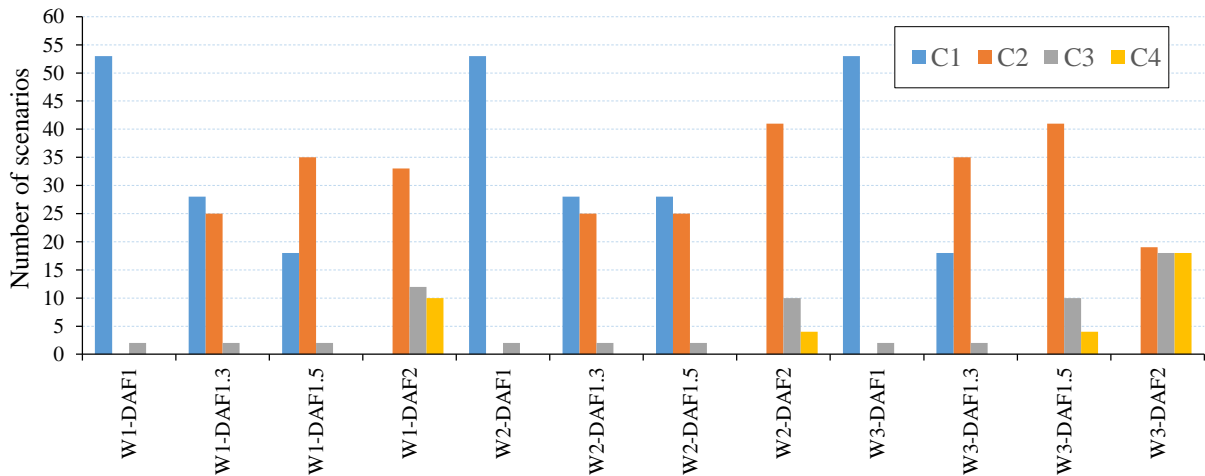


Figure V.3: Number of local failure scenarios within C1 to C4 under the combinations of actions W1, W2 and W3, when one column is lost.

The increment of the applied load W_d on the directly affected part, by increasing the DAF or the combination of actions, increases the consequences under the local failure scenarios. Figure V.4 presents the results in this way in ascending order of W_d . Considering the loss of one column, it shows that when $W_d \leq 47.7 \text{ kN/m}$, the structure achieves to resist the majority of the scenarios (53 scenarios) without collapse (categories C1 or C2), some

collapse being observed only for two scenarios ($i = 5$ and 55). When $W_d \geq 55.1 \text{ kN/m}$, the number of scenarios that corresponds to the categories C1 or C2 starts to decrease, and the number of scenarios in categories C3 or C4 increases. The worst case is W3-DAF2 (73.2 kN/m), for which there are 19 scenarios without collapse and 36 scenarios that lead to a collapse in the structure.

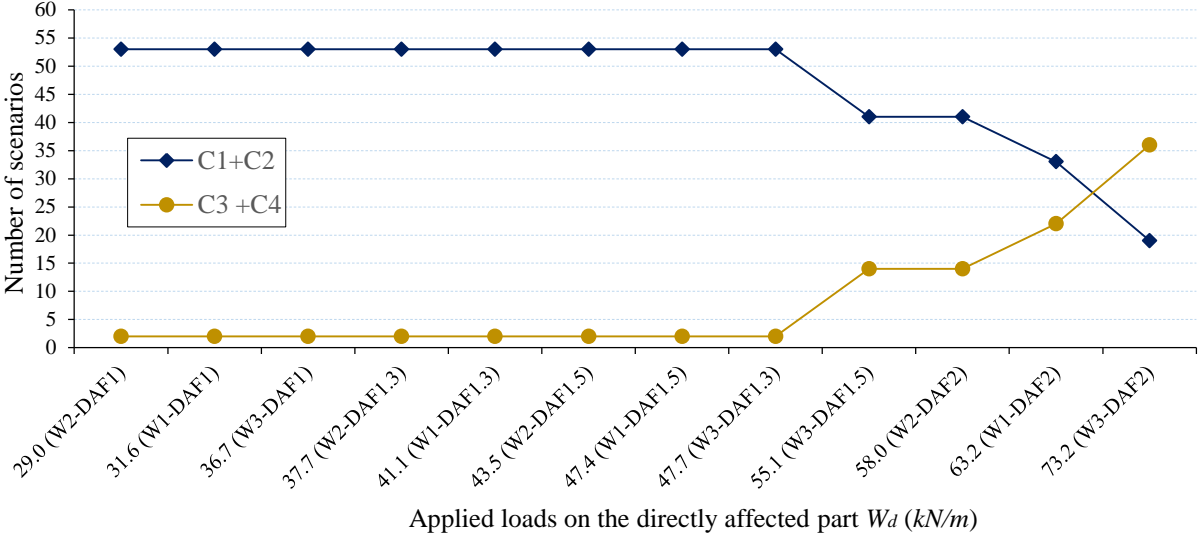


Figure V.4: Number of local failure scenarios without (C1 + C2) or with (C3 + C4) partial/total collapse according to W_d , when one column is lost.

Figure V.5, Figure V.6 and Figure V.7 show that the combination of loads (W1, W2 or W3) and the dynamic amplification factor DAF also have a major effect on the structural response with the loss of two, three and four columns, respectively. The number of scenarios without collapse (category C1 or C2) decreases when W_d increases, while the collapse can be found under a larger number of scenarios (category C3 or C4). Under the combination W3-DAF2 (73.2 kN/m), all the scenarios correspond to the categories C3 or C4. Moreover, the structure succeeds to find a second line of defence (category C2) under two scenarios ($i = 170$ and 175) with the loss of four columns when the dynamic effect is ignored for the different combinations of loads (W1-DAF1, W2-DAF1 and W3-DAF1), or when the DAF is fixed at 1.3 under load combination W2.

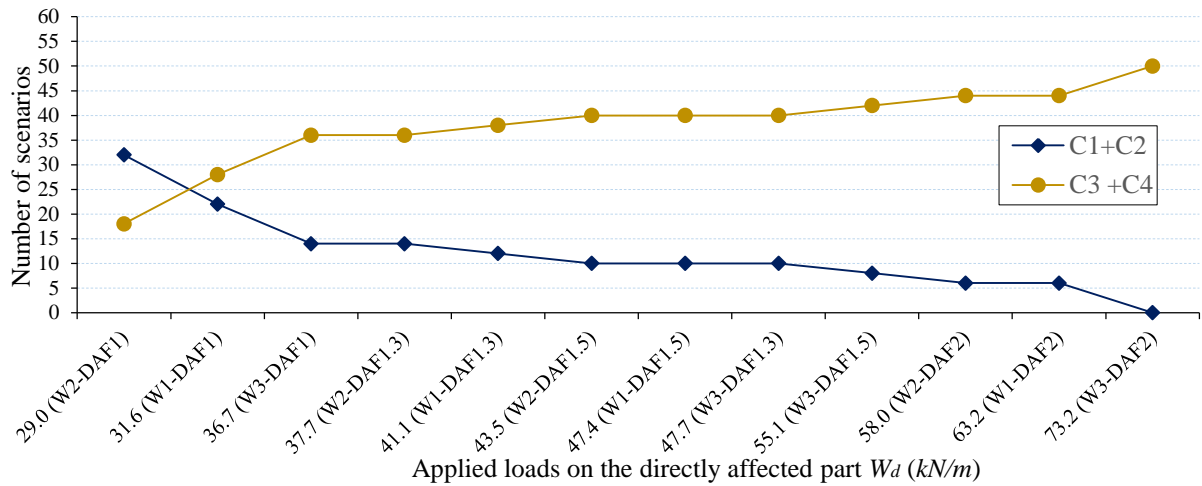


Figure V.5: Number of local failure scenarios without (C1 + C2) or with (C3 + C4) partial/total collapse according to W_a , when two columns are lost.

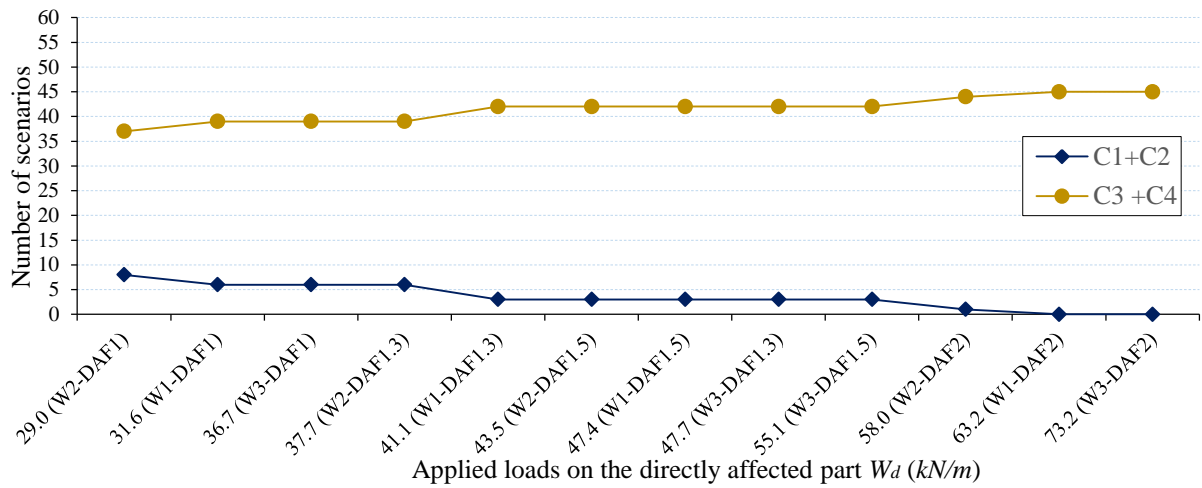


Figure V.6: Number of local failure scenarios without (C1 + C2) or with (C3 + C4) partial/total collapse according to W_a , when three columns are lost.

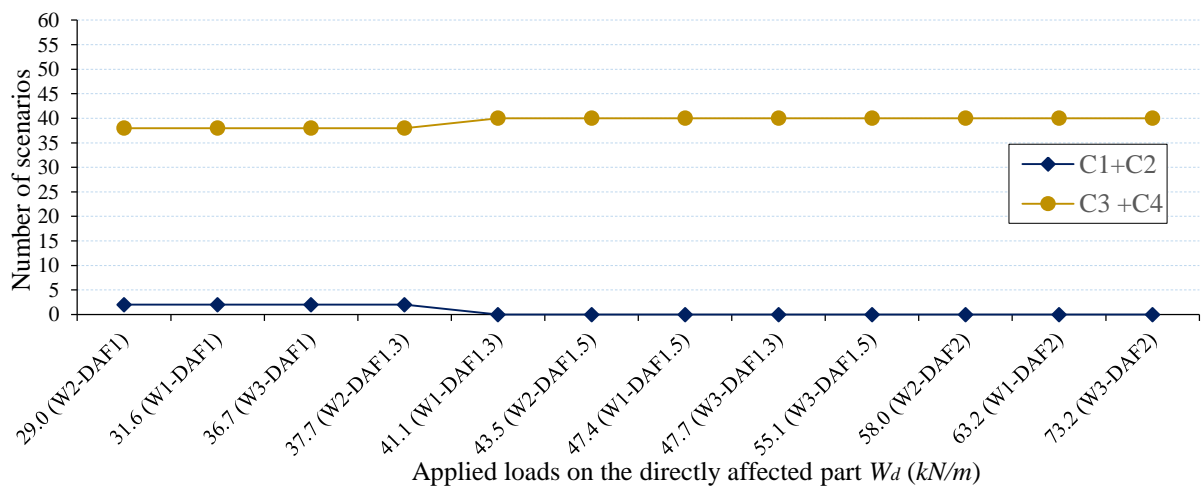


Figure V.7: Number of local failure scenarios without (C1 + C2) or with (C3 + C4) partial/total collapse according to W_a , when four columns are lost.

The numbers of scenarios without (C1 + C2) or with (C3 + C4) partial/total collapse for the 190 applied local failure scenarios (loss of one, two, three, or four columns in Table IV.3) presented in Figure V.8 reveal how the increase of the applied loads on the directly affected part W_d can significantly change the structural response under the applied scenarios. One finds that under the lowest W_d value of 29 kN/m for W2-DAF1, the number of scenarios in the categories C1 and C2 is $n_{C1+C2}^{W2-DAF1} = 95$, and this number decreases to 19 under the highest W_d value of 73.2 kN/m for W3-DAF2. Conversely, the number of scenarios in the categories C3 and C4 increases from $n_{C3+C4}^{W2-DAF1} = 95$ to $n_{C3+C4}^{W3-DAF2} = 171$.

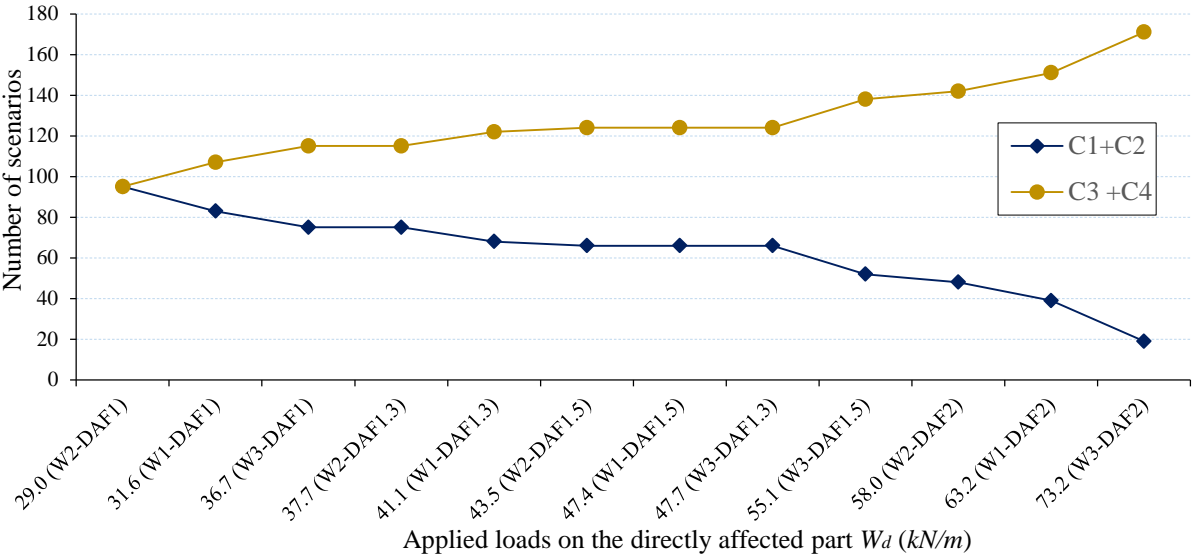


Figure V.8: Number of local failure scenarios without (C1 + C2) or with (C3 + C4) partial/total collapse according to W_d , for all the scenarios of Table IV.3.

V.2.3 Assessment of structural robustness with RPF1

The degree of failure propagation DFP_i for each scenario i and each load combination of Table V.1 is detailed in Annex B (Table B.2, Table B.3 and Table B.4). In order to show the effect of the assumptions on load combination and dynamic amplification factor choices on the structural robustness assessment, one shows in Figure V.9 the maximum degree of failure propagation $max(DFP_i)$ according to the number of removed columns and W_d . One observes that the increase of W_d changes $max(DFP_i)$ only under the loss of one or two column(s). Moreover, the ranking order of $max(DFP_i)$ according to the number of removed columns depends on W_d .

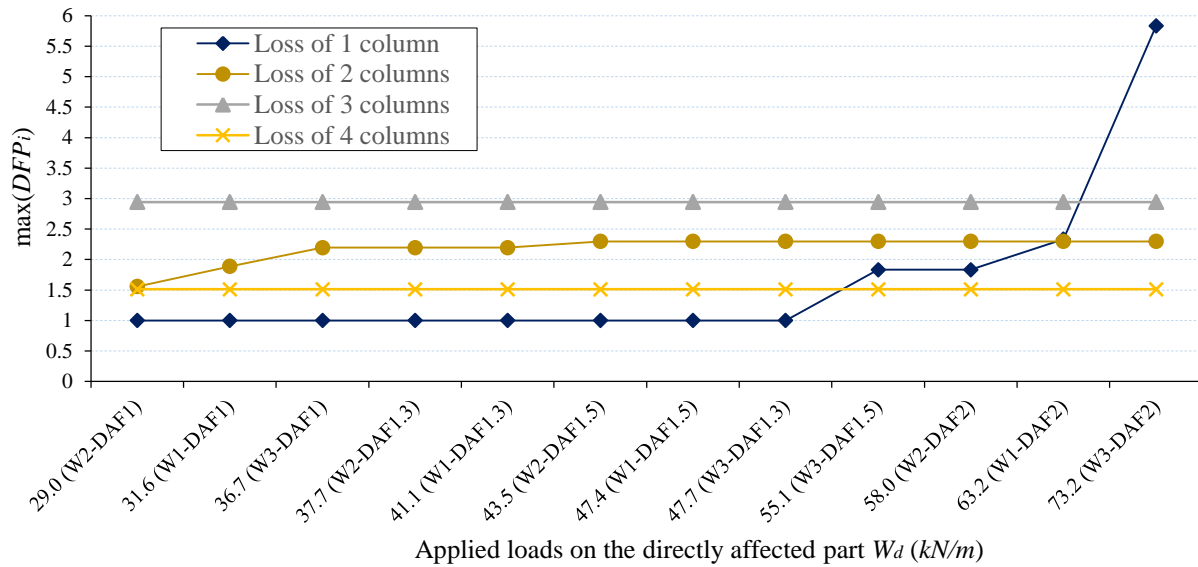


Figure V.9: Maximum degree of failure propagation $\max(DFP_i)$ according to the number of removed columns and W_d .

When $29 \text{ kN/m} \leq W_d \leq 47.7 \text{ kN/m}$, the scenarios 5 and 55 are the only scenarios with the loss of one column that lead to the collapse of the directly affected part with $DFP_{5 \text{ or } 55} = 1$. The increase of W_d under W3-DAF1.5 and W2-DAF2 leads to a progressive collapse with the scenarios 16 and 36. The maximum degree of failure propagation then increases with $\max(DFP_i | \text{loss of 1 column}) = 1.8$. The collapse under scenario 21 for $W_d = 63.2 \text{ kN/m}$ increases the failure propagation to 2.3, while the worst collapse for W3-DAF2 ($W_d = 73.2 \text{ kN/m}$) is under the scenario 27 with $DFP_{27} = 5.8$.

For the scenarios with the loss of two columns, the lowest degree of failure propagation is 1.6 found with W2-DAF1 ($W_d = 29 \text{ kN/m}$), which corresponds to the scenarios 71 and 86. The combination W1-DAF1 leads to a progressive collapse under the scenarios 76 and 81 with $DFP_{76 \text{ or } 81} = 1.9$. When $36.7 \text{ kN/m} \leq W_d \leq 41.1 \text{ kN/m}$, the worst collapse is under the scenarios 77 and 82 with $DFP_{77 \text{ or } 82} = 2.2$. Finally, the progressive collapse under the scenarios 78 and 83 for $W_d \geq 43.5 \text{ kN/m}$ presents the highest degree of failure propagation ($DFP_{78 \text{ or } 83} = 2.3$) under the loss of two columns.

As mentioned previously, the highest degree of failure propagation remains constant under the local failure scenarios with the loss of three or four columns for all case studies. In particular, there is a progressive collapse under the most critical scenarios # 128 (with the loss of 3 columns), # 168 and # 173 (with the loss of 4 columns). Besides, the scenarios with the loss of three columns have a higher degree of failure propagation than other scenarios under $29 \text{ kN/m} \leq W_d \leq 63.2 \text{ kN/m}$, which indicates that these scenarios are the most critical. To be more precise, the scenario 128 is the most critical with $\max(DFP_{128}) = 2.9$. Under W3-

DAF2 ($W_d = 73.2 \text{ kN/m}$), the scenarios with the loss of one column become the most critical as $\max_{W3-DAF2}(DFP_i | \text{loss of 1 column}) = 5.8$.

The Robustness Propagation Failure Index (RPF_i) corresponds to the highest degree of failure propagation among all the applied scenarios. In this example, the robustness index is $RPF_i = 2.9$, and it remains constant for $29 \text{ kN/m} \leq W_d \leq 63.2 \text{ kN/m}$, as shown in Figure V.10. This index then increases under W3-DAF2, where $RPF_i = 5.8$, which corresponds to the scenario # 27.

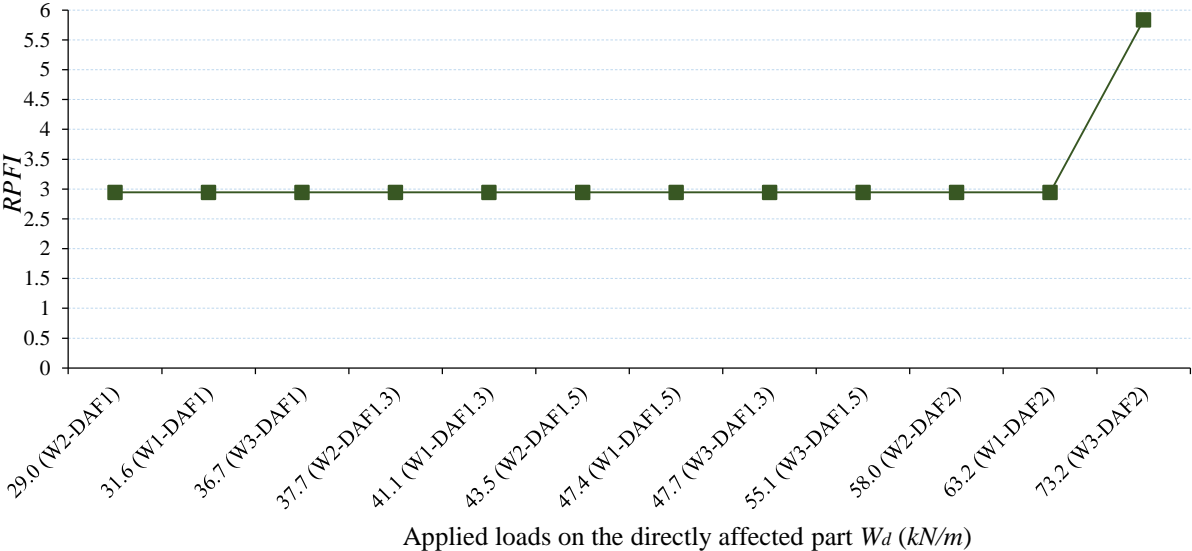


Figure V.10: Robustness Propagation Failure Index (RPF_i) according W_d .

V.2.4 Assessment of structural robustness with $REI(UC)$

The evaluation of structural robustness is also performed according to the threshold UC , with a view to identify the minimum energy-based magnitude of local failure scenario i with $\mathcal{M}(CP_i) \geq UC$. The adopted threshold UC in this example is fixed at 90 m . Figures B.1 to B.12 in Annex B provide the diagrams of the local failure energy E_i with the measure of collapsed part $\mathcal{M}(CP_i)$ for each scenario i under the case studies of Table V.1.

Table V.3 presents the Robustness Energy Index $REI(UC = 90m)$ with the associated local failure scenarios. The highest $REI(UC = 90m) = 164.9 \text{ kJ}$ corresponds to the W2 load-combination (W2-DAF1, W2-DAF1.3 and W2-DAF1.5) with scenarios 71, 76, 81 and 86 that consist of the loss of two columns. The same scenarios lead to $UC \geq 90m$ for some of the W1 and W3 combinations (W1-DAF1, W1-DAF1.3, W1-DAF1.5, W3-DAF1 and W3-DAF1.3). The robustness index $REI(UC = 90m)$ is lower than with W2 as the failure energy of columns under W2 is higher than with W1 or W3, as explained in Section V.2.2 (see Figure V.1 and Figure V.2).

When $W_d \geq 55.1 \text{ kN/m}$ for the case studies W1-DAF2, W2-DAF2, W3-DAF1.5 and W3-DAF2, the scenario 16 and 36 lead to a progressive collapse with $UC \geq 90\text{m}$, which decreases the robustness index $REI(UC = 90\text{m})$. The lowest failure energy is under the load combination W3, the cases with the DAF fixed at 1.5 or 2.0 having the lowest REI with $REI_{W3-DAF1.5 \text{ or } W3-DAF2}(UC = 90\text{m}) = 77 \text{ kJ}$. One can conclude that the worst collapse case is obtained with W3-DAF1.5 and W3-DAF2 with the lowest magnitude of local failure scenario.

	$REI(UC = 90 \text{ m})$ [kJ]	Scenario #
W1-DAF1	161.2	71; 76; 81; 86
W1-DAF1.3	161.2	71; 76; 81; 86
W1-DAF1.5	161.2	71; 76; 81; 86
W1-DAF2	80.6	16; 21; 31; 36
W2-DAF1	164.9	71; 86
W2-DAF1.3	164.9	71; 76; 81; 86
W2-DAF1.5	164.9	71; 76; 81; 86
W2-DAF2	82.5	16; 36
W3-DAF1	153.9	71; 76; 81; 86
W3-DAF1.3	153.9	71; 76; 81; 86
W3-DAF1.5	77.0	16; 36
W3-DAF2	77.0	16; 21; 26; 31; 36

Table V.3: Robustness Energy Index REI with unacceptable collapse threshold $UC = 90 \text{ m}$ for each case study of Table V.1.

The sensitivity of the Robustness Energy Index $REI(UC)$ according to the threshold $UC \in [10 \text{ m}; 280 \text{ m}]$ under the combinations of actions W1, W2 and W3 is presented in Figure V.11, Figure V.12 and Figure V.13, respectively. For the load combination W1, the robustness index $REI(UC)$ under W1-DAF1, W1-DAF1.3 and W1-DAF1.5 is equal for $UC \in [10 \text{ m}; 280 \text{ m}]$. The scenarios 76 and 81 with $\mathcal{M}(CP_{76 \text{ or } 81}) = 170 \text{ m}$ are the most critical for $UC \in [10 \text{ m}; 170 \text{ m}]$, and therefore $REI(UC \in [10 \text{ m}; 170 \text{ m}]) = 161.2 \text{ kJ}$. These scenarios are no longer critical when the unacceptable collapse $UC \geq 180 \text{ m}$, where the scenario 126 that leads to a total collapse of the structure becomes the most critical ($REI(UC \in [180 \text{ m}; 280 \text{ m}]) = 241.9 \text{ kJ}$). Besides, the applied loads for W1-DAF2 lead to a progressive collapse under the scenarios 21 and 31 with $\mathcal{M}(CP_{21 \text{ or } 31}) = 140 \text{ m}$, which makes these scenarios the most critical ones with the robustness index $REI(UC \in$

[10 m; 140 m]) = 80.6 kJ, as shown in Figure V.11. For $UC \geq 150$ m, the results are similar to the other cases of DAF .

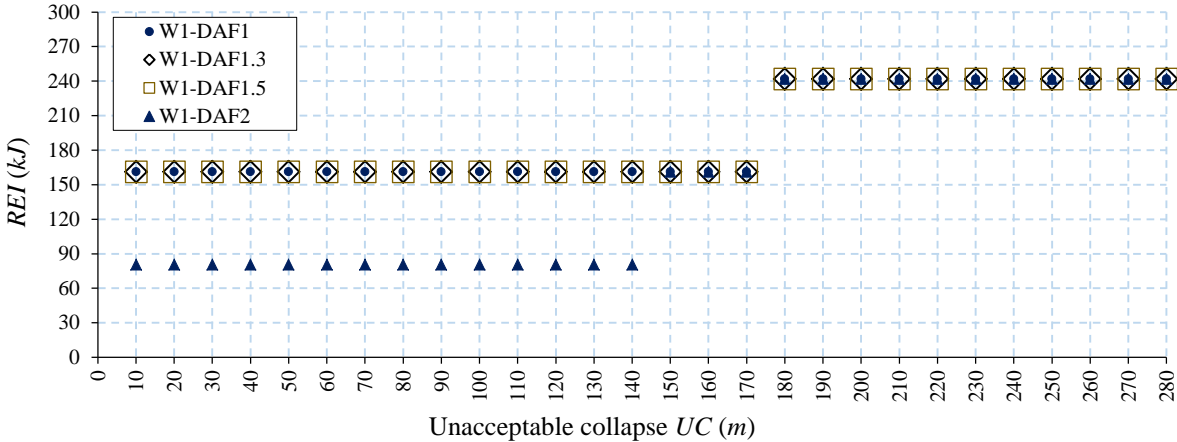


Figure V.11: Sensitivity of REI index with UC under load combination W1.

Figure V.12 shows that the $REI(UC)$ values under W2-DAF1.3 and W2-DAF1.5 are quite similar to those of W1-DAF1.3 and W1-DAF1.5, respectively. The decrease of applied load under the loads combination W2 helps the structure to resist the scenarios 76 and 81 under W2-DAF1, which were critical under W1-DAF1. Moreover, the scenarios 71 and 86 with $\mathcal{M}(CP_{71 \text{ or } 86}) = 140$ m are critical, which causes the increment of $REI(UC)$ when $UC > 140$ m. Similarly, the scenarios 21 and 31 are not critical under W2-DAF2 when compared to W1-DAF2, and the scenarios 16 and 36 with $\mathcal{M}(CP_{16 \text{ or } 36}) = 110$ m represent the most critical scenarios for $UC \leq 110$ m.

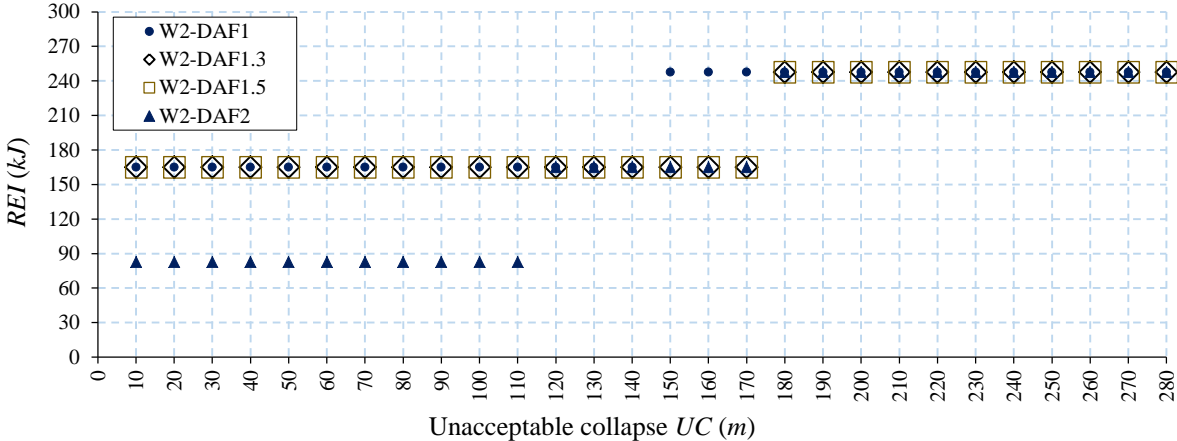


Figure V.12: Sensitivity of REI index with UC under load combination W2.

The increment of the load by using the combination W3 changes the results under the different dynamic amplification factor $DAF = 1.5$ or 2 compared to those of W1, while they

are quite similar with $DAF = 1$ or 1.3 (compare Figure V.11 and Figure V.13). The $REI(UC \in [10\text{ m}; 110\text{ m}])$ under W3-DAF1.3 is lower than that under W1-DAF1.3 since the scenarios 16 and 36 with $\mathcal{M}(CP_{16\text{ or }36}) = 110\text{ m}$ are critical scenarios under W3-DAF1.3. As the scenario 26 leads to the total collapse of the structure under W3-DAF2, $REI(UC)$ is constant and is equal to the failure energy of scenario 26 ($E_{26} = 77\text{ kJ}$, see Figure V.13), which is the critical scenario with the lowest energy.

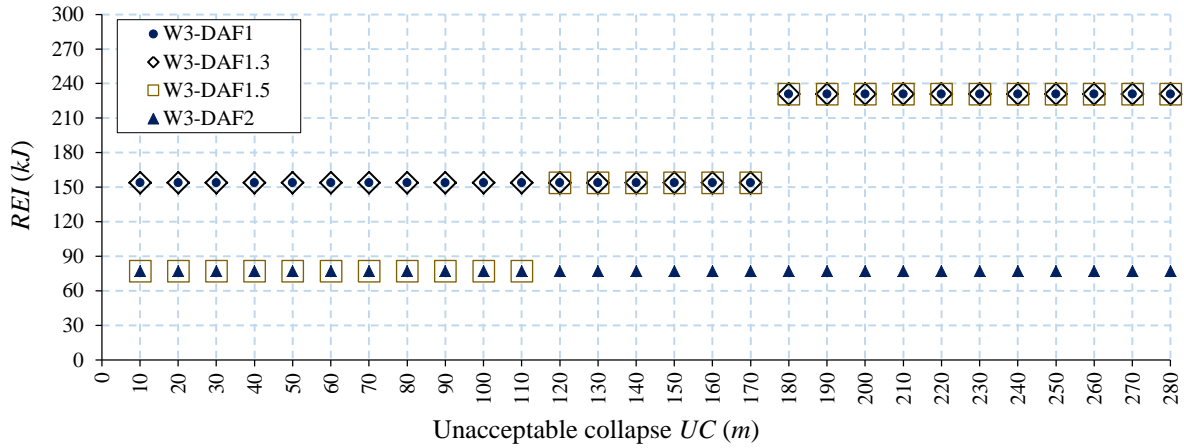


Figure V.13: Sensitivity of REI index with UC under load combination W3.

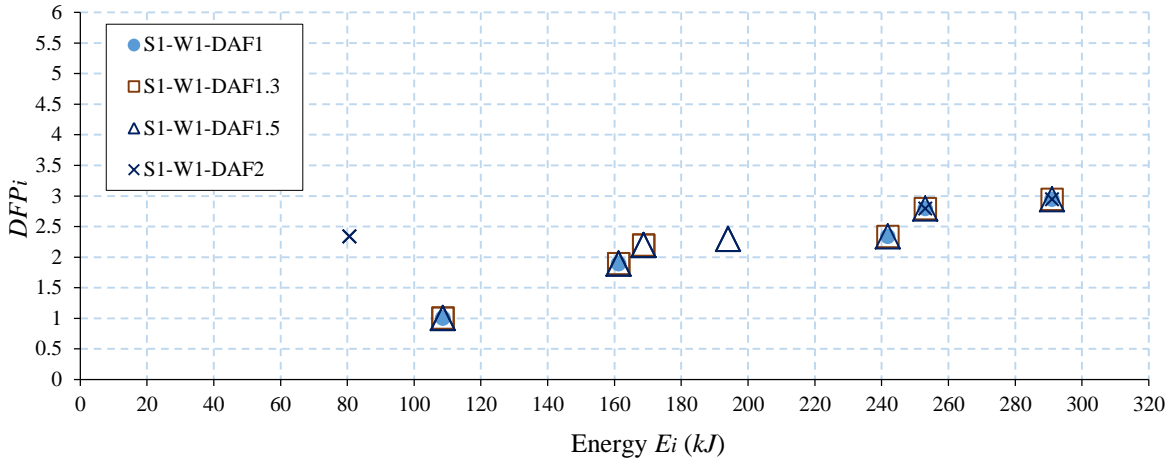
V.2.5 Assessment of structural robustness with several criteria

Several criteria can be used in the structural robustness assessment to identify the scenarios with maximal propagation extent and minimal initial failure magnitude. In this context, the bi-objective problems introduced in Equations IV.8, IV.12 and IV.13 are considered in this section.

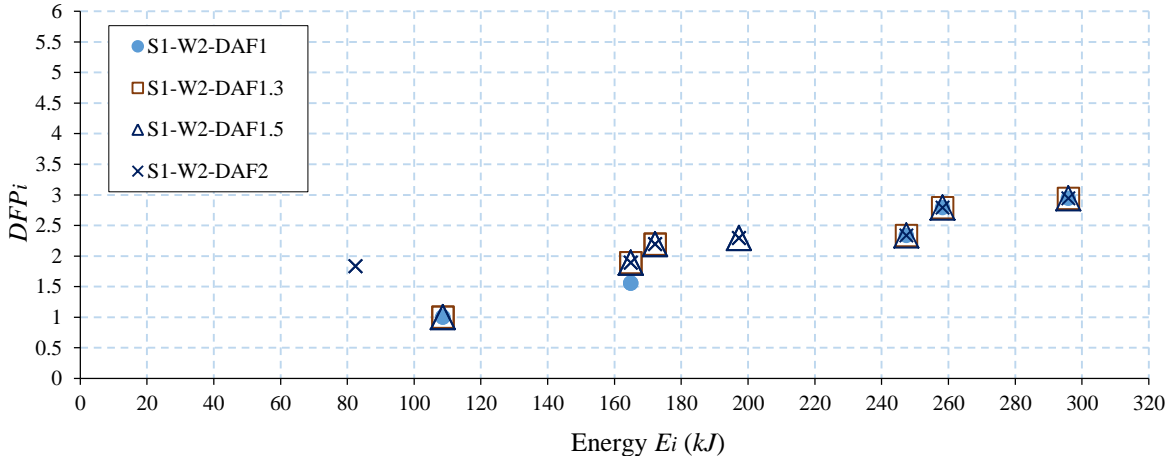
Based on the bi-objective problem of Equation IV.8, Figure V.14 (a, b and c) shows the non-dominated solutions (Pareto front) for each case study of Table V.1 when simultaneously minimizing E_i and maximizing DFP_i . It is shown how the choice of load combination (between W1, W2 and W3) can change the most critical scenarios (non-dominated solutions). Also, for each load combination, the most critical scenarios change under the chosen dynamic amplification factor DAF . In particular, the Pareto fronts under the load combination W1 with $DAF = 1.0, 1.3$ or 1.5 are quite similar, where 7 scenarios ($i = 5, 55, 76, 81, 126, 127$ and 128) are common for S1-W1-DAF1, S1-W1-DAF1.3 and S1-W1-DAF1.5, as shown in Table V.4. With a higher DAF fixed at 2.0, the scenarios 21 and 31 cause a progressive collapse with $DFP_{21\text{ or }31}^{W1-DAF2} = 2.3$, which makes these scenarios non-dominated compared to the scenarios 5, 55, 76, 81 and 126 (see Figure V.14-a).

Under the loads combination W2, one shows that the scenarios of the Pareto fronts with the different values of DAF are (i) grouped (see Figure V.14-b), and (ii) close to those found with W1-DAF1, W1-DAF1.3 and W1-DAF1.5 (in Figure V.14-a). As for W1, when fixing a high DAF value to 2.0, some new scenarios appear such as # 16 and 36 with $DFP_{16\text{ or }36}^{W2-DAF2} = 1.8$, where the collapse under these scenarios has a higher degree of failure propagation with a lower failure energy than some scenarios found with DAF fixed at 1.0, 1.3 or 1.5.

Under the load combination W3, the Pareto fronts of W3-DAF1 and W3-DAF1.3 are close to those identified under the combinations W1 and W2, as shown in Figure V.14(c). If some difference appears for $DAF = 1.5$, the most spectacular change when comparing Figure V.14 (a, b and c) is for DAF fixed at 2.0. Indeed, the Pareto front under the applied loads of W3-DAF2, which has the highest load on the directly affected part ($W_d = 73.2\text{ kN/m}$), has two non-dominated scenarios ($i = 26$ and 27). These scenarios can be considered as the most critical when compared to the scenarios of the other Pareto fronts as they have a higher degree of failure propagation ($DFP_{26}^{W3-DAF2} = 4.7$ and $DFP_{27}^{W3-DAF2} = 5.8$) and a lower failure energy ($E_{26} = 77\text{ kJ}$ and $E_{27} = 82.4\text{ kJ}$).



(a) Combination of actions W1



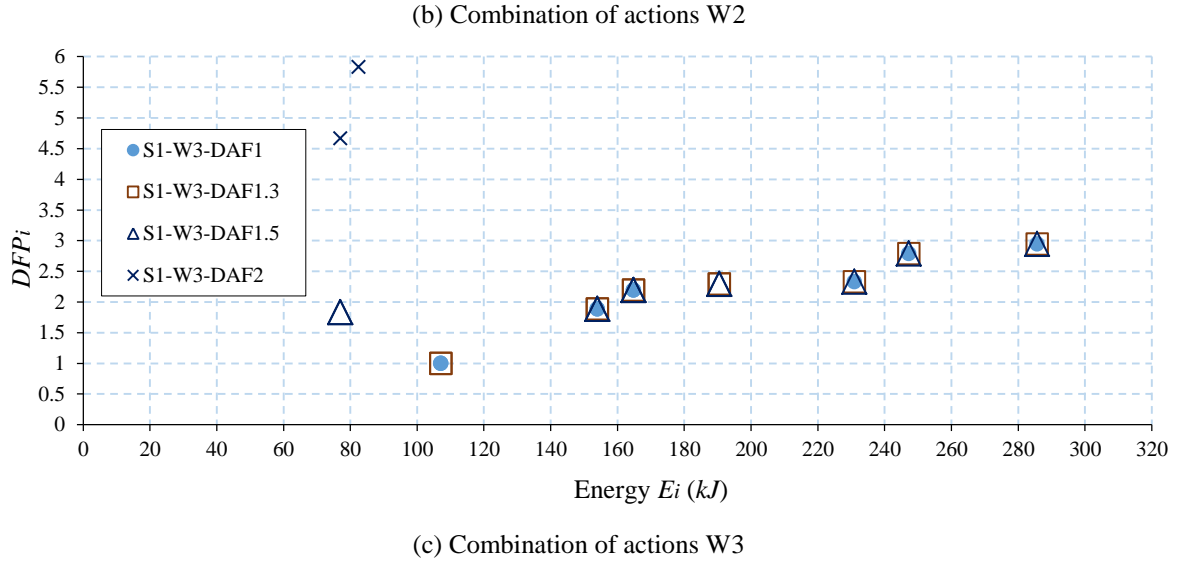


Figure V.14: Identification of non-dominated solutions for each case study of Table V.1 when simultaneously minimizing E_i and maximizing DFP_i (Equation IV.8).

Pareto front	i	E_i (kJ)	DFP_i	Pareto front	i	E_i (kJ)	DFP_i
S1-W1-DAF1	5	108.6	1.0	S1-W2-DAF1.5	77	172.1	2.2
	55	108.6	1.0		82	172.1	2.2
	76	161.2	1.9		78	197.3	2.3
	81	161.2	1.9		83	197.3	2.3
	126	241.9	2.3		126	247.4	2.3
	127	253.1	2.8		127	258.2	2.8
	128	291.0	2.9		128	295.9	2.9
S1-W1-DAF1.3	5	108.6	1.0	S1-W2-DAF2	16	82.5	1.8
	55	108.6	1.0		36	82.5	1.8
	76	161.2	1.9		76	164.9	1.9
	81	161.2	1.9		81	164.9	1.9
	77	168.7	2.2		77	172.1	2.2
	82	168.7	2.2		82	172.1	2.2
	126	241.9	2.3		78	197.3	2.3
	127	253.1	2.8		83	197.3	2.3
	128	291.0	2.9		126	247.4	2.3
S1-W1-DAF1.5	5	108.6	1.0	127	258.2	2.8	
	55	108.6	1.0	128	295.9	2.9	
	76	161.2	1.9	S1-W3-DAF1	5	107.0	1.0
	81	161.2	1.9		55	107.0	1.0
	77	168.7	2.2		76	153.9	1.9
	82	168.7	2.2		81	153.9	1.9
	78	194.0	2.3		77	164.8	2.2
	83	194.0	2.3		82	164.8	2.2
	126	241.9	2.3		126	230.9	2.3
	127	253.1	2.8		127	247.2	2.8
128	291.0	2.9	128		285.6	2.9	
S1-W1-DAF2	21	80.6	2.3		S1-W3-DAF1.3	5	107.0
	31	80.6	2.3	55		107.0	1.0
	127	253.1	2.8	76		153.9	1.9
	128	291.0	2.9	81		153.9	1.9
S1-W2-DAF1	5	108.5	1.0	77		164.8	2.2
	55	108.5	1.0	82		164.8	2.2
	71	164.9	1.6	78		190.4	2.3
	86	164.9	1.6	83		190.4	2.3

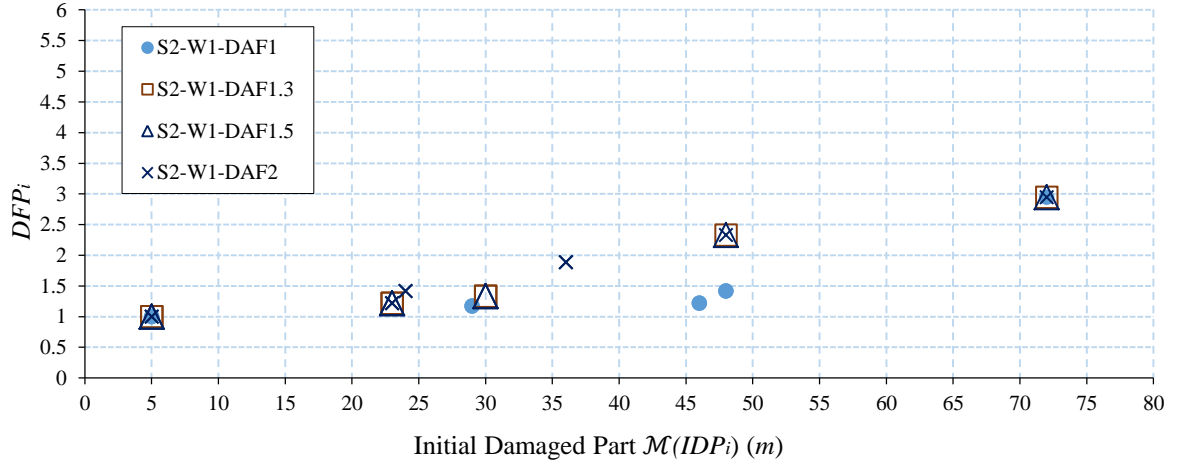
	126	247.4	2.3		126	230.9	2.3
	127	258.2	2.8		127	247.2	2.8
	128	295.9	2.9		128	285.6	2.9
S1-W2-DAF1.3	5	108.5	1.0	S1-W3-DAF1.5	16	77.0	1.8
	55	108.5	1.0		36	77.0	1.8
	76	164.9	1.9		76	153.9	1.9
	81	164.9	1.9		81	153.9	1.9
	77	172.1	2.2		77	164.8	2.2
	82	172.1	2.2		82	164.8	2.2
	126	247.4	2.3		78	190.4	2.3
	127	258.2	2.8		83	190.4	2.3
128	295.9	2.9	126	230.9	2.3		
S1-W2-DAF1.5	5	108.5	1.0	127	247.2	2.8	
	55	108.5	1.0	128	285.6	2.9	
	76	164.9	1.9	S1-W3-DAF2	26	77.0	4.7
	81	164.9	1.9		27	82.4	5.8

Table V.4: Non-dominated scenarios for each case study of Table V.1 related to Equation (IV.8).

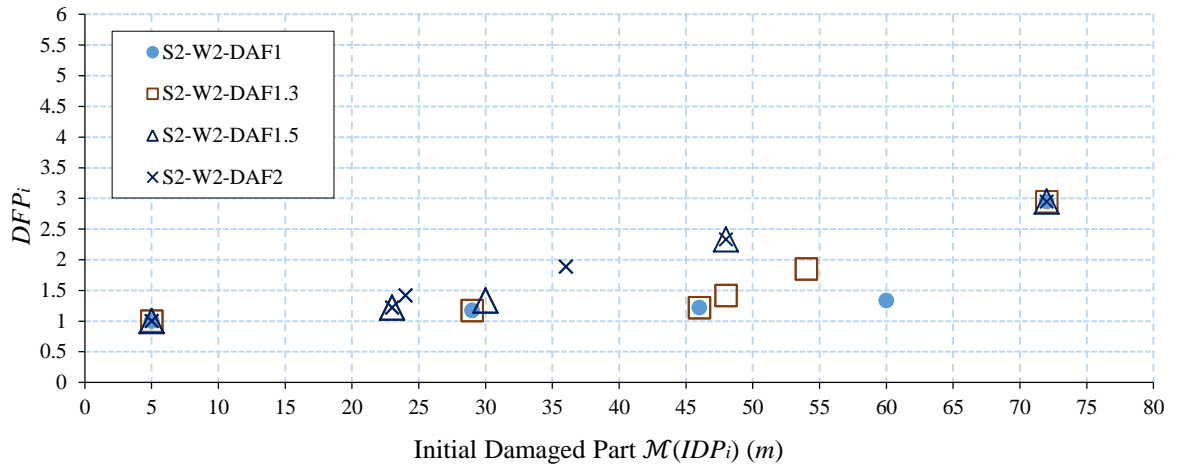
The bi-objective solutions of Equation (IV.12) (minimizing $\mathcal{M}(IDP_i)$ and maximizing DFP_i) for each case study of Table V.1 are presented in Figure V.15(a, b and c). Under the combination of actions W1, the Pareto fronts S2-W1-DAF1.3, S2-W1-DAF1.5 and S2-W1-DAF2 are quite close. Some scenarios of the Pareto front S2-W1-DAF1 have a lower degree of failure propagation DFP_i than for the others Pareto fronts (see Figure V.15-a), which unsurprisingly indicates that the applied scenarios when ignoring the dynamic effect (W1-DAF1) are less critical in terms of failure propagation.

Figure V.15(b) indicates that the Pareto fronts S2-W2-DAF1.5 and S2-W2-DAF2 include similar scenarios such as 5, 55, 120, 128, 129 and 140 (see Table V.5), and that they are close to the Pareto fronts of W1-DAF1.3, W1-DAF1.5 and W1-DAF2 (see Figure V.15-a). The scenarios of the Pareto front S2-W2-DAF1 and S2-W2-DAF1.3 have a lower degree of failure propagation DFP_i with a larger initial damaged part $\mathcal{M}(IDP_i)$ than the others Pareto fronts, which indicates that these Pareto fronts are less critical than the others under the combination W2.

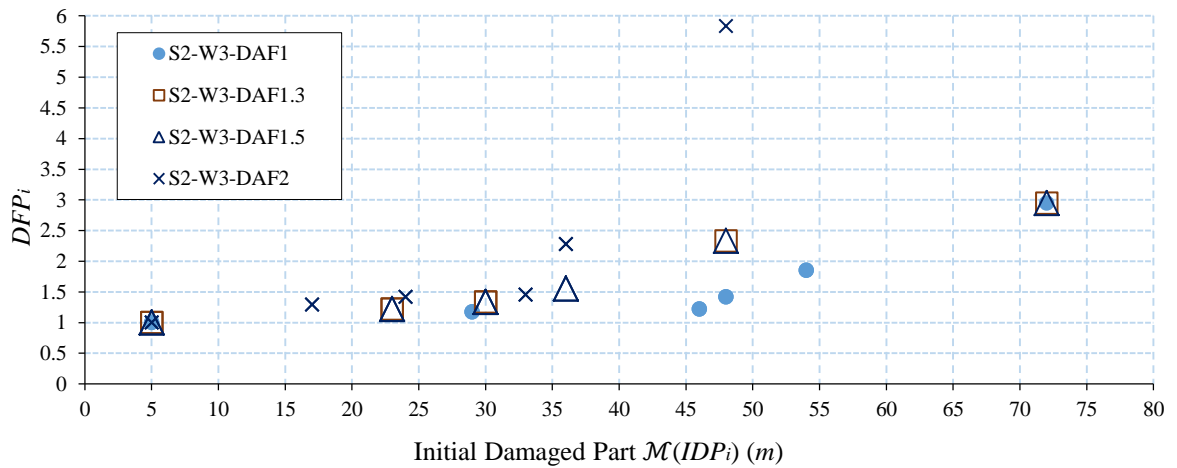
More space between the Pareto fronts with different dynamic amplification factors are found under the load combination W3 (see Figure V.15-c). Those with W3-DAF1.3 and W3-DAF1.5 are quite similar, where all the scenarios of S2-W3-DAF1.3 belong to S2-W3-DAF1.5 (see Table V.5). One observes that these Pareto fronts are located between the Pareto fronts S2-W3-DAF1 and S2-W3-DAF2. Indeed, S2-W3-DAF1 solutions have a lower degree of failure propagation DFP_i than in the others Pareto fronts. Conversely, S2-W3-DAF2 presents the most critical scenarios compared to the other Pareto fronts of the other combinations. In particular, the scenario 27 with $DFP_{27} = 5.8$ leads to the highest degree of failure propagation.



(a) Combination of actions W1



(b) Combination of actions W2



(c) Combination of actions W3

Figure V.15: Identification of non-dominated solutions for each case study of Table V.1 when simultaneously minimizing $\mathcal{M}(IDP_i)$ and maximizing DFP_i (Equation IV.12).

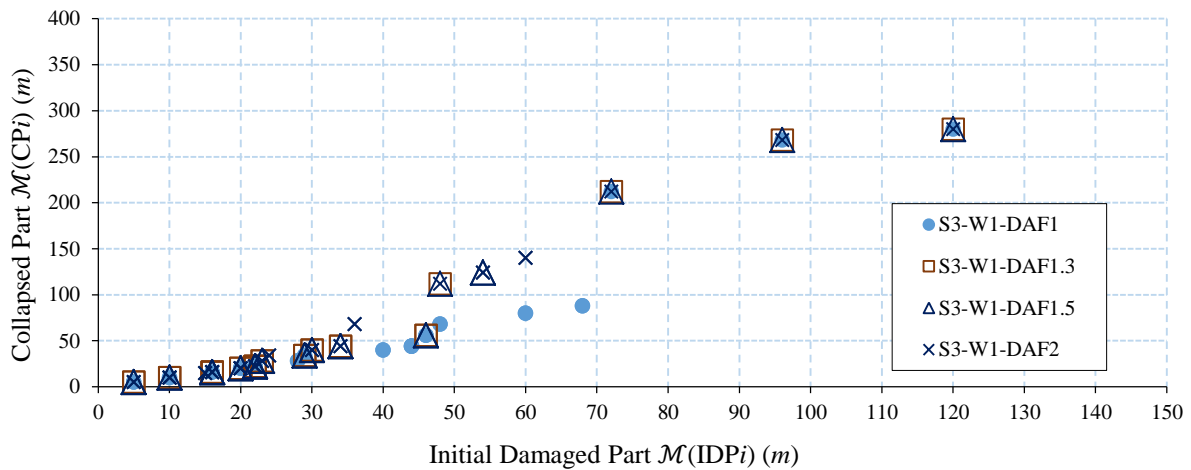
Pareto front	i	$\mathcal{M}(IDP_i)$ (m)	DFP_i	Pareto front	i	$\mathcal{M}(IDP_i)$ (m)	DFP_i
S2-W1-DAF1	5	5	1.0	S2-W2-DAF1.5	120	23	1.2
	55	5	1.0		140	23	1.2

	165	29	1.2		170	30	1.3
	180	29	1.2		175	30	1.3
	119	46	1.2		129	48	2.3
	139	46	1.2		128	72	2.9
	124	48	1.4		5	5	1.0
	134	48	1.4		55	5	1.0
	128	72	2.9		120	23	1.2
S2-W1-DAF1.3	5	5	1.0	S2-W2-DAF2	140	23	1.2
	55	5	1.0		125	24	1.4
	120	23	1.2		135	24	1.4
	140	23	1.2		79	36	1.9
	170	30	1.3		84	36	1.9
	175	30	1.3		129	48	2.3
	129	48	2.3		128	72	2.9
S2-W1-DAF1.5	128	72	2.9	S2-W3-DAF1	5	5	1.0
	5	5	1.0		55	5	1.0
	55	5	1.0		165	29	1.2
	120	23	1.2		180	29	1.2
	140	23	1.2		119	46	1.2
	170	30	1.3		139	46	1.2
	175	30	1.3		124	48	1.4
S2-W1-DAF2	129	48	2.3	S2-W3-DAF1.3	134	48	1.4
	128	72	2.9		73	54	1.9
	5	5	1.0		88	54	1.9
	55	5	1.0		128	72	2.9
	120	23	1.2		5	5	1.0
	140	23	1.2		55	5	1.0
	125	24	1.4		120	23	1.2
S2-W2-DAF1	135	24	1.4	S2-W3-DAF1.5	140	23	1.2
	79	36	1.9		170	30	1.3
	84	36	1.9		175	30	1.3
	129	48	2.3		74	36	1.6
	128	72	2.9		89	36	1.6
	5	5	1.0		129	48	2.3
	55	5	1.0		128	72	2.9
S2-W2-DAF1.3	165	29	1.2	S2-W3-DAF2	5	5	1.0
	180	29	1.2		55	5	1.0
	119	46	1.2		70	17	1.3
	139	46	1.2		95	17	1.3
	124	48	1.4		125	24	1.4
	134	48	1.4		135	24	1.4
	73	54	1.9		13	33	1.5
S2-W2-DAF1.5	88	54	1.9		43	33	1.5
	128	72	2.9		18	36	2.3
	5	5	1.0		38	36	2.3
	55	5	1.0		27	48	5.8

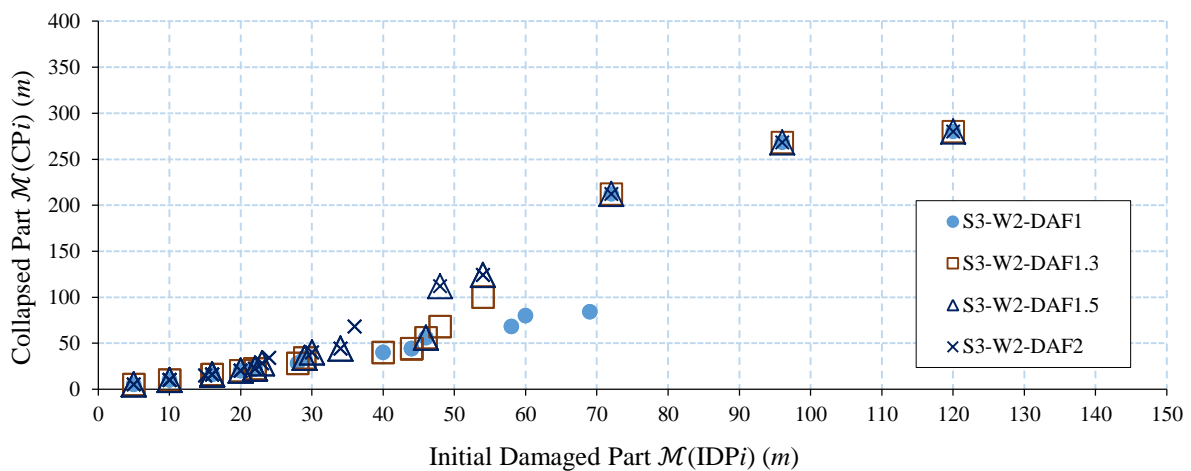
Table V.5: Non-dominated scenarios for each case study of Table V.1 related to Equation (IV.12).

Figure V.16 (a, b and c) presents the non-dominated solutions (Pareto front) for each case study of Table V.1 according to the bi-objective problem of Equation IV.13 (simultaneously minimizing $\mathcal{M}(IDP_i)$ and maximizing $\mathcal{M}(CP_i)$). The corresponding solutions are described in Table B.5 (Annex B). One illustrates that the Pareto fronts S3-W1-DAF1.3, S3-W1-DAF1.5, S3-W1-DAF2, S3-W2-DAF1.5 and S3-W2-DAF2 are quite similar, where solutions are close to each other's (see Figure V.16 a and b) with 24 common scenarios. Similar to the previous results identified by Equation IV.12 (Figure V.15 a and b), the Pareto fronts S3-W1-DAF1, S3-W2-DAF1 and S3-W2-DAF1.3 have scenarios with lower values of $\mathcal{M}(CP_i)$ than the other Pareto fronts under load combinations W1 and W2.

The Pareto front S3-W3-DAF2 can be considered as the most critical one according to Equation IV.13. Indeed, it is associated with the most critical scenario 27 that leads to a total collapse of the structure with $\mathcal{M}(CP_{27}^{W3-DAF2}) = 280\text{ m}$ and $\mathcal{M}(IDP_{27}^{W3-DAF2}) = 48\text{ m}$, as shown in Figure V.16(c). The same total collapse of the structure is found under the scenario 126 for the other case studies but with an initial damaged part of 120 m.



(a) Combination of actions W1



(b) Combination of actions W2

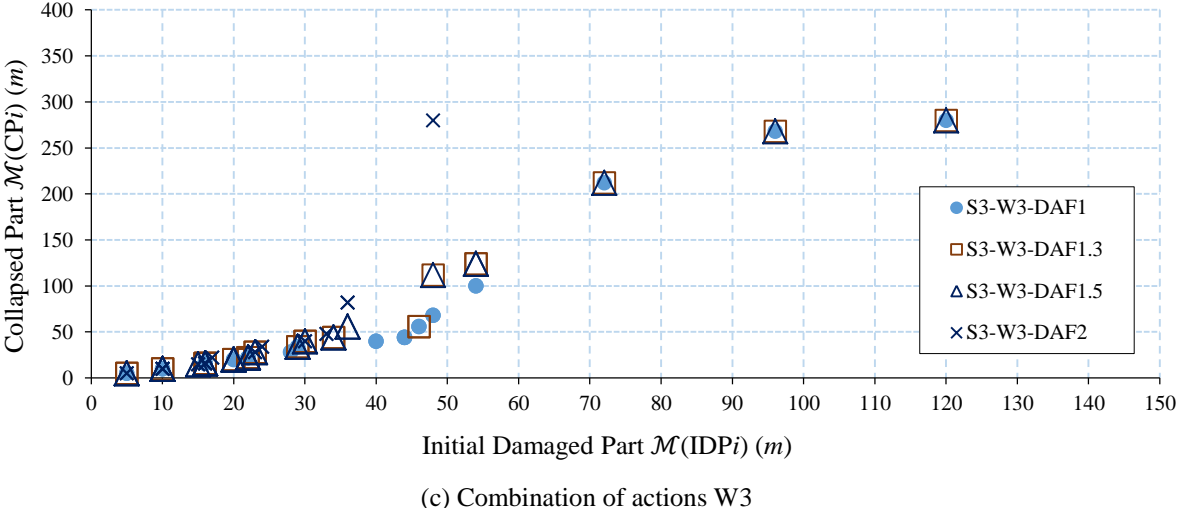


Figure V.16: Identification of non-dominated solutions for each case study of Table V.1 when simultaneously minimizing $\mathcal{M}(IDP_i)$ and maximizing $\mathcal{M}(CP_i)$ (Equation IV.13).

Similarly to what was observed with *RFPI* and *REI* indices, the structural robustness assessment with the different bi-objective problems of Equations IV.8, IV.12 and IV.13 shows how the applied scenarios become more critical (in the sense of being dominated or not when dealing with several conflicting criteria, see Equation IV.10) when increasing the applied loads on the whole structure or when increasing the dynamic amplification factor.

V.2.6 General discussion

This section illustrates that the assumptions that concern the applied load in the accidental situation have an important effect on the structural robustness assessment. The analysis of the number of local failure scenarios within categories C1 to C4 shows how the structural response under some scenarios changes according to the applied loads, in particular W_d . Besides, these differences are detected when comparing the different load combinations (W1, W2 and W3) with a similar dynamic amplification factor (*DAF*), or when comparing different values of *DAF* (1.0, 1.3, 1.5 or 2.0) for a same accidental load combination.

The results with $DAF = 1.0$ indicate that ignoring the dynamic effects can influence the structural response under some scenarios, which can also change the values of the proposed indices (*RPFi* and *REI(UC)*). It is then crucial to take these dynamic effects into account in the structural robustness assessment and to identify the appropriate dynamic amplification factor (*DAF*) to represent these effects in the progressive collapse analysis.

V.3 EFFECT OF BAY DIMENSION

V.3.1 Presentation of case study

In this section, the steel framed structure of Section III.4.3.1 is tested with a larger span between columns (see Figure V.17), where the bays of 6 m span are extended to 7 m (bays of 5 m remain unchanged). In the following, the structures with 6 m and 7 m span are denoted ST6 and ST7, respectively. The objective is to study the effect of the geometrical configuration on the structural robustness while still respecting the recommendations of Eurocodes for the serviceability and ultimate limit states.

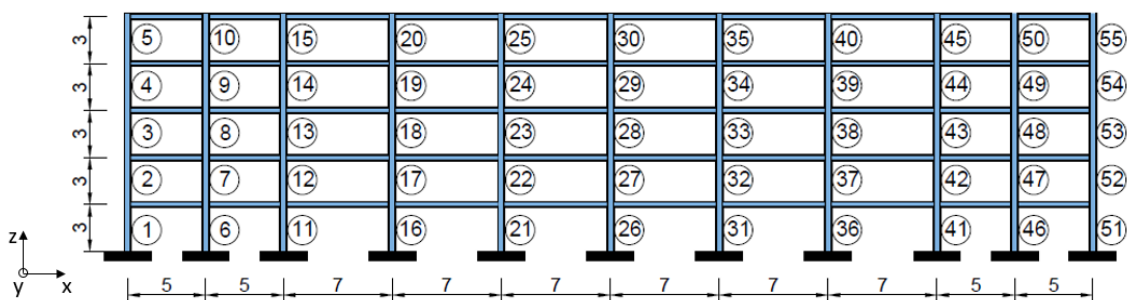


Figure V.17: Layout of steel-frame building ST7 with 7 m span (dimensions in meter).

The applied local failure scenarios are those presented in Table IV.3. The gravity load supported by the column P increases with the bay dimensions (see Figure IV.1), which leads to decrease the failure energy of each column, as shown in Table V.6. The failure energy of some columns (e.g. 1, 2, 3, etc.) does not change due to the fact that the span above these columns remains unchanged. The failure energy of each scenario i is described in Table B.6 (Annex B).

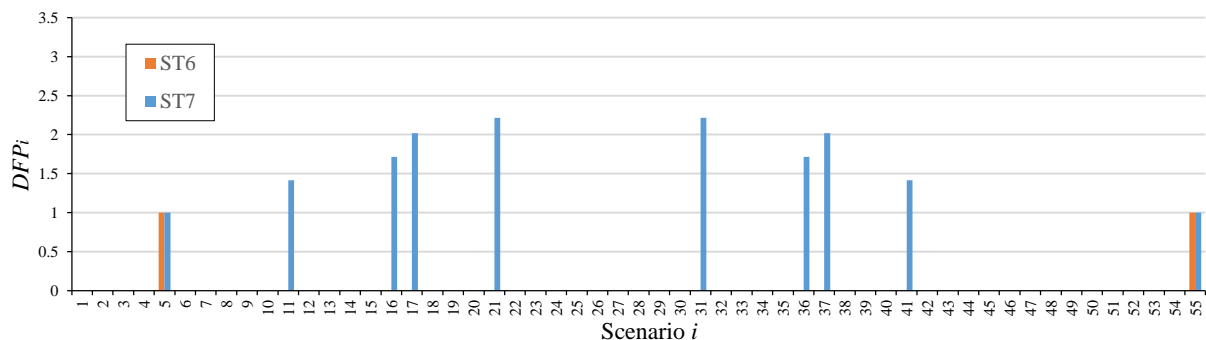
Column #	ST6		ST7	
	Vertical load (P) [kN]	Energy [kJ]	Vertical load (P) [kN]	Energy [kJ]
1; 51	395.0	100.4	395.0	100.4
2; 52	316.0	102.1	316.0	102.1
3; 53	237.0	103.8	237.0	103.8
4; 54	158.0	105.4	158.0	105.4
5; 55	79.0	108.6	79.0	108.6
6; 46	790.0	84.2	790.0	84.2
7; 47	632.0	87.8	632.0	87.8
8; 48	474.0	98.8	474.0	98.8
9; 49	316.0	102.1	316.0	102.1
10; 50	158.0	105.4	158.0	105.4
11; 41	869.0	82.5	948.0	80.6

12; 42	695.2	86.1	758.4	84.4
13; 43	521.4	98.6	568.8	97.0
14; 44	347.6	102.0	379.2	101.5
15; 45	173.8	105.4	189.6	105.3
16; 21; 26; 31; 36	948.0	80.6	1106.0	77.0
17; 22; 27; 32; 37	758.4	84.4	884.8	82.4
18; 23; 28; 33; 38	568.8	97.0	663.6	95.2
19; 24; 29; 34; 39	379.2	101.9	442.4	100.3
20; 25; 30; 35; 40	189.6	105.4	221.2	105.2

Table V.6: Vertical load P and failure energy of each column for the design configurations ST6 and ST7.

V.3.2 Assessment of structural robustness with RPM

The structural response of the configuration ST7 under each scenario i is described in Table B.6 (Annex B). In comparison with the results of the configuration ST6, increasing the span between columns reduces the ability to resist some scenarios. Figure V.18 shows that ST7 does not achieve to resist the scenarios 11, 16, 17, 21, 31, 36, 37 and 41 with the loss of one column (see Figure V.18 a), while it did not lead to a collapse in the configuration ST6. In fact, the indirectly affected part in ST7 fails to resist the tension forces developed in the directly affected part. Also, some scenarios with the loss of two ($i = 74, 79, 84$ and 89) or three columns ($i = 125$ and 135) have a high degree of failure propagation for the configuration ST7 (see Figure V.18 b and c), while there was no collapse for the configuration ST6. As all the scenarios with the loss of four columns lead to a collapse for the configuration ST6, they also lead to a collapse with the configuration ST7, as shown in Figure V.18(d). It is worth to note that the degree of failure propagation under the scenarios that have an expanded collapse ($DFP_i > 1$) is larger for ST6 than ST7. Despite the fact that the structural members affected under these scenarios, initially and after failure propagation, are the same for ST6 and ST7, the variation of beams dimension automatically leads to a larger value $\mathcal{M}(IDP_i)$ and $\mathcal{M}(CP_i)$ for ST7, while the ratio between them when calculating DFP_i (see Equation IV.4) is larger for ST6 in this example.



(a) Scenarios i with the loss of one column

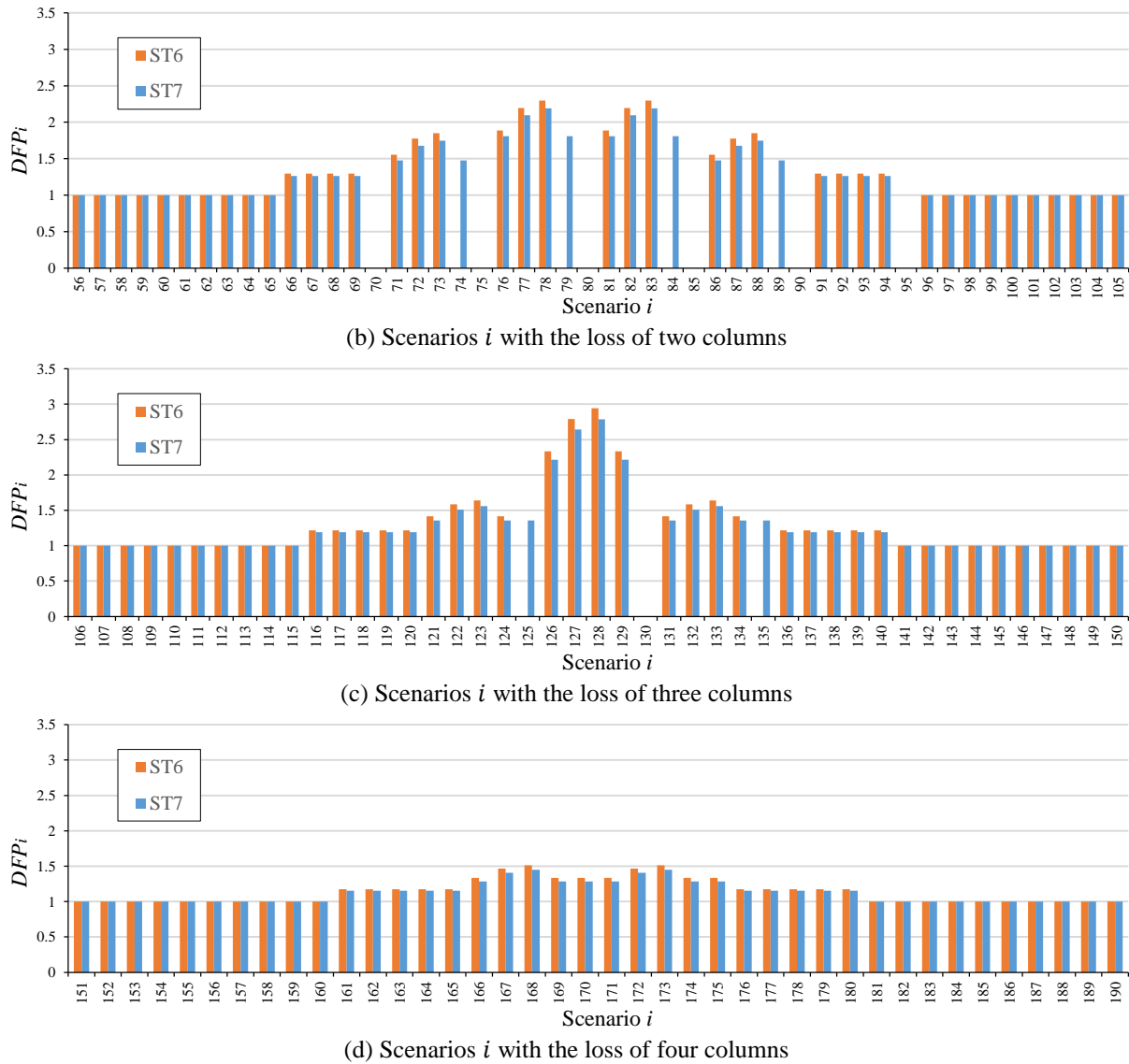


Figure V.18: Comparison in the degree of failure propagation between the design configurations ST6 and ST7.

Based on these results, the number of local failure scenarios within the categories C1 to C4 changes from ST6 to ST7. One illustrates in Figure V.19(a, b and c) that the number of scenarios for the configuration ST7 in category C2 decreases compared to ST6 under the scenarios with the loss of one, two or three column(s). Hence, ST7 does not succeed to find a second line of defence under some scenarios. These scenarios fall in category C4 for the configuration ST7, where Figure V.19(a, b and c) shows how the number of scenarios in category C4 increases from ST6 to ST7. For the scenarios with the loss of four columns, there is no change on the number of scenarios within the categories C1 to C4, as shown in Figure V.19(d).

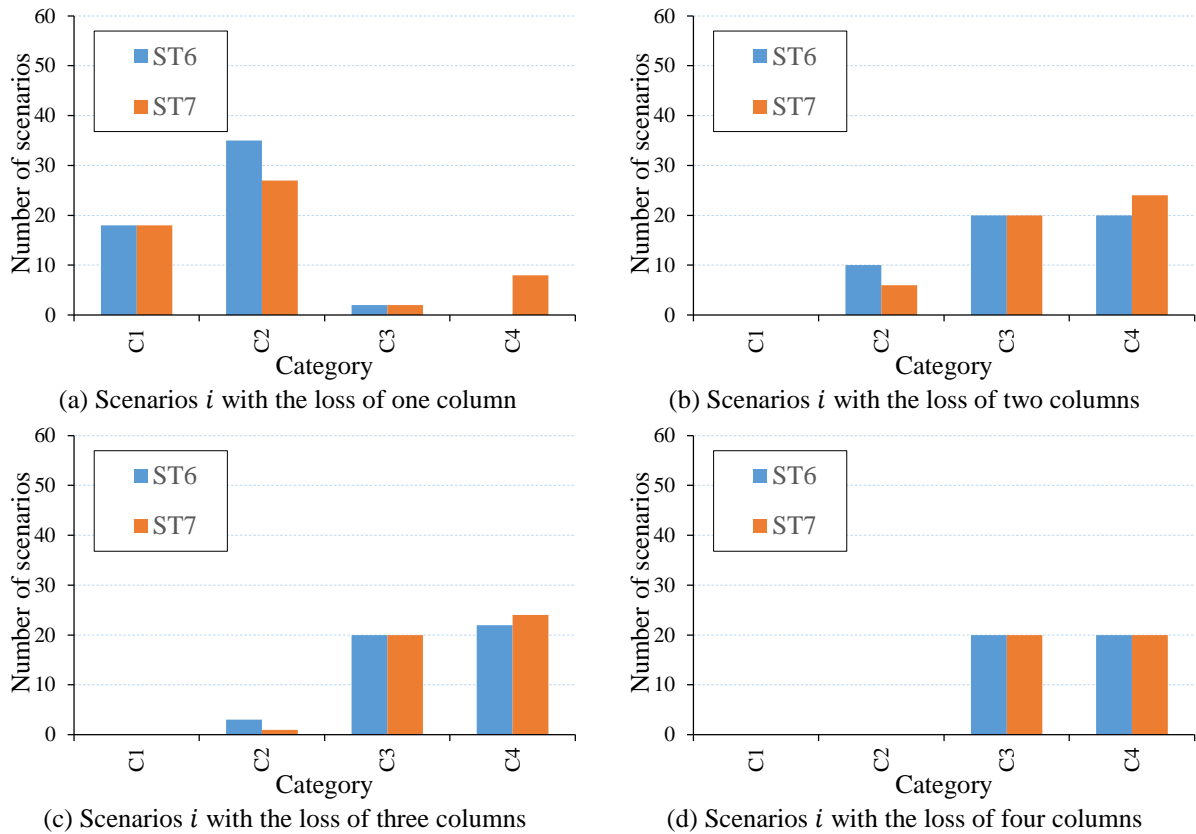


Figure V.19: Number of local failure scenarios within C1 to C4 according to the number of removed columns for the design configurations ST6 and ST7.

In order to identify how the maximal failure propagation can change according to the number of removed columns, Table V.7 presents the maximum degree of failure propagation $max(DFP_i)$ for the configurations ST6 and ST7. There is an increase of $max(DFP_i)$ for ST7 under the scenarios with the loss of one column. The scenarios 21 and 31 with the configuration ST7 lead to the worst collapse propagation with $DFP_{21\ or\ 31}^{ST7} = 2.2$, while the configuration ST6 achieves to resist these scenarios without collapse (see Figure V.18-a). Under the scenarios with the loss of two, three or four columns, $max(DFP_i)$ is slightly decreased from ST6 to ST7, as shown in Table V.7. Indeed, the most critical scenarios that correspond to $max(DFP_i)$ are the same for ST6 and ST7, while the degree of failure propagation is lower for ST7 than that of ST6, for the reasons of beam dimensions mentioned previously.

	Loss of 1 column	Loss of 2 columns	Loss of 3 columns	Loss of 4 columns
ST6	1.0	2.3	2.9	1.5
ST7	2.2	2.2	2.8	1.4

Table V.7: Maximum value of degree of failure propagation $max(DFP_i)$ according to the number of removed columns for the design configurations ST6 and ST7.

As the Robustness Propagation Failure Index ($RPMI$) is equal to the maximum degree of failure propagation among the applied scenarios, the $RPMI$ index for configuration ST6 is $RPMI_{ST6} = 2.9$, and the one for configuration ST7 is $RPMI_{ST7} = 2.8$. Considering all scenarios, $RPMI$ finally does not increase with ST7, and it could even indicate an improvement in the robustness with a lower $RPMI$ value than with ST6. As explained previously: (i) the most critical scenario ($i = 128$) that leads to the highest DFP_i is the same for ST6 and ST7, and (ii) the degree of failure propagation is lower for ST7 than for ST6 due to the definition of the $RPMI$ index which is based on the structural dimensions.

V.3.3 Assessment of structural robustness with $REI(UC)$

The Robustness Energy Index $REI(UC)$ according to the threshold $UC \in [10; 280]$ for the configurations ST6 and ST7 is presented in Figure V.20. Design configuration ST7 has a lower $REI(UC)$ when $10 \text{ m} \leq UC \leq 150 \text{ m}$ as scenarios 21 and 31 ($\mathcal{M}(CP_{21 \text{ or } 31}^{ST7}) = 155 \text{ m}$) that lead to an expanded collapse are the most critical scenarios. For $UC > 150 \text{ m}$, the critical scenarios for ST6 and ST7 are the same, as shown in Table V.8. Besides, an increase of $REI(UC)$ for ST7 is observed when $UC > 190 \text{ m}$, while for ST6 it occurs when $UC > 170 \text{ m}$. The reason is that the collapsed part under the critical scenarios is different between the two configurations ($\mathcal{M}(CP_{76 \text{ or } 81}^{ST7}) = 190 \text{ m} > \mathcal{M}(CP_{76 \text{ or } 81}^{ST6}) = 170 \text{ m}$). Based on these results, the robustness index $REI(UC)$ shows how the change of the geometry in ST7 leads to decrease the robustness level of the structure compared to ST6, in particular for $UC \in [10; 150]$ and $UC \in [180; 190]$.

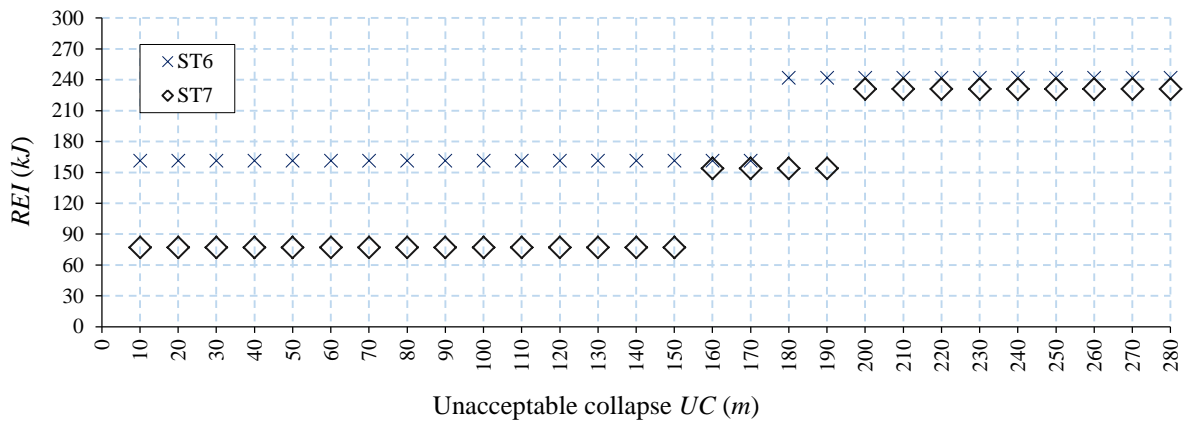


Figure V.20: REI index according to UC for the design configurations ST6 and ST7.

Configuration	UC	$REI(UC)$ (kJ)	Critical scenarios
ST6	[10 m; 170 m]	161	76; 81
	[180 m; 280 m]	242	126

ST7	[10 m; 150 m]	77	21; 31
	[160 m; 190 m]	154	76; 81
	[200 m; 280 m]	231	126

Table V.8: Critical scenarios according to UC for the design configurations ST6 and ST7.

V.3.4 Assessment of structural robustness with several criteria

The critical scenarios identified with the bi-objective problems of Equations IV.8, IV.12 and IV.13 are presented in Figure V.21, Figure V.22 and Figure V.23, respectively. The Pareto front S1-ST6 has 11 non-dominated scenarios according to Equation IV.8, while S1-ST7 has 4 scenarios, as described in Table B.7 (Annex B). The Pareto fronts S1-ST6 and S1-ST7 have only two common scenarios ($i = 127$ and 128), and the collapse under the scenarios 21 and 31 for ST7 ($DFP_{21 \text{ or } 31}^{ST7} = 2.2$) is more critical than for the other scenarios identified in S1-ST6 (which explains the vanishing of some non-dominated scenarios from S1-ST6 to S1-ST7).

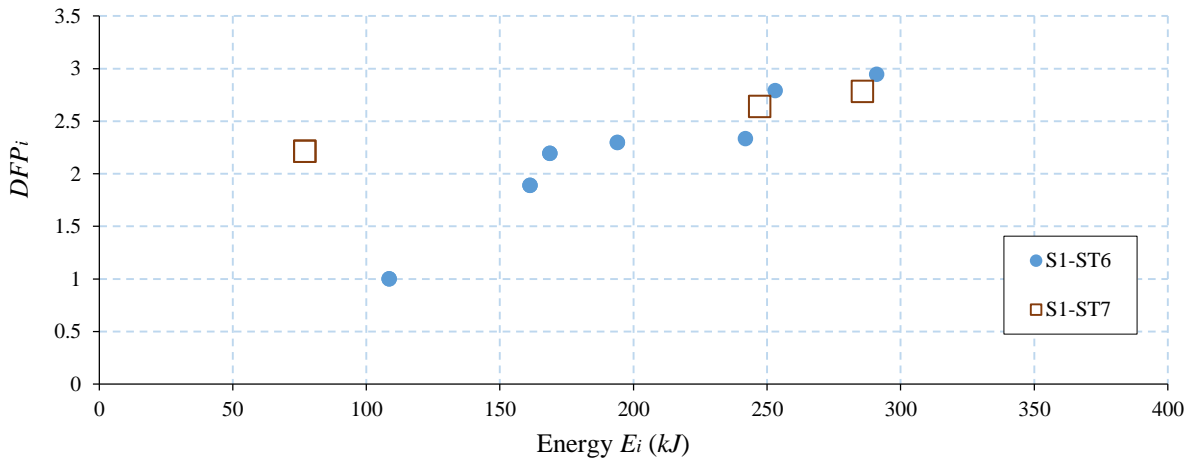


Figure V.21: Identification of non-dominated solutions for the design configurations ST6 and ST7 when simultaneously minimizing E_i and maximizing DFP_i (Equation IV.8).

One notes that the majority of non-dominated scenarios of the Pareto fronts for ST6 and ST7 according to Equations IV.12 and IV.13 are common (see Table B.8 and Table B.9 in Annex B), which indicates that most of the critical scenarios are similar for both configurations. The points in Figure V.22 and Figure V.23 do not exactly overlap for both configurations due to the fact that the values of DFP_i , $\mathcal{M}(IDP_i)$ and $\mathcal{M}(CP_i)$ are not similar for ST6 and ST7. As some scenarios (e.g. $i=21, 31, 79, 84$, etc.) lead to a collapse for ST7 but not for ST6, the Pareto fronts S2-ST7 and S3-ST7 have some different non-dominated scenarios compared to S2-ST6 and S3-ST6, respectively. Figure V.22 (when minimizing

$\mathcal{M}(IDP_i)$ and maximizing DFP_i) shows that some scenarios of S2-ST6 are above the scenarios of S2-ST7, which indicates that they have a larger DFP_i than those of S2-ST7. One observes in Figure V.23 (when minimizing $\mathcal{M}(IDP_i)$ and maximizing $\mathcal{M}(CP_i)$) that there is more space between the points of ST6 and ST7 that correspond to the same scenarios. According to Equation IV.13, the larger values of $\mathcal{M}(CP_i)$ for ST7 than for ST6 do not obviously mean that the scenarios of S3-ST7 are more critical than those of S3-ST6 due the fact that they also have a larger value of $\mathcal{M}(IDP_i)$.

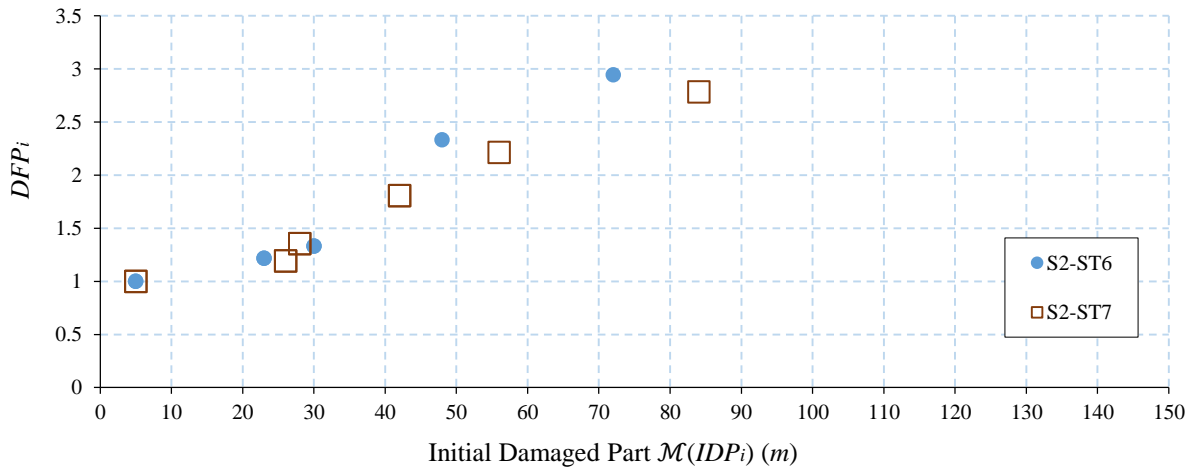


Figure V.22: Identification of non-dominated solutions for the design configurations ST6 and ST7 when simultaneously minimizing $\mathcal{M}(IDP_i)$ and maximizing DFP_i (Equation IV.12).

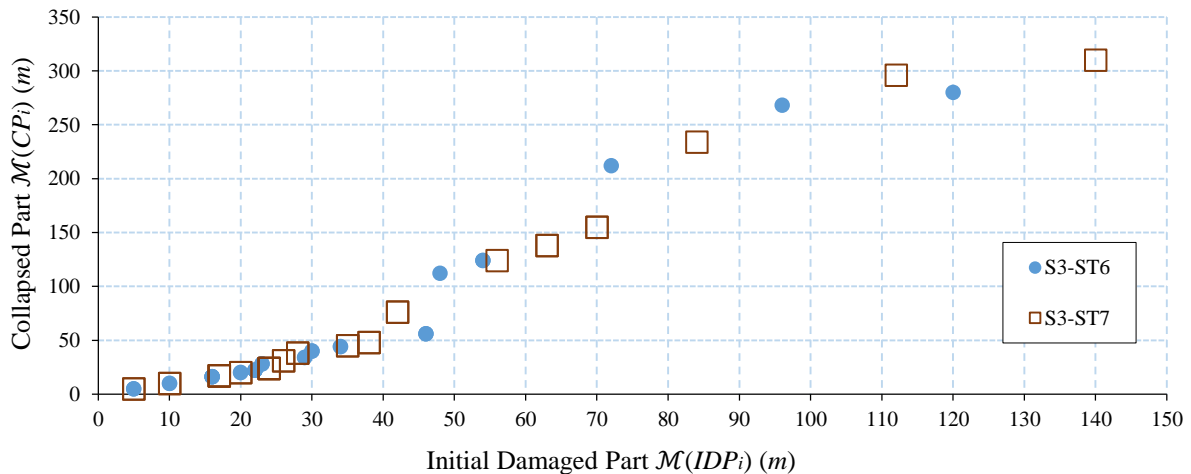


Figure V.23: Identification of non-dominated solutions for the design configurations ST6 and ST7 when simultaneously minimizing $\mathcal{M}(IDP_i)$ and maximizing $\mathcal{M}(CP_i)$ (Equation IV.13).

V.3.5 General discussion

This example shows how a change in the geometrical configuration of the structure can change the structural response under some scenarios. If the structural robustness

assessment indicates that the Robustness Propagation Failure Index (RPF_i) is lower for ST7 than ST6, this aspect is not due to the fact that ST7 has a better performance than ST6 under the applied scenarios (the critical scenario with the highest level of propagation is the same for both configurations), but rather can be explained by the beam dimensions and the definition of DFP_i . In contrast, the structural robustness assessment based on the Robustness Energy Index $REI(UC)$ shows that the configuration losses in terms of robustness as ST7 has a lower value $REI(UC)$ than ST6. One also shows that the number of scenarios falling within category C3 or C4 increases when moving from ST6 to ST7.

These results raise the question of which is the best robustness index to use for structural robustness assessment. In fact, both indices (RPF_i and $REI(UC)$) as well as the analysis of scenario categories are important to assess the structural robustness, where each measure provides a different and complementary aspect of structural robustness.

V.4 EFFECT OF STEEL DUCTILITY

The material ductility of the structural elements plays a crucial role on the structural capacity to develop a second line of defence with the tensile membrane action. It influences the maximal displacement that the directly affected part can reach before the rupture of material, which leads to the failure. In order to study the effect of the steel ductility on the structural robustness, the ductility of the steel is restrained by a strain of fracture $\varepsilon_f = 22\%$ (see Figure V.24) according to the catalogue of ArcelorMittal (2018). In case the strain of a layer reaches the strain of fracture ε_f , one considers the failure of this layer, where the strength becomes almost zero, as shown in Figure V.24.

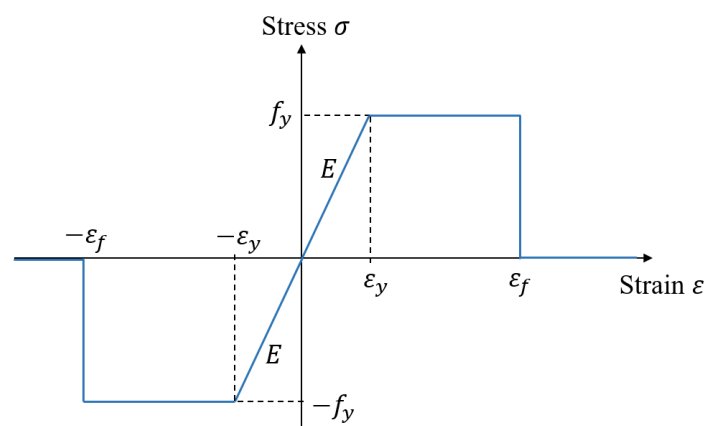


Figure V.24: Constitutive law of steel with a strain of fracture.

In the proposed strategy of iterative coupling between the yield design approach and the non-linear analysis, the material ductility might influence the results of non-linear analysis, where this aspect is not considered in the yield design calculation. In this section, the analyses without or with considering the fracture limit of steel are denoted DUC1 and DUC2, respectively. When applying the assumption DUC2, the substructures corresponding to the scenarios with the loss one column achieve to support the applied loads after a certain deflection without reaching the fracture limit ε_f . For example, Figure V.25(b) shows that the substructure corresponding to the loss of column # 26 achieves to find an alternative equilibrium state under $W_a = 31.6 \text{ kN/m}$ with deflection $\delta_{26} = 0.63 \text{ m}$ on the top of the removed column. The analysis under the assumption DUC1 leads to the same results of DUC2 (see Figure V.25-a). Besides, Figure V.26 shows that the axial strain of the cross-section layers at the joint A (where the strain values are the highest on the substructure) does not reach the fracture limit ε_f .

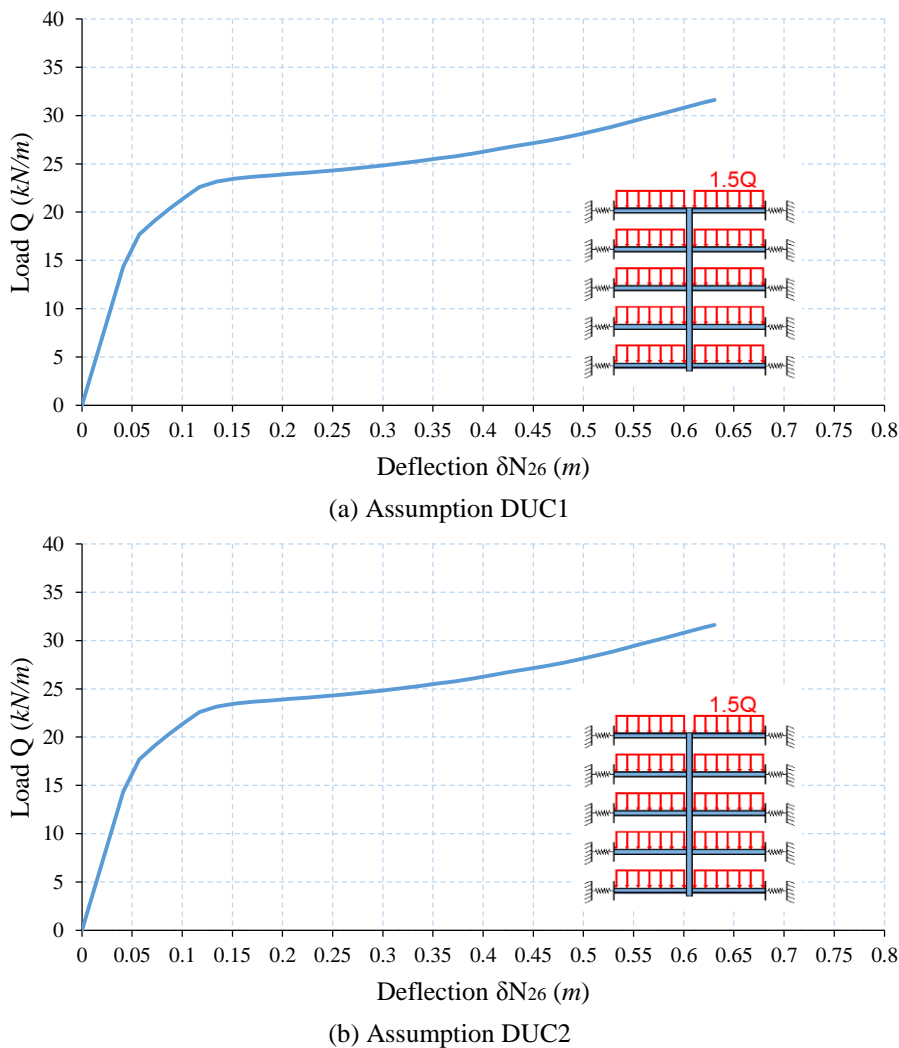


Figure V.25: Deflection-load diagram of non-linear static analysis of the initial damaged part after the loss of column # 26 for the assumptions (a) DUC1 and (b) DUC2.

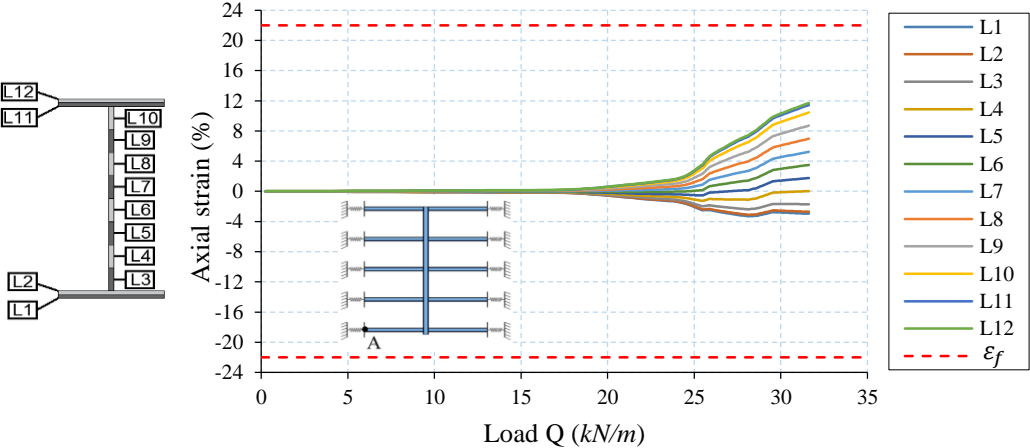
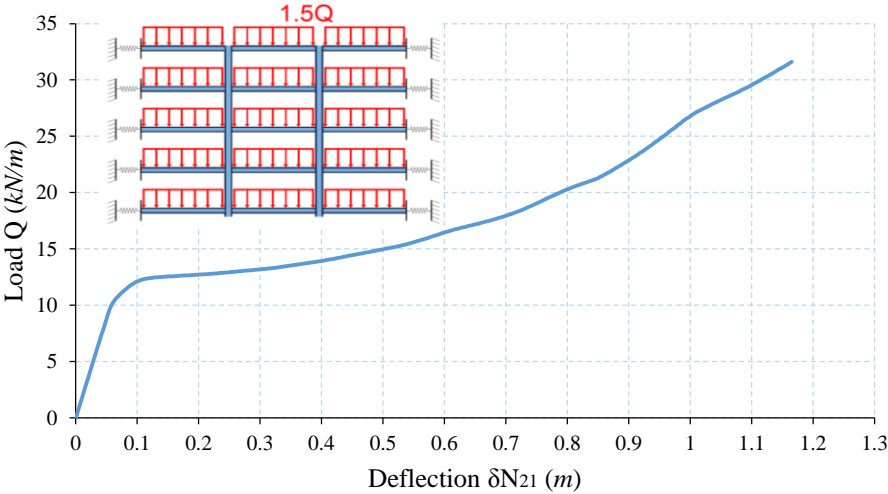


Figure V.26: Axial strain of the cross-section layers at the joint A in the directly affected part after the loss of column # 26 for the assumption DUC2.

In contrast, under the scenarios with the loss of more than one column, the associated substructure never achieves to support W_a (31.6 kN/m) due to the high strain that can exist at some points and the subsequent failure of some layers. For example, the non-linear analysis applied to the substructure associated with the loss of columns # 21 and 26 indicates that under the assumption DUC1 the substructure achieves to support $W_a = 31.6 \text{ kN/m}$ with deflection $\delta_{21} = 1.16 \text{ m}$ (see Figure V.27-a). Conversely, under the assumption DUC2, the maximum load capacity is $Q = 22.7 \text{ kN/m}$ (which corresponds to point P^* in Figure V.27-b). Under this load, the strain at some joints reaches ϵ_f , as shown in Figure V.28 at the joint B, where the layers L11 and L12 rupture fail to the tension force.



(a) Assumption DUC1

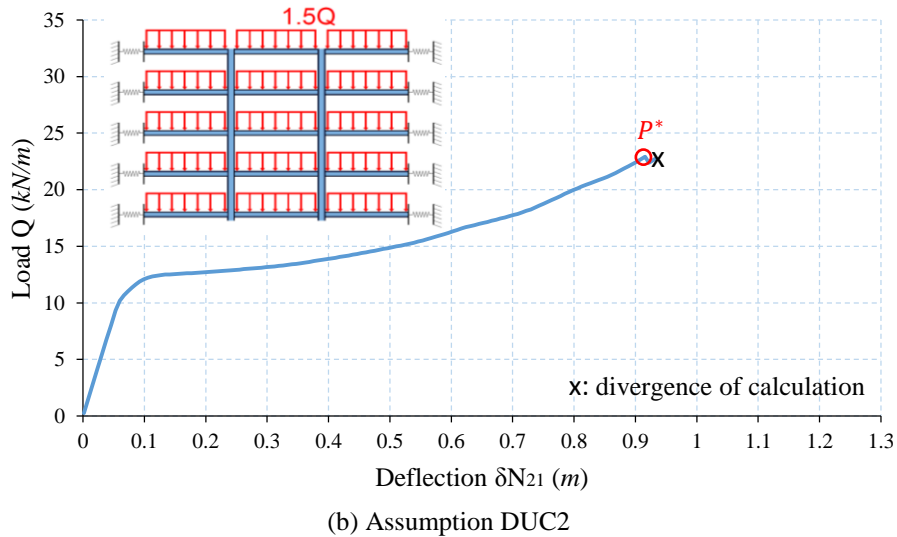


Figure V.27: Deflection-load diagram of non-linear static analysis of the initial damaged part after the loss of columns # 21 and 26 for the assumptions DUC1 and DUC2.

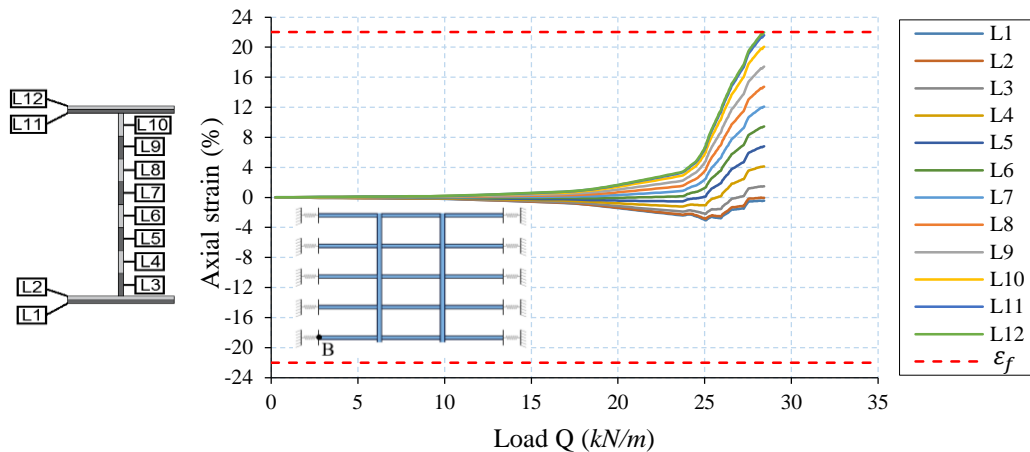
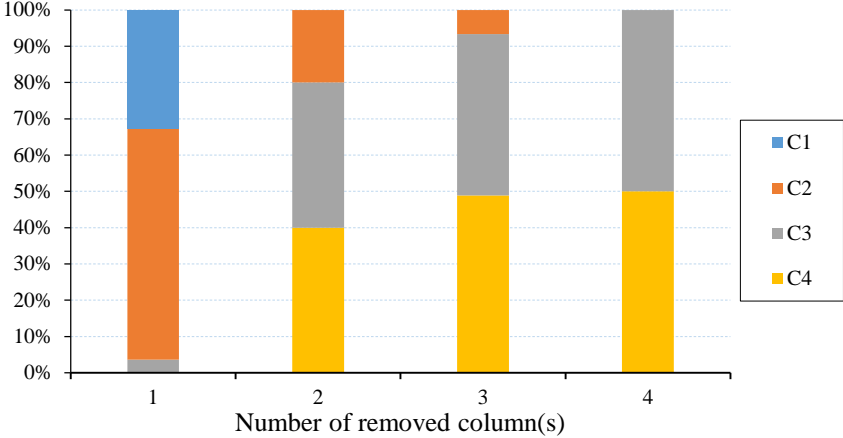


Figure V.28: Axial strain of the cross-section layers at the joint B in the directly affected part after the loss of columns # 21 and 26 for the assumption DUC2.

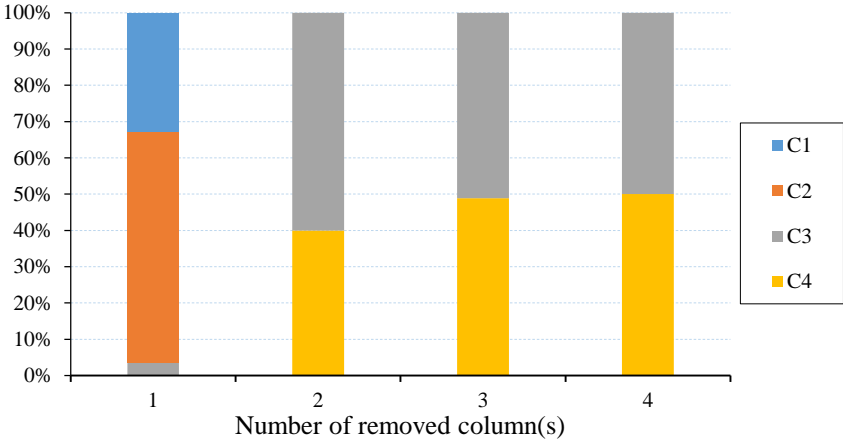
These examples illustrate that the consideration of a fracture threshold (DUC2) on the constitutive law of steel material can change the structural response under some scenarios. Hence, the assumption that the materials are elastic perfectly plastic (DUC1) is not fully objective for progressive collapse simulation.

The percentage of the applied local failure scenarios with the loss of one column within categories C1 to C4 is the same for DUC1 and DUC2, as shown in Figure V.29(a and b), due to that the structure with the assumption DUC2 achieves to find a second line of defence without reaching the fracture limit of steel material. For the assumption DUC1, Figure V.29(a) shows that the structure prevents the collapse under some scenarios (category C2) with the loss of two or three columns. For the assumption DUC2, the non-linear analysis iteration of the proposed strategy indicates that there is a rupture of steel at the joints of the

directly affected part under the scenarios with the loss of more than one column. Therefore, there is no scenario in the category C2 (see Figure V.29-b). The structural response of the structure under each scenario is described in Table B.10 (Annex B).



(a) Assumption DUC1



(b) Assumption DUC2

Figure V.29: Percentage of local failure scenarios within categories C1 to C4 according to the number of removed columns for the assumptions DUC1 and DUC2.

Figure V.30 shows that there is no change for the maximum value of degree of failure propagation $\max(DFP_i)$ according to the number of removed columns for the assumptions DUC1 and DUC2. Hence, despite the change on the structural response under some scenarios when a fracture limit is integrated ϵ_f (assumption DUC2), the structural robustness assessment with considering DFP_i indicates the same results for the assumptions DUC1 and DUC2 with a Robustness Propagation Failure Index $RPF I_{DUC1 \text{ or } DUC2} = 2.9$.

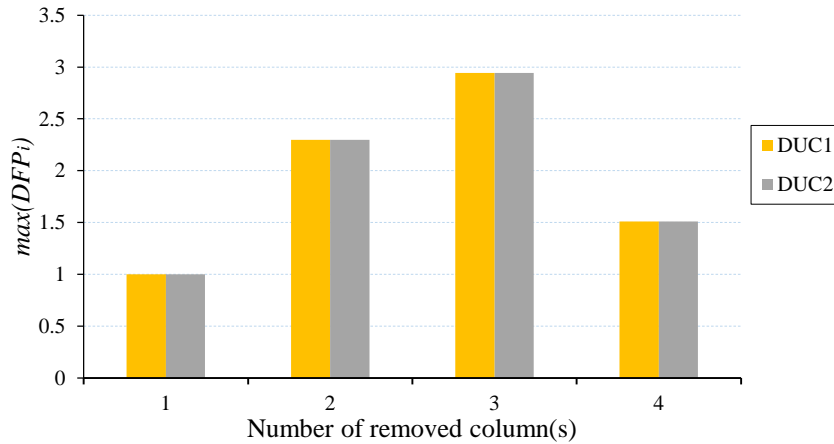


Figure V.30: Maximum value of degree of failure propagation according to the number of removed columns for the assumptions DUC1 and DUC2.

Also, the structural robustness assessment with considering the Robustness Energy Index $REI(UC)$ indicates that for both assumptions DUC1 and DUC2, this index has the same value when $UC \in [10\text{ m}; 280\text{ m}]$, as shown in Figure V.31. The most critical scenarios associated to $REI(UC)$ are similar for both cases (Scenarios 76 and 81 for $UC \in [10\text{ m}; 170\text{ m}]$, and scenario 126 for $UC \in [180\text{ m}; 280\text{ m}]$), which explains the overlapping of the results between DUC1 and DUC2.

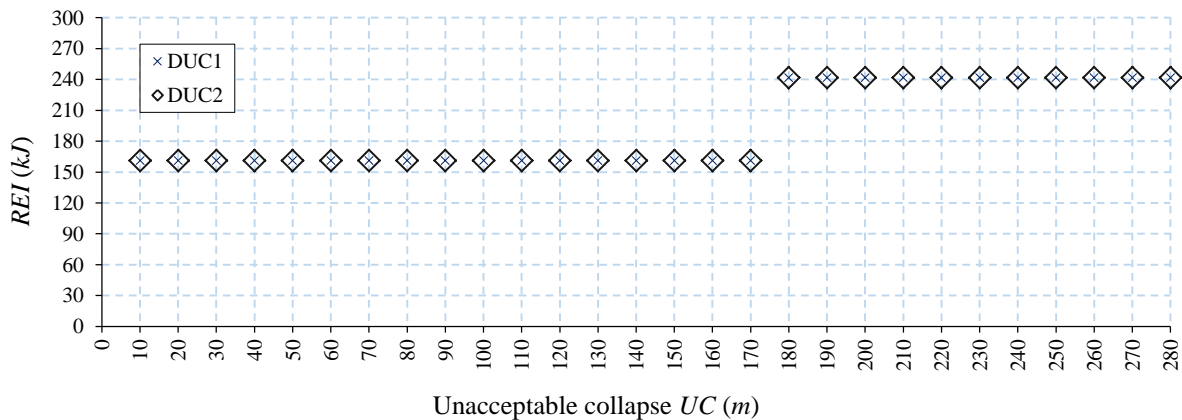


Figure V.31: Sensitivity of REI index with UC for the assumptions DUC1 and DUC2.

Similarly, the non-dominated scenarios identified according to the bi-objective problems of Equations IV.8 and IV.12 are the same for both assumptions DUC1 and DUC2, as shown in Figure V.32 and Figure V.33, respectively. Furthermore, all the scenarios of S3-DUC1 identified by the bi-objective problem of Equation IV.13 belong to S3-DUC2 (see Figure V.34). However, some of the scenarios lead to a collapse with DUC2 but not with DUC1 ($i = 70, 75, 80, 85, 90$ and 95 , see the dotted line area in Figure V.34). These critical scenarios are non-dominated for DUC2 but not for DUC1.

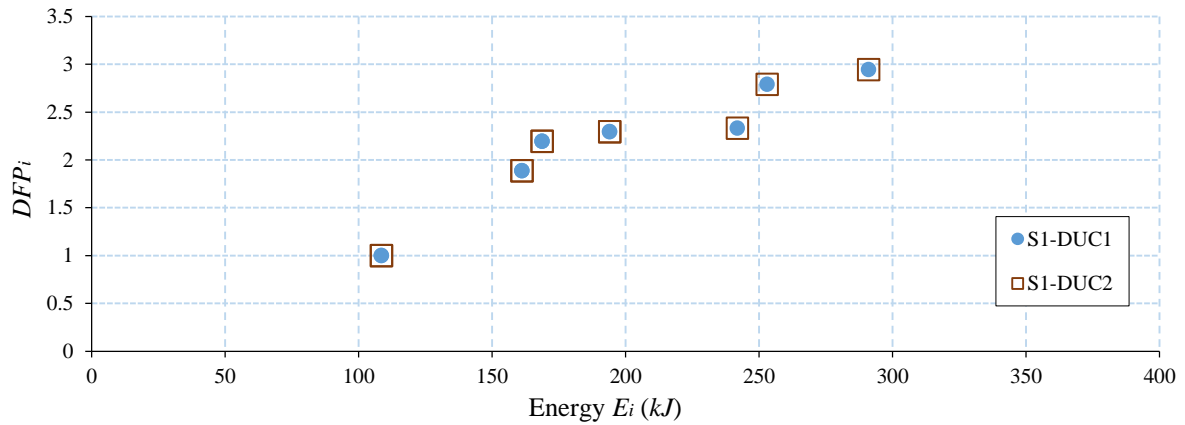


Figure V.32: Non-dominated solutions when simultaneously minimizing E_i and maximizing DFP_i (Equation IV.8) for the assumptions DUC1 and DUC2.

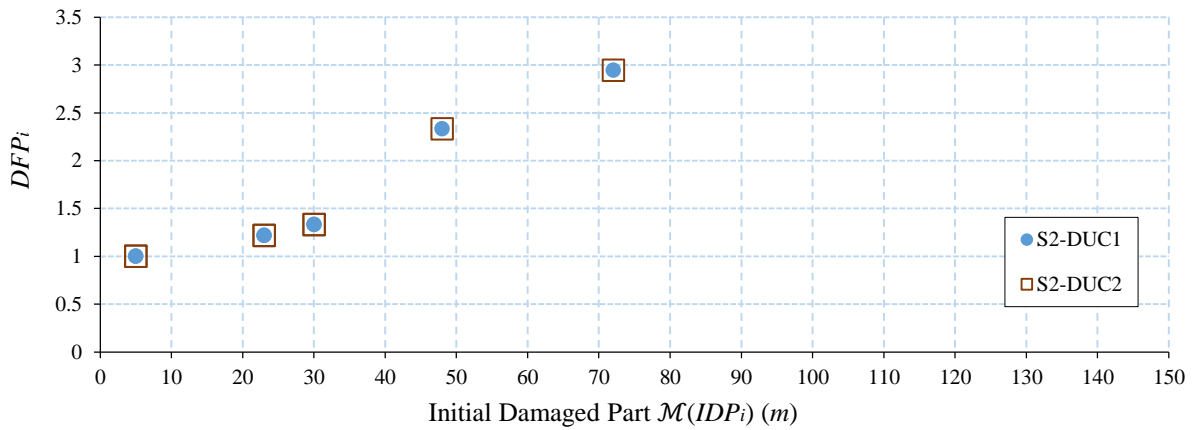


Figure V.33: Non-dominated solutions when simultaneously minimizing $\mathcal{M}(IDP_i)$ and maximizing DFP_i (Equation IV.12) for the assumptions DUC1 and DUC2.

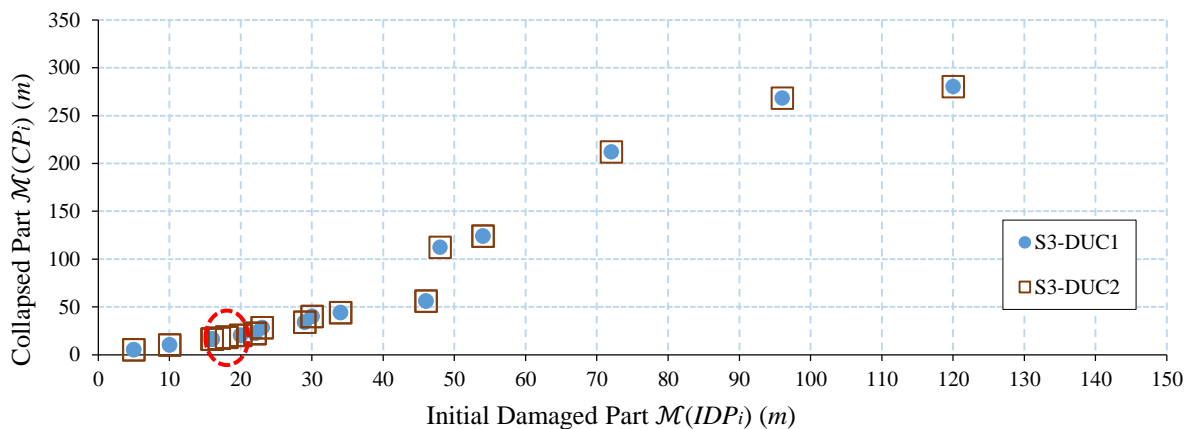


Figure V.34: Non-dominated solutions when simultaneously minimizing $\mathcal{M}(IDP_i)$ and maximizing $\mathcal{M}(CP_i)$ (Equation IV.13) for the assumptions DUC1 and DUC2.

In this section, one concludes that the restraint of steel ductility by a fracture limit ε_f (DUC2) changes the structural response under some scenarios. However, these differences do not modify the overall robustness assessment in this example due to the high ductility of the considered structural steel and to the fact that the most critical scenarios are the same for both assumptions.

V.5 DISCUSSION ON THE OTHER FACTORS INFLUENCING THE STRUCTURAL ROBUSTNESS ASSESSMENT

In the previous sections, the effect of some key factors on the structural robustness assessment has been analyzed. In fact, several other parameters have been considered in the previous chapters whose selected value or associated assumption may impact in the end the proposed robustness indices. In this section, a selection of these factors is proposed among which: (i) the threshold associated with an unacceptable collapse, (ii) the boundary conditions of the substructure when modelling the directly affected part, (iii) the identification of the local failure scenarios and the way they are characterized, (iv) the consideration of debris loading in the progressive collapse analysis, and (v) the consideration of a three-dimensional analysis.

V.5.1 Threshold UC associated with an unacceptable collapse

The threshold UC associated with an unacceptable collapse is mainly related to the calculation of the Robustness Energy Index (REI) (see Equations IV.6 and IV.7). The sensitivity of this index to the threshold UC was tested for each example presented in Chapters IV and V. One has shown how the robustness index depends on UC (Figure IV.19) and how UC can change the ranking order between design options (Figure IV.41 and Figure V.20). It was also illustrated how the Robustness Energy Index was sensitive to the load combinations in addition to the threshold UC (Figure V.11 to Figure V.13). The Eurocodes (NF EN 1991-1-7, 2007) mention that the limit of admissible damage may be different for each type of building, while recommending a maximal value of 100 m^2 or 15 % of the floor area as threshold for buildings, whichever is less, on two adjacent floors caused by the removal of any supporting column, pier or wall. If considering a range of UC values enables a global comparison of several design options, further research work is still needed to select the best criterion to be associated to such threshold.

V.5.2 Boundary conditions of the substructure

In the proposed strategy for progressive collapse analysis, the non-linear analysis is performed only on the directly affected part by extracting the corresponding area of the structure. A refined non-linear analysis is performed on this part by calibrating boundary conditions with horizontal springs at the extremities of the substructure (a simplified approach identifies the stiffness of each spring, see Section III.4.1) to represent the effect of the indirectly affected part. Through the iterative procedure, the integration of the geometric changes (identified by the non-linear analysis) that may lead to the development of catenary action in later iterations of the yield design calculation is only considered for the directly affected part, and not for the indirectly affected part (which finally causes the removal of some P-delta effect). In order to improve the accuracy of such coupling approach, further development is required to (i) integrate advanced macroelements at the extremities of the substructure to better model the displacements and the rotations of the indirectly affected part (several macromodels were proposed to simulate the behaviour of the beam-column joints, see Demonceau, 2008; Vidalis, 2014; Huvelle et al., 2015), (ii) better calibrate the boundary conditions, for example by considering the displacement field computed at the areas boundaries; and (iii) take into account not only the geometric changes in the directly affected part, but also the displacements in the other parts of the structure to fully take into account the P-delta effects.

V.5.3 Local failure scenarios

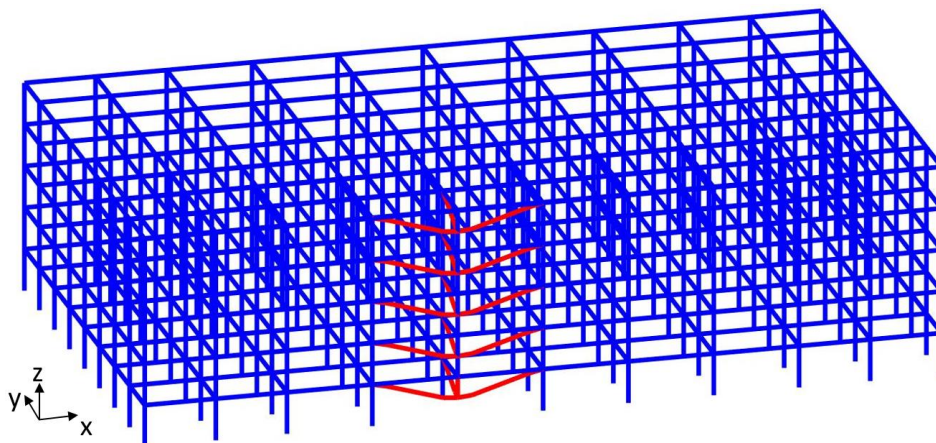
In this dissertation, the adopted local initial failure scenarios are event-independent and limited to the loss of some adjacent columns. Some virtual loading actions are associated to estimate the corresponding level of energy required for the failure of such element(s). This strong assumption does not reflect the fact that the loss of column(s) might probably cause the damage or the total loss of other types of elements such as beams. Considering the damage of beams in the initial local failure scenarios seems a necessary step in future investigations, to properly assess structural robustness. Indeed, for framed structures, the tensile membrane action allows to provide a second line of defence and avoid the collapse. The damage of beams in the directly affected part might then reduce the ability of the structure to resist the local failure scenarios. However, the consideration of the loss of beam elements can significantly increase the number of local failure scenarios to be investigated and the overall computation cost. In the proposed steel-framed building of Section III.4.3, the number of scenarios would increase from 190 to 3219 scenarios.

V.5.4 Debris loading

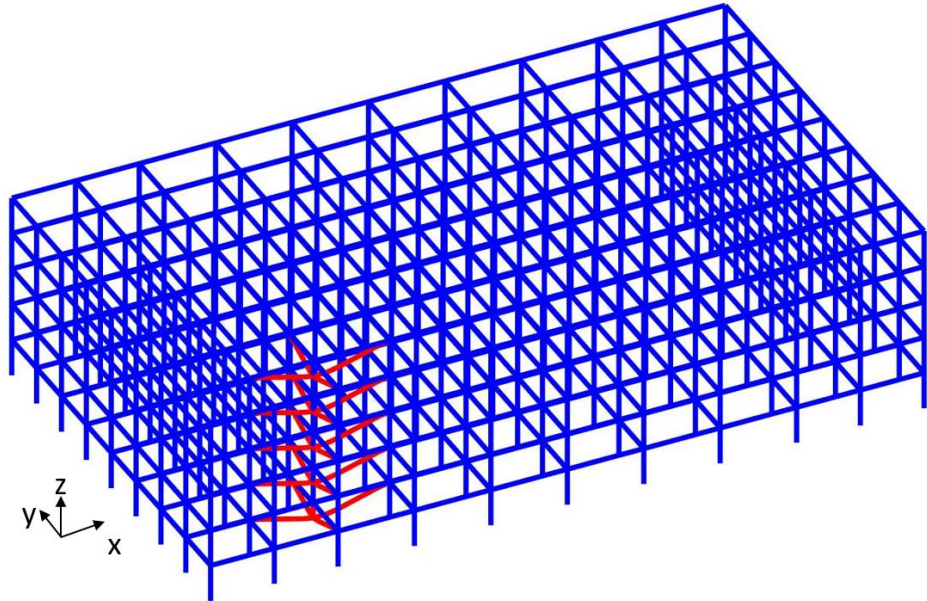
The effect of the debris loading is ignored in this dissertation, while it is an important aspect in progressive collapse analyses. The simulation of the collision between falling debris and other structural components is a complex issue that can be modelled in a simplified manner by adding the load of the collapsed floors (using an amplification factor) on the lower floor. The identification of an appropriate amplification factor (to take into account the dynamic effects of the collision) needs further research work, as there is no guidance currently to take into account this type of loading. The consideration of this aspect might change the structural response for some scenarios presented in this dissertation, and, consequently, the overall structural robustness assessment.

V.5.5 Three-dimensional analysis

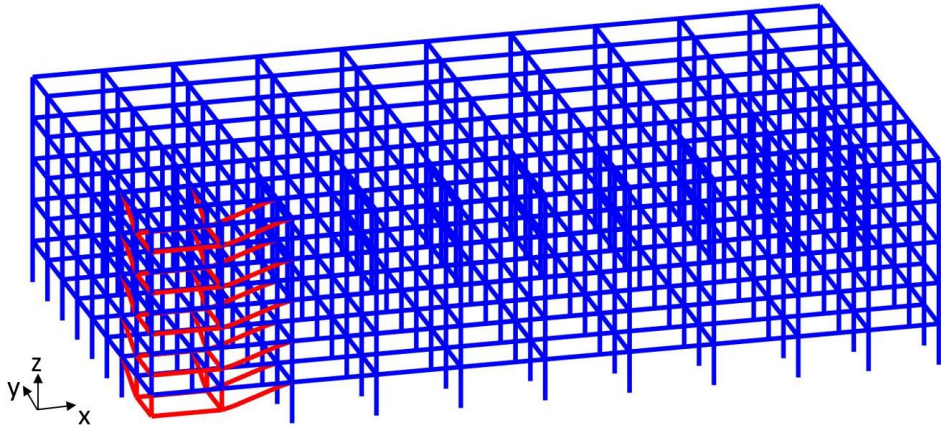
The three-dimensional analysis allows a more realistic simulation than the two-dimensional modelling used in this dissertation. With a 2D approach, the effect of a part of the structure is ignored, which might influence the structural response for several reasons. First, the distribution of forces and then the ability of the structure to resist the local failure is different. Second, the 3D analysis allows to take into account the effect of some structural elements such as the floor slabs, which is ignored in the 2D analysis. The consideration of this effect might increase the ability of the structure to develop the tensile membrane action. Finally, the measures of the initially damaged part $\mathcal{M}(IDP_i)$ and the collapsed part $\mathcal{M}(CP_i)$ are significantly different in 2D and 3D analyses. The numerical implementation of the yield design calculation presented in Section III.3 already enables a 3D modelling. An illustration of the results obtained with the kinematic approach is provided in Figure V.35 (a, b and c) by considering an 8-bay building in y direction. One identifies the failure mechanism under some scenarios with the loss of column(s). This figure shows how the directly and indirectly affected parts are linked with a redistribution of forces proper to the 3D modelling.



(a) Loss of an peripheral column



(b) Loss of an internal column



(c) Loss of four columns

Figure V.35: Failure mechanism identified by the yield design calculation calculation under some scenarios with the loss of column(s) (the displacement are not representative).

V.6 CONCLUSIONS

The sensitivity of the model to some parameters has been considered in this chapter to identify how some fluctuations in inputs might change in an important way or not the conclusions. Three types of changes have been considered for the steel frame structure previously considered in Chapter III and IV (i) the accidental combination of action loads when the exceptional event occurs (including the use of dynamic amplification factors for the directly affected part), (ii) the structural geometry by modifying the bay dimensions of the steel framed case study, and (iii) the steel ductility by adding a fracture strain on the constitutive law.

Considering the combination of actions, the investigations have been made according to Eurocodes Limit State and also to US standards in order to compare how different the robustness level can be when using different design rules. Several dynamic amplification factors have been combined to this analysis to illustrate that the number of scenarios with collapse (partial or total) increases with the applied loads on the structure. It was shown that the proposed index $RPF I$ (respectively $REI(UC)$) increases (respectively decreases) with the applied loads.

Considering the structural geometry, it was shown how longer beam elements can reduce the ability of the structure to develop catenary action, then leading to a higher number of scenarios with collapse (partial or total). However, for some scenarios, the degree of failure propagation was found to be lower due to the beam dimensions and the definition of the degree of failure propagation. For $REI(UC)$, one showed that the level of structural robustness decreases when increasing the span length. In this case, it was highlighted that both indices ($RPF I$ and $REI(UC)$) as well as the analysis of scenario categories provide a complementary aspect when assessing structural robustness.

The analysis of the ductility effect indicates that the assumption of considering the materials as elastic perfectly plastic may lead in a few cases to an overestimation of the material ductility, and then of the structural capacity. It was shown that adding a fracture limit changes the structural response for some scenarios, while not changing the robustness indices in the end. In this sense, the proposed robustness indices tend to smooth the fluctuations observed for some scenarios when moving to the overall robustness assessment (as the robustness indices are associated with the worst-case scenarios).

Other factors are also discussed in this chapter that might influence the structural robustness analysis. Some of these factors relate to the definition of the proposed indices, such as the threshold UC associated with an unacceptable collapse. Indeed, the identification of the threshold UC needs further research work so that some recommendations can be formulated in the end. As there is a high uncertainty level associated with the local failure scenarios, more analysis is needed to investigate scenarios with the damage or the total loss of different types of elements such as beams and columns.

In order to improve the proposed approach, the modelling of the progressive collapse needs further development. An essential point relates to the boundary conditions of the substructure in the non-linear analysis, all the more when choosing a three-dimensional analysis. Also, the debris loading, while ignored in this dissertation, should be considered to provide a more realistic analysis. These points should be further considered to improve the accuracy of the progressive collapse simulation.

CHAPTER VI

GENERAL CONCLUSIONS

The main purpose of this thesis was to develop a strategy to assess the capacity of a structure to withstand actions and the safety against progressive collapse, with a focus on quantification approaches for design and construction codes and standards.

This work started by analyzing the existing approaches related to structural robustness proposed by the engineering and scientific communities, in order to identify some scientific and technical issues. The engineering community takes into account robustness requirements by relying on indirect or direct resistance provisions such as the tying method, the alternative load path method, the specific local resistance design method or the risk-based assessment method, the choice between these methods depending on the consequence class of a structure. The scientific community has thoroughly investigated the concept of robustness from different perspectives that can be summarized in the two following groups: the quantification of structural robustness through indicators (deterministic or probabilistic), and the modelling of progressive collapse with numerical or experimental tests that reach or go beyond ultimate limits. Based on this analysis, three main questions below were identified:

- How to propose a simplified modelling of progressive collapse by taking into account the dynamic effects, the geometrical and the material non-linearities?
- How to identify the degree of failure propagation, in order to evaluate and quantify the extent of failure after an initial event?
- How to assess the maximum structural capacity with respect to some performance criteria?

The proposed research activity has focused on these three questions by analyzing progressive collapse, and the robustness quantification through the use of indicators. One

details below some conclusions for each of these three questions by presenting each time the main assumptions considered in the analysis.

I.1 HOW TO PROPOSE A SIMPLIFIED MODELLING OF PROGRESSIVE COLLAPSE?

The structural modelling based on a coupling between yield design and non-linear analyses is introduced in Chapter III to discretize progressive collapse. Such an iterative procedure aims to check if an alternative load path can be found in the directly affected part of a structure, and if not, how the failure propagation can be discretized until one reaches a final state.

The philosophy is to iteratively identify with a yield design approach the part of the structure concerned by a failure mechanism and to further analyze the corresponding subsystem with a non-linear model. With the yield design theory, one estimates the macroscopic yield criterion of an element based on the microscopic yield criteria of the constitutive materials, and the geometric shape of the element cross-section. Ultimate load is determined by looking at the compatibility between the equilibrium of the structure and the local verification of a criterion of resistance at any point of the structure. Hence, the yield design approach avoids a step-by-step non-linear analysis of the structure along the full loading path, and is a good candidate to the robustness analysis where main motivation is to determine the set of ultimate loads as well as the most probable failure mechanism. Besides, one aims to avoid potential convergence issues associated with loss of stability.

The yield design approach relies on several assumptions among which infinitesimal assumption, considering that the materials are elastic perfectly plastic. Also, the numerical implementation depends on the structure, its structural components and the chosen mechanical model influences the numerical equilibrium equations and the yield criteria of elements.

A comparison with a non-linear analysis was proposed on basic elements by considering different assumptions for the non-linear model (without or with taking into account geometrical non-linearities). It was shown how the yield design approach enables to estimate the ultimate load for initiation of failure mechanism, though missing to identify the capacity of the structure to find a new behaviour (catenary action) under large displacements as this behaviour is not investigated by this theory. This observation led to the proposition of coupling the yield design approach with a non-linear analysis based on a corotational formulation, to better analyze the structural response of the part concerned by the failure mechanism. According to this method, one can identify the initially affected part under the

applied scenario by the first iteration of the yield design approach. If there is a possibility to develop an alternative functioning, a non-linear analysis is performed on this part to characterize the geometrical and the material non-linearities. The successive iterations of the yield design approach with the deformed geometrical configuration allow to verify the ability of the structure to develop a second line of defence.

I.2 HOW TO IDENTIFY THE DEGREE OF FAILURE PROPAGATION?

One aims to capture multiple aspects of robustness with respect to the definition of the Eurocodes including (i) the situation that the structure is facing (an action that leads to a localised failure in the structure, where the local failure is the part of structure that is assumed to have collapsed, or been severely disabled, by the accidental event (NF EN 1991-1-7, 2007)), and (ii) the fact that the local failure should not propagate disproportionately.

To deal with this second question, progressive and disproportionate collapse concepts have been dissociated. The former initiates with a localized damage to a single or a few structural components and develops throughout the structural system, affecting other components. The latter is characterized by a disproportion in size compared to the initial event or its resulting local failure.

The iterative strategy for progressive collapse analysis is used to compare a metric of the initial damaged part with a metric of the total collapse part at the end, and then build a robustness index. The approach identifies four categories of structural response for a framed structure: (i) without consequences (category C1), (ii) without collapse of the directly affected part (category C2), (iii) with collapse of the directly affected part (category C3), and (iv) with expanded collapse out of the directly affected part (category C4). This procedure enables to check if an alternative load path can be found and to follow failure propagation by identifying a directly and indirectly affected part of the structure. The initial damaged part is identified by the first iteration of the yield design calculation. The collapsed part is identified by the last iteration of the proposed modelling strategy, which represents the total part of the structure that has lost the mechanical stability under the applied loads. Hence, this simplified structural modelling method can follow the propagation of failure by identifying the initial and the final stages, which finally can be used to measure the degree of the failure propagation. Besides, it enables to model the structural response under the applied scenario (including some geometrical and materials non-linearities) with a reasonable computation time and then to consider a large number of scenarios. Indeed, it was observed in previous works that the majority of proposed robustness indices are related to only one scenario that can be threat-dependent or threat-independent, where there is one value of the robustness index for each scenario. Such indices might fail to evaluate the structural robustness in a general manner

based on several significant scenarios. The objective was then to consider various multiple scenarios and to identify those with highest propagation. When comparing several design options, it has been shown how the number of elements that are removed can change the ranking order of options based on the degree of propagation. The Robustness Propagation Failure Index (*RPMI*) has then been proposed with the aim to quantify the largest propagation extent among all scenarios of local failure occurrence.

I.3 HOW TO ASSESS THE MAXIMUM STRUCTURAL CAPACITY WITH RESPECT TO SOME PERFORMANCE CRITERIA?

By relating the applied local failure scenarios to some criterion such as the energy required to cause such failure, one aims to characterize the scenario itself and provide a magnitude of the worst-case scenario (considering the state after failure propagation). This strategy aims to capture the magnitude of local failure and characterize the adopted scenarios to evaluate the subsequent structural response.

In the proposed approach, the required energy to cause the failure (and loss) of an element (exceptional event) is equal to the external work done by the load of action to reach the ultimate strain of the material. The energy is calculated according to different types of actions such as distributed loads that can represent the effect of an explosion action, or a concentrated load that can represent the effect of an impact. A non-linear static analysis is performed to calculate the energy of the corresponding local failure scenario. It was shown how one load type can be sufficient to perform a relative comparison of cross-sections, based on an energy-based approach, as there is some proportional ratio among energy levels. In fact, the characterization of the local failure scenarios aims to provide a quantitative indication of the magnitude of local failure. The Robustness Energy Index (*REI(UC)*), equal to the minimum energy value of the critical scenarios (based on a threshold *UC*), identifies the lowest magnitude of local failure scenarios that lead to an unacceptable collapse, based on some criteria defined beforehand. In other words, it indicates the maximum capacity of a structure to withstand exceptional events by identifying those events that are relatively not significant in magnitude but lead to an unacceptable collapse. As for the Robustness Propagation Failure Index (*RPMI*), the Robustness Energy Index (*REI(UC)*) was used to discriminate several design configurations.

The above mentioned criteria, based on propagation extent or energy related to initial failure scenario have been considered separately, and also simultaneously since robustness can be understood as a combined research of minimal causes with maximal consequences. A some methodology relying on the concepts of multi-objective optimization has been proposed in this direction to find scenarios with minimal initial magnitude (based on energy or part of

the structure initially affected) and maximal extent (based on failure propagation, or part of the structure that failed at the end). In particular, when minimizing the energy requested for initial failure, there is no need to define any threshold in advance. Such Pareto front was determined for the steel framed structure considered as illustration and it was shown how a finite set of scenarios can be identified (most critical scenarios being the non dominated Pareto front) for a set of objective functions. When considering several strengthening options, Pareto fronts were compared and the sorting process was used to give a clue on the robustness levels of each option.

I.4 GENERAL PERSPECTIVES

The discussion on the obtained results shows the need for future research, considering main assumptions, and the potential for future developments in link with the current works in the scientific and engineering communities on the topic of robustness. It should be noted that this dissertation includes several parts in the proposed framework that can be used in an independent way.

In the frame case study considered for illustration of the proposed approach, the affected part was each time isolated for non-linear analysis with a simplified modelling of the joints at the edges. This modelling obviously requires some further development as the omission of the rotations of the supports in the sub-structure can cause an error in the prediction of the deflection. Also, including the displacement of the indirectly affected part should be considered to properly take into account P-delta effects. Several research works in the literature have already developed macromodels for modelling in an accurate way the response of supports in submodels and integration of these developments in the proposed framework represents an interesting perspective. Also, some analytical methods (Demonceau, 2008; Huvelle et al., 2015) are proposed in the literature to predict the response of a frame structure submitted to a column loss with isolating the directly affected part. As these methods enable to identify the geometrical deformation under the applied loads, they can replace the iteration of the non-linear analysis in the proposed iterative strategy, which may significantly reduce the computation cost.

The methodology was applied to steel framed structures. An application to other materials such as reinforced concrete elements should be considered to investigate the potential of coupling between the yield design theory and non-linear analyses. Future research is needed to test other non-linear finite element models (with different formulations, Lagrangian, updated Lagrangian and corotational) and/or adapt the iterative coupling strategy for different types of materials. Indeed, this is a great challenge to illustrate how failure might propagate in different ways for different construction materials and how the proposed

approach could capture these differences. Nutal (2014) previously proposed a comparative study between steel and concrete structures by investigating the behaviour in case of a column loss for two identical buildings (same geometry and applied loads) with different construction materials. Similar application should be considered for the proposed modelling approach as a necessary continuation of this research work.

In this dissertation, only two-dimension simulations were considered to investigate how some non-linear catenary actions can be introduced in a simplified modelling when following progressive collapse. Out-plane instabilities were not taken into account in the verifications. As mentioned above, further two-dimension simulations are still needed to improve the structural modelling, the choice in the numerical modelling and assumptions when discretizing substructures as failure propagates to help streamline the input assumptions and convergence efficiency before considering three-dimension run in the future.

This work aims to be used in the future, either by providing some recommendations on design for robustness (for example tying approach, membrane actions, calculation rules) based on prior calculation using the proposed approach (no calculation needed for low consequence class) or by integrating calculations for high consequence class with full risk analysis, in link with the evolution of standards (revision of Eurocodes related to robustness, development of technical recommendations for robustness for *fib* Model Code 2020). Also, even if the proposed concepts were illustrated throughout this dissertation with a framed building structure at a design stage, the approach intends to be applicable for other types of structures such as bridges, not only for the design stage, but also during the life-cycle of an existing structure, when robustness issues are at stake.

REFERENCES

- Adam, J.M., Parisi, F., Sagaseta, J., Lu, X., 2018. Research and practice on progressive collapse and robustness of building structures in the 21st century. *Engineering Structures* 173, 122–149. <https://doi.org/10.1016/j.engstruct.2018.06.082>
- Agarwal, J., Blockley, D., Woodman, N., 2003. Vulnerability of structural systems. *Structural Safety* 25, 263–286. [https://doi.org/10.1016/S0167-4730\(02\)00068-1](https://doi.org/10.1016/S0167-4730(02)00068-1)
- Agarwal, J., England, J., 2008. Recent developments in robustness and relation with risk. *Proceedings of the Institution of Civil Engineers - Structures and Buildings* 161, 183–188. <https://doi.org/10.1680/stbu.2008.161.4.183>
- AlHafian, S., 2013. *Seismic Progressive Collapse of Reinforced Concrete Frame Structures using the Applied Element Method*. Heriot-Watt University.
- Alsafadie, R., Hjiij, M., Battini, J.-M., 2011. Three-dimensional formulation of a mixed corotational thin-walled beam element incorporating shear and warping deformation. *Thin-Walled Structures* 49, 523–533. <https://doi.org/10.1016/j.tws.2010.12.002>
- American Society of Civil Engineers (ASCE), 2016. *Minimum design loads and associated criteria for buildings and other structures (ASCE/SEI 7-16)*.
- Anderies, J.M., Janssen, M.A., Ostrom, E., 2004. A framework to analyze the robustness of social-ecological systems from an institutional perspective.
- ArcelorMittal, 2018a. *Sections and Merchant Bars*.
- ArcelorMittal, 2018b. *Square hollow structural sections*.
- Arup, 2011. *Review of international research on structural robustness and disproportionate collapse*. Department for Communities and Local Government, and Centre for the Protection of National Infrastructure, London.

- Azéma, E., Radjaï, F., Peyroux, R., Richefeu, V., Saussine, G., 2008. Short-time dynamics of a packing of polyhedral grains under horizontal vibrations. *Eur. Phys. J. E* 26, 327–335. <https://doi.org/10.1140/epje/i2007-10331-0>
- Babazadeh, A., Burgueño, R., Silva, P.F., 2016. P- δ Effects on the Plastic Region of RC Bridge Columns: Closed-Form Solution. *Journal of Structural Engineering* 142, 04016116. [https://doi.org/10.1061/\(ASCE\)ST.1943-541X.0001595](https://doi.org/10.1061/(ASCE)ST.1943-541X.0001595)
- Baker, J.F., Williams, E.L., Lax, D., 1948. The design of framed buildings against high explosive bombs, in: *The Civil Engineer in War: Properties of Materials, Structures, Hydraulics, Tunnelling and Surveying*. pp. 80–112. <https://doi.org/10.1680/tceiwv2.45170>
- Baker, J.W., Schubert, M., Faber, M.H., 2008. On the assessment of robustness. *Structural Safety* 30, 253–267. <https://doi.org/10.1016/j.strusafe.2006.11.004>
- Bao, Y., Kunnath, S.K., El-Tawil, S., Lew, H.S., 2008. Macromodel-Based Simulation of Progressive Collapse: RC Frame Structures. *Journal of Structural Engineering* 134, 1079–1091. [https://doi.org/10.1061/\(ASCE\)0733-9445\(2008\)134:7\(1079\)](https://doi.org/10.1061/(ASCE)0733-9445(2008)134:7(1079))
- Bao, Y., Main, J.A., Lew, H.S., Sadek, F., 2014. Robustness Assessment of RC Frame Buildings under Column Loss Scenarios, in: *Structures Congress 2014*. Presented at the Structures Congress 2014, American Society of Civil Engineers, Boston, Massachusetts, United States, pp. 988–1001. <https://doi.org/10.1061/9780784413357.088>
- Biggs, M.C., 1975. *Constrained Minimization Using Recursive Quadratic Programming. Towards Global Optimization* (L.C.W. Dixon and G.P. Szergo, eds.) 341–349.
- Biondini, F., Frangopol, D.M., Restelli, S., 2008. On Structural Robustness, Redundancy, and Static Indeterminacy, in: *Structures Congress 2008*. Presented at the Structures Congress 2008, American Society of Civil Engineers, Vancouver, British Columbia, Canada, pp. 1–10. [https://doi.org/10.1061/41016\(314\)237](https://doi.org/10.1061/41016(314)237)
- Bleyer, J., 2015. *Méthodes numériques pour le calcul à la rupture des structures de génie civil*. Paris-Est University, Doctoral School of Sciences, Ingénierie et Environnement.
- Bleyer, J., de Buhan, P., 2013. Yield surface approximation for lower and upper bound yield design of 3D composite frame structures. *Computers & Structures* 129, 86–98. <https://doi.org/10.1016/j.compstruc.2013.08.011>
- Bontempi, F., Giuliani, L.G., Gkoumas, K., 2007. Handling the exceptions: Robustness assessment of a complex structural system. *Proceedings of the 3rd international conference on structural engineering, mechanics and computation (SEMC 2007)* 1747–1752.

-
- Botte, W., Caspeele, R., Gouverneur, D., Taerwe, L., 2014. Influence of membrane action on robustness indicators and a global resistance factor design, in: *Bridge Maintenance, Safety, Management and Life Extension*. CRC Press, pp. 2038–2046. <https://doi.org/10.1201/b17063-315>
- Brett, C., Lu, Y., 2013. Assessment of robustness of structures: Current state of research. *Frontiers of Structural and Civil Engineering* 7, 356–368. <https://doi.org/10.1007/s11709-013-0220-z>
- Briscoe, T., 1997. Robust Parsing, in: *Survey of the State of the Art in Human Language Technology*. Cambridge University Press and Giardini, p. 513.
- Brozzetti, J., 1996. EUROCODE 3 CALCUL DES STRUCTURES EN ACIER. Partie 1-1, Règles générales et règles pour les bâtiments.
- Byrd, R.H., Gilbert, J.C., Nocedal, J., 2000. A trust region method based on interior point techniques for nonlinear programming. *Math. Program.* 89, 149–185. <https://doi.org/10.1007/PL00011391>
- Carlson, J.M., Doyle, J., 2002. Complexity and robustness.
- Cavaco, E.S., Neves, L.A.C., Casas, J.R., 2018. On the robustness to corrosion in the life cycle assessment of an existing reinforced concrete bridge. *Structure and Infrastructure Engineering* 14, 137–150. <https://doi.org/10.1080/15732479.2017.1333128>
- Chen, Y.-L., Huang, L., Lu, Y.-Q., Deng, L., Tan, H.-Z., 2016. Assessment of Structural Robustness under Different Events according to Vulnerability. *Journal of Performance of Constructed Facilities* 30, 04016004. [https://doi.org/10.1061/\(ASCE\)CF.1943-5509.0000854](https://doi.org/10.1061/(ASCE)CF.1943-5509.0000854)
- COST Action TU0601, 2011. Robustness of Structures-THEORETICAL FRAMEWORK ON STRUCTURAL ROBUSTNESS.
- Cundall, P.A., Strack, O.D.L., 1979. A discrete numerical model for granular assemblies. *Géotechnique* 29, 47–65. <https://doi.org/10.1680/geot.1979.29.1.47>
- DCLG, 2013. The building regulations 2010 - structure: approved document A.
- de Buhan, P., 2007. Plasticité et calcul à la rupture.
- Deb, K., Pratap, A., Agarwal, S., Meyarivan, T., 2002. A fast and elitist multiobjective genetic algorithm: NSGA-II. *IEEE Trans. Evol. Computat.* 6, 182–197. <https://doi.org/10.1109/4235.996017>

- Demonceau, J.-F., 2008. Steel and composite building frames: sway response under conventional loading and development of membrane effects in beams further to an exceptional action. University of Liege.
- Demonceau, J.-F., D'Antimo, M., Jaspard, J.-P., 2018. Robustness of steel structures subjected to a column loss scenario. Presented at the 6th International Symposium on Life-Cycle Civil Engineering, Ghent, Belgium.
- Desprez, C.A., 2010. Analyse et Réduction de la Vulnérabilité Sismique des Structures Existantes : Renforcement par Collage de Tissus de Fibres de Carbone (TFC). Grenoble University-Institut Polytechnique de Grenoble.
- Dinu, F., Marginean, I., Dubina, D., 2017. Experimental testing and numerical modelling of steel moment-frame connections under column loss. *Engineering Structures* 151, 861–878. <https://doi.org/10.1016/j.engstruct.2017.08.068>
- Droogné, D., Botte, B., Caspeepele, R., Taerwe, L., 2016. Quantitative evaluation of Eurocode provisions with respect to structural robustness on the basis of numerical analysis of RC beams including membrane action. Presented at the Fib symposium 2016, Cape Town, South Africa.
- Droogné, D., Botte, W., Caspeepele, R., 2018. A multilevel calculation scheme for risk-based robustness quantification of reinforced concrete frames. *Engineering Structures* 160, 56–70. <https://doi.org/10.1016/j.engstruct.2017.12.052>
- El Hajj Diab, M., Orcesi, A., Desprez, C., Bleyer, J., 2019a. An embedded yield design approach within a non-linear analysis for structural modeling of progressive collapse. Presented at the RILEM spring convention and sustainable materials, systems and structures conference, Rovinj, Croatia.
- El Hajj Diab, M., Orcesi, A., Desprez, C., Bleyer, J., 2019b. A scenario-based procedure for structural robustness assessment. Presented at the IABSE symposium 2019 Guimarães, towards a resilient built environment - risk and asset management, Guimarães, Portugal.
- Elsanadedy, H.M., Almusallam, T.H., Al-Salloum, Y.A., Abbas, H., 2017. Investigation of precast RC beam-column assemblies under column-loss scenario. *Construction and Building Materials* 142, 552–571. <https://doi.org/10.1016/j.conbuildmat.2017.03.120>
- EN 1990, 2003. EN 1990: Eurocode - basis of structural design.
- Faber, M.H., 2007. Risk and Safety in Civil Engineering.
- Faber, M.H., Maes, M.A., Straub, D., Baker, J., 2006. On the Quantification of Robustness of Structures, in: Volume 3: Safety and Reliability; Materials Technology; Douglas Faulkner Symposium on Reliability and Ultimate Strength of Marine Structures.

-
- Presented at the 25th International Conference on Offshore Mechanics and Arctic Engineering, ASME, Hamburg, Germany, pp. 79–87.
<https://doi.org/10.1115/OMAE2006-92095>
- Fallon, C.T., Quiel, S.E., Naito, C.J., 2016. Uniform Pushdown Approach for Quantifying Building-Frame Robustness and the Consequence of Disproportionate Collapse. *Journal of Performance of Constructed Facilities* 30, 04016060.
[https://doi.org/10.1061/\(ASCE\)CF.1943-5509.0000912](https://doi.org/10.1061/(ASCE)CF.1943-5509.0000912)
- Fang, Z.-X., Li, H.-Q., 2009. Robustness of engineering structures and its role in risk mitigation. *Civil Engineering and Environmental Systems* 26, 223–230.
<https://doi.org/10.1080/10286600802058975>
- Fascetti, A., Kunnath, S.K., Nisticò, N., 2015. Robustness evaluation of RC frame buildings to progressive collapse. *Engineering Structures* 86, 242–249.
<https://doi.org/10.1016/j.engstruct.2015.01.008>
- fib, 2012. Model Code 2010 - Final draft, Volume 2.
- fib bulletin 82, 2017. Precast segmental bridges.
- Filippou, F.C., Constantinides, M., 2004. FEDEASLab getting started guide and simulation examples. Technical report NEEsgrid-TR22.
- Frangopol, D., Nakib, R., 1991. Redundancy in highway bridges. *Engineering Journal* 45–50.
- Frangopol, D.M., Curley, J.P., 1987. Effects of Damage and Redundancy on Structural Reliability. *Journal of Structural Engineering* 113, 1533–1549.
[https://doi.org/10.1061/\(ASCE\)0733-9445\(1987\)113:7\(1533\)](https://doi.org/10.1061/(ASCE)0733-9445(1987)113:7(1533))
- Franz-Josef, U.L.M., 1996. Un modèle d'endommagement plastique: application aux bétons de structure. Laboratoire central des ponts et chaussées.
- Fu, G., 1987. Modeling of lifetime structural system reliability (No. 87–9). Department of Civil Engineering, Case Western Reserve University, Cleveland.
- Fu, G., Frangopol, D.M., 1990. Balancing weight, system reliability and redundancy in a multiobjective optimization framework. *Structural Safety* 7, 165–175.
[https://doi.org/10.1016/0167-4730\(90\)90066-X](https://doi.org/10.1016/0167-4730(90)90066-X)
- Furuta, H., Shinozuka, M., Yao, J.T., 1985. Probabilistic and Fuzzy Representation of Redundancy in Structural Systems. Presented at the First International Fuzzy Systems Associated Congress, Palma de Mallorca, Spain.
- Ghosn, M., Dueñas-Osorio, L., Frangopol, D.M., McAllister, T.P., Bocchini, P., Manuel, L., Ellingwood, B.R., Arangio, S., Bontempi, F., Shah, M., Akiyama, M., Biondini, F., Hernandez, S., Tsiatas, G., 2016. Performance Indicators for Structural Systems and

- Infrastructure Networks. *Journal of Structural Engineering* 142, F4016003. [https://doi.org/10.1061/\(ASCE\)ST.1943-541X.0001542](https://doi.org/10.1061/(ASCE)ST.1943-541X.0001542)
- Griffiths, H., Pugsley, A., Saunders, O., 1968. Report of the Inquiry into the Collapse of Flats at Ronan Point, Canning Town.
- Grujicic, M., Snipes, J.S., Ramaswami, S., Yavari, R., 2013. Discrete Element Modeling and Analysis of Structural Collapse/Survivability of a Building Subjected to Improvised Explosive Device (IED) Attack. *Advances in Materials Science and Applications* 2, 9–24. <https://doi.org/10.5963/AMSA0201002>
- GSA, 2013. Alternative path analysis and design guidelines for progressive collapse resistance.
- GSA, 2003. Progressive Collapse Analysis and Design Guidelines for New Federal Office Buildings and Major Modernization Projects. Washington, DC: Office of Chief Architects.
- Gu, X., Wang, X., Yin, X., Lin, F., Hou, J., 2014. Collapse simulation of reinforced concrete moment frames considering impact actions among blocks. *Engineering Structures* 65, 30–41. <https://doi.org/10.1016/j.engstruct.2014.01.046>
- Guo, L., Gao, S., Fu, F., 2015. Structural performance of semi-rigid composite frame under column loss. *Engineering Structures* 95, 112–126. <https://doi.org/10.1016/j.engstruct.2015.03.049>
- Guo, L., Gao, S., Fu, F., Wang, Y., 2013. Experimental study and numerical analysis of progressive collapse resistance of composite frames. *Journal of Constructional Steel Research* 89, 236–251. <https://doi.org/10.1016/j.jcsr.2013.07.006>
- Haberland, M., 2007a. Progressive collapse and robustness. Structural Analysis and Steel structures Institute.
- Haberland, M., 2007b. Progressiver Kollaps und Robustheit (Progressive collapse and robustness). Hamburg University of Technology, Structural Analysis and Steel Structures Institute.
- Han, S.P., 1977. A globally convergent method for nonlinear programming. *J Optim Theory Appl* 22, 297–309. <https://doi.org/10.1007/BF00932858>
- Hoffmann, N., Kuhlmann, U., Demonceau, J.-F., Jaspard, J.-P., Colomer, C., Hoffmeister, B., Zandonini, R., Hjiiaj, M., Mohler, C., 2015. Robust Impact Design of Steel and Composite Buildings. *IABSE Symposium Report* 103, 38–45. <https://doi.org/10.2749/222137815815622663>

-
- Huber, P.J., 1996. Robust statistical procedures, 2nd ed. ed, CBMS-NSF regional conference series in applied mathematics. Society for Industrial and Applied Mathematics, Philadelphia.
- Huber, P.J., Ronchetti, E.M., 2009. Robust Statistics, Wiley Series in Probability and Statistics. John Wiley & Sons, Inc., Hoboken, NJ, USA. <https://doi.org/10.1002/9780470434697>
- Huvelle, C., 2011. Contribution à l'étude de la robustesse des structures de bâtiments - Prise en compte de la plastification progressive de la partie de la structure "non directement affectée" par l'événement exceptionnel considéré.
- Huvelle, C., Hoang, V.-L., Jaspard, J.-P., Demonceau, J.-F., 2015. Complete analytical procedure to assess the response of a frame submitted to a column loss. *Engineering Structures* 86, 33–42. <https://doi.org/10.1016/j.engstruct.2014.12.018>
- Insua, D.R., Ruggeri, F., 2000. Robust Bayesian Analysis, Lecture Notes in Statistics. Springer New York, New York, NY. <https://doi.org/10.1007/978-1-4612-1306-2>
- Izzuddin, B.A., Vlassis, A.G., Elghazouli, A.Y., Nethercot, D.A., 2008. Progressive collapse of multi-storey buildings due to sudden column loss — Part I: Simplified assessment framework. *Engineering Structures* 30, 1308–1318. <https://doi.org/10.1016/j.engstruct.2007.07.011>
- Izzuddin, B.A., Vlassis, A.G., Elghazouli, A.Y., Nethercot OBE, D.A., 2007. Assessment of progressive collapse in multi-storey buildings. *Proceedings of the Institution of Civil Engineers - Structures and Buildings* 160, 197–205. <https://doi.org/10.1680/stbu.2007.160.4.197>
- Janssens, V.M., 2012. Modelling Progressive Collapse in Steel Structures. Trinity College Dublin.
- Jaspard, J.P., Demonceau, J.F., Ludivine, C., 2011. Robustness of steel and composite building structures. Presented at the 7th National conference on steel structures, Grèce Volos.
- JCSS, 2008. Risk assessment in engineering – principles, system representation and risk criteria.
- Johnson, E.S., Meissner, J.E., Fahnestock, L.A., 2016. Experimental Behavior of a Half-Scale Steel Concrete Composite Floor System Subjected To Column Removal Scenarios. *Journal of Structural Engineering* 142, 04015133. [https://doi.org/10.1061/\(ASCE\)ST.1943-541X.0001398](https://doi.org/10.1061/(ASCE)ST.1943-541X.0001398)
- Juster-Lermitte, S., 2010. Benchmark SMART 2008, phase 1, Synthetics results report.

- Kagho Gouadjio, N.C., 2013. Etude de la vulnérabilité et de la robustesse des ouvrages (Study of vulnerability and robustness of structures). Paris-Est University.
- Kazemi-Moghaddam, A., Sasani, M., 2015. Progressive collapse evaluation of Murrah Federal Building following sudden loss of column G20. *Engineering Structures* 89, 162–171. <https://doi.org/10.1016/j.engstruct.2015.02.003>
- Khandelwal, K., El-Tawil, S., 2011. Pushdown resistance as a measure of robustness in progressive collapse analysis. *Engineering Structures* 33, 2653–2661. <https://doi.org/10.1016/j.engstruct.2011.05.013>
- Khandelwal, K., El-Tawil, S., 2008. Assessment of Progressive Collapse Residual Capacity Using Pushdown Analysis, in: *Structures Congress 2008*. Presented at the Structures Congress 2008, American Society of Civil Engineers, Vancouver, British Columbia, Canada, pp. 1–8. [https://doi.org/10.1061/41016\(314\)94](https://doi.org/10.1061/41016(314)94)
- Knoll, F., Vogel, T., 2009. Design for robustness.
- Kokot, S., Anthoine, A., Negro, P., Solomos, G., 2012. Static and dynamic analysis of a reinforced concrete flat slab frame building for progressive collapse. *Engineering Structures* 40, 205–217. <https://doi.org/10.1016/j.engstruct.2012.02.026>
- Korndorfer, J., Hoffmeister, B., Feldmann, M., Heng, P., Hjiiaj, M., 2015. Robust impact design of steel and composite buildings Advances in the Residual Strength Method. IABSE Symposium Report 103, 54–61.
- Kouvelis, P., Yu, G., 1997. Robust discrete optimization and its applications, Nonconvex optimization and its applications. Kluwer Academic Publishers, Dordrecht ; Boston.
- Kunnath, S.K., Bao, Y., El-Tawil, S., 2018. Advances in Computational Simulation of Gravity-Induced Disproportionate Collapse of RC Frame Buildings. *Journal of Structural Engineering* 144, 03117003. [https://doi.org/10.1061/\(ASCE\)ST.1943-541X.0001938](https://doi.org/10.1061/(ASCE)ST.1943-541X.0001938)
- Le, J.-L., Xue, B., 2014. Probabilistic analysis of reinforced concrete frame structures against progressive collapse. *Engineering Structures* 76, 313–323. <https://doi.org/10.1016/j.engstruct.2014.07.016>
- Le, T.N., 2013. Nonlinear dynamics of lexible structures using corotational beam elements. INSA Rennes.
- Le, T.-N., Battini, J.-M., Hjiiaj, M., 2014. Corotational formulation for nonlinear dynamics of beams with arbitrary thin-walled open cross-sections. *Computers & Structures* 134, 112–127. <https://doi.org/10.1016/j.compstruc.2013.11.005>
- Le, T.-N., Battini, J.-M., Hjiiaj, M., 2011. Efficient formulation for dynamics of corotational 2D beams. *Comput Mech* 48, 153–161. <https://doi.org/10.1007/s00466-011-0585-6>

-
- Lew, H.S., Main, J.A., Robert, S.D., Sadek, F., Chiarito, V.P., 2013. Performance of Steel Moment Connections under a Column Removal Scenario. I: Experiments. *Journal of Structural Engineering* 139, 98–107. [https://doi.org/10.1061/\(ASCE\)ST.1943-541X.0000618](https://doi.org/10.1061/(ASCE)ST.1943-541X.0000618)
- Li, S., Shan, S., Zhai, C., Xie, L., 2016. Experimental and numerical study on progressive collapse process of RC frames with full-height infill walls. *Engineering Failure Analysis* 59, 57–68. <https://doi.org/10.1016/j.engfailanal.2015.11.020>
- Li, Y., Lu, X., Guan, H., Ren, P., Qian, L., 2016. Probability-based progressive collapse-resistant assessment for reinforced concrete frame structures. *Advances in Structural Engineering* 19, 1723–1735. <https://doi.org/10.1177/1369433216649385>
- Li, Z.X., Izzuddin, B.A., Vu-Quoc, L., 2008. A 9-node co-rotational quadrilateral shell element. *Comput Mech* 42, 873–884. <https://doi.org/10.1007/s00466-008-0289-8>
- Liu, C., Tan, K.H., Fung, T.C., 2015. Investigations of nonlinear dynamic performance of top-and-seat with web angle connections subjected to sudden column removal. *Engineering Structures* 99, 449–461. <https://doi.org/10.1016/j.engstruct.2015.05.010>
- Lu, X., Lin, X., Ye, L., 2009. Simulation of Structural Collapse with Coupled Finite Element-Discrete Element Method, in: Yuan, Y., Cui, J., Mang, H.A. (Eds.), *Computational Structural Engineering*. Springer Netherlands, Dordrecht, pp. 127–135. https://doi.org/10.1007/978-90-481-2822-8_14
- Magalhães de Souza, R., 2000. Force-based Finite Element for Large Displacement Inelastic Analysis of Frames. University of California, Berkeley.
- Marchand, K.A., Alfawakhiri, F., 2005. Facts for Steel Buildings-Blast and Progressive Collapse.
- Marginean, I., Dinu, F., Dubina, D., 2018. Simulation of the dynamic response of steel moment frames following sudden column loss. Experimental calibration of the numerical model and application. *Steel Construction* 11, 57–64. <https://doi.org/10.1002/stco.201810012>
- Masoero, E., Wittel, F.K., Herrmann, H.J., Chiaia, B.M., 2012. Hierarchical Structures for a Robustness-Oriented Capacity Design. *Journal of Engineering Mechanics* 138, 1339–1347. [https://doi.org/10.1061/\(ASCE\)EM.1943-7889.0000437](https://doi.org/10.1061/(ASCE)EM.1943-7889.0000437)
- Mazars, J., Grange, S., 2017. Simplified strategies based on damage mechanics for concrete under dynamic loading. *Philosophical Transactions of the Royal Society A: Mathematical, Physical and Engineering Sciences* 375, 20160170. <https://doi.org/10.1098/rsta.2016.0170>
-

- Mazars, J., Kotronis, P., Ragueneau, F., Casaux, G., 2006. Using multifiber beams to account for shear and torsion. *Computer Methods in Applied Mechanics and Engineering* 195, 7264–7281. <https://doi.org/10.1016/j.cma.2005.05.053>
- Meyer, B., 1997. *Object-Oriented Software Construction*, 2nd ed. Interactive Software Engineering.
- Minister of Housing and Local Government, 1970. *The Building (Fifth Amendment) Regulations 1970*.
- Mohammadkhani-Shali, S., 2007. Study of systeme redundancy in bridges: failure machanism analysis using response surface methods. Ecole des Ponts ParisTech.
- Munjiza, A., Bangash, T., John, N.W.M., 2004. The combined finite–discrete element method for structural failure and collapse. *Engineering Fracture Mechanics* 71, 469–483. [https://doi.org/10.1016/S0013-7944\(03\)00044-4](https://doi.org/10.1016/S0013-7944(03)00044-4)
- Nafday, A.M., 2011. Consequence-based structural design approach for black swan events. *Structural Safety* 33, 108–114. <https://doi.org/10.1016/j.strusafe.2010.09.003>
- NF EN 1990, 2003. Basis of structural design. Comité européen de Normalisation (CEN).
- NF EN 1991-1-1, 2003. Eurocode 1, Actions on structures, Part 1-1: General actions — Densities, self weight, imposed loads for buildings.
- NF EN 1991-1-7, 2007. Eurocode 1 - Actions on structures - Part 1-7: General actions - Accidental actions. European Commlltee for Standardization (CEN).
- NF EN 1992-1-1, 2005. Design of concrete structures.
- NF EN 1993-1-1, 2005. Design of steel structures.
- Nimse, R.B., Joshi, D.D., Patel, P.V., 2014. Behavior of wet precast beam column connections under progressive collapse scenario: an experimental study. *International Journal of Advanced Structural Engineering* 6, 149–159. <https://doi.org/10.1007/s40091-014-0072-3>
- NTSB, 2008. Collapse of I-35W Highway Bridge Minneapolis, Minnesota August 1, 2007.
- Nutal, B., 2014. *Robustness of Steel and Concrete Structures*. Université de Liège.
- Orton, S.L., Kirby, J.E., 2014. Dynamic Response of a RC Frame under Column Removal. *Journal of Performance of Constructed Facilities* 28, 04014010. [https://doi.org/10.1061/\(ASCE\)CF.1943-5509.0000464](https://doi.org/10.1061/(ASCE)CF.1943-5509.0000464)
- Pearson, C., Delatte, N., 2005. Ronan Point Apartment Tower Collapse and its Effect on Building Codes. *Journal of Performance of Constructed Facilities* 172–177.

-
- Pham, D.T., 2014. Analyse par le calcul à la rupture de la stabilité au feu des panneaux en béton armé de grandes dimensions. Paris-Est University.
- Powell, M.J.D., 1978. THE CONVERGENCE OF VARIABLE METRIC METHODS FOR NONLINEARLY CONSTRAINED OPTIMIZATION CALCULATIONS, in: *Nonlinear Programming 3*. Elsevier, pp. 27–63. <https://doi.org/10.1016/B978-0-12-468660-1.50007-4>
- Qian, K., Li, B., 2017a. Effects of Masonry Infill Wall on the Performance of RC Frames to Resist Progressive Collapse. *Journal of Structural Engineering* 143, 04017118. [https://doi.org/10.1061/\(ASCE\)ST.1943-541X.0001860](https://doi.org/10.1061/(ASCE)ST.1943-541X.0001860)
- Qian, K., Li, B., 2017b. Dynamic and residual behavior of reinforced concrete floors following instantaneous removal of a column. *Engineering Structures* 148, 175–184. <https://doi.org/10.1016/j.engstruct.2017.06.059>
- Ross, C.T.F., 2001. Elastic Instability, in: *Encyclopedia of Materials: Science and Technology*. Elsevier, pp. 2425–2427. <https://doi.org/10.1016/B0-08-043152-6/00430-7>
- Rousseau, J., 2009. Modélisation numérique du comportement dynamique de structures sous impact sévère avec un couplage éléments discrets / éléments finis. Université Joseph Fourier.
- Sadek, F., El-Tawil, S., Lew, H.S., 2008. Robustness of Composite Floor Systems with Shear Connections: Modeling, Simulation, and Evaluation. *Journal of Structural Engineering* 134, 1717–1725. [https://doi.org/10.1061/\(ASCE\)0733-9445\(2008\)134:11\(1717\)](https://doi.org/10.1061/(ASCE)0733-9445(2008)134:11(1717))
- Sadek, F., Main, J.A., Lew, H.S., Bao, Y., 2011. Testing and Analysis of Steel and Concrete Beam-Column Assemblies under a Column Removal Scenario. *Journal of Structural Engineering* 137, 881–892. [https://doi.org/10.1061/\(ASCE\)ST.1943-541X.0000422](https://doi.org/10.1061/(ASCE)ST.1943-541X.0000422)
- Salençon, J., 2013. Yield design, Mechanical engineering and solid mechanics series. ISTE ; Wiley, London : Hoboken, NJ.
- Sasani, M., 2008. Response of a reinforced concrete infilled-frame structure to removal of two adjacent columns. *Engineering Structures* 30, 2478–2491. <https://doi.org/10.1016/j.engstruct.2008.01.019>
- Sasani, M., Kazemi, A., Sagioglu, S., Forest, S., 2011a. Progressive Collapse Resistance of an Actual 11-Story Structure Subjected to Severe Initial Damage. *Journal of Structural Engineering* 137, 893–902. [https://doi.org/10.1061/\(ASCE\)ST.1943-541X.0000418](https://doi.org/10.1061/(ASCE)ST.1943-541X.0000418)
- Sasani, M., Sagioglu, S., 2010. Gravity Load Redistribution and Progressive Collapse Resistance of 20-Story Reinforced Concrete Structure following Loss of Interior Column. *Structural Journal* 107. <https://doi.org/10.14359/51664011>
-

- Sasani, M., Sagioglu, S., 2008. Progressive Collapse Resistance of Hotel San Diego. *Journal of Structural Engineering* 134, 478–488. [https://doi.org/10.1061/\(ASCE\)0733-9445\(2008\)134:3\(478\)](https://doi.org/10.1061/(ASCE)0733-9445(2008)134:3(478))
- Sasani, M., Werner, A., Kazemi, A., 2011b. Bar fracture modeling in progressive collapse analysis of reinforced concrete structures. *Engineering Structures* 33, 401–409. <https://doi.org/10.1016/j.engstruct.2010.10.023>
- Scholz, H., 1990. P- Delta Effect Under Repeated Loading. *Journal of Structural Engineering* 116, 2070–2082. [https://doi.org/10.1061/\(ASCE\)0733-9445\(1990\)116:8\(2070\)](https://doi.org/10.1061/(ASCE)0733-9445(1990)116:8(2070))
- Seck, E.H.B., 2018. Contribution au développement d’outils analytiques et numériques pour quantifier et qualifier la robustesse des structures (Contribution to the development of analytical and numerical tools to quantify and qualify the robustness of structures). Paris Lumières University.
- Sétra, 2013a. Robustesse des ouvrages, in: *Maîtrise Des Risques-Application Aux Ouvrages d’art*. Service d’études sur les transports, les routes et leurs aménagements, pp. 61–88.
- Sétra, 2013b. Robustesse des ouvrages.
- Shan, S., Li, S., Xu, S., Xie, L., 2016. Experimental study on the progressive collapse performance of RC frames with infill walls. *Engineering Structures* 111, 80–92. <https://doi.org/10.1016/j.engstruct.2015.12.010>
- Slotine, J.-J.E., Li, W., 1991. *Applied Nonlinear Control*. Prentice-Hall, Englewood Cliffs, New Jersey.
- Song, B.I., Giriunas, K.A., Sezen, H., 2014. Progressive collapse testing and analysis of a steel frame building. *Journal of Constructional Steel Research* 94, 76–83. <https://doi.org/10.1016/j.jcsr.2013.11.002>
- Spacone, E., Filippou, F.C., Taucer, F.F., 1996. FIBRE BEAM-COLUMN MODEL FOR NON-LINEAR ANALYSIS OF R/C FRAMES: PART I. FORMULATION. *Earthquake Engineering & Structural Dynamics* 25, 711–725. [https://doi.org/10.1002/\(SICI\)1096-9845\(199607\)25:7<711::AID-EQE576>3.0.CO;2-9](https://doi.org/10.1002/(SICI)1096-9845(199607)25:7<711::AID-EQE576>3.0.CO;2-9)
- Starossek, U., Haberland, M., 2011. Approaches to measures of structural robustness. *Structure and Infrastructure Engineering* 7, 625–631. <https://doi.org/10.1080/15732479.2010.501562>
- Starossek, U., Haberland, M., 2010. Disproportionate Collapse: Terminology and Procedures. *Journal of Performance of Constructed Facilities* 24, 519–528. [https://doi.org/10.1061/\(ASCE\)CF.1943-5509.0000138](https://doi.org/10.1061/(ASCE)CF.1943-5509.0000138)

-
- Starossek, U., Haberland, M., 2008. Measures of Structural Robustness — Requirements and Applications, in: Structures Congress 2008. Presented at the Structures Congress 2008, American Society of Civil Engineers, Vancouver, British Columbia, Canada, pp. 1–10. [https://doi.org/10.1061/41016\(314\)235](https://doi.org/10.1061/41016(314)235)
- Stinger, S.M., Orton, S.L., 2013. Experimental Evaluation of Disproportionate Collapse Resistance in Reinforced Concrete Frames. *Structural Journal* 110. <https://doi.org/10.14359/51685609>
- Stylianidis, P., 2011. Progressive collapse response of steel and composite buildings. Department of Civil and Environmental Engineering-Imperial College London.
- Sun, R., Huang, Z., Burgess, I.W., 2012. Progressive collapse analysis of steel structures under fire conditions. *Engineering Structures* 34, 400–413. <https://doi.org/10.1016/j.engstruct.2011.10.009>
- Sunder, S.S., Gann, R.G., Grosshandler, W.L., Lew, H.S., Bukowski, R.W., Sadek, F., Gayle, F.W., Gross, J.L., McAllister, T.P., Averill, J.D., Lawson, J.R., Nelson, H.E., Cauffman, S.A., 2005. Final report on the collapse of the World Trade Center towers :: federal building and fire safety investigation of the World Trade Center disaster (No. NIST NCSTAR 1). National Institute of Standards and Technology, Gaithersburg, MD. <https://doi.org/10.6028/NIST.NCSTAR.1>
- Tagel-Din, H., 2009. High Fidelity Modeling of Building Collapse with Realistic Visualization of Resulting Damage and Debris Using the Applied Element Method.
- Tagel-Din, H., Meguro, K., 2000. Applied element method for simulation of nonlinear materials: theory and application for RC structures. *Structural Eng./Earthquake Eng., International Journal of the Japan Society of Civil Engineers (JSCE)* 17, 137–148.
- Taguchi, G., Chowdhury, S., 1999. Robust engineering – learn how to boost quality while reducing costs and time to market. McGraw Hill Professional, New York, NY.
- Takeda, T., Sozen, M.A., Neilsen, N.N., 1970. Reinforced concrete response to simulated earthquakes 96, 2557–2573.
- UFC 4-023-03, 2009. Design of buildings to resist progressive collapse.
- Vidalis, C.A., 2014. Improving the resistance to progressive collapse of steel and composite frames. Imperial College London-Department of Civil and Environmental Engineering.
- Vincent, H., Arquier, M., Bleyer, J., de Buhan, P., 2017. Yield design based numerical analysis of three-dimensional reinforced concrete structures.
- Vlassis, A.G., Izzuddin, B.A., Elghazouli, A.Y., Nethercot, D.A., 2008. Progressive collapse of multi-storey buildings due to sudden column loss—Part II: Application.

- Engineering Structures 30, 1424–1438.
<https://doi.org/10.1016/j.engstruct.2007.08.011>
- Vrouwenvelder, T., 2008. Treatment of risk and reliability in the Eurocodes. Proceedings of the Institution of Civil Engineers - Structures and Buildings 161, 209–214.
<https://doi.org/10.1680/stbu.2008.161.4.209>
- Vu, X.D., 2013. Vulnérabilité des ouvrages en béton sous impact: Caractérisation, modélisation, et validation. University of Grenoble.
- Waltz, R.A., Morales, J.L., Nocedal, J., Orban, D., 2006. An interior algorithm for nonlinear optimization that combines line search and trust region steps. Math. Program. 107, 391–408. <https://doi.org/10.1007/s10107-004-0560-5>
- Xiao, Y., Kunnath, S., Li, F.W., Zhao, Y.B., Lew, H., Bao, Y., 2015. Collapse test of three-storey half-scale reinforced concrete frame building. ACI Structural Journal 112, 429–438.
- Xue, B., Le, J.-L., 2016a. Stochastic Computational Model for Progressive Collapse of Reinforced Concrete Buildings. Journal of Structural Engineering 142, 04016031.
[https://doi.org/10.1061/\(ASCE\)ST.1943-541X.0001485](https://doi.org/10.1061/(ASCE)ST.1943-541X.0001485)
- Xue, B., Le, J.-L., 2016b. Simplified energy-based analysis of collapse risk of reinforced concrete buildings. Structural Safety 63, 47–58.
<https://doi.org/10.1016/j.strusafe.2016.07.003>
- Yi, W.-J., He, Q.-F., Xiao, Y., Kunnath, S.K., 2008. Experimental Study on Progressive Collapse-Resistant Behavior of Reinforced Concrete Frame Structures. Structural Journal 105. <https://doi.org/10.14359/19857>
- Yin, H., Shi, G., 2018. Finite element analysis on the seismic behavior of fully prefabricated steel frames. Engineering Structures 173, 28–51.
<https://doi.org/10.1016/j.engstruct.2018.06.096>
- Yu, J., Tan, K.H., 2017. Structural Behavior of Reinforced Concrete Frames Subjected to Progressive Collapse. Structural Journal 114. <https://doi.org/10.14359/51689424>
- Yu, J., Tan, K.H., 2014. Special Detailing Techniques to Improve Structural Resistance against Progressive Collapse. Journal of Structural Engineering 140, 04013077.
[https://doi.org/10.1061/\(ASCE\)ST.1943-541X.0000886](https://doi.org/10.1061/(ASCE)ST.1943-541X.0000886)
- Yu, J., Tan, K.-H., 2013. Experimental and numerical investigation on progressive collapse resistance of reinforced concrete beam column sub-assemblages. Engineering Structures 55, 90–106. <https://doi.org/10.1016/j.engstruct.2011.08.040>
- Zandonini, R., Baldassino, N., Freddi, F., 2014. Robustness of steel-concrete flooring systems - An experimental assessment: Robustness of steel-concrete flooring systems - An

experimental assessment. Stahlbau 83, 608–613.
<https://doi.org/10.1002/stab.201410192>

Zhao, X.-L., Wilkinson, T., Hancock, G., 2005. Members Subjected to Bending and Compression, in: Cold-Formed Tubular Members and Connections. Elsevier, pp. 91–116. <https://doi.org/10.1016/B978-008044101-6/50006-2>

ANNEX A

DETAILED RESULTS FOR THE STRUCTURAL ROBUSTNESS ASSESSMENT IN CHAPTER IV

This annex provides detailed results of the structural robustness investigation in Chapter IV, in particular for the five design configurations D0, D1, D2, D3 and D4 considered in Section IV.5. For each of these design configurations, Table A.1 presents the failure energy E_i relevant to each scenario i (Table IV.3), and Table A.2 details the measure of the initial damaged part $\mathcal{M}(IDP_i)$ and the collapsed part $\mathcal{M}(CP_i)$ under each scenario i .

i	D0	D1	D2	D3	D4	i	D0	D1	D2	D3	D4
1	100.4	100.4	137.6	137.6	100.4	96	166.7	166.6	261.2	261.2	166.7
2	102.1	102.1	138.7	138.7	102.1	97	173.9	173.9	266.7	265.7	173.9
3	103.8	103.8	139.8	139.8	103.8	98	197.4	197.4	272.1	271.1	197.4
4	105.4	105.4	140.8	140.8	105.4	99	204.2	204.1	276.4	276.4	204.2
5	108.6	108.6	141.9	141.9	108.6	100	210.8	210.8	281.7	281.7	210.8
6	84.2	84.2	131.2	131.2	84.2	101	184.7	184.6	268.8	268.8	184.7
7	87.8	87.8	133.4	133.4	87.8	102	190.0	189.9	272.1	272.1	190.0
8	98.8	98.8	136.6	135.6	98.8	103	202.6	202.5	276.4	275.4	202.6
9	102.1	102.1	138.7	138.7	102.1	104	207.6	207.5	279.6	279.6	207.6
10	105.4	105.4	140.8	140.8	105.4	105	214.0	214.0	282.8	282.8	214.0
11	82.5	82.4	130.1	130.0	82.5	106	267.1	267.0	398.9	398.8	267.1
12	86.1	86.1	133.3	132.3	86.1	107	276.0	276.0	405.4	404.4	276.0
13	98.6	98.6	135.5	135.5	98.6	108	301.2	301.1	411.9	410.9	301.2
14	102.0	102.0	137.7	137.7	102.0	109	309.6	309.6	417.3	417.3	309.6
15	105.4	105.4	140.8	140.8	105.4	110	319.4	319.4	423.6	423.6	319.4
16	80.6	80.6	129.0	128.9	80.6	111	247.3	247.1	390.2	390.1	247.3
17	84.4	84.3	132.2	132.2	84.4	112	258.3	258.2	398.9	397.9	258.3
18	97.0	97.0	134.5	134.5	97.0	113	294.4	294.3	406.6	405.6	294.4
19	101.9	101.9	137.7	137.7	101.9	114	306.1	306.1	414.1	414.1	306.1
20	105.4	105.4	139.9	139.9	105.4	115	316.2	316.2	421.6	421.5	316.2
21	80.6	80.6	129.0	128.9	80.6	116	243.7	243.5	388.0	387.9	243.7
22	84.4	84.3	132.2	132.2	84.4	117	254.8	254.7	397.7	396.7	254.8
23	97.0	97.0	134.5	134.5	97.0	118	292.7	292.6	404.5	404.5	292.7
24	101.9	101.9	137.7	137.7	101.9	119	305.9	305.9	413.0	413.0	305.9
25	105.4	105.4	139.9	139.9	105.4	120	316.2	316.1	420.6	420.6	316.2
26	80.6	80.6	129.0	128.9	80.6	121	241.9	241.7	386.9	386.8	241.9

Annex A: Detailed results for the structural robustness assessment in Chapter IV

27	84.4	84.3	132.2	132.2	84.4	122	253.1	253.0	396.6	396.5	253.1
28	97.0	97.0	134.5	134.5	97.0	123	291.0	291.0	403.5	403.5	291.0
29	101.9	101.9	137.7	137.7	101.9	124	305.8	305.8	413.0	413.0	305.8
30	105.4	105.4	139.9	139.9	105.4	125	316.1	316.1	419.6	419.6	316.1
31	80.6	80.6	129.0	128.9	80.6	126	241.9	241.7	386.9	386.8	241.9
32	84.4	84.3	132.2	132.2	84.4	127	253.1	253.0	396.6	396.5	253.1
33	97.0	97.0	134.5	134.5	97.0	128	291.0	291.0	403.5	403.5	291.0
34	101.9	101.9	137.7	137.7	101.9	129	305.8	305.8	413.0	413.0	305.8
35	105.4	105.4	139.9	139.9	105.4	130	316.1	316.1	419.6	419.6	316.1
36	80.6	80.6	129.0	128.9	80.6	131	241.9	241.7	386.9	386.8	241.9
37	84.4	84.3	132.2	132.2	84.4	132	253.1	253.0	396.6	396.5	253.1
38	97.0	97.0	134.5	134.5	97.0	133	291.0	291.0	403.5	403.5	291.0
39	101.9	101.9	137.7	137.7	101.9	134	305.8	305.8	413.0	413.0	305.8
40	105.4	105.4	139.9	139.9	105.4	135	316.1	316.1	419.6	419.6	316.1
41	82.5	82.4	130.1	130.0	82.5	136	243.7	243.5	388.0	387.9	243.7
42	86.1	86.1	133.3	132.3	86.1	137	254.8	254.7	397.7	396.7	254.8
43	98.6	98.6	135.5	135.5	98.6	138	292.7	292.6	404.5	404.5	292.7
44	102.0	102.0	137.7	137.7	102.0	139	305.9	305.9	413.0	413.0	305.9
45	105.4	105.4	140.8	140.8	105.4	140	316.2	316.1	420.6	420.6	316.2
46	84.2	84.2	131.2	131.2	84.2	141	247.3	247.1	390.2	390.1	247.3
47	87.8	87.8	133.4	133.4	87.8	142	258.3	258.2	398.9	397.9	258.3
48	98.8	98.8	136.6	135.6	98.8	143	294.4	294.3	406.6	405.6	294.4
49	102.1	102.1	138.7	138.7	102.1	144	306.1	306.1	414.1	414.1	306.1
50	105.4	105.4	140.8	140.8	105.4	145	316.2	316.2	421.6	421.5	316.2
51	100.4	100.4	137.6	137.6	100.4	146	267.1	267.0	398.9	398.8	267.1
52	102.1	102.1	138.7	138.7	102.1	147	276.0	276.0	405.4	404.4	276.0
53	103.8	103.8	139.8	139.8	103.8	148	301.2	301.1	411.9	410.9	301.2
54	105.4	105.4	140.8	140.8	105.4	149	309.6	309.6	417.3	417.3	309.6
55	108.6	108.6	141.9	141.9	108.6	150	319.4	319.4	423.6	423.6	319.4
56	184.7	184.6	268.8	268.8	184.7	151	347.7	347.6	527.9	527.8	347.7
57	190.0	189.9	272.1	272.1	190.0	152	360.4	360.3	537.6	536.6	360.4
58	202.6	202.5	276.4	275.4	202.6	153	398.2	398.1	546.4	545.4	398.2
59	207.6	207.5	279.6	279.6	207.6	154	411.6	411.5	555.0	554.9	411.6
60	214.0	214.0	282.8	282.8	214.0	155	424.8	424.8	563.5	563.5	424.8
61	166.7	166.6	261.2	261.2	166.7	156	327.9	327.7	519.2	519.1	327.9
62	173.9	173.9	266.7	265.7	173.9	157	342.6	342.5	531.1	530.1	342.6
63	197.4	197.4	272.1	271.1	197.4	158	391.4	391.3	541.1	540.1	391.4
64	204.2	204.1	276.4	276.4	204.2	159	408.1	408.0	551.8	551.7	408.1
65	210.8	210.8	281.7	281.7	210.8	160	421.6	421.6	561.4	561.4	421.6
66	163.1	163.0	259.0	259.0	163.1	161	324.3	324.1	517.0	516.8	324.3
67	170.4	170.4	265.5	264.5	170.4	162	339.2	339.1	529.9	528.9	339.2
68	195.7	195.6	270.0	270.0	195.7	163	389.7	389.6	539.0	539.0	389.7
69	204.0	204.0	275.4	275.4	204.0	164	407.9	407.8	550.7	550.7	407.9
70	210.8	210.8	280.7	280.7	210.8	165	421.6	421.5	560.4	560.4	421.6
71	161.2	161.1	257.9	257.9	161.2	166	322.5	322.2	515.9	515.8	322.5
72	168.7	168.7	264.4	264.4	168.7	167	337.5	337.3	528.9	528.7	337.5
73	194.0	194.0	269.0	269.0	194.0	168	388.1	387.9	538.0	538.0	388.1
74	203.9	203.9	275.3	275.3	203.9	169	407.8	407.7	550.7	550.6	407.8
75	210.8	210.7	279.7	279.7	210.8	170	421.5	421.5	559.4	559.4	421.5
76	161.2	161.1	257.9	257.9	161.2	171	322.5	322.2	515.9	515.8	322.5
77	168.7	168.7	264.4	264.4	168.7	172	337.5	337.3	528.9	528.7	337.5
78	194.0	194.0	269.0	269.0	194.0	173	388.1	387.9	538.0	538.0	388.1
79	203.9	203.9	275.3	275.3	203.9	174	407.8	407.7	550.7	550.6	407.8
80	210.8	210.7	279.7	279.7	210.8	175	421.5	421.5	559.4	559.4	421.5
81	161.2	161.1	257.9	257.9	161.2	176	324.3	324.1	517.0	516.8	324.3
82	168.7	168.7	264.4	264.4	168.7	177	339.2	339.1	529.9	528.9	339.2
83	194.0	194.0	269.0	269.0	194.0	178	389.7	389.6	539.0	539.0	389.7
84	203.9	203.9	275.3	275.3	203.9	179	407.9	407.8	550.7	550.7	407.9

85	210.8	210.7	279.7	279.7	210.8	180	421.6	421.5	560.4	560.4	421.6
86	161.2	161.1	257.9	257.9	161.2	181	327.9	327.7	519.2	519.1	327.9
87	168.7	168.7	264.4	264.4	168.7	182	342.6	342.5	531.1	530.1	342.6
88	194.0	194.0	269.0	269.0	194.0	183	391.4	391.3	541.1	540.1	391.4
89	203.9	203.9	275.3	275.3	203.9	184	408.1	408.0	551.8	551.7	408.1
90	210.8	210.7	279.7	279.7	210.8	185	421.6	421.6	561.4	561.4	421.6
91	163.1	163.0	259.0	259.0	163.1	186	347.7	347.6	527.9	527.8	347.7
92	170.4	170.4	265.5	264.5	170.4	187	360.4	360.3	537.6	536.6	360.4
93	195.7	195.6	270.0	270.0	195.7	188	398.2	398.1	546.4	545.4	398.2
94	204.0	204.0	275.4	275.4	204.0	189	411.6	411.5	555.0	554.9	411.6
95	210.8	210.8	280.7	280.7	210.8	190	424.8	424.8	563.5	563.5	424.8

Table A.1: Energy $E_i(kJ)$ required to cause the local failure of scenario i for design configurations D0, D1, D2, D3 and D4 (see Table IV.3 for identification of removed column(s)).

i	D0		D1		D2		D3		D4	
	$\mathcal{M}(IDP_i)$ (m)	$\mathcal{M}(CP_i)$ (m)								
1	0	0	0	0	0	0	0	0	0	0
2	0	0	0	0	0	0	0	0	0	0
3	0	0	0	0	0	0	0	0	0	0
4	0	0	0	0	0	0	0	0	0	0
5	5	5	0	0	5	5	0	0	5	5
6	0	0	0	0	0	0	0	0	0	0
7	0	0	0	0	0	0	0	0	0	0
8	0	0	0	0	0	0	0	0	0	0
9	0	0	0	0	0	0	0	0	0	0
10	0	0	0	0	0	0	0	0	0	0
11	55	0	0	0	55	0	0	0	0	0
12	44	0	0	0	44	0	0	0	0	0
13	33	0	0	0	33	0	0	0	0	0
14	22	0	0	0	22	0	0	0	0	0
15	11	0	0	0	11	0	0	0	11	0
16	60	0	0	0	60	0	0	0	60	0
17	48	0	0	0	48	0	0	0	48	0
18	36	0	0	0	36	0	0	0	36	0
19	24	0	0	0	24	0	0	0	24	0
20	12	0	0	0	12	0	0	0	12	0
21	60	0	0	0	60	0	0	0	60	0
22	48	0	0	0	48	0	0	0	48	0
23	36	0	0	0	36	0	0	0	36	0
24	24	0	0	0	24	0	0	0	24	0
25	12	0	0	0	12	0	0	0	12	0
26	60	0	0	0	60	0	0	0	60	0
27	48	0	0	0	48	0	0	0	48	0
28	36	0	0	0	36	0	0	0	36	0
29	24	0	0	0	24	0	0	0	24	0
30	12	0	0	0	12	0	0	0	12	0
31	60	0	0	0	60	0	0	0	60	0
32	48	0	0	0	48	0	0	0	48	0
33	36	0	0	0	36	0	0	0	36	0
34	24	0	0	0	24	0	0	0	24	0
35	12	0	0	0	12	0	0	0	12	0
36	60	0	0	0	60	0	0	0	60	0
37	48	0	0	0	48	0	0	0	48	0
38	36	0	0	0	36	0	0	0	36	0
39	24	0	0	0	24	0	0	0	24	0
40	12	0	0	0	12	0	0	0	12	0
41	55	0	0	0	55	0	0	0	0	0
42	44	0	0	0	44	0	0	0	0	0
43	33	0	0	0	33	0	0	0	0	0
44	22	0	0	0	22	0	0	0	0	0

Annex A: Detailed results for the structural robustness assessment in Chapter IV

45	11	0	0	0	11	0	0	0	11	0
46	0	0	0	0	0	0	0	0	0	0
47	0	0	0	0	0	0	0	0	0	0
48	0	0	0	0	0	0	0	0	0	0
49	0	0	0	0	0	0	0	0	0	0
50	0	0	0	0	0	0	0	0	0	0
51	0	0	0	0	0	0	0	0	0	0
52	0	0	0	0	0	0	0	0	0	0
53	0	0	0	0	0	0	0	0	0	0
54	0	0	0	0	0	0	0	0	0	0
55	5	5	0	0	5	5	0	0	5	5
56	50	50	0	0	50	50	0	0	0	0
57	40	40	0	0	40	40	0	0	0	0
58	30	30	0	0	30	30	0	0	0	0
59	20	20	20	20	20	20	20	20	0	0
60	10	10	10	10	10	10	10	10	10	10
61	80	80	0	0	80	80	0	0	0	0
62	64	64	0	0	64	69	0	0	0	0
63	48	48	0	0	48	53	0	0	0	0
64	32	32	0	0	32	37	0	0	0	0
65	16	16	0	0	16	0	0	0	16	16
66	85	110	0	0	85	110	0	0	85	110
67	68	88	0	0	68	98	0	0	68	88
68	51	66	0	0	51	76	0	0	51	0
69	34	44	0	0	34	0	0	0	34	0
70	17	0	0	0	17	0	0	0	17	0
71	90	140	0	0	90	140	0	0	90	140
72	72	128	0	0	72	128	0	0	72	128
73	54	100	0	0	54	100	0	0	54	0
74	36	0	0	0	36	0	0	0	36	0
75	18	0	18	0	18	0	18	0	18	0
76	90	170	0	0	90	170	0	0	90	170
77	72	158	0	0	72	158	0	0	72	0
78	54	124	0	0	54	0	0	0	54	0
79	36	0	0	0	36	0	0	0	36	0
80	18	0	18	0	18	0	18	0	18	0
81	90	170	0	0	90	170	0	0	90	170
82	72	158	0	0	72	158	0	0	72	0
83	54	124	0	0	54	0	0	0	54	0
84	36	0	0	0	36	0	0	0	36	0
85	18	0	18	0	18	0	18	0	18	0
86	90	140	0	0	90	140	0	0	90	140
87	72	128	0	0	72	128	0	0	72	128
88	54	100	0	0	54	100	0	0	54	0
89	36	0	0	0	36	0	0	0	36	0
90	18	0	18	0	18	0	18	0	18	0
91	85	110	0	0	85	110	0	0	85	110
92	68	88	0	0	68	98	0	0	68	88
93	51	66	0	0	51	76	0	0	51	0
94	34	44	0	0	34	0	0	0	34	0
95	17	0	0	0	17	0	0	0	17	0
96	80	80	0	0	80	80	0	0	0	0
97	64	64	0	0	64	69	0	0	0	0
98	48	48	0	0	48	53	0	0	0	0
99	32	32	0	0	32	37	0	0	0	0
100	16	16	0	0	16	0	0	0	16	16
101	50	50	0	0	50	50	0	0	0	0
102	40	40	0	0	40	40	0	0	0	0
103	30	30	0	0	30	30	0	0	0	0
104	20	20	20	20	20	20	20	20	0	0
105	10	10	10	10	10	10	10	10	10	10
106	80	80	80	80	80	80	80	80	80	80
107	64	64	64	64	64	64	64	64	64	64
108	48	48	48	48	48	48	48	48	48	48

Annex A: Detailed results for the structural robustness assessment in Chapter IV

109	32	32	32	32	32	32	32	32	32	32
110	16	16	16	16	16	16	16	16	16	16
111	110	110	110	110	110	110	110	110	110	110
112	88	88	88	88	88	93	88	88	88	88
113	66	66	66	66	66	71	66	66	66	66
114	44	44	44	44	44	49	44	44	44	44
115	22	22	22	22	22	22	22	22	22	22
116	115	140	115	140	115	140	115	140	115	140
117	92	112	92	112	92	122	92	112	92	112
118	69	84	69	84	69	94	69	84	69	84
119	46	56	46	56	46	66	46	0	46	56
120	23	28	23	0	23	0	23	0	23	0
121	120	170	120	170	120	170	120	170	120	170
122	96	152	96	136	96	152	96	152	96	152
123	72	118	72	102	72	118	72	0	72	118
124	48	68	48	0	48	84	48	0	48	0
125	24	0	24	0	24	0	24	0	24	0
126	120	280	120	280	120	280	120	280	120	280
127	96	268	96	268	96	268	96	0	96	268
128	72	212	72	0	72	212	72	0	72	0
129	48	112	48	0	48	0	48	0	48	0
130	24	0	24	0	24	0	24	0	24	0
131	120	170	120	170	120	170	120	170	120	170
132	96	152	96	136	96	152	96	152	96	152
133	72	118	72	102	72	118	72	0	72	118
134	48	68	48	0	48	84	48	0	48	0
135	24	0	24	0	24	0	24	0	24	0
136	115	140	115	140	115	140	115	140	115	140
137	92	112	92	112	92	122	92	112	92	112
138	69	84	69	84	69	94	69	84	69	84
139	46	56	46	56	46	66	46	0	46	56
140	23	28	23	0	23	0	23	0	23	0
141	110	110	110	110	110	110	110	110	110	110
142	88	88	88	88	88	88	88	88	88	88
143	66	66	66	66	66	66	66	66	66	66
144	44	44	44	44	44	44	44	44	44	44
145	22	22	22	22	22	22	22	22	22	22
146	80	80	80	80	80	80	80	80	80	80
147	64	64	64	64	64	64	64	64	64	64
148	48	48	48	48	48	48	48	48	48	48
149	32	32	32	32	32	32	32	32	32	32
150	16	16	16	16	16	16	16	16	16	16
151	110	110	110	110	110	110	110	110	110	110
152	88	88	88	88	88	88	88	88	88	88
153	66	66	66	66	66	66	66	66	66	66
154	44	44	44	44	44	44	44	44	44	44
155	22	22	22	22	22	22	22	22	22	22
156	140	140	140	140	140	140	140	140	140	140
157	112	112	112	112	112	117	112	112	112	112
158	84	84	84	84	84	89	84	84	84	84
159	56	56	56	56	56	61	56	56	56	56
160	28	28	28	28	28	28	28	28	28	28
161	145	170	145	170	145	170	145	170	145	170
162	116	136	116	136	116	146	116	136	116	136
163	87	102	87	102	87	112	87	102	87	102
164	58	68	58	68	58	78	58	68	58	68
165	29	34	29	34	29	0	29	0	29	0
166	150	200	150	216	150	200	150	200	150	200
167	120	176	120	160	120	176	120	176	120	176
168	90	136	90	120	90	136	90	120	90	136
169	60	80	60	80	60	96	60	0	60	60
170	30	40	30	0	30	0	30	0	30	0
171	150	200	150	216	150	200	150	200	150	200
172	120	176	120	160	120	176	120	176	120	176

173	90	136	90	120	90	136	90	120	90	136
174	60	80	60	80	60	96	60	0	60	60
175	30	40	30	0	30	0	30	0	30	0
176	145	170	145	170	145	170	145	170	145	170
177	116	136	116	136	116	146	116	136	116	136
178	87	102	87	102	87	112	87	102	87	102
179	58	68	58	68	58	78	58	68	58	68
180	29	34	29	34	29	0	29	0	29	0
181	140	140	140	140	140	140	140	140	140	140
182	112	112	112	112	112	117	112	112	112	112
183	84	84	84	84	84	89	84	84	84	84
184	56	56	56	56	56	61	56	56	56	56
185	28	28	28	28	28	28	28	28	28	28
186	110	110	110	110	110	110	110	110	110	110
187	88	88	88	88	88	88	88	88	88	88
188	66	66	66	66	66	66	66	66	66	66
189	44	44	44	44	44	44	44	44	44	44
190	22	22	22	22	22	22	22	22	22	22

Table A.2: Structural response under each local failure scenario i for design configurations D0, D1, D2, D3 and D4.

ANNEX B

DETAILED RESULTS FOR THE STRUCTURAL ROBUSTNESS ASSESSMENT IN CHAPTER V

This annex details some results of the sensitivity analysis presented led in Chapter V. Section V.2 aims to study the effect of the combinations of loads and the dynamic amplification factor on the structural robustness assessment. Table B.1 presents the failure energy E_i for each scenario i under the load combinations W1, W2 and W3. The structural response under each load combination with the several dynamic amplification factor ($DAF=1.0, 1.3, 1.5$ or 2.0) is presented in Table B.2, Table B.3 and Table B.4. The diagrams of the local failure energy E_i with the measure of collapsed part $\mathcal{M}(CP_i)$ for the case studies of Table V.1 are presented in Figures B.1 to B.12. Further, Table B.5 presents the non-dominated scenarios that maximize $\mathcal{M}(CP_i)$ and minimize initial damaged part $\mathcal{M}(IDP_i)$ according to Equation (IV.13).

Scenario i	E_i^{W1} (kJ)	E_i^{W2} (kJ)	E_i^{W3} (kJ)	Scenario i	E_i^{W1} (kJ)	E_i^{W2} (kJ)	E_i^{W3} (kJ)
1	100.4	102.0	100.3	96	166.7	170.2	159.6
2	102.1	103.7	102.0	97	173.9	175.8	168.6
3	103.8	105.3	103.7	98	197.4	199.1	194.0
4	105.4	107.0	105.4	99	204.2	205.8	202.4
5	108.6	108.6	107.0	100	210.8	212.4	210.7
6	84.2	86.0	80.8	101	184.7	188.0	181.1
7	87.8	89.5	84.5	102	190.0	193.2	186.5
8	98.8	100.3	97.1	103	202.6	205.6	200.8
9	102.1	103.7	102.0	104	207.6	210.6	207.4
10	105.4	107.0	105.4	105	214.0	215.5	212.4
11	82.5	84.2	78.9	106	267.1	272.2	260.0
12	86.1	86.3	84.2	107	276.0	279.5	270.6
13	98.6	98.8	96.9	108	301.2	304.4	297.7
14	102.0	102.1	100.4	109	309.6	312.7	307.8
15	105.4	105.4	105.3	110	319.4	321.0	317.8

Annex B: Detailed results for the structural robustness assessment in Chapter V

16	80.6	82.5	77.0	111	247.3	252.6	236.6
17	84.4	86.1	82.4	112	258.3	261.9	251.0
18	97.0	98.6	95.2	113	294.4	297.7	289.2
19	101.9	102.0	100.3	114	306.1	307.8	302.7
20	105.4	105.4	105.3	115	316.2	317.8	316.0
21	80.6	82.5	77.0	116	243.7	249.1	232.8
22	84.4	86.1	82.4	117	254.8	258.5	248.9
23	97.0	98.6	95.2	118	292.7	296.0	287.3
24	101.9	102.0	100.3	119	305.9	306.2	301.1
25	105.4	105.4	105.3	120	316.2	316.3	316.0
26	80.6	82.5	77.0	121	241.9	247.4	230.9
27	84.4	86.1	82.4	122	253.1	258.2	247.2
28	97.0	98.6	95.2	123	291.0	295.9	285.6
29	101.9	102.0	100.3	124	305.8	306.1	300.9
30	105.4	105.4	105.3	125	316.1	316.2	315.9
31	80.6	82.5	77.0	126	241.9	247.4	230.9
32	84.4	86.1	82.4	127	253.1	258.2	247.2
33	97.0	98.6	95.2	128	291.0	295.9	285.6
34	101.9	102.0	100.3	129	305.8	306.1	300.9
35	105.4	105.4	105.3	130	316.1	316.2	315.9
36	80.6	82.5	77.0	131	241.9	247.4	230.9
37	84.4	86.1	82.4	132	253.1	258.2	247.2
38	97.0	98.6	95.2	133	291.0	295.9	285.6
39	101.9	102.0	100.3	134	305.8	306.1	300.9
40	105.4	105.4	105.3	135	316.1	316.2	315.9
41	82.5	84.2	78.9	136	243.7	249.1	232.8
42	86.1	86.3	84.2	137	254.8	258.5	248.9
43	98.6	98.8	96.9	138	292.7	296.0	287.3
44	102.0	102.1	100.4	139	305.9	306.2	301.1
45	105.4	105.4	105.3	140	316.2	316.3	316.0
46	84.2	86.0	80.8	141	247.3	252.6	236.6
47	87.8	89.5	84.5	142	258.3	261.9	251.0
48	98.8	100.3	97.1	143	294.4	297.7	289.2
49	102.1	103.7	102.0	144	306.1	307.8	302.7
50	105.4	107.0	105.4	145	316.2	317.8	316.0
51	100.4	102.0	100.3	146	267.1	272.2	260.0
52	102.1	103.7	102.0	147	276.0	279.5	270.6
53	103.8	105.3	103.7	148	301.2	304.4	297.7
54	105.4	107.0	105.4	149	309.6	312.7	307.8
55	108.6	108.6	107.0	150	319.4	321.0	317.8
56	184.7	188.0	181.1	151	347.7	354.6	336.9
57	190.0	193.2	186.5	152	360.4	365.6	353.0
58	202.6	205.6	200.8	153	398.2	403.0	392.9
59	207.6	210.6	207.4	154	411.6	414.8	408.1
60	214.0	215.5	212.4	155	424.8	426.4	423.1
61	166.7	170.2	159.6	156	327.9	335.1	313.6
62	173.9	175.8	168.6	157	342.6	348.0	333.4

63	197.4	199.1	194.0	158	391.4	396.4	384.4
64	204.2	205.8	202.4	159	408.1	409.9	403.0
65	210.8	212.4	210.7	160	421.6	423.2	421.4
66	163.1	166.6	155.8	161	324.3	331.5	309.8
67	170.4	172.4	166.5	162	339.2	344.5	331.3
68	195.7	197.4	192.1	163	389.7	394.7	382.5
69	204.0	204.2	200.7	164	407.9	408.2	401.4
70	210.8	210.9	210.7	165	421.6	421.7	421.3
71	161.2	164.9	153.9	166	322.5	329.8	307.9
72	168.7	172.1	164.8	167	337.5	344.3	329.6
73	194.0	197.3	190.4	168	388.1	394.5	380.8
74	203.9	204.1	200.6	169	407.8	408.2	401.3
75	210.8	210.8	210.6	170	421.5	421.7	421.2
76	161.2	164.9	153.9	171	322.5	329.8	307.9
77	168.7	172.1	164.8	172	337.5	344.3	329.6
78	194.0	197.3	190.4	173	388.1	394.5	380.8
79	203.9	204.1	200.6	174	407.8	408.2	401.3
80	210.8	210.8	210.6	175	421.5	421.7	421.2
81	161.2	164.9	153.9	176	324.3	331.5	309.8
82	168.7	172.1	164.8	177	339.2	344.5	331.3
83	194.0	197.3	190.4	178	389.7	394.7	382.5
84	203.9	204.1	200.6	179	407.9	408.2	401.4
85	210.8	210.8	210.6	180	421.6	421.7	421.3
86	161.2	164.9	153.9	181	327.9	335.1	313.6
87	168.7	172.1	164.8	182	342.6	348.0	333.4
88	194.0	197.3	190.4	183	391.4	396.4	384.4
89	203.9	204.1	200.6	184	408.1	409.9	403.0
90	210.8	210.8	210.6	185	421.6	423.2	421.4
91	163.1	166.6	155.8	186	347.7	354.6	336.9
92	170.4	172.4	166.5	187	360.4	365.6	353.0
93	195.7	197.4	192.1	188	398.2	403.0	392.9
94	204.0	204.2	200.7	189	411.6	414.8	408.1
95	210.8	210.9	210.7	190	424.8	426.4	423.1

Table B.1: Energy E_i required to cause the local failure of scenario i under the combinations of actions W1, W2 and W3.

i	W1-DAF1			W1-DAF1.3			W1-DAF1.5			W1-DAF2		
	$\mathcal{M}(IDP_i)$ (m)	$\mathcal{M}(CP_i)$ (m)	DFP_i									
1	0	0	0.0	0	0	0.0	0	0	0.0	25	25	1.0
2	0	0	0.0	0	0	0.0	0	0	0.0	20	20	1.0
3	0	0	0.0	0	0	0.0	0	0	0.0	15	15	1.0
4	0	0	0.0	0	0	0.0	0	0	0.0	10	10	1.0
5	5	5	1.0	5	5	1.0	5	5	1.0	5	5	1.0
6	0	0	0.0	0	0	0.0	0	0	0.0	50	50	1.0
7	0	0	0.0	0	0	0.0	0	0	0.0	40	0	0.0
8	0	0	0.0	0	0	0.0	0	0	0.0	30	0	0.0
9	0	0	0.0	0	0	0.0	0	0	0.0	20	0	0.0
10	0	0	0.0	0	0	0.0	0	0	0.0	10	0	0.0

Annex B: Detailed results for the structural robustness assessment in Chapter V

11	0	0	0.0	0	0	0.0	55	0	0.0	55	80	1.5
12	0	0	0.0	0	0	0.0	44	0	0.0	44	64	1.5
13	0	0	0.0	0	0	0.0	33	0	0.0	33	0	0.0
14	0	0	0.0	0	0	0.0	22	0	0.0	22	0	0.0
15	0	0	0.0	0	0	0.0	11	0	0.0	11	0	0.0
16	0	0	0.0	60	0	0.0	60	0	0.0	60	110	1.8
17	0	0	0.0	48	0	0.0	48	0	0.0	48	104	2.2
18	0	0	0.0	36	0	0.0	36	0	0.0	36	0	0.0
19	0	0	0.0	24	0	0.0	24	0	0.0	24	0	0.0
20	0	0	0.0	12	0	0.0	12	0	0.0	12	0	0.0
21	0	0	0.0	60	0	0.0	60	0	0.0	60	140	2.3
22	0	0	0.0	48	0	0.0	48	0	0.0	48	0	0.0
23	0	0	0.0	36	0	0.0	36	0	0.0	36	0	0.0
24	0	0	0.0	24	0	0.0	24	0	0.0	24	0	0.0
25	0	0	0.0	12	0	0.0	12	0	0.0	12	0	0.0
26	0	0	0.0	60	0	0.0	60	0	0.0	60	0	0.0
27	0	0	0.0	48	0	0.0	48	0	0.0	48	0	0.0
28	0	0	0.0	36	0	0.0	36	0	0.0	36	0	0.0
29	0	0	0.0	24	0	0.0	24	0	0.0	24	0	0.0
30	0	0	0.0	12	0	0.0	12	0	0.0	12	0	0.0
31	0	0	0.0	60	0	0.0	60	0	0.0	60	140	2.3
32	0	0	0.0	48	0	0.0	48	0	0.0	48	0	0.0
33	0	0	0.0	36	0	0.0	36	0	0.0	36	0	0.0
34	0	0	0.0	24	0	0.0	24	0	0.0	24	0	0.0
35	0	0	0.0	12	0	0.0	12	0	0.0	12	0	0.0
36	0	0	0.0	60	0	0.0	60	0	0.0	60	110	1.8
37	0	0	0.0	48	0	0.0	48	0	0.0	48	104	2.2
38	0	0	0.0	36	0	0.0	36	0	0.0	36	0	0.0
39	0	0	0.0	24	0	0.0	24	0	0.0	24	0	0.0
40	0	0	0.0	12	0	0.0	12	0	0.0	12	0	0.0
41	0	0	0.0	0	0	0.0	55	0	0.0	55	80	1.5
42	0	0	0.0	0	0	0.0	44	0	0.0	44	64	1.5
43	0	0	0.0	0	0	0.0	33	0	0.0	33	0	0.0
44	0	0	0.0	0	0	0.0	22	0	0.0	22	0	0.0
45	0	0	0.0	0	0	0.0	11	0	0.0	11	0	0.0
46	0	0	0.0	0	0	0.0	0	0	0.0	50	50	1.0
47	0	0	0.0	0	0	0.0	0	0	0.0	40	0	0.0
48	0	0	0.0	0	0	0.0	0	0	0.0	30	0	0.0
49	0	0	0.0	0	0	0.0	0	0	0.0	20	0	0.0
50	0	0	0.0	0	0	0.0	0	0	0.0	10	0	0.0
51	0	0	0.0	0	0	0.0	0	0	0.0	25	25	1.0
52	0	0	0.0	0	0	0.0	0	0	0.0	20	20	1.0
53	0	0	0.0	0	0	0.0	0	0	0.0	15	15	1.0
54	0	0	0.0	0	0	0.0	0	0	0.0	10	10	1.0
55	5	5	1.0	5	5	1.0	5	5	1.0	5	5	1.0
56	50	50	1.0	50	50	1.0	50	50	1.0	50	50	1.0
57	40	40	1.0	40	40	1.0	40	40	1.0	40	40	1.0
58	30	30	1.0	30	30	1.0	30	30	1.0	30	30	1.0
59	20	20	1.0	20	20	1.0	20	20	1.0	20	20	1.0
60	10	10	1.0	10	10	1.0	10	10	1.0	10	10	1.0
61	80	80	1.0	80	80	1.0	80	80	1.0	80	80	1.0
62	64	64	1.0	64	64	1.0	64	64	1.0	64	64	1.0
63	48	48	1.0	48	48	1.0	48	48	1.0	48	48	1.0
64	32	32	1.0	32	32	1.0	32	32	1.0	32	32	1.0
65	16	0	0.0	16	16	1.0	16	16	1.0	16	16	1.0
66	85	110	1.3	85	110	1.3	85	110	1.3	85	110	1.3
67	68	88	1.3	68	88	1.3	68	88	1.3	68	88	1.3
68	51	0	0.0	51	66	1.3	51	66	1.3	51	66	1.3

Annex B: Detailed results for the structural robustness assessment in Chapter V

69	34	0	0.0	34	44	1.3	34	44	1.3	34	44	1.3
70	17	0	0.0	17	0	0.0	17	0	0.0	17	0	0.0
71	90	140	1.6	90	140	1.6	90	140	1.6	90	140	1.6
72	72	128	1.8	72	128	1.8	72	128	1.8	72	128	1.8
73	54	0	0.0	54	100	1.9	54	100	1.9	54	100	1.9
74	36	0	0.0	36	0	0.0	36	0	0.0	36	56	1.6
75	18	0	0.0	18	0	0.0	18	0	0.0	18	0	0.0
76	90	170	1.9	90	170	1.9	90	170	1.9	90	170	1.9
77	72	0	0.0	72	158	2.2	72	158	2.2	72	158	2.2
78	54	0	0.0	54	0	0.0	54	124	2.3	54	124	2.3
79	36	0	0.0	36	0	0.0	36	0	0.0	36	68	1.9
80	18	0	0.0	18	0	0.0	18	0	0.0	18	0	0.0
81	90	170	1.9	90	170	1.9	90	170	1.9	90	170	1.9
82	72	0	0.0	72	158	2.2	72	158	2.2	72	158	2.2
83	54	0	0.0	54	0	0.0	54	124	2.3	54	124	2.3
84	36	0	0.0	36	0	0.0	36	0	0.0	36	68	1.9
85	18	0	0.0	18	0	0.0	18	0	0.0	18	0	0.0
86	90	140	1.6	90	140	1.6	90	140	1.6	90	140	1.6
87	72	128	1.8	72	128	1.8	72	128	1.8	72	128	1.8
88	54	0	0.0	54	100	1.9	54	100	1.9	54	100	1.9
89	36	0	0.0	36	0	0.0	36	0	0.0	36	56	1.6
90	18	0	0.0	18	0	0.0	18	0	0.0	18	0	0.0
91	85	110	1.3	85	110	1.3	85	110	1.3	85	110	1.3
92	68	88	1.3	68	88	1.3	68	88	1.3	68	88	1.3
93	51	0	0.0	51	66	1.3	51	66	1.3	51	66	1.3
94	34	0	0.0	34	44	1.3	34	44	1.3	34	44	1.3
95	17	0	0.0	17	0	0.0	17	0	0.0	17	0	0.0
96	80	80	1.0	80	80	1.0	80	80	1.0	80	80	1.0
97	64	64	1.0	64	64	1.0	64	64	1.0	64	64	1.0
98	48	48	1.0	48	48	1.0	48	48	1.0	48	48	1.0
99	32	32	1.0	32	32	1.0	32	32	1.0	32	32	1.0
100	16	0	0.0	16	16	1.0	16	16	1.0	16	16	1.0
101	50	50	1.0	50	50	1.0	50	50	1.0	50	50	1.0
102	40	40	1.0	40	40	1.0	40	40	1.0	40	40	1.0
103	30	30	1.0	30	30	1.0	30	30	1.0	30	30	1.0
104	20	20	1.0	20	20	1.0	20	20	1.0	20	20	1.0
105	10	10	1.0	10	10	1.0	10	10	1.0	10	10	1.0
106	80	80	1.0	80	80	1.0	80	80	1.0	80	80	1.0
107	64	64	1.0	64	64	1.0	64	64	1.0	64	64	1.0
108	48	48	1.0	48	48	1.0	48	48	1.0	48	48	1.0
109	32	32	1.0	32	32	1.0	32	32	1.0	32	32	1.0
110	16	16	1.0	16	16	1.0	16	16	1.0	16	16	1.0
111	110	110	1.0	110	110	1.0	110	110	1.0	110	110	1.0
112	88	88	1.0	88	88	1.0	88	88	1.0	88	88	1.0
113	66	66	1.0	66	66	1.0	66	66	1.0	66	66	1.0
114	44	44	1.0	44	44	1.0	44	44	1.0	44	44	1.0
115	22	22	1.0	22	22	1.0	22	22	1.0	22	22	1.0
116	115	140	1.2	115	140	1.2	115	140	1.2	115	140	1.2
117	92	112	1.2	92	112	1.2	92	112	1.2	92	112	1.2
118	69	84	1.2	69	84	1.2	69	84	1.2	69	84	1.2
119	46	56	1.2	46	56	1.2	46	56	1.2	46	56	1.2
120	23	0	0.0	23	28	1.2	23	28	1.2	23	28	1.2
121	120	170	1.4	120	170	1.4	120	170	1.4	120	170	1.4
122	96	152	1.6	96	152	1.6	96	152	1.6	96	152	1.6
123	72	118	1.6	72	118	1.6	72	118	1.6	72	118	1.6
124	48	68	1.4	48	68	1.4	48	68	1.4	48	68	1.4
125	24	0	0.0	24	0	0.0	24	0	0.0	24	34	1.4
126	120	280	2.3	120	280	2.3	120	280	2.3	120	280	2.3

Annex B: Detailed results for the structural robustness assessment in Chapter V

127	96	268	2.8	96	268	2.8	96	268	2.8	96	268	2.8
128	72	212	2.9	72	212	2.9	72	212	2.9	72	212	2.9
129	48	0	0.0	48	112	2.3	48	112	2.3	48	112	2.3
130	24	0	0.0	24	0	0.0	24	0	0.0	24	24	1.0
131	120	170	1.4	120	170	1.4	120	170	1.4	120	170	1.4
132	96	152	1.6	96	152	1.6	96	152	1.6	96	152	1.6
133	72	118	1.6	72	118	1.6	72	118	1.6	72	118	1.6
134	48	68	1.4	48	68	1.4	48	68	1.4	48	68	1.4
135	24	0	0.0	24	0	0.0	24	0	0.0	24	34	1.4
136	115	140	1.2	115	140	1.2	115	140	1.2	115	140	1.2
137	92	112	1.2	92	112	1.2	92	112	1.2	92	112	1.2
138	69	84	1.2	69	84	1.2	69	84	1.2	69	84	1.2
139	46	56	1.2	46	56	1.2	46	56	1.2	46	56	1.2
140	23	0	0.0	23	28	1.2	23	28	1.2	23	28	1.2
141	110	110	1.0	110	110	1.0	110	110	1.0	110	110	1.0
142	88	88	1.0	88	88	1.0	88	88	1.0	88	88	1.0
143	66	66	1.0	66	66	1.0	66	66	1.0	66	66	1.0
144	44	44	1.0	44	44	1.0	44	44	1.0	44	44	1.0
145	22	22	1.0	22	22	1.0	22	22	1.0	22	22	1.0
146	80	80	1.0	80	80	1.0	80	80	1.0	80	80	1.0
147	64	64	1.0	64	64	1.0	64	64	1.0	64	64	1.0
148	48	48	1.0	48	48	1.0	48	48	1.0	48	48	1.0
149	32	32	1.0	32	32	1.0	32	32	1.0	32	32	1.0
150	16	16	1.0	16	16	1.0	16	16	1.0	16	16	1.0
151	110	110	1.0	110	110	1.0	110	110	1.0	110	110	1.0
152	88	88	1.0	88	88	1.0	88	88	1.0	88	88	1.0
153	66	66	1.0	66	66	1.0	66	66	1.0	66	66	1.0
154	44	44	1.0	44	44	1.0	44	44	1.0	44	44	1.0
155	22	22	1.0	22	22	1.0	22	22	1.0	22	22	1.0
156	140	140	1.0	140	140	1.0	140	140	1.0	140	140	1.0
157	112	112	1.0	112	112	1.0	112	112	1.0	112	112	1.0
158	84	84	1.0	84	84	1.0	84	84	1.0	84	84	1.0
159	56	56	1.0	56	56	1.0	56	56	1.0	56	56	1.0
160	28	28	1.0	28	28	1.0	28	28	1.0	28	28	1.0
161	145	170	1.2	145	170	1.2	145	170	1.2	145	170	1.2
162	116	136	1.2	116	136	1.2	116	136	1.2	116	136	1.2
163	87	102	1.2	87	102	1.2	87	102	1.2	87	102	1.2
164	58	68	1.2	58	68	1.2	58	68	1.2	58	68	1.2
165	29	34	1.2	29	34	1.2	29	34	1.2	29	34	1.2
166	150	200	1.3	150	200	1.3	150	200	1.3	150	200	1.3
167	120	176	1.5	120	176	1.5	120	176	1.5	120	176	1.5
168	90	136	1.5	90	136	1.5	90	136	1.5	90	136	1.5
169	60	80	1.3	60	80	1.3	60	80	1.3	60	80	1.3
170	30	0	0.0	30	40	1.3	30	40	1.3	30	40	1.3
171	150	200	1.3	150	200	1.3	150	200	1.3	150	200	1.3
172	120	176	1.5	120	176	1.5	120	176	1.5	120	176	1.5
173	90	136	1.5	90	136	1.5	90	136	1.5	90	136	1.5
174	60	80	1.3	60	80	1.3	60	80	1.3	60	80	1.3
175	30	0	0.0	30	40	1.3	30	40	1.3	30	40	1.3
176	145	170	1.2	145	170	1.2	145	170	1.2	145	170	1.2
177	116	136	1.2	116	136	1.2	116	136	1.2	116	136	1.2
178	87	102	1.2	87	102	1.2	87	102	1.2	87	102	1.2
179	58	68	1.2	58	68	1.2	58	68	1.2	58	68	1.2
180	29	34	1.2	29	34	1.2	29	34	1.2	29	34	1.2
181	140	140	1.0	140	140	1.0	140	140	1.0	140	140	1.0
182	112	112	1.0	112	112	1.0	112	112	1.0	112	112	1.0
183	84	84	1.0	84	84	1.0	84	84	1.0	84	84	1.0
184	56	56	1.0	56	56	1.0	56	56	1.0	56	56	1.0

185	28	28	1.0	28	28	1.0	28	28	1.0	28	28	1.0
186	110	110	1.0	110	110	1.0	110	110	1.0	110	110	1.0
187	88	88	1.0	88	88	1.0	88	88	1.0	88	88	1.0
188	66	66	1.0	66	66	1.0	66	66	1.0	66	66	1.0
189	44	44	1.0	44	44	1.0	44	44	1.0	44	44	1.0
190	22	22	1.0	22	22	1.0	22	22	1.0	22	22	1.0

Table B.2: Structural response under each local failure scenario i when applying the combination of actions W1 with several dynamic amplification factors.

i	W2-DAF1			W2-DAF1.3			W2-DAF1.5			W2-DAF2		
	$\mathcal{M}(IDP_i)$ (m)	$\mathcal{M}(CP_i)$ (m)	DFP_i									
1	0	0	0.0	0	0	0.0	0	0	0.0	25	25	1.0
2	0	0	0.0	0	0	0.0	0	0	0.0	20	20	1.0
3	0	0	0.0	0	0	0.0	0	0	0.0	15	15	1.0
4	0	0	0.0	0	0	0.0	0	0	0.0	10	10	1.0
5	5	5	1.0	5	5	1.0	5	5	1.0	5	5	1.0
6	0	0	0.0	0	0	0.0	0	0	0.0	50	0	0.0
7	0	0	0.0	0	0	0.0	0	0	0.0	40	0	0.0
8	0	0	0.0	0	0	0.0	0	0	0.0	30	0	0.0
9	0	0	0.0	0	0	0.0	0	0	0.0	20	0	0.0
10	0	0	0.0	0	0	0.0	0	0	0.0	10	0	0.0
11	0	0	0.0	0	0	0.0	0	0	0.0	55	80	1.5
12	0	0	0.0	0	0	0.0	0	0	0.0	44	0	0.0
13	0	0	0.0	0	0	0.0	0	0	0.0	33	0	0.0
14	0	0	0.0	0	0	0.0	0	0	0.0	22	0	0.0
15	0	0	0.0	0	0	0.0	0	0	0.0	11	0	0.0
16	0	0	0.0	60	0	0.0	60	0	0.0	60	110	1.8
17	0	0	0.0	48	0	0.0	48	0	0.0	48	0	0.0
18	0	0	0.0	36	0	0.0	36	0	0.0	36	0	0.0
19	0	0	0.0	24	0	0.0	24	0	0.0	24	0	0.0
20	0	0	0.0	12	0	0.0	12	0	0.0	12	0	0.0
21	0	0	0.0	60	0	0.0	60	0	0.0	60	0	0.0
22	0	0	0.0	48	0	0.0	48	0	0.0	48	0	0.0
23	0	0	0.0	36	0	0.0	36	0	0.0	36	0	0.0
24	0	0	0.0	24	0	0.0	24	0	0.0	24	0	0.0
25	0	0	0.0	12	0	0.0	12	0	0.0	12	0	0.0
26	0	0	0.0	60	0	0.0	60	0	0.0	60	0	0.0
27	0	0	0.0	48	0	0.0	48	0	0.0	48	0	0.0
28	0	0	0.0	36	0	0.0	36	0	0.0	36	0	0.0
29	0	0	0.0	24	0	0.0	24	0	0.0	24	0	0.0
30	0	0	0.0	12	0	0.0	12	0	0.0	12	0	0.0
31	0	0	0.0	60	0	0.0	60	0	0.0	60	0	0.0
32	0	0	0.0	48	0	0.0	48	0	0.0	48	0	0.0
33	0	0	0.0	36	0	0.0	36	0	0.0	36	0	0.0
34	0	0	0.0	24	0	0.0	24	0	0.0	24	0	0.0
35	0	0	0.0	12	0	0.0	12	0	0.0	12	0	0.0
36	0	0	0.0	60	0	0.0	60	0	0.0	60	110	1.8
37	0	0	0.0	48	0	0.0	48	0	0.0	48	0	0.0
38	0	0	0.0	36	0	0.0	36	0	0.0	36	0	0.0
39	0	0	0.0	24	0	0.0	24	0	0.0	24	0	0.0
40	0	0	0.0	12	0	0.0	12	0	0.0	12	0	0.0
41	0	0	0.0	0	0	0.0	0	0	0.0	55	80	1.5
42	0	0	0.0	0	0	0.0	0	0	0.0	44	0	0.0
43	0	0	0.0	0	0	0.0	0	0	0.0	33	0	0.0
44	0	0	0.0	0	0	0.0	0	0	0.0	22	0	0.0

Annex B: Detailed results for the structural robustness assessment in Chapter V

45	0	0	0.0	0	0	0.0	0	0	0.0	11	0	0.0
46	0	0	0.0	0	0	0.0	0	0	0.0	50	0	0.0
47	0	0	0.0	0	0	0.0	0	0	0.0	40	0	0.0
48	0	0	0.0	0	0	0.0	0	0	0.0	30	0	0.0
49	0	0	0.0	0	0	0.0	0	0	0.0	20	0	0.0
50	0	0	0.0	0	0	0.0	0	0	0.0	10	0	0.0
51	0	0	0.0	0	0	0.0	0	0	0.0	25	25	1.0
52	0	0	0.0	0	0	0.0	0	0	0.0	20	20	1.0
53	0	0	0.0	0	0	0.0	0	0	0.0	15	15	1.0
54	0	0	0.0	0	0	0.0	0	0	0.0	10	10	1.0
55	5	5	1.0	5	5	1.0	5	5	1.0	5	5	1.0
56	50	50	1.0	50	50	1.0	50	50	1.0	50	50	1.0
57	40	40	1.0	40	40	1.0	40	40	1.0	40	40	1.0
58	30	30	1.0	30	30	1.0	30	30	1.0	30	30	1.0
59	20	20	1.0	20	20	1.0	20	20	1.0	20	20	1.0
60	10	10	1.0	10	10	1.0	10	10	1.0	10	10	1.0
61	80	80	1.0	80	80	1.0	80	80	1.0	80	80	1.0
62	64	64	1.0	64	64	1.0	64	64	1.0	64	64	1.0
63	48	0	0.0	48	48	1.0	48	48	1.0	48	48	1.0
64	32	0	0.0	32	32	1.0	32	32	1.0	32	32	1.0
65	16	0	0.0	16	16	1.0	16	16	1.0	16	16	1.0
66	85	110	1.3	85	110	1.3	85	110	1.3	85	110	1.3
67	68	0	0.0	68	88	1.3	68	88	1.3	68	88	1.3
68	51	0	0.0	51	66	1.3	51	66	1.3	51	66	1.3
69	34	0	0.0	34	0	0.0	34	44	1.3	34	44	1.3
70	17	0	0.0	17	0	0.0	17	0	0.0	17	0	0.0
71	90	140	1.6	90	140	1.6	90	140	1.6	90	140	1.6
72	72	0	0.0	72	128	1.8	72	128	1.8	72	128	1.8
73	54	0	0.0	54	100	1.9	54	100	1.9	54	100	1.9
74	36	0	0.0	36	0	0.0	36	0	0.0	36	56	1.6
75	18	0	0.0	18	0	0.0	18	0	0.0	18	0	0.0
76	90	0	0.0	90	170	1.9	90	170	1.9	90	170	1.9
77	72	0	0.0	72	158	2.2	72	158	2.2	72	158	2.2
78	54	0	0.0	54	0	0.0	54	124	2.3	54	124	2.3
79	36	0	0.0	36	0	0.0	36	0	0.0	36	68	1.9
80	18	0	0.0	18	0	0.0	18	0	0.0	18	0	0.0
81	90	0	0.0	90	170	1.9	90	170	1.9	90	170	1.9
82	72	0	0.0	72	158	2.2	72	158	2.2	72	158	2.2
83	54	0	0.0	54	0	0.0	54	124	2.3	54	124	2.3
84	36	0	0.0	36	0	0.0	36	0	0.0	36	68	1.9
85	18	0	0.0	18	0	0.0	18	0	0.0	18	0	0.0
86	90	140	1.6	90	140	1.6	90	140	1.6	90	140	1.6
87	72	0	0.0	72	128	1.8	72	128	1.8	72	128	1.8
88	54	0	0.0	54	100	1.9	54	100	1.9	54	100	1.9
89	36	0	0.0	36	0	0.0	36	0	0.0	36	56	1.6
90	18	0	0.0	18	0	0.0	18	0	0.0	18	0	0.0
91	85	110	1.3	85	110	1.3	85	110	1.3	85	110	1.3
92	68	0	0.0	68	88	1.3	68	88	1.3	68	88	1.3
93	51	0	0.0	51	66	1.3	51	66	1.3	51	66	1.3
94	34	0	0.0	34	0	0.0	34	44	1.3	34	44	1.3
95	17	0	0.0	17	0	0.0	17	0	0.0	17	0	0.0
96	80	80	1.0	80	80	1.0	80	80	1.0	80	80	1.0
97	64	64	1.0	64	64	1.0	64	64	1.0	64	64	1.0
98	48	0	0.0	48	48	1.0	48	48	1.0	48	48	1.0
99	32	0	0.0	32	32	1.0	32	32	1.0	32	32	1.0
100	16	0	0.0	16	16	1.0	16	16	1.0	16	16	1.0
101	50	50	1.0	50	50	1.0	50	50	1.0	50	50	1.0
102	40	40	1.0	40	40	1.0	40	40	1.0	40	40	1.0

Annex B: Detailed results for the structural robustness assessment in Chapter V

103	30	30	1.0	30	30	1.0	30	30	1.0	30	30	1.0
104	20	20	1.0	20	20	1.0	20	20	1.0	20	20	1.0
105	10	10	1.0	10	10	1.0	10	10	1.0	10	10	1.0
106	80	80	1.0	80	80	1.0	80	80	1.0	80	80	1.0
107	64	64	1.0	64	64	1.0	64	64	1.0	64	64	1.0
108	48	48	1.0	48	48	1.0	48	48	1.0	48	48	1.0
109	32	32	1.0	32	32	1.0	32	32	1.0	32	32	1.0
110	16	16	1.0	16	16	1.0	16	16	1.0	16	16	1.0
111	110	110	1.0	110	110	1.0	110	110	1.0	110	110	1.0
112	88	88	1.0	88	88	1.0	88	88	1.0	88	88	1.0
113	66	66	1.0	66	66	1.0	66	66	1.0	66	66	1.0
114	44	44	1.0	44	44	1.0	44	44	1.0	44	44	1.0
115	22	22	1.0	22	22	1.0	22	22	1.0	22	22	1.0
116	115	140	1.2	115	140	1.2	115	140	1.2	115	140	1.2
117	92	112	1.2	92	112	1.2	92	112	1.2	92	112	1.2
118	69	84	1.2	69	84	1.2	69	84	1.2	69	84	1.2
119	46	56	1.2	46	56	1.2	46	56	1.2	46	56	1.2
120	23	0	0.0	23	0	0.0	23	28	1.2	23	28	1.2
121	120	170	1.4	120	170	1.4	120	170	1.4	120	170	1.4
122	96	152	1.6	96	152	1.6	96	152	1.6	96	152	1.6
123	72	118	1.6	72	118	1.6	72	118	1.6	72	118	1.6
124	48	0	0.0	48	68	1.4	48	68	1.4	48	68	1.4
125	24	0	0.0	24	0	0.0	24	0	0.0	24	34	1.4
126	120	280	2.3	120	280	2.3	120	280	2.3	120	280	2.3
127	96	268	2.8	96	268	2.8	96	268	2.8	96	268	2.8
128	72	212	2.9	72	212	2.9	72	212	2.9	72	212	2.9
129	48	0	0.0	48	0	0.0	48	112	2.3	48	112	2.3
130	24	0	0.0	24	0	0.0	24	0	0.0	24	0	0.0
131	120	170	1.4	120	170	1.4	120	170	1.4	120	170	1.4
132	96	152	1.6	96	152	1.6	96	152	1.6	96	152	1.6
133	72	118	1.6	72	118	1.6	72	118	1.6	72	118	1.6
134	48	0	0.0	48	68	1.4	48	68	1.4	48	68	1.4
135	24	0	0.0	24	0	0.0	24	0	0.0	24	34	1.4
136	115	140	1.2	115	140	1.2	115	140	1.2	115	140	1.2
137	92	112	1.2	92	112	1.2	92	112	1.2	92	112	1.2
138	69	84	1.2	69	84	1.2	69	84	1.2	69	84	1.2
139	46	56	1.2	46	56	1.2	46	56	1.2	46	56	1.2
140	23	0	0.0	23	0	0.0	23	28	1.2	23	28	1.2
141	110	110	1.0	110	110	1.0	110	110	1.0	110	110	1.0
142	88	88	1.0	88	88	1.0	88	88	1.0	88	88	1.0
143	66	66	1.0	66	66	1.0	66	66	1.0	66	66	1.0
144	44	44	1.0	44	44	1.0	44	44	1.0	44	44	1.0
145	22	22	1.0	22	22	1.0	22	22	1.0	22	22	1.0
146	80	80	1.0	80	80	1.0	80	80	1.0	80	80	1.0
147	64	64	1.0	64	64	1.0	64	64	1.0	64	64	1.0
148	48	48	1.0	48	48	1.0	48	48	1.0	48	48	1.0
149	32	32	1.0	32	32	1.0	32	32	1.0	32	32	1.0
150	16	16	1.0	16	16	1.0	16	16	1.0	16	16	1.0
151	110	110	1.0	110	110	1.0	110	110	1.0	110	110	1.0
152	88	88	1.0	88	88	1.0	88	88	1.0	88	88	1.0
153	66	66	1.0	66	66	1.0	66	66	1.0	66	66	1.0
154	44	44	1.0	44	44	1.0	44	44	1.0	44	44	1.0
155	22	22	1.0	22	22	1.0	22	22	1.0	22	22	1.0
156	140	140	1.0	140	140	1.0	140	140	1.0	140	140	1.0
157	112	112	1.0	112	112	1.0	112	112	1.0	112	112	1.0
158	84	84	1.0	84	84	1.0	84	84	1.0	84	84	1.0
159	56	56	1.0	56	56	1.0	56	56	1.0	56	56	1.0
160	28	28	1.0	28	28	1.0	28	28	1.0	28	28	1.0

161	145	170	1.2	145	170	1.2	145	170	1.2	145	170	1.2
162	116	136	1.2	116	136	1.2	116	136	1.2	116	136	1.2
163	87	102	1.2	87	102	1.2	87	102	1.2	87	102	1.2
164	58	68	1.2	58	68	1.2	58	68	1.2	58	68	1.2
165	29	34	1.2	29	34	1.2	29	34	1.2	29	34	1.2
166	150	200	1.3	150	200	1.3	150	200	1.3	150	200	1.3
167	120	176	1.5	120	176	1.5	120	176	1.5	120	176	1.5
168	90	136	1.5	90	136	1.5	90	136	1.5	90	136	1.5
169	60	80	1.3	60	80	1.3	60	80	1.3	60	80	1.3
170	30	0	0.0	30	0	0.0	30	40	1.3	30	40	1.3
171	150	200	1.3	150	200	1.3	150	200	1.3	150	200	1.3
172	120	176	1.5	120	176	1.5	120	176	1.5	120	176	1.5
173	90	136	1.5	90	136	1.5	90	136	1.5	90	136	1.5
174	60	80	1.3	60	80	1.3	60	80	1.3	60	80	1.3
175	30	0	0.0	30	0	0.0	30	40	1.3	30	40	1.3
176	145	170	1.2	145	170	1.2	145	170	1.2	145	170	1.2
177	116	136	1.2	116	136	1.2	116	136	1.2	116	136	1.2
178	87	102	1.2	87	102	1.2	87	102	1.2	87	102	1.2
179	58	68	1.2	58	68	1.2	58	68	1.2	58	68	1.2
180	29	34	1.2	29	34	1.2	29	34	1.2	29	34	1.2
181	140	140	1.0	140	140	1.0	140	140	1.0	140	140	1.0
182	112	112	1.0	112	112	1.0	112	112	1.0	112	112	1.0
183	84	84	1.0	84	84	1.0	84	84	1.0	84	84	1.0
184	56	56	1.0	56	56	1.0	56	56	1.0	56	56	1.0
185	28	28	1.0	28	28	1.0	28	28	1.0	28	28	1.0
186	110	110	1.0	110	110	1.0	110	110	1.0	110	110	1.0
187	88	88	1.0	88	88	1.0	88	88	1.0	88	88	1.0
188	66	66	1.0	66	66	1.0	66	66	1.0	66	66	1.0
189	44	44	1.0	44	44	1.0	44	44	1.0	44	44	1.0
190	22	22	1.0	22	22	1.0	22	22	1.0	22	22	1.0

Table B.3: Structural response under each local failure scenario i when applying the combination of actions W2 with several dynamic amplification factors.

i	W3-DAF1			W3-DAF1.3			W3-DAF1.5			W3-DAF2		
	$\mathcal{M}(IDP_i)$ (m)	$\mathcal{M}(CP_i)$ (m)	DFP_i									
1	0	0	0.0	0	0	0.0	25	25	1.0	25	25	1.0
2	0	0	0.0	0	0	0.0	20	20	1.0	20	20	1.0
3	0	0	0.0	0	0	0.0	15	15	1.0	15	15	1.0
4	0	0	0.0	0	0	0.0	10	10	1.0	10	10	1.0
5	5	5	1.0	5	5	1.0	5	5	1.0	5	5	1.0
6	0	0	0.0	0	0	0.0	50	0	0.0	50	50	1.0
7	0	0	0.0	0	0	0.0	40	0	0.0	40	40	1.0
8	0	0	0.0	0	0	0.0	30	0	0.0	30	30	1.0
9	0	0	0.0	0	0	0.0	20	0	0.0	20	20	1.0
10	0	0	0.0	0	0	0.0	10	0	0.0	10	0	0.0
11	0	0	0.0	55	0	0.0	55	80	1.5	55	80	1.5
12	0	0	0.0	44	0	0.0	44	0	0.0	44	64	1.5
13	0	0	0.0	33	0	0.0	33	0	0.0	33	48	1.5
14	0	0	0.0	22	0	0.0	22	0	0.0	22	0	0.0
15	0	0	0.0	11	0	0.0	11	0	0.0	11	0	0.0
16	0	0	0.0	60	0	0.0	60	110	1.8	60	110	1.8
17	0	0	0.0	48	0	0.0	48	0	0.0	48	104	2.2
18	0	0	0.0	36	0	0.0	36	0	0.0	36	82	2.3
19	0	0	0.0	24	0	0.0	24	0	0.0	24	0	0.0
20	0	0	0.0	12	0	0.0	12	0	0.0	12	0	0.0

Annex B: Detailed results for the structural robustness assessment in Chapter V

21	0	0	0.0	60	0	0.0	60	0	0.0	60	140	2.3
22	0	0	0.0	48	0	0.0	48	0	0.0	48	134	2.8
23	0	0	0.0	36	0	0.0	36	0	0.0	36	0	0.0
24	0	0	0.0	24	0	0.0	24	0	0.0	24	0	0.0
25	0	0	0.0	12	0	0.0	12	0	0.0	12	0	0.0
26	0	0	0.0	60	0	0.0	60	0	0.0	60	280	4.7
27	0	0	0.0	48	0	0.0	48	0	0.0	48	280	5.8
28	0	0	0.0	36	0	0.0	36	0	0.0	36	0	0.0
29	0	0	0.0	24	0	0.0	24	0	0.0	24	0	0.0
30	0	0	0.0	12	0	0.0	12	0	0.0	12	0	0.0
31	0	0	0.0	60	0	0.0	60	0	0.0	60	140	2.3
32	0	0	0.0	48	0	0.0	48	0	0.0	48	134	2.8
33	0	0	0.0	36	0	0.0	36	0	0.0	36	0	0.0
34	0	0	0.0	24	0	0.0	24	0	0.0	24	0	0.0
35	0	0	0.0	12	0	0.0	12	0	0.0	12	0	0.0
36	0	0	0.0	60	0	0.0	60	110	1.8	60	110	1.8
37	0	0	0.0	48	0	0.0	48	0	0.0	48	104	2.2
38	0	0	0.0	36	0	0.0	36	0	0.0	36	82	2.3
39	0	0	0.0	24	0	0.0	24	0	0.0	24	0	0.0
40	0	0	0.0	12	0	0.0	12	0	0.0	12	0	0.0
41	0	0	0.0	55	0	0.0	55	80	1.5	55	80	1.5
42	0	0	0.0	44	0	0.0	44	0	0.0	44	64	1.5
43	0	0	0.0	33	0	0.0	33	0	0.0	33	48	1.5
44	0	0	0.0	22	0	0.0	22	0	0.0	22	0	0.0
45	0	0	0.0	11	0	0.0	11	0	0.0	11	0	0.0
46	0	0	0.0	0	0	0.0	50	0	0.0	50	50	1.0
47	0	0	0.0	0	0	0.0	40	0	0.0	40	40	1.0
48	0	0	0.0	0	0	0.0	30	0	0.0	30	30	1.0
49	0	0	0.0	0	0	0.0	20	0	0.0	20	20	1.0
50	0	0	0.0	0	0	0.0	10	0	0.0	10	0	0.0
51	0	0	0.0	0	0	0.0	25	25	1.0	25	25	1.0
52	0	0	0.0	0	0	0.0	20	20	1.0	20	20	1.0
53	0	0	0.0	0	0	0.0	15	15	1.0	15	15	1.0
54	0	0	0.0	0	0	0.0	10	10	1.0	10	10	1.0
55	5	5	1.0	5	5	1.0	5	5	1.0	5	5	1.0
56	50	50	1.0	50	50	1.0	50	50	1.0	50	50	1.0
57	40	40	1.0	40	40	1.0	40	40	1.0	40	40	1.0
58	30	30	1.0	30	30	1.0	30	30	1.0	30	30	1.0
59	20	20	1.0	20	20	1.0	20	20	1.0	20	20	1.0
60	10	10	1.0	10	10	1.0	10	10	1.0	10	10	1.0
61	80	80	1.0	80	80	1.0	80	80	1.0	80	80	1.0
62	64	64	1.0	64	64	1.0	64	64	1.0	64	64	1.0
63	48	48	1.0	48	48	1.0	48	48	1.0	48	48	1.0
64	32	32	1.0	32	32	1.0	32	32	1.0	32	32	1.0
65	16	16	1.0	16	16	1.0	16	16	1.0	16	16	1.0
66	85	110	1.3	85	110	1.3	85	110	1.3	85	110	1.3
67	68	88	1.3	68	88	1.3	68	88	1.3	68	88	1.3
68	51	66	1.3	51	66	1.3	51	66	1.3	51	66	1.3
69	34	0	0.0	34	44	1.3	34	44	1.3	34	44	1.3
70	17	0	0.0	17	0	0.0	17	0	0.0	17	22	1.3
71	90	140	1.6	90	140	1.6	90	140	1.6	90	140	1.6
72	72	128	1.8	72	128	1.8	72	128	1.8	72	128	1.8
73	54	100	1.9	54	100	1.9	54	100	1.9	54	100	1.9
74	36	0	0.0	36	0	0.0	36	56	1.6	36	56	1.6
75	18	0	0.0	18	0	0.0	18	0	0.0	18	18	1.0
76	90	170	1.9	90	170	1.9	90	170	1.9	90	170	1.9
77	72	158	2.2	72	158	2.2	72	158	2.2	72	158	2.2
78	54	0	0.0	54	124	2.3	54	124	2.3	54	124	2.3

Annex B: Detailed results for the structural robustness assessment in Chapter V

79	36	0	0.0	36	0	0.0	36	0	0.0	36	68	1.9
80	18	0	0.0	18	0	0.0	18	0	0.0	18	18	1.0
81	90	170	1.9	90	170	1.9	90	170	1.9	90	170	1.9
82	72	158	2.2	72	158	2.2	72	158	2.2	72	158	2.2
83	54	0	0.0	54	124	2.3	54	124	2.3	54	124	2.3
84	36	0	0.0	36	0	0.0	36	0	0.0	36	68	1.9
85	18	0	0.0	18	0	0.0	18	0	0.0	18	18	1.0
86	90	140	1.6	90	140	1.6	90	140	1.6	90	140	1.6
87	72	128	1.8	72	128	1.8	72	128	1.8	72	128	1.8
88	54	100	1.9	54	100	1.9	54	100	1.9	54	100	1.9
89	36	0	0.0	36	0	0.0	36	56	1.6	36	56	1.6
90	18	0	0.0	18	0	0.0	18	0	0.0	18	18	1.0
91	85	110	1.3	85	110	1.3	85	110	1.3	85	110	1.3
92	68	88	1.3	68	88	1.3	68	88	1.3	68	88	1.3
93	51	66	1.3	51	66	1.3	51	66	1.3	51	66	1.3
94	34	0	0.0	34	44	1.3	34	44	1.3	34	44	1.3
95	17	0	0.0	17	0	0.0	17	0	0.0	17	22	1.3
96	80	80	1.0	80	80	1.0	80	80	1.0	80	80	1.0
97	64	64	1.0	64	64	1.0	64	64	1.0	64	64	1.0
98	48	48	1.0	48	48	1.0	48	48	1.0	48	48	1.0
99	32	32	1.0	32	32	1.0	32	32	1.0	32	32	1.0
100	16	16	1.0	16	16	1.0	16	16	1.0	16	16	1.0
101	50	50	1.0	50	50	1.0	50	50	1.0	50	50	1.0
102	40	40	1.0	40	40	1.0	40	40	1.0	40	40	1.0
103	30	30	1.0	30	30	1.0	30	30	1.0	30	30	1.0
104	20	20	1.0	20	20	1.0	20	20	1.0	20	20	1.0
105	10	10	1.0	10	10	1.0	10	10	1.0	10	10	1.0
106	80	80	1.0	80	80	1.0	80	80	1.0	80	80	1.0
107	64	64	1.0	64	64	1.0	64	64	1.0	64	64	1.0
108	48	48	1.0	48	48	1.0	48	48	1.0	48	48	1.0
109	32	32	1.0	32	32	1.0	32	32	1.0	32	32	1.0
110	16	16	1.0	16	16	1.0	16	16	1.0	16	16	1.0
111	110	110	1.0	110	110	1.0	110	110	1.0	110	110	1.0
112	88	88	1.0	88	88	1.0	88	88	1.0	88	88	1.0
113	66	66	1.0	66	66	1.0	66	66	1.0	66	66	1.0
114	44	44	1.0	44	44	1.0	44	44	1.0	44	44	1.0
115	22	22	1.0	22	22	1.0	22	22	1.0	22	22	1.0
116	115	140	1.2	115	140	1.2	115	140	1.2	115	140	1.2
117	92	112	1.2	92	112	1.2	92	112	1.2	92	112	1.2
118	69	84	1.2	69	84	1.2	69	84	1.2	69	84	1.2
119	46	56	1.2	46	56	1.2	46	56	1.2	46	56	1.2
120	23	0	0.0	23	28	1.2	23	28	1.2	23	28	1.2
121	120	170	1.4	120	170	1.4	120	170	1.4	120	170	1.4
122	96	152	1.6	96	152	1.6	96	152	1.6	96	152	1.6
123	72	118	1.6	72	118	1.6	72	118	1.6	72	118	1.6
124	48	68	1.4	48	68	1.4	48	68	1.4	48	68	1.4
125	24	0	0.0	24	0	0.0	24	0	0.0	24	34	1.4
126	120	280	2.3	120	280	2.3	120	280	2.3	120	280	2.3
127	96	268	2.8	96	268	2.8	96	268	2.8	96	268	2.8
128	72	212	2.9	72	212	2.9	72	212	2.9	72	212	2.9
129	48	0	0.0	48	112	2.3	48	112	2.3	48	112	2.3
130	24	0	0.0	24	0	0.0	24	0	0.0	24	24	1.0
131	120	170	1.4	120	170	1.4	120	170	1.4	120	170	1.4
132	96	152	1.6	96	152	1.6	96	152	1.6	96	152	1.6
133	72	118	1.6	72	118	1.6	72	118	1.6	72	118	1.6
134	48	68	1.4	48	68	1.4	48	68	1.4	48	68	1.4
135	24	0	0.0	24	0	0.0	24	0	0.0	24	34	1.4
136	115	140	1.2	115	140	1.2	115	140	1.2	115	140	1.2

137	92	112	1.2	92	112	1.2	92	112	1.2	92	112	1.2
138	69	84	1.2	69	84	1.2	69	84	1.2	69	84	1.2
139	46	56	1.2	46	56	1.2	46	56	1.2	46	56	1.2
140	23	0	0.0	23	28	1.2	23	28	1.2	23	28	1.2
141	110	110	1.0	110	110	1.0	110	110	1.0	110	110	1.0
142	88	88	1.0	88	88	1.0	88	88	1.0	88	88	1.0
143	66	66	1.0	66	66	1.0	66	66	1.0	66	66	1.0
144	44	44	1.0	44	44	1.0	44	44	1.0	44	44	1.0
145	22	22	1.0	22	22	1.0	22	22	1.0	22	22	1.0
146	80	80	1.0	80	80	1.0	80	80	1.0	80	80	1.0
147	64	64	1.0	64	64	1.0	64	64	1.0	64	64	1.0
148	48	48	1.0	48	48	1.0	48	48	1.0	48	48	1.0
149	32	32	1.0	32	32	1.0	32	32	1.0	32	32	1.0
150	16	16	1.0	16	16	1.0	16	16	1.0	16	16	1.0
151	110	110	1.0	110	110	1.0	110	110	1.0	110	110	1.0
152	88	88	1.0	88	88	1.0	88	88	1.0	88	88	1.0
153	66	66	1.0	66	66	1.0	66	66	1.0	66	66	1.0
154	44	44	1.0	44	44	1.0	44	44	1.0	44	44	1.0
155	22	22	1.0	22	22	1.0	22	22	1.0	22	22	1.0
156	140	140	1.0	140	140	1.0	140	140	1.0	140	140	1.0
157	112	112	1.0	112	112	1.0	112	112	1.0	112	112	1.0
158	84	84	1.0	84	84	1.0	84	84	1.0	84	84	1.0
159	56	56	1.0	56	56	1.0	56	56	1.0	56	56	1.0
160	28	28	1.0	28	28	1.0	28	28	1.0	28	28	1.0
161	145	170	1.2	145	170	1.2	145	170	1.2	145	170	1.2
162	116	136	1.2	116	136	1.2	116	136	1.2	116	136	1.2
163	87	102	1.2	87	102	1.2	87	102	1.2	87	102	1.2
164	58	68	1.2	58	68	1.2	58	68	1.2	58	68	1.2
165	29	34	1.2	29	34	1.2	29	34	1.2	29	34	1.2
166	150	200	1.3	150	200	1.3	150	200	1.3	150	200	1.3
167	120	176	1.5	120	176	1.5	120	176	1.5	120	176	1.5
168	90	136	1.5	90	136	1.5	90	136	1.5	90	136	1.5
169	60	80	1.3	60	80	1.3	60	80	1.3	60	80	1.3
170	30	0	0.0	30	40	1.3	30	40	1.3	30	40	1.3
171	150	200	1.3	150	200	1.3	150	200	1.3	150	200	1.3
172	120	176	1.5	120	176	1.5	120	176	1.5	120	176	1.5
173	90	136	1.5	90	136	1.5	90	136	1.5	90	136	1.5
174	60	80	1.3	60	80	1.3	60	80	1.3	60	80	1.3
175	30	0	0.0	30	40	1.3	30	40	1.3	30	40	1.3
176	145	170	1.2	145	170	1.2	145	170	1.2	145	170	1.2
177	116	136	1.2	116	136	1.2	116	136	1.2	116	136	1.2
178	87	102	1.2	87	102	1.2	87	102	1.2	87	102	1.2
179	58	68	1.2	58	68	1.2	58	68	1.2	58	68	1.2
180	29	34	1.2	29	34	1.2	29	34	1.2	29	34	1.2
181	140	140	1.0	140	140	1.0	140	140	1.0	140	140	1.0
182	112	112	1.0	112	112	1.0	112	112	1.0	112	112	1.0
183	84	84	1.0	84	84	1.0	84	84	1.0	84	84	1.0
184	56	56	1.0	56	56	1.0	56	56	1.0	56	56	1.0
185	28	28	1.0	28	28	1.0	28	28	1.0	28	28	1.0
186	110	110	1.0	110	110	1.0	110	110	1.0	110	110	1.0
187	88	88	1.0	88	88	1.0	88	88	1.0	88	88	1.0
188	66	66	1.0	66	66	1.0	66	66	1.0	66	66	1.0
189	44	44	1.0	44	44	1.0	44	44	1.0	44	44	1.0
190	22	22	1.0	22	22	1.0	22	22	1.0	22	22	1.0

Table B.4: Structural response under each local failure scenario i when applying the combination of actions W3 with several dynamic amplification factors.

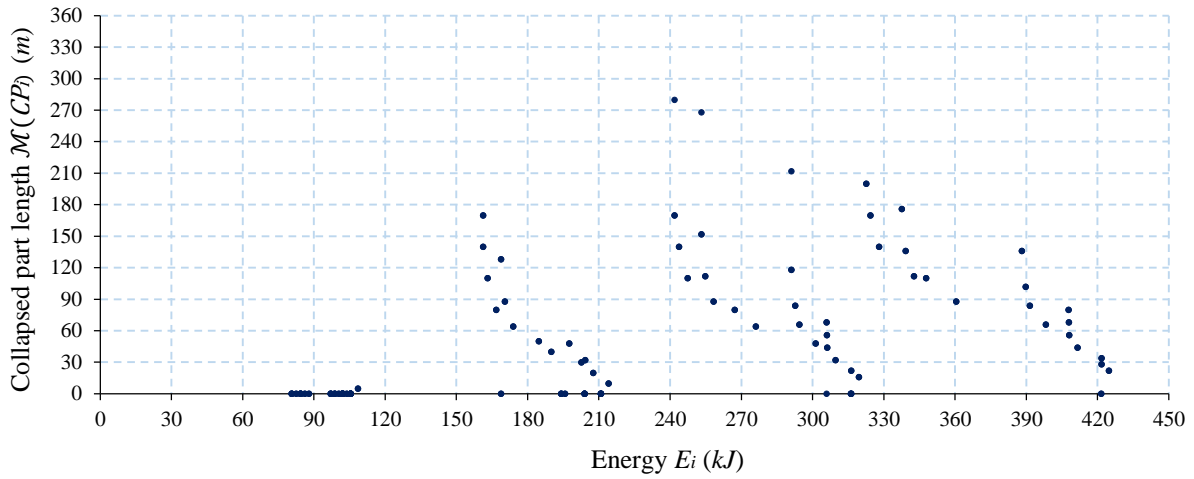


Figure B.1: Local failure energy – collapsed part length diagrams under W1-DAF1.

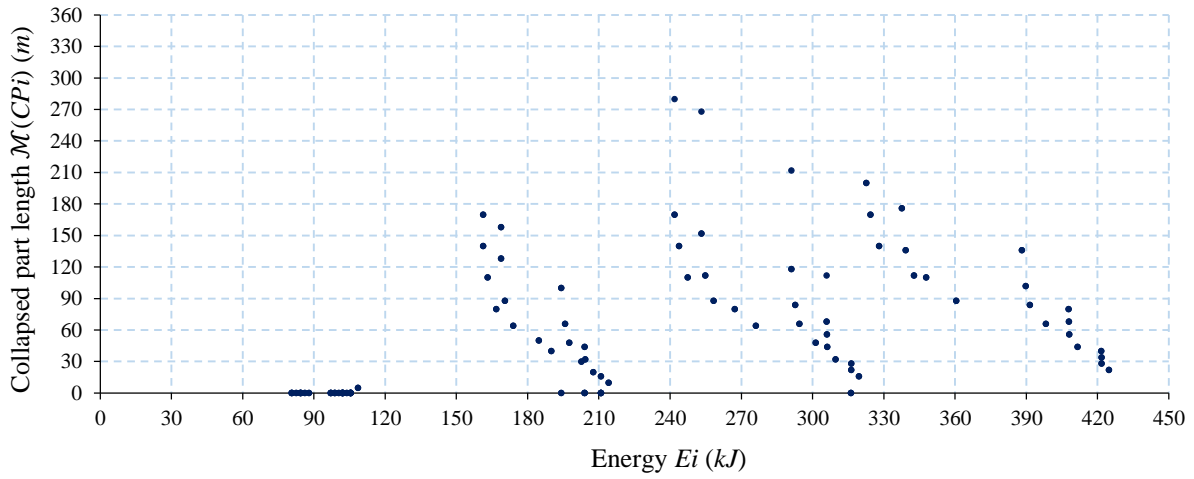


Figure B.2: Local failure energy – collapsed part length diagrams under W1-DAF1.3.

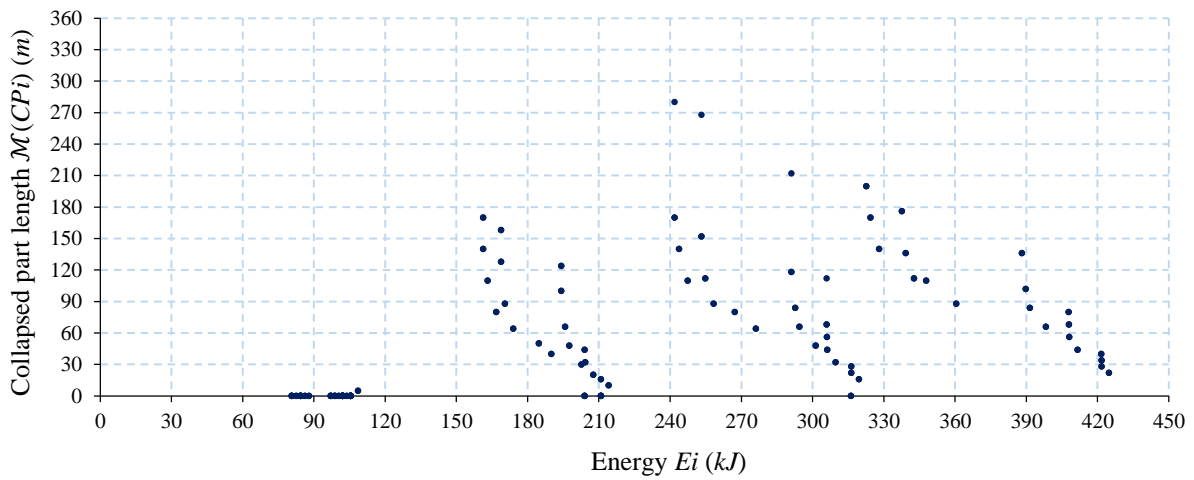


Figure B.3: Local failure energy – collapsed part length diagrams under W1-DAF1.5.

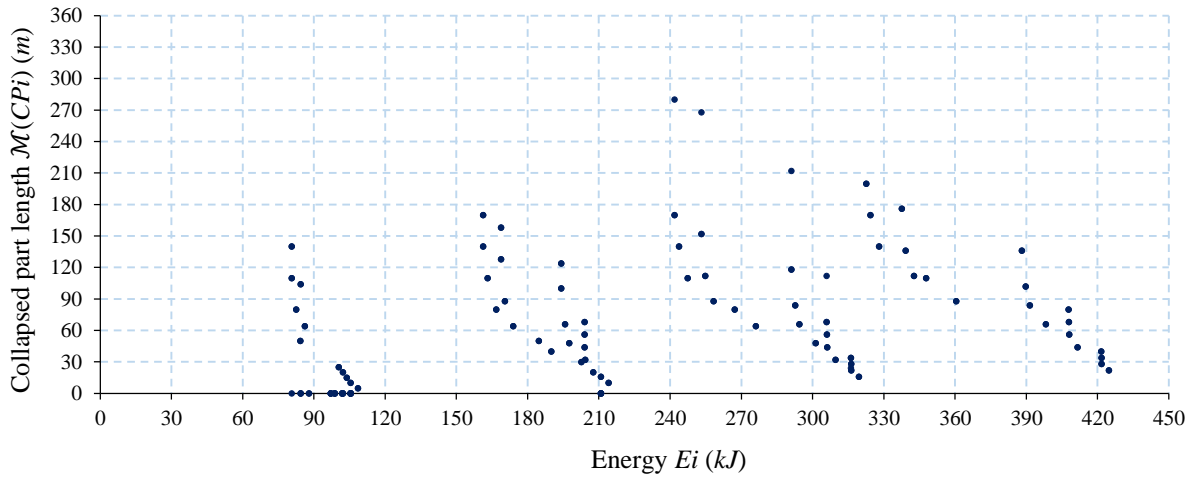


Figure B.4: Local failure energy – collapsed part length diagrams under W1-DAF2.

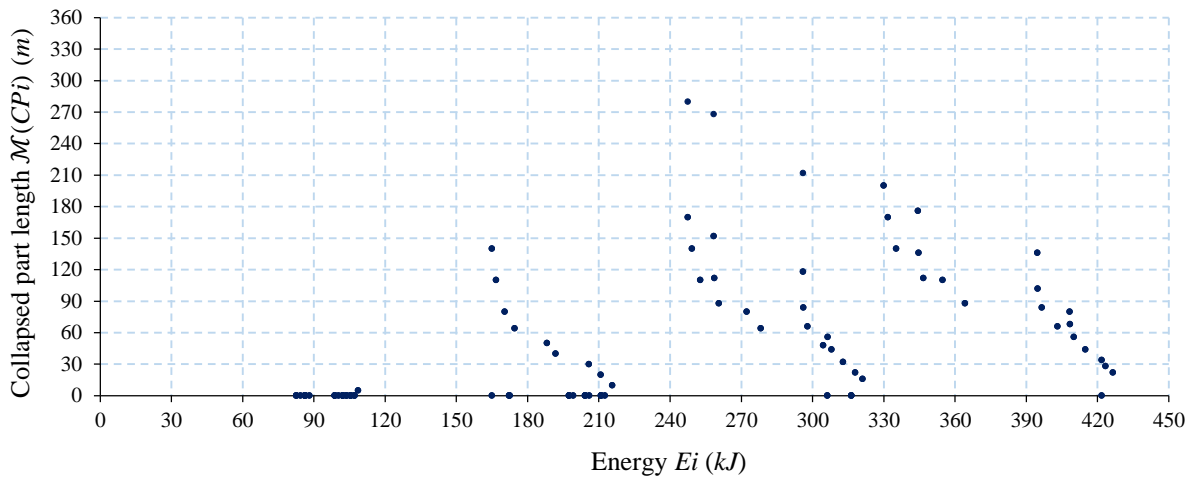


Figure B.5: Local failure energy – collapsed part length diagrams under W2-DAF1.

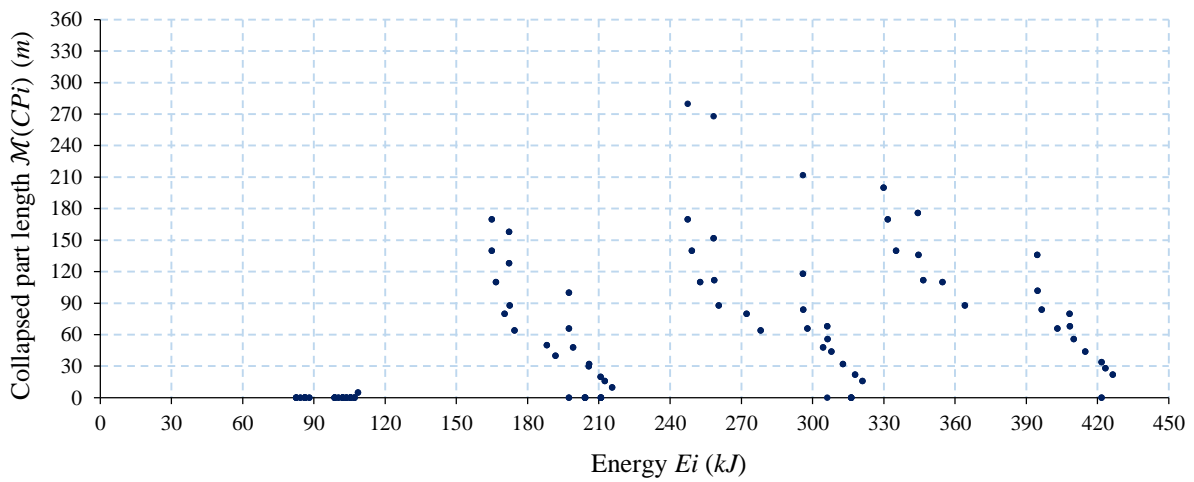


Figure B.6: Local failure energy – collapsed part length diagrams under W2-DAF1.3.

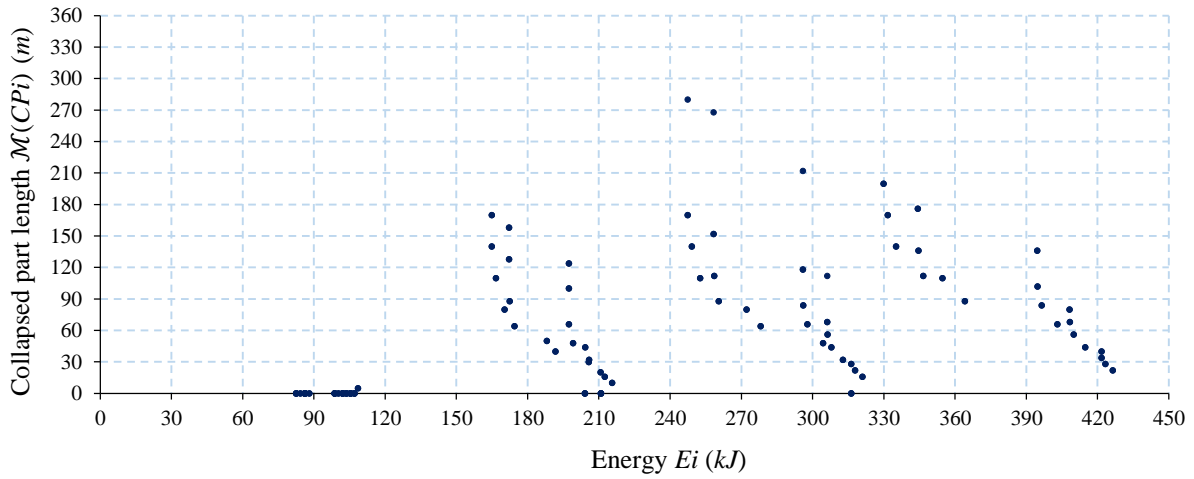


Figure B.7: Local failure energy – collapsed part length diagrams under W2-DAF1.5.

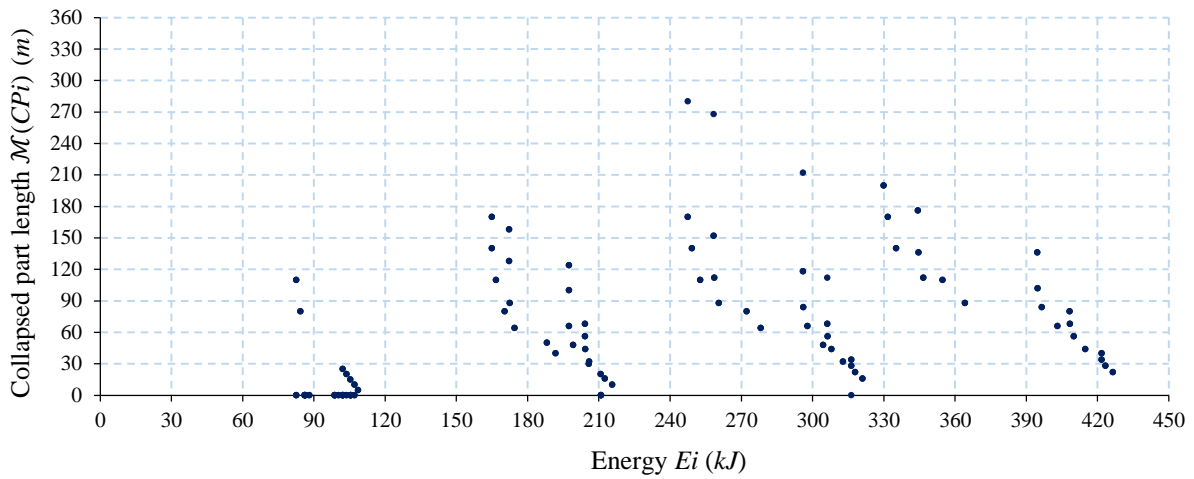


Figure B.8: Local failure energy – collapsed part length diagrams under W2-DAF2.

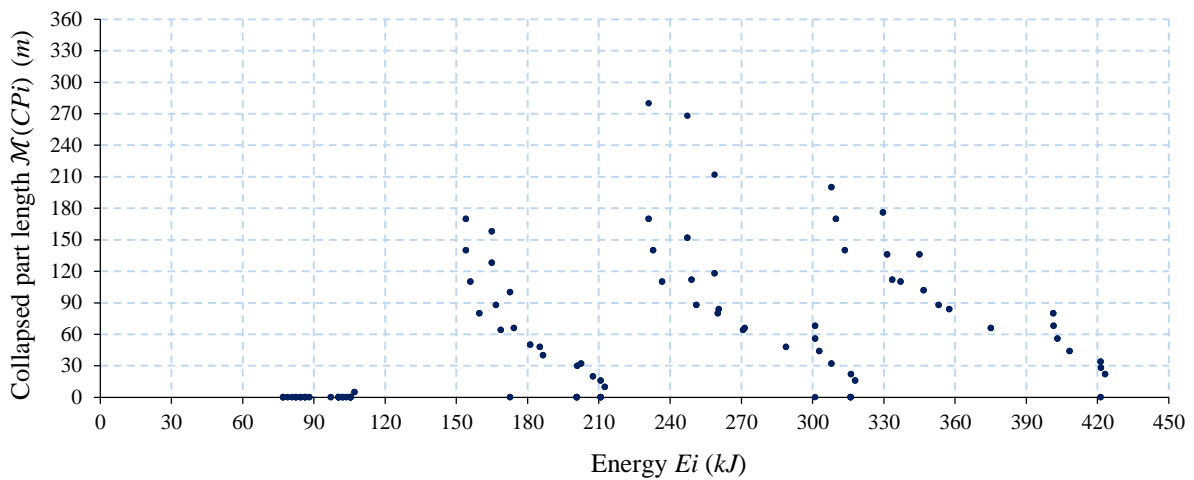


Figure B.9: Local failure energy – collapsed part length diagrams under W3-DAF1.

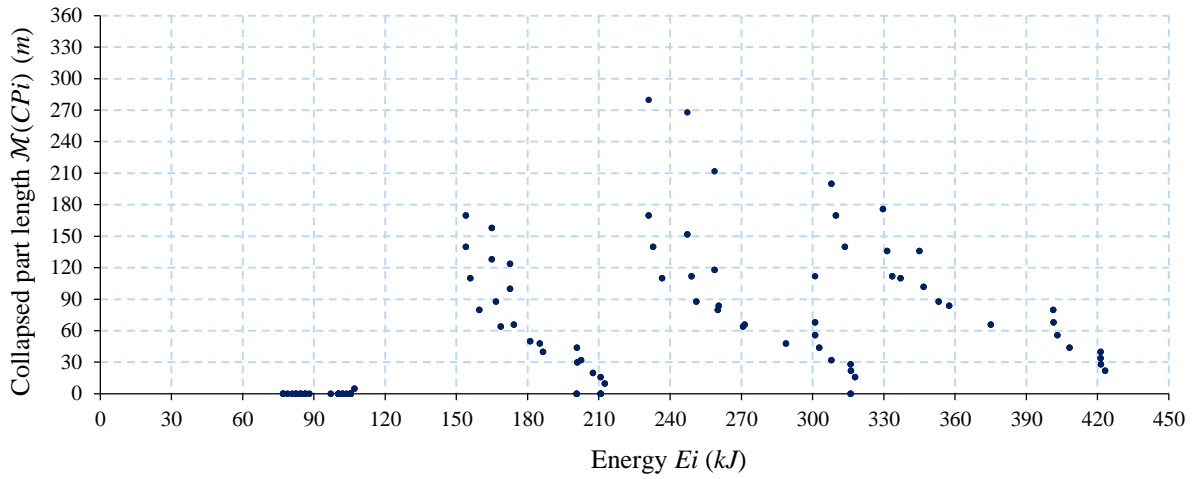


Figure B.10: Local failure energy – collapsed part length diagrams under W3-DAF1.3.

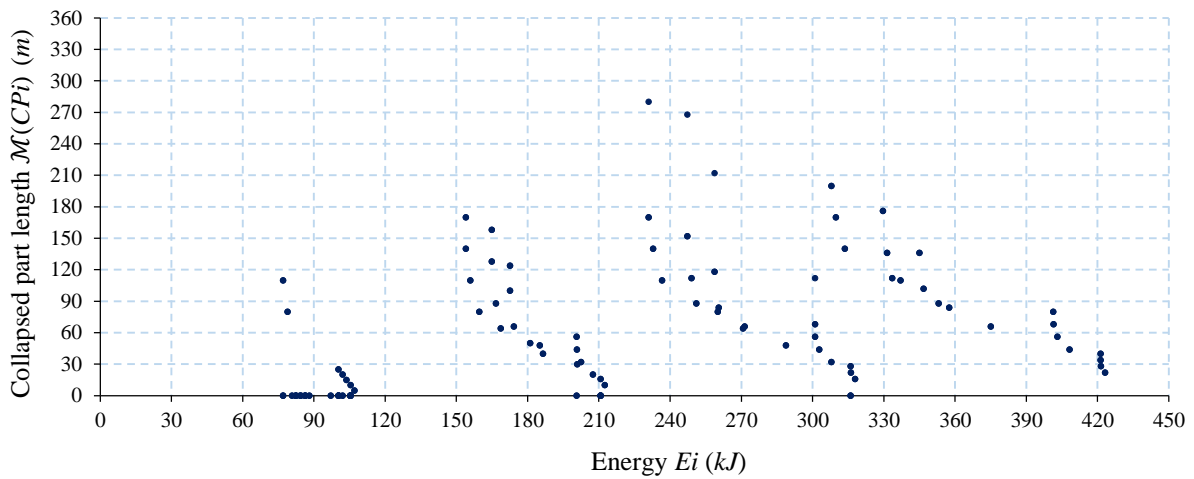


Figure B.11: Local failure energy – collapsed part length diagrams under W3-DAF1.5.

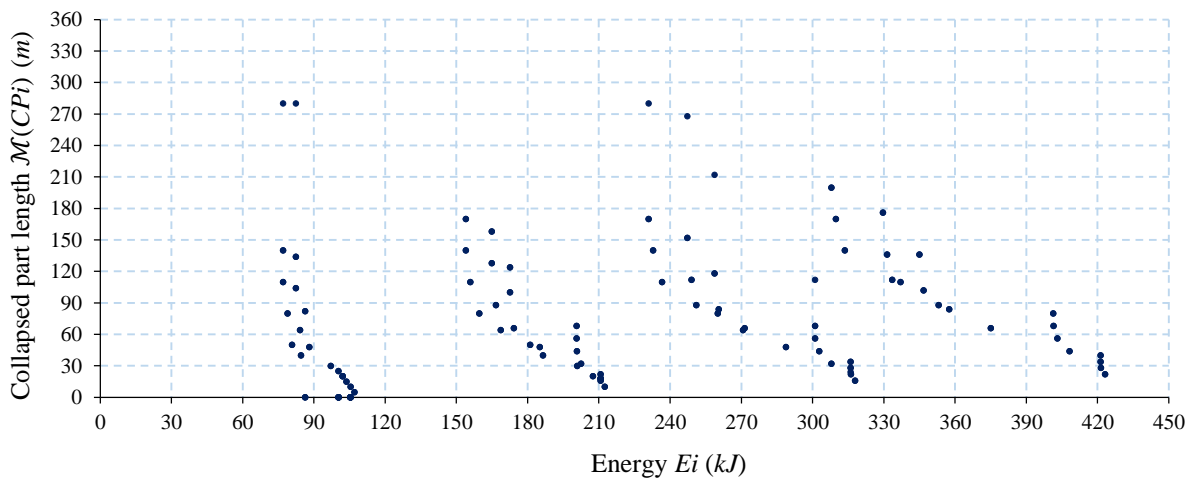


Figure B.12: Local failure energy – collapsed part length diagrams under W3-DAF2.

Pareto front	i	$\mathcal{M}(IDP_i)$ (m)	$\mathcal{M}(CP_i)$ (m)	Pareto front	i	$\mathcal{M}(IDP_i)$ (m)	$\mathcal{M}(CP_i)$ (m)
S3-W1-DAF1	5	5	5	S3-W2-DAF1.3	127	96	268
	55	5	5		126	120	280
	60	10	10		5	5	5
	105	10	10		55	5	5
	110	16	16		60	10	10
	150	16	16		105	10	10
	59	20	20		65	16	16
	104	20	20		100	16	16
	115	22	22		110	16	16
	145	22	22		150	16	16
	155	22	22		59	20	20
	190	22	22		104	20	20
	160	28	28		115	22	22
	185	28	28		145	22	22
	165	29	34		155	22	22
	180	29	34		190	22	22
	57	40	40	120	23	28	
	102	40	40	140	23	28	
	114	44	44	165	29	34	
	144	44	44	180	29	34	
	154	44	44	170	30	40	
	189	44	44	175	30	40	
	119	46	56	69	34	44	
	139	46	56	94	34	44	
	124	48	68	119	46	56	
	134	48	68	139	46	56	
	169	60	80	129	48	112	
	174	60	80	78	54	124	
	67	68	88	83	54	124	
	92	68	88	128	72	212	
	128	72	212	127	96	268	
	127	96	268	126	120	280	
126	120	280	5	5	5		
S3-W1-DAF1.3	5	5	5	S3-W2-DAF2	55	5	5
	55	5	5		4	10	10
	60	10	10		54	10	10
	105	10	10		60	10	10
	65	16	16		105	10	10
	100	16	16		3	15	15
	110	16	16		53	15	15
	150	16	16		65	16	16
	59	20	20		100	16	16
	104	20	20		110	16	16
	115	22	22		150	16	16
	145	22	22		2	20	20
	155	22	22		52	20	20
	190	22	22		59	20	20
	120	23	28		104	20	20
	140	23	28		115	22	22
	165	29	34		145	22	22
	180	29	34		155	22	22
	170	30	40		190	22	22
	175	30	40		120	23	28
	69	34	44		140	23	28
	94	34	44		125	24	34
	119	46	56		135	24	34

	139	46	56		170	30	40
	129	48	112		175	30	40
	128	72	212		69	34	44
	127	96	268		94	34	44
	126	120	280		79	36	68
S3-W1-DAF1.5	5	5	5	S3-W3-DAF1	84	36	68
	55	5	5		129	48	112
	60	10	10		78	54	124
	105	10	10		83	54	124
	65	16	16		128	72	212
	100	16	16		127	96	268
	110	16	16		126	120	280
	150	16	16		5	5	5
	59	20	20		55	5	5
	104	20	20		60	10	10
	115	22	22		105	10	10
	145	22	22		65	16	16
	155	22	22		100	16	16
	190	22	22		110	16	16
	120	23	28		150	16	16
	140	23	28		59	20	20
	165	29	34		104	20	20
	180	29	34		115	22	22
	170	30	40		145	22	22
	175	30	40		155	22	22
	69	34	44		190	22	22
	94	34	44		160	28	28
	119	46	56		185	28	28
	139	46	56		165	29	34
	129	48	112		180	29	34
	78	54	124		57	40	40
	83	54	124		102	40	40
	128	72	212		114	44	44
	127	96	268		144	44	44
	126	120	280		154	44	44
S3-W1-DAF2	5	5	5	189	44	44	
	55	5	5	119	46	56	
	4	10	10	139	46	56	
	54	10	10	124	48	68	
	60	10	10	134	48	68	
	105	10	10	73	54	100	
	3	15	15	88	54	100	
	53	15	15	128	72	212	
	65	16	16	127	96	268	
	100	16	16	126	120	280	
	110	16	16	5	5	5	
	150	16	16	55	5	5	
	2	20	20	60	10	10	
	52	20	20	105	10	10	
	59	20	20	65	16	16	
	104	20	20	100	16	16	
	115	22	22	110	16	16	
	145	22	22	150	16	16	
	155	22	22	59	20	20	
	190	22	22	104	20	20	
120	23	28	115	22	22		
140	23	28	145	22	22		
125	24	34	155	22	22		

115	22	22	105	10	10
145	22	22	3	15	15
155	22	22	53	15	15
190	22	22	65	16	16
160	28	28	100	16	16
185	28	28	110	16	16
165	29	34	150	16	16
180	29	34	70	17	22
57	40	40	95	17	22
102	40	40	120	23	28
114	44	44	140	23	28
144	44	44	125	24	34
154	44	44	135	24	34
189	44	44	170	30	40
119	46	56	175	30	40
139	46	56	13	33	48
124	48	68	43	33	48
134	48	68	18	36	82
73	54	100	38	36	82
88	54	100	27	48	280
128	72	212			

Table B.5: Non-dominated scenarios for each case study of Table V.1 related to Equation (IV.13).

One provides now the detailed results on the structural robustness assessment of the design configurations ST6 and ST7 considered in Section V.3. Table B.6 presents the failure energy E_i and structural response under each local failure scenario i for configuration ST7. The non-dominated scenarios (Pareto fronts) according to the bi-objective problems of Equations IV.8, IV.12 and IV.13 are presented in Table B.7, Table B.8 and Table B.9, respectively.

i	Column (s) #	E_i (kJ)	$\mathcal{M}(IDP_i)$ (m)	$\mathcal{M}(CP_i)$ (m)	DFP_i	Category
1	1	100.4	0	0	0.0	C1
2	2	102.1	0	0	0.0	C1
3	3	103.8	0	0	0.0	C1
4	4	105.4	0	0	0.0	C1
5	5	108.6	5	5	1.0	C3
6	6	84.2	0	0	0.0	C1
7	7	87.8	0	0	0.0	C1
8	8	98.8	0	0	0.0	C1
9	9	102.1	0	0	0.0	C1
10	10	105.4	0	0	0.0	C1
11	11	80.6	60	85	1.4	C4
12	12	84.4	48	0	0.0	C2
13	13	97.0	36	0	0.0	C2
14	14	101.5	24	0	0.0	C2
15	15	105.3	12	0	0.0	C2
16	16	77.0	70	120	1.7	C4
17	17	82.4	56	113	2.0	C4
18	18	95.2	42	0	0.0	C2
19	19	100.3	28	0	0.0	C2
20	20	105.2	14	0	0.0	C2
21	21	77.0	70	155	2.2	C4
22	22	82.4	56	0	0.0	C2

Annex B: Detailed results for the structural robustness assessment in Chapter V

23	23	95.2	42	0	0.0	C2
24	24	100.3	28	0	0.0	C2
25	25	105.2	14	0	0.0	C2
26	26	77.0	70	0	0.0	C2
27	27	82.4	56	0	0.0	C2
28	28	95.2	42	0	0.0	C2
29	29	100.3	28	0	0.0	C2
30	30	105.2	14	0	0.0	C2
31	31	77.0	70	155	2.2	C4
32	32	82.4	56	0	0.0	C2
33	33	95.2	42	0	0.0	C2
34	34	100.3	28	0	0.0	C2
35	35	105.2	14	0	0.0	C2
36	36	77.0	70	120	1.7	C4
37	37	82.4	56	113	2.0	C4
38	38	95.2	42	0	0.0	C2
39	39	100.3	28	0	0.0	C2
40	40	105.2	14	0	0.0	C2
41	41	80.6	60	85	1.4	C4
42	42	84.4	48	0	0.0	C2
43	43	97.0	36	0	0.0	C2
44	44	101.5	24	0	0.0	C2
45	45	105.3	12	0	0.0	C2
46	46	84.2	0	0	0.0	C1
47	47	87.8	0	0	0.0	C1
48	48	98.8	0	0	0.0	C1
49	49	102.1	0	0	0.0	C1
50	50	105.4	0	0	0.0	C1
51	51	100.4	0	0	0.0	C1
52	52	102.1	0	0	0.0	C1
53	53	103.8	0	0	0.0	C1
54	54	105.4	0	0	0.0	C1
55	55	108.6	5	5	1.0	C3
56	1-6	184.7	50	50	1.0	C3
57	2-7	190.0	40	40	1.0	C3
58	3-8	202.6	30	30	1.0	C3
59	4-9	207.6	20	20	1.0	C3
60	5-10	214.0	10	10	1.0	C3
61	6-11	164.8	85	85	1.0	C3
62	7-12	172.2	68	68	1.0	C3
63	8-13	195.8	51	51	1.0	C3
64	9-14	203.6	34	34	1.0	C3
65	10 - 15	210.7	17	17	1.0	C3
66	11-16	157.6	95	120	1.3	C4
67	12-17	166.7	76	96	1.3	C4
68	13-18	192.2	57	72	1.3	C4
69	14-19	201.8	38	48	1.3	C4
70	15-20	210.5	19	0	0.0	C2
71	16-21	153.9	105	155	1.5	C4
72	17-22	164.8	84	141	1.7	C4
73	18-23	190.4	63	110	1.7	C4
74	19-24	200.6	42	62	1.5	C4
75	20-25	210.4	21	0	0.0	C2
76	21-26	153.9	105	190	1.8	C4
77	22-27	164.8	84	176	2.1	C4
78	23-28	190.4	63	138	2.2	C4
79	24-29	200.6	42	76	1.8	C4
80	25-30	210.4	21	0	0.0	C2

Annex B: Detailed results for the structural robustness assessment in Chapter V

81	26-31	153.9	105	190	1.8	C4
82	27-32	164.8	84	176	2.1	C4
83	28-33	190.4	63	138	2.2	C4
84	29-34	200.6	42	76	1.8	C4
85	30-35	210.4	21	0	0.0	C2
86	31-36	153.9	105	155	1.5	C4
87	32-37	164.8	84	141	1.7	C4
88	33-38	190.4	63	110	1.7	C4
89	34-39	200.6	42	62	1.5	C4
90	35-40	210.4	21	0	0.0	C2
91	36-41	157.6	95	120	1.3	C4
92	37-42	166.7	76	96	1.3	C4
93	38-43	192.2	57	72	1.3	C4
94	39-44	201.8	38	48	1.3	C4
95	40-45	210.5	19	0	0.0	C2
96	41-46	164.8	85	85	1.0	C3
97	42 - 47	172.2	68	68	1.0	C3
98	43-48	195.8	51	51	1.0	C3
99	44-49	203.6	34	34	1.0	C3
100	45-50	210.7	17	17	1.0	C3
101	46-51	184.7	50	50	1.0	C3
102	47-52	190.0	40	40	1.0	C3
103	48-53	202.6	30	30	1.0	C3
104	49-54	207.6	20	20	1.0	C3
105	50-55	214.0	10	10	1.0	C3
106	1-6-11	265.3	85	85	1.0	C3
107	2-7-12	274.3	68	68	1.0	C3
108	3-8-13	299.6	51	51	1.0	C3
109	4-9-14	309.1	34	34	1.0	C3
110	5-10-15	319.3	17	17	1.0	C3
111	6-11-16	241.8	120	120	1.0	C3
112	7-12-17	254.6	96	96	1.0	C3
113	8-13-18	291.0	72	72	1.0	C3
114	9-14-19	303.9	48	48	1.0	C3
115	10-15-20	315.9	24	24	1.0	C3
116	11-16-21	234.5	130	155	1.2	C4
117	12-17-22	249.1	104	124	1.2	C4
118	13-18-23	287.4	78	93	1.2	C4
119	14-19-24	302.1	52	62	1.2	C4
120	15-20-25	315.7	26	31	1.2	C4
121	16-21-26	230.9	140	190	1.4	C4
122	17-22-27	247.1	112	169	1.5	C4
123	18-23-28	285.6	84	131	1.6	C4
124	19-24-29	300.9	56	76	1.4	C4
125	20-25-30	315.6	28	38	1.4	C4
126	21-26-31	230.9	140	310	2.2	C4
127	22-27-32	247.1	112	296	2.6	C4
128	23-28-33	285.6	84	234	2.8	C4
129	24-29-34	300.9	56	124	2.2	C4
130	25-30-35	315.6	28	0	0.0	C2
131	26-31-36	230.9	140	190	1.4	C4
132	27-32-37	247.1	112	169	1.5	C4
133	28-33-38	285.6	84	131	1.6	C4
134	29-34-39	300.9	56	76	1.4	C4
135	30-35-40	315.6	28	38	1.4	C4
136	31-36-41	234.5	130	155	1.2	C4
137	32-37-42	249.1	104	124	1.2	C4
138	33-38-43	287.4	78	93	1.2	C4

139	34-39-44	302.1	52	62	1.2	C4
140	35-40-45	315.7	26	31	1.2	C4
141	36-41-46	241.8	120	120	1.0	C3
142	37-42-47	254.6	96	96	1.0	C3
143	38-43-48	291.0	72	72	1.0	C3
144	39-44-49	303.9	48	48	1.0	C3
145	40-45-50	315.9	24	24	1.0	C3
146	41-46-51	265.3	85	85	1.0	C3
147	42-47-52	274.3	68	68	1.0	C3
148	43-48-53	299.6	51	51	1.0	C3
149	44-49-54	309.1	34	34	1.0	C3
150	45-50-55	319.3	17	17	1.0	C3
151	1-6-11-16	342.2	120	120	1.0	C3
152	2-7-12-17	356.7	96	96	1.0	C3
153	3-8-13-18	394.8	72	72	1.0	C3
154	4-9-14-19	409.4	48	48	1.0	C3
155	5-10-15-20	424.5	24	24	1.0	C3
156	6-11-16-21	318.7	155	155	1.0	C3
157	7-12-17-22	337.0	124	124	1.0	C4
158	8-13-18-23	386.2	93	93	1.0	C3
159	9-14-19-24	404.3	62	62	1.0	C3
160	10-15-20-25	421.1	31	31	1.0	C3
161	11-16-21-26	311.5	165	190	1.2	C4
162	12-17-22-27	331.5	132	152	1.2	C4
163	13-18-23-28	382.6	99	114	1.2	C4
164	14-19-24-29	402.4	66	76	1.2	C4
165	15-20-25-30	420.9	33	38	1.2	C4
166	16-21-26-31	307.8	175	225	1.3	C4
167	17-22-27-32	329.5	140	197	1.4	C4
168	18-23-28-33	380.8	105	152	1.4	C4
169	19-24-29-34	401.3	70	90	1.3	C4
170	20-25-30-35	420.8	35	45	1.3	C4
171	21-26-31-36	307.8	175	225	1.3	C4
172	22-27-32-37	329.5	140	197	1.4	C4
173	23-28-33-38	380.8	105	152	1.4	C4
174	24-29-34-39	401.3	70	90	1.3	C4
175	25-30-35-40	420.8	35	45	1.3	C4
176	26-31-36-41	311.5	165	190	1.2	C4
177	27-32-37-42	331.5	132	152	1.2	C4
178	28-33-38-43	382.6	99	114	1.2	C4
179	29-34-39-44	402.4	66	76	1.2	C4
180	30-35-40-45	420.9	33	38	1.2	C4
181	31-36-41-46	318.7	155	155	1.0	C3
182	32-37-42-47	337.0	124	124	1.0	C4
183	33-38-43-48	386.2	93	93	1.0	C3
184	34-39-44-49	404.3	62	62	1.0	C3
185	35-40-45-50	421.1	31	31	1.0	C3
186	36-41-46-51	342.2	120	120	1.0	C3
187	37-42-47-52	356.7	96	96	1.0	C3
188	38-43-48-53	394.8	72	72	1.0	C3
189	39-44-49-54	409.4	48	48	1.0	C3
190	40-45-50-55	424.5	24	24	1.0	C3

Table B.6: Failure energy and structural response under each local failure scenario i for the configuration ST7.

Pareto front	i	Column #	E_i (kJ)	DFP_i
--------------	-----	----------	------------	---------

S1-ST6	5	5	108.6	1.0
	55	55	108.6	1.0
	76	21-26	161.2	1.9
	77	26-31	168.7	2.2
	78	22-27	194.0	2.3
	81	27-32	161.2	1.9
	82	23-28	168.7	2.2
	83	28-33	194.0	2.3
	126	21-26-31	241.9	2.3
	127	22-27-32	253.1	2.8
	128	23-28-33	291.0	2.9
S1-ST7	21	21	77.0	2.2
	31	31	77.0	2.2
	127	22-27-32	247.1	2.6
	128	23-28-33	285.6	2.8

Table B.7: Non-dominated scenarios for the design configurations ST6 and ST7 related to Equation (IV.8).

Pareto front	i	Column #	$\mathcal{M}(IDP_i) (m)$	DFP_i
S2-ST6	5	5	5	1.0
	55	55	5	1.0
	120	15-20-25	23	1.2
	140	35-40-45	23	1.2
	170	20-25-30-35	30	1.3
	175	25-30-35-40	30	1.3
	129	24-29-34	48	2.3
	128	23-28-33	72	2.9
S2-ST7	5	5	5	1.0
	55	55	5	1.0
	120	15-20-25	26	1.2
	140	35-40-45	26	1.2
	125	20-25-30	28	1.4
	135	30-35-40	28	1.4
	79	24-29	42	1.8
	84	29-34	42	1.8
	129	24-29-34	56	2.2
	128	23-28-33	84	2.8

Table B.8: Non-dominated scenarios for the design configurations ST6 and ST7 related to Equation (IV.12).

Pareto front	i	Column #	$\mathcal{M}(IDP_i) (m)$	$\mathcal{M}(IDP_i) (m)$
S3-ST6	5	5	5	5
	55	55	5	5
	60	5-10	10	10
	105	50-55	10	10
	65	10-15	16	16
	100	45-50	16	16

	110	5-10-15	16	16
	150	45-50-55	16	16
	59	4-9	20	20
	104	49-54	20	20
	115	10-15-20	22	22
	145	40-45-50	22	22
	155	5-10-15-20	22	22
	190	40-45-50-55	22	22
	120	15-20-25	23	28
	140	35-40-45	23	28
	165	15-20-25-30	29	34
	180	30-35-40-45	29	34
	170	20-25-30-35	30	40
	175	25-30-35-40	30	40
	69	14-19	34	44
	94	39-44	34	44
	119	14-19-24	46	56
	139	34-39-44	46	56
	129	24-29-34	48	112
	78	23-28	54	124
	83	28-33	54	124
	128	23-28-33	72	212
	127	22-27-32	96	268
	126	21-26-31	120	280
S3-ST7	5	5	5	5
	55	55	5	5
	60	5-10	10	10
	105	50-55	10	10
	65	10-15	17	17
	100	45-50	17	17
	110	5-10-15	17	17
	150	45-50-55	17	17
	59	4-9	20	20
	104	49-54	20	20
	115	10-15-20	24	24
	145	40-45-50	24	24
	155	5-10-15-20	24	24
	190	40-45-50-55	24	24
	120	15-20-25	26	31
	140	35-40-45	26	31
	125	20-25-30	28	38
	135	30-35-40	28	38
	170	20-25-30-35	35	45
	175	25-30-35-40	35	45
69	14-19	38	48	
94	39-44	38	48	
79	24-29	42	76	

	84	29-34	42	76
	129	24-29-34	56	124
	78	23-28	63	138
	83	28-33	63	138
	21	21	70	155
	31	31	70	155
	128	23-28-33	84	234
	127	22-27-32	112	296
	126	21-26-31	140	310

Table B.9: Non-dominated scenarios for the design configurations ST6 and ST7 related to Equation (IV.13).

Finally, the failure energy and the structural response under each local failure scenario i for the assumption DUC2 are described in Table B.10.

i	Column(s) #	E_i (kJ)	$\mathcal{M}(IDP_i)$ (m)	$\mathcal{M}(CP_i)$ (m)	DFP_i	Category
1	1	100.4	0	0	0.0	C1
2	2	102.1	0	0	0.0	C1
3	3	103.8	0	0	0.0	C1
4	4	105.4	0	0	0.0	C1
5	5	108.6	5	5	1.0	C3
6	6	84.2	0	0	0.0	C1
7	7	87.8	0	0	0.0	C1
8	8	98.8	0	0	0.0	C1
9	9	102.1	0	0	0.0	C1
10	10	105.4	0	0	0.0	C1
11	11	82.5	55	0	0.0	C2
12	12	86.1	44	0	0.0	C2
13	13	98.6	33	0	0.0	C2
14	14	102.0	22	0	0.0	C2
15	15	105.4	11	0	0.0	C2
16	16	80.6	60	0	0.0	C2
17	17	84.4	48	0	0.0	C2
18	18	97.0	36	0	0.0	C2
19	19	101.9	24	0	0.0	C2
20	20	105.4	12	0	0.0	C2
21	21	80.6	60	0	0.0	C2
22	22	84.4	48	0	0.0	C2
23	23	97.0	36	0	0.0	C2
24	24	101.9	24	0	0.0	C2
25	25	105.4	12	0	0.0	C2
26	26	80.6	60	0	0.0	C2
27	27	84.4	48	0	0.0	C2
28	28	97.0	36	0	0.0	C2
29	29	101.9	24	0	0.0	C2
30	30	105.4	12	0	0.0	C2
31	31	80.6	60	0	0.0	C2
32	32	84.4	48	0	0.0	C2
33	33	97.0	36	0	0.0	C2
34	34	101.9	24	0	0.0	C2
35	35	105.4	12	0	0.0	C2
36	36	80.6	60	0	0.0	C2
37	37	84.4	48	0	0.0	C2
38	38	97.0	36	0	0.0	C2

Annex B: Detailed results for the structural robustness assessment in Chapter V

39	39	101.9	24	0	0.0	C2
40	40	105.4	12	0	0.0	C2
41	41	82.5	55	0	0.0	C2
42	42	86.1	44	0	0.0	C2
43	43	98.6	33	0	0.0	C2
44	44	102.0	22	0	0.0	C2
45	45	105.4	11	0	0.0	C2
46	46	84.2	0	0	0.0	C1
47	47	87.8	0	0	0.0	C1
48	48	98.8	0	0	0.0	C1
49	49	102.1	0	0	0.0	C1
50	50	105.4	0	0	0.0	C1
51	51	100.4	0	0	0.0	C1
52	52	102.1	0	0	0.0	C1
53	53	103.8	0	0	0.0	C1
54	54	105.4	0	0	0.0	C1
55	55	108.6	5	5	1.0	C3
56	1-6	184.7	50	50	1.0	C3
57	2-7	190.0	40	40	1.0	C3
58	3-8	202.6	30	30	1.0	C3
59	4-9	207.6	20	20	1.0	C3
60	5-10	214.0	10	10	1.0	C3
61	6-11	166.7	80	80	1.0	C3
62	7-12	173.9	64	64	1.0	C3
63	8-13	197.4	48	48	1.0	C3
64	9-14	204.2	32	32	1.0	C3
65	10 - 15	210.8	16	16	1.0	C3
66	11-16	163.1	85	110	1.3	C4
67	12-17	170.4	68	88	1.3	C4
68	13-18	195.7	51	66	1.3	C4
69	14-19	204.0	34	44	1.3	C4
70	15-20	210.8	17	17	1.0	C3
71	16-21	161.2	90	140	1.6	C4
72	17-22	168.7	72	128	1.8	C4
73	18-23	194.0	54	100	1.9	C4
74	19-24	203.9	36	36	1.0	C3
75	20-25	210.8	18	18	1.0	C3
76	21-26	161.2	90	170	1.9	C4
77	22-27	168.7	72	158	2.2	C4
78	23-28	194.0	54	124	2.3	C4
79	24-29	203.9	36	36	1.0	C3
80	25-30	210.8	18	18	1.0	C3
81	26-31	161.2	90	170	1.9	C4
82	27-32	168.7	72	158	2.2	C4
83	28-33	194.0	54	124	2.3	C4
84	29-34	203.9	36	36	1.0	C3
85	30-35	210.8	18	18	1.0	C3
86	31-36	161.2	90	140	1.6	C4
87	32-37	168.7	72	128	1.8	C4
88	33-38	194.0	54	100	1.9	C4
89	34-39	203.9	36	36	1.0	C3
90	35-40	210.8	18	18	1.0	C3
91	36-41	163.1	85	110	1.3	C4
92	37-42	170.4	68	88	1.3	C4
93	38-43	195.7	51	66	1.3	C4
94	39-44	204.0	34	44	1.3	C4
95	40-45	210.8	17	17	1.0	C3
96	41-46	166.7	80	80	1.0	C3

Annex B: Detailed results for the structural robustness assessment in Chapter V

97	42 - 47	173.9	64	64	1.0	C3
98	43-48	197.4	48	48	1.0	C3
99	44-49	204.2	32	32	1.0	C3
100	45-50	210.8	16	16	1.0	C3
101	46-51	184.7	50	50	1.0	C3
102	47-52	190.0	40	40	1.0	C3
103	48-53	202.6	30	30	1.0	C3
104	49-54	207.6	20	20	1.0	C3
105	50-55	214.0	10	10	1.0	C3
106	1-6-11	267.1	80	80	1.0	C3
107	2-7-12	276.0	64	64	1.0	C3
108	3-8-13	301.2	48	48	1.0	C3
109	4-9-14	309.6	32	32	1.0	C3
110	5-10-15	319.4	16	16	1.0	C3
111	6-11-16	247.3	110	110	1.0	C3
112	7-12-17	258.3	88	88	1.0	C3
113	8-13-18	294.4	66	66	1.0	C3
114	9-14-19	306.1	44	44	1.0	C3
115	10-15-20	316.2	22	22	1.0	C3
116	11-16-21	243.7	115	140	1.2	C4
117	12-17-22	254.8	92	112	1.2	C4
118	13-18-23	292.7	69	84	1.2	C4
119	14-19-24	305.9	46	56	1.2	C4
120	15-20-25	316.2	23	28	1.2	C4
121	16-21-26	241.9	120	170	1.4	C4
122	17-22-27	253.1	96	152	1.6	C4
123	18-23-28	291.0	72	118	1.6	C4
124	19-24-29	305.8	48	68	1.4	C4
125	20-25-30	316.1	24	24	1.0	C3
126	21-26-31	241.9	120	280	2.3	C4
127	22-27-32	253.1	96	268	2.8	C4
128	23-28-33	291.0	72	212	2.9	C4
129	24-29-34	305.8	48	112	2.3	C4
130	25-30-35	316.1	24	24	1.0	C3
131	26-31-36	241.9	120	170	1.4	C4
132	27-32-37	253.1	96	152	1.6	C4
133	28-33-38	291.0	72	118	1.6	C4
134	29-34-39	305.8	48	68	1.4	C4
135	30-35-40	316.1	24	24	1.0	C3
136	31-36-41	243.7	115	140	1.2	C4
137	32-37-42	254.8	92	112	1.2	C4
138	33-38-43	292.7	69	84	1.2	C4
139	34-39-44	305.9	46	56	1.2	C4
140	35-40-45	316.2	23	28	1.2	C4
141	36-41-46	247.3	110	110	1.0	C3
142	37-42-47	258.3	88	88	1.0	C3
143	38-43-48	294.4	66	66	1.0	C3
144	39-44-49	306.1	44	44	1.0	C3
145	40-45-50	316.2	22	22	1.0	C3
146	41-46-51	267.1	80	80	1.0	C3
147	42-47-52	276.0	64	64	1.0	C3
148	43-48-53	301.2	48	48	1.0	C3
149	44-49-54	309.6	32	32	1.0	C3
150	45-50-55	319.4	16	16	1.0	C3
151	1-6-11-16	347.7	110	110	1.0	C3
152	2-7-12-17	360.4	88	88	1.0	C3
153	3-8-13-18	398.2	66	66	1.0	C3
154	4-9-14-19	411.6	44	44	1.0	C3

155	5-10-15-20	424.8	22	22	1.0	C3
156	6-11-16-21	327.9	140	140	1.0	C3
157	7-12-17-22	342.6	112	112	1.0	C3
158	8-13-18-23	391.4	84	84	1.0	C3
159	9-14-19-24	408.1	56	56	1.0	C3
160	10-15-20-25	421.6	28	28	1.0	C3
161	11-16-21-26	324.3	145	170	1.2	C4
162	12-17-22-27	339.2	116	136	1.2	C4
163	13-18-23-28	389.7	87	102	1.2	C4
164	14-19-24-29	407.9	58	68	1.2	C4
165	15-20-25-30	421.6	29	34	1.2	C4
166	16-21-26-31	322.5	150	200	1.3	C4
167	17-22-27-32	337.5	120	176	1.5	C4
168	18-23-28-33	388.1	90	136	1.5	C4
169	19-24-29-34	407.8	60	80	1.3	C4
170	20-25-30-35	421.5	30	40	1.3	C4
171	21-26-31-36	322.5	150	200	1.3	C4
172	22-27-32-37	337.5	120	176	1.5	C4
173	23-28-33-38	388.1	90	136	1.5	C4
174	24-29-34-39	407.8	60	80	1.3	C4
175	25-30-35-40	421.5	30	40	1.3	C4
176	26-31-36-41	324.3	145	170	1.2	C4
177	27-32-37-42	339.2	116	136	1.2	C4
178	28-33-38-43	389.7	87	102	1.2	C4
179	29-34-39-44	407.9	58	68	1.2	C4
180	30-35-40-45	421.6	29	34	1.2	C4
181	31-36-41-46	327.9	140	140	1.0	C3
182	32-37-42-47	342.6	112	112	1.0	C3
183	33-38-43-48	391.4	84	84	1.0	C3
184	34-39-44-49	408.1	56	56	1.0	C3
185	35-40-45-50	421.6	28	28	1.0	C3
186	36-41-46-51	347.7	110	110	1.0	C3
187	37-42-47-52	360.4	88	88	1.0	C3
188	38-43-48-53	398.2	66	66	1.0	C3
189	39-44-49-54	411.6	44	44	1.0	C3
190	40-45-50-55	424.8	22	22	1.0	C3

Table B.10: Failure energy and structural response under each local failure scenario i for the assumption DUC2.